4-16-2004

Behavior and Design of Precast Prestressed Inverted Tee Girders with Multiple Web Openings for Service Systems

James M. Thompson

Stephen Pessiki

BEHAVIOR AND DESIGN OF PRECAST PRESTRESSED CONCRETE INVERTED TEE GIRDERS WITH MULTIPLE WEB OPENINGS FOR SERVICE SYSTEMS

by

James M. Thompson
Assistant Professor
Civil Engineering
Ohio University
(Former Graduate Research Assistant
Civil and Environmental Engineering
Lehigh University)

Stephen Pessiki
Associate Professor
Civil and Environmental Engineering

ATLSS Report No. 04-07

April 16, 2004

ATLSS is a National Center for Engineering Research on Advanced Technology for Large Structural Systems

117 ATLSS Drive
Bethlehem, PA 18015-4728

Phone: (610)758-3525
Fax: (610)758-5902

www.atlss.lehigh.edu
Email: inatl@lehigh.edu

[This page intentionally blank]

ACKNOWLEDGMENTS

This research was supported by the Precast/Prestressed Concrete Institute, High Concrete Structures, Inc., and the Center for Advanced Technology for Large Structural Systems (ATLSS) at Lehigh University. The authors gratefully acknowledge the sponsors' support. The authors also appreciate and acknowledge the assistance provided by the laboratory staff at Imbt and Fritz Laboratories. The opinions, findings and conclusions expressed in this report are those of the authors and do not necessarily reflect the views of the sponsors.

[This page intentionally blank]

TABLE OF CONTENTS

Page

[This page intentionally blank]

LIST OF TABLES

Page

[This page intentionally blank]

LIST OF FIGURES

Page

[This page intentionally blank]

LIST OF NOTATION

A	=	area, in.^{2}
a	=	depth of equivalent rectangular stress block, in.
A_{ab}	=	area of abutment reinforcement, in.^{2}
A_{bt}	=	area of the bottom chord, in.^{2}
A_{gt}	=	top chord gross area, in.^{2}
A_l	=	area of reinforcement for longitudinal bending of the ledge, in.^{2}
A_p	=	area of (1) ½" diameter "special" prestressing strand, in.^{2}
A_{ps}	=	area of prestressed reinforcement in tension zone, in.^{2}
A_{sh}	=	area of hanger reinforcement, in.^{2}
A_{sl}	=	area of reinforcement for transverse bending of the ledge, in.^{2}
A_v	=	area of shear reinforcement within a distance s, in.^{2}
A_{vb}	=	area of shear reinforcement in the bottom chord, in.^{2}
A_{vt}	=	area of shear reinforcement in the top chord, in.^{2}
A_s	=	area of tension reinforcement, in.^{2}
A'_s	=	area of compression reinforcement, or area of reinforcement provided to resist the total tensile force in concrete at release, in.^{2}
A_t	=	top chord area, in.^{2}
b_l	=	width of the projecting ledge of the IT girder, in.
b_w	=	web width of the IT girder, in.
C	=	compression force, kips
c_b	=	distance from the neutral axis to the bottom of the section, in.
c_t	=	distance from the neutral axis to the top of the section, in.
d	=	distance from extreme compression fiber to centroid of longitudinal tension reinforcement, in.
d_e	=	distance from end of beam to first DT stem, in.
d_p	=	distance from extreme compression fiber to prestressed reinforcement centroid in.
e	=	eccentricity of centroid of prestress force from centroid of section, in.
E_c	=	modulus of elasticity of concrete at 28 day strength, psi
E_{ci}	=	modulus of elasticity of concrete at release strength, psi
E_p	=	modulus of elasticity of prestressed reinforcement, ksi
E_s	=	modulus of elasticity of mild steel reinforcement, ksi
f_{ct}	=	splitting tensile strength of concrete, psi
f_{pe}	=	tensile stress in prestressing tendons after long term losses, ksi
f_{pi}	=	tensile stress in prestressing tendons immediately after prestress transfer, ksi
f_{pj}	=	tensile stress in prestressing tendons due to tendon jacking force, ksi
f_{ps}	=	stress in prestressed reinforcement at nominal strength, ksi
f_{pu}	=	specified tensile strength of prestressing tendons, ksi
f_{py}	=	yield stress of prestressed reinforcement, ksi
f_r	=	modulus of rupture or expected average concrete cracking stress, psi (Section 4.9.1)
f_y	=	specified yield strength of nonprestressed reinforcement, ksi
f'_c	=	specified compressive strength of concrete, psi

f'_{ci}	=	compressive strength of concrete at time of initial prestress, psi
h	=	total depth of the IT girder, in.
h_b	=	height of the bottom chord, in.
h_l	=	depth of the projecting ledge of the IT girder, in.
h_o	=	height of an opening, in.
h_p	=	depth of a post, in.
h_t	=	height of the top chord, in.
h_w	=	web depth of the IT girder, in.
I	=	moment of inertia, in.^{4}
I_b	=	moment of inertia of the bottom chord, in.^{4}
I_t	=	moment of inertia of the top chord, in.^{4}
L_B	=	column center-to-center spacing in the span direction of the DT beams, ft
L_{DT}	=	actual length of the DT beams, ft
L_e	=	distance from end of beam to theoretical location of reaction, in.
L_{eff}	=	effective length of beam between reactions, in.
L_G	=	column center-to-center spacing in the span direction of the girder, ft
L_{IT}	=	actual length of the IT girder, ft
l_b	=	length of the bottom chord, in.
l_o	=	length of an opening, in.
l_p	=	length of a post, in.
l_t	=	length of the top chord, in.
M	=	moment at a section, in.-kip
M_b	=	moment in the bottom chord, in.-kip
M_i	=	moment at the left side of an opening, in.-kip
M_j	=	moment at the right side of an opening, in.-kip
M_n	=	nominal moment strength, in.-kip
M_t	=	moment in the top chord, in.-kip
M_u	=	factored moment, in.-kip
M_{ub}	=	factored bottom chord moment, in.-kip
M_{ut}	=	factored top chord moment, in.-kip
N	=	normal force at a section, in.-kip
N_b	=	normal force in the bottom chord, kip
N_t	=	normal force in the top chord, kip
N_u	=	factored axial force, kip
N_{ub}	=	factored normal force in the bottom chord, kip
N_{ut}	=	factored normal force in the top chord, kip
P	=	equivalent load from the prestressed reinforcement, due to jacking force, initial prestress force, or effective prestress force, kip
P_e	=	prestressing force after long term losses have occurred, kip
P_i	=	prestressing force immediately after transfer, kip
P_j	=	prestressing force due to jacking of the tendons, kip
Q	=	total load transferred to the girder from two DT stems, opposite each other on each side of the girder web, kip
Q_{DL}	=	concentrated load on girder due to superimposed dead load, kip

Q_{DT} = concentrated load on girder due to DT beams, kip
Q_f = concentrated load on the girder at which capacity and demand are equal for a failure mode, kip
Q_{IT} = concentrated load on girder due to self-weight, kip
Q_{LL} = concentrated load on girder due to superimposed live load, kip
Q_s = service load on girder, kip
Q_{TP} = concentrated load on girder due to cast-in-place topping slab, kip
Q_u = factored load on girder, kip
q = pressure load on FE model, ksi
R = beam reaction, kip
R_y = translational restraint in the y-direction in the finite element model
R_z = translational restraint in the z-direction in the finite element model
ρ_b = reinforcement ratio producing balanced strain conditions
S_{DT} = spacing of the DT stems, ft
T = tension force, kip
V = shear force at a section, kip
V_b = shear force in the bottom chord, kip
V_c = nominal shear strength provided by concrete, kip
V_{cb} = nominal shear strength provided by concrete in the bottom chord, kip
V_{ci} = nominal shear strength provided by concrete when diagonal cracking results from combined shear and moment, kip
V_{ct} = nominal shear strength provided by concrete in the top chord, kip
V_{cw} = nominal shear strength provided by concrete when diagonal cracking results excessive principal tensile stress in web, kip
V_n = nomianl shear strength, kip
V_s = nominal shear strength provided by shear reinforcement, kip
V_t = shear force in the top chord, kip
V_u = factored shear force at section
V_{ub} = factored shear force in the bottom chord, kip
V_{uc} = factored shear force in a chord, kip
V_{ut} = factored shear force in the top chord, kip
w_D = dead load per unit length of beam, plf, or unit area of surface, psf,
w_{DL} = dead load per unit length of beam, plf, or unit area of surface, psf, due to fixed service equipment and architectural finishes
w_{DT} = dead load per unit length of beam, plf, or unit area of surface, psf, due to DT beam
w_{IT} = dead load per unit length of beam, plf, or unit area of surface, psf, due to IT girder
w_L = live load per unit length of beam, plf, or unit area of surface, psf
w_s = service load per unit length of beam, plf, or unit area of surface, psf
w_{TP} = dead load per unit length of beam, plf, or unit area of surface, psf, due to concrete topping slab
w_u = factored load per unit length of beam, plf, or unit area of surface, psf
y = distance from the neutral axis of a section to a point on the section, in.
y_b = depth from the top of the section to the centroid of the bottom chord, in.

z	=	distance between the centroids of the top and bottom chords, in.
α_b	=	proportion of the shear force resisted by the bottom chord
α_t	=	proportion of the shear force resisted by the top chord
ϵ	=	strain, in./in.
ϵ_n	=	normal strain, in./in.
ϵ_a	=	strain at a section, in./in.
ϵ_b	=	strain at a section, in./in.
γ_p	=	factor for type of prestressing tendon
σ_{xx}	=	normal stress on the x face of an element in the x direction, psi
σ_{zz}	=	normal stress on the z face of an element in the z direction, psi
ϕ	=	strength reduction factor

ABSTRACT

A precast, prestressed inverted tee (IT) girder with multiple large web openings (ITO) allows building services to cross the girder line within the member's depth, reducing a building's floor-to-floor and overall height. This research's objectives are to understand how web openings alter an IT girder's serviceability and ultimate strength, and develop a design procedure for this structural member.

A prototype ITO girder was designed based on the available literature on concrete beams with web openings. Three full-scale ITO girders and an IT girder were tested to evaluate and compare their behavior. The test variables were the transverse reinforcement details between and above the openings. The ITO's behavior was investigated with linear elastic (FE) and nonlinear(fiber model) finite element analyses and truss models.

The tests show an ITO satisfies the required limit states. Until the ITOs' failure, their behavior was similar to the IT's. The ITOs failed suddenly when a diagonal crack occurred above the opening nearest the support, while the IT had a ductile midspan failure. The literature's design approach did not predict the ITOs' failure load or mode. The transverse reinforcement variations between the openings did not affect the ITO's serviceability, behavior or strength. The transverse reinforcement variations above the openings did not affect the ITO's serviceability or behavior, but did affect its strength.

The ITO's openings exhibit frame behavior, confirming previous researchers' findings. The fiber models show that the chord shear forces and moments depend on cracking in the chords, while the chord axial forces depend primarily on the moment at a section and the distance between the chords. The fiber model's midspan opening failure load is nearly identical with an IT's plane section failure load.

Strut-and-tie models show that the opening's span side abutment reinforcement transfers shear to the top chord, and on its support side, transfers shear force from the bottom chord to the section. The design procedure limits the chord forces by limiting the abutment reinforcement. Knowing the chord forces, the chords are designed for strength.

[This page intentionally blank]

CHAPTER 1

INTRODUCTION

1.1 INTRODUCTION

Figures 1.1 and 1.2 show a typical interior bay of the U.S. conventional precast, prestressed concrete gravity load resisting system (hereafter referred to as the conventional system). A precast, prestressed (pretensioned) inverted tee (IT) girder is one of the conventional system's three primary components. The other two primary components are the double tee (DT) beam floor members, and the supports for the IT girder (columns in Figures 1.1 and 1.2). Gravity loads act directly on the DT beams, which transfer these loads to the IT girders. The IT girders transfer the gravity loads to the columns, which in turn transfer the loads to the foundation.

The conventional system has many attributes that make it suitable for constructing multistory buildings with a regular, rectangular plan. Its components can span long distances, reducing the number of pieces fabricated, transported and erected and the time associated with each operation, allowing the building frame's rapid erection. Its long spans provide large column-free spaces, resulting in greater flexibility in interior space arrangements. Component fabrication occurs at a precast plant, away from the building site, improving quality control and allowing site work and foundation construction to occur simultaneously with component fabrication.

Parking garages and occupied buildings such as residential, commercial, educational, and office buildings are typical examples of buildings that benefit from the conventional system's attributes. Occupied buildings, as opposed to parking garages, require many different types of building service systems. These systems include plumbing (i.e., supply, drain-waste-vent, and fire protection), HVAC (i.e., heating, ventilating and air conditioning), and electrical systems (i.e., power, security and communication). Occupied buildings typically have a 2 in. thick cast-in-place concrete topping slab that provides the finished floor surface and acts compositely with the floor members and the IT girder.

The typical practice for occupied buildings employing the conventional system is to place the building's service systems below the IT girder where they cross the girder line. Figures 1.2 and 1.3 show the typical arrangement of building service systems in an office building constructed with the conventional system. Figure 1.2 shows the resulting two-layer floor system in a section through the IT girder. This figure also defines and shows the structural depth, the service depth, and the floor system depth.

Despite the conventional system's advantages, it is not widely used for occupied buildings, and instead is primarily used for parking garages. This is due partly to the large floor system depth needed to hold the service systems in occupied buildings. A large floor system depth increases the building's height, volume and weight for a fixed number of stories. This increases the required quantity of exterior architectural finishes, the demand on building services, the size of foundation elements and the costs associated with these items. In jurisdictions where building height limits exist, a large floor system depth may reduce the number of stories that fit within the limit, resulting

in a project that is not economically viable. Finally, in seismic regions a taller, heavier building increases the demand on the lateral load resisting system and its cost.

An IT girder with multiple web openings for service systems has the potential to make the conventional system more suitable for occupied buildings. The web openings allow the building's service systems to pass through the girder, eliminating the service depth. If the web openings do not require an offsetting increase in the girder's depth, their inclusion reduces the floor system depth. This reduces the floor-to-floor height and the overall height of a building for a given number of stories, with the attendant advantages.

Figure 1.4 shows a prototype for an IT girder with multiple web openings. Regularly spaced openings along the girder's length standardize production and eliminate the need to coordinate individual openings with specific service systems. Referring to Figure 1.4, this research calls the diagonally hatched areas above and below the openings chords, calls the vertically hatched areas between the openings posts, and calls the regions at the openings' edges abutments. This research calls the resulting structural member an ITO girder.

Figure 1.5 shows the prototype ITO girder replacing the IT girder in Figure 1.2. Figure 1.5 shows the service systems placed between the DT stems and routed through the ITO girder's web, which eliminates the service depth. The secondary HVAC ducts' size dictates the opening's minimum height, and structural requirements limit the maximum height.

Placing multiple web openings in an IT girder alters the manner in which it resists the loads applied to it and the girder's response to those loads. These openings have the potential to affect several parameters, such as, (1) the distribution of internal forces on the cross-section, (2) the concrete stresses' magnitude and distribution, (3) the cracking load and crack patterns (location, type, extent and width), (4) the load-deflection response, (5) the peak load, and (6) the failure mechanism and failure load. These changes need to be investigated and their effects understood to design a safe and serviceable ITO girder.

1.2 RESEARCH OBJECTIVES

The research has two main objectives, which are:

1. To understand and explain the behavior of a precast, prestressed inverted tee girder with multiple large web openings.
2. To develop a design procedure for a precast, prestressed inverted tee girder with multiple web openings.

1.3 SUMMARY OF APPROACH

This research investigates the effects of placing multiple large web openings in an IT girder through an experimental program, linear and nonlinear finite element analyses, and strut-and-tie models. The results from the experimental program and the linear finite element analyses (task 1 through part of

task 5 in the following list) are presented in Thompson and Pessiki (2001). This report covers the fiber model analyses in task 5 and tasks 6 and 7.

1. Review the current literature on concrete beams with large web openings, including research on nonprestressed, pretensioned and post-tensioned beams.
2. Design a prototype ITO girder for a typical interior bay in a representative office building using current industry standard practices, code requirements, and a design approach identified in the literature.
3. Design and test three full-scale ITO girders and a full-scale IT girder reference specimen, all based on the prototype ITO girder.
4. Evaluate the experimental program's results to (a) assess the openings' effect on the ITO girder's response, (b) evaluate the applicability of the design approach in the literature to the ITO girder, and (c) assess the ITO girder's ability to satisfy applicable code requirements.
5. Conduct linear elastic and nonlinear finite element analyses to investigate the ITO girder's behavior and compare these results with the design approach in the literature and the experimental results.
6. Investigate strut-and-tie models for insight on the ITO girder's behavior.
7. Develop a design procedure for an ITO girder based on the experimental results, the finite element analyses, and the strut-and-tie models. The goal is to reduce the knowledge obtained from the research to a simplified set of design rules or guidelines, and to note the conditions for their applicability.

1.4 SUMMARY OF FINDINGS

An inverted tee girder with large web openings can provide satisfactory service load performance and adequate strength. In the experimental program, the ITO specimens' overall service load behavior was similar to that of the comparably longitudinally reinforced IT specimen. The similarity in behavior continued to the point at which the ITO specimens failed, at a load approximately 27% less than the IT specimen. The ITO specimens failed when a diagonal crack occurred in the top chord at the opening nearest the support. This prevented them from reaching their flexural strength at midspan and failing in a ductile manner.

The amount of transverse reinforcement and its distribution in the posts was not found to affect the test specimens' peak load. It was found to affect the width of the cracks that formed between openings. The amount of transverse reinforcement in the top chord did affect the girder's peak load capacity, and the extent of the cracks that occurred.

The ITO specimens' behavior confirms the findings of previous researchers that a beam with large web openings exhibits frame behavior at the openings. The results also show that the findings of the previous research, primarily on double tee beams, are not completely applicable to this cross-section. The recommendations of the previous research did not result in an accurate failure load or failure mode prediction for the ITO specimens. The opening location along the span was found to affect the

cracking at the opening significantly. This is due to the relative shear force and moment values at the opening.

The finite element analyses and the experimental program show that the proportion of the shear force resisted by each chord is dependent on their relative stiffness. The fiber model analyses show that the proportion of the shear force resisted by each chord changes as cracking occurs in the chords. These results also show that the relative stiffness is not only dependent on the moments of inertia, but also depends on the rigidity of the connection between the chords and the girder web. Once cracking occurs, these supports are not sufficiently rigid at the opening edges to allow the assumption of a fully fixed end condition for computing the relative stiffness.

The fiber model shows that the midspan opening failure load for a symmetrically loaded ITO girder is nearly identical with the failure load determined from a plane section analysis of an IT girder with the identical cross-section. This observation shows that if the failure loads for the other possible failure modes exceed the midspan opening failure load, an ITO girder can reach approximately the same load as the identical IT girder.

This research shows that treating an ITO girder as a flexural member with regions requiring special detailing does not produce completely satisfactory results. The desired ductile failure mode, prestressed reinforcement yielding at midspan, does not occur. Instead, an undesirable failure mode, diagonal cracking in the top chord, occurs. Capacity design provides an alternate way to approach the ITO girder's design. This approach's objective is to provide sufficient strength for the undesirable failure modes so they do not occur before the desired failure mode. To implement a capacity design approach, the demand must be known with certainty.

The test and fiber model results show that the chord shear forces and moments are highly dependent on the extent of cracking in the chords, while the chord axial forces depend primarily on the total moment at a section and the distance between the chords' centroids. The bottom chord cracking controls the shear distribution between the top and bottom chords, and the top chord cracking influences the top chord inflection point location. The chords' moments vary with the chord's normal and shear forces and the inflection point location, and therefore are a function of how much cracking occurs in the chords. These observations indicate an elastic analysis similar to the assumptions made for the analysis of a Vierendeel truss is inadequate for estimating the chord shear forces and moments. They also indicate a conservative approach for the chord's axial-flexural design is needed.

These analyses also show that cracking occurs in the bottom chord at both openings while the chord's axial force is compressive. This observation shows that the sign of the chord's axial force is not sufficient as a criterion for apportioning the shear force between the chords. The experimental results also show that a properly reinforced opening can be located within the strand development length. Because strand slip can result in a sudden failure, the bottom chord at an opening within the strand development length should not be designed for an excessive amount of shear force, which leads to large moments and extensive cracking.

The fiber model shows that the depth of the uncracked concrete in the top chords at openings 1 and 2 makes it unlikely the chord reinforcement will yield. This indicates flexural hinging of the top chord at both ends of the opening is not a viable mechanism to control the top chord shear force. The

strut-and-tie models reveal the function of the ITO girder's various types of reinforcement and show that the abutment reinforcement on an opening's span side transfers shear force to the top chord, and on an opening's support side, transfers shear force from the bottom chord to the section. Once the abutment reinforcement's function in the transfer of forces to the chords is understood, it is apparent that this reinforcement can be used to limit the chord forces to known values through controlled yielding. Once the chord forces are known and limited, the chords can be designed to provide adequate strength, allowing the ITO girder to fail in the desired failure mode.

A design procedure is presented that provides a means to quantify and limit the chord forces for strength design, using the abutment reinforcement to control the chord forces. The design procedure provides recommendations on the sizing of the various types of reinforcement required for the ITO girder. It also provides a method to ensure that a ductile midspan failure occurs prior to a brittle failure like those observed in the experimental program. Full-scale testing is necessary to validate the design procedure and ensure the resulting ITO girder behaves as intended.

1.5 OUTLINE OF REPORT

Chapter 2 reviews the work covered in Thompson and Pessiki (2001), including the conclusions from the experimental program and the linear finite element analyses. Chapter 3 presents the nonlinear fiber model analyses, which include analysis of the test specimens to predict the observed failure, and a parameter study to investigate the influence of several design parameters on the ITO girder. Chapter 4 presents strut-and-tie models used to investigate the internal forces in the ITO girder and identify the function of the various types of reinforcement. Chapter 5 presents the design procedure, which is based on the experimental results, the finite element analyses, and the strut-and-tie models. Chapter 6 provides a summary of the work, the conclusions drawn from it, and suggestions for future work.

1.6 UNIT CONVERSIONS

1 in.	=	25.4 mm
1 $in.^2$	=	645 mm^2
1 $in.^4$	=	416 x 10^3 mm^4
1 ft	=	304.8 mm
1 lb	=	4.448 N
1 kip	=	4.448 kN
1 psi	=	6.895 kPa
1 ksi	=	6.895 MPa
1 psf	=	47.9 N/m^2
1 plf	=	14.59 N/m

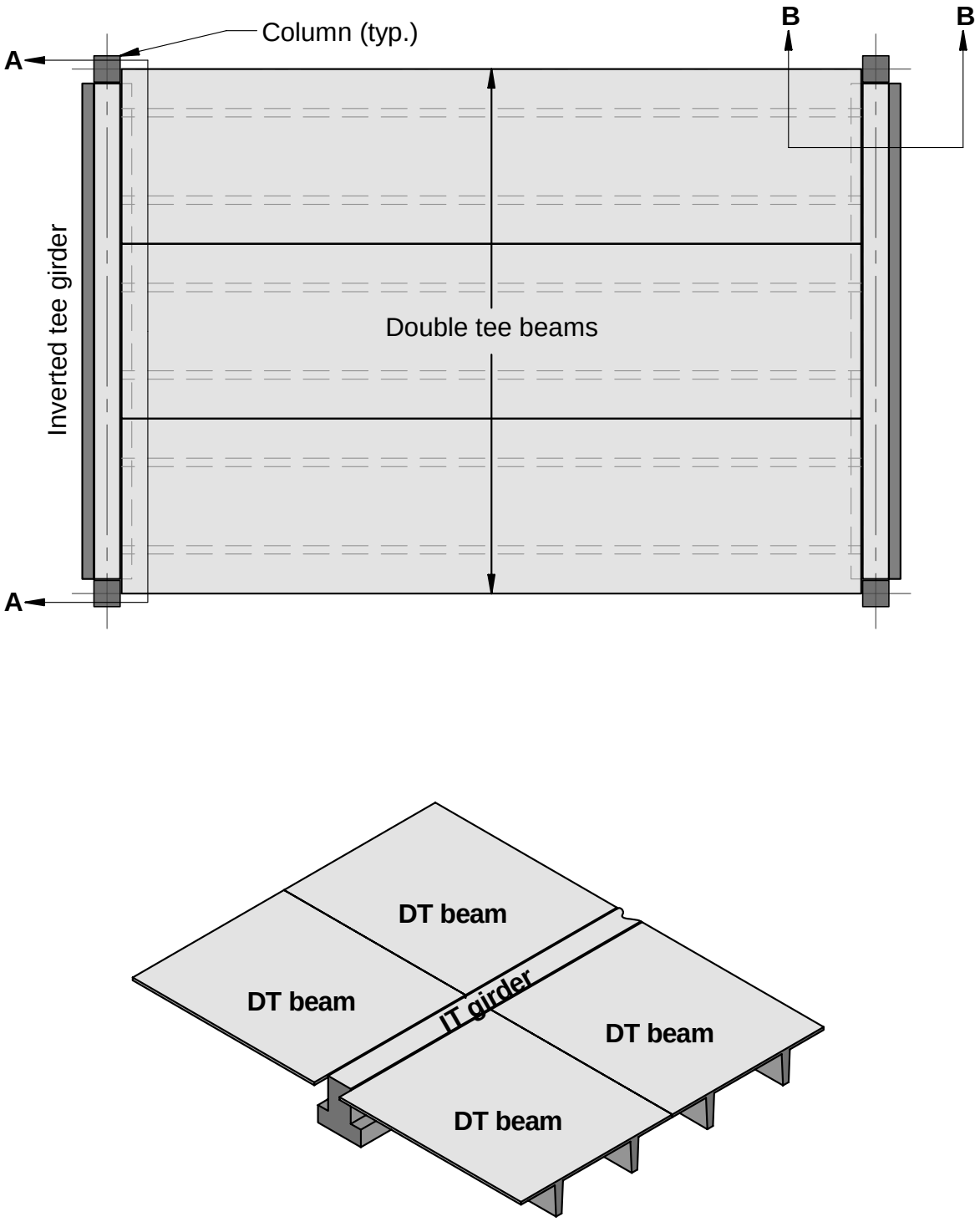

Figure 1.1 Plan and isometric views of a typical interior bay of the U.S. conventional precast, prestressed gravity load resisting system

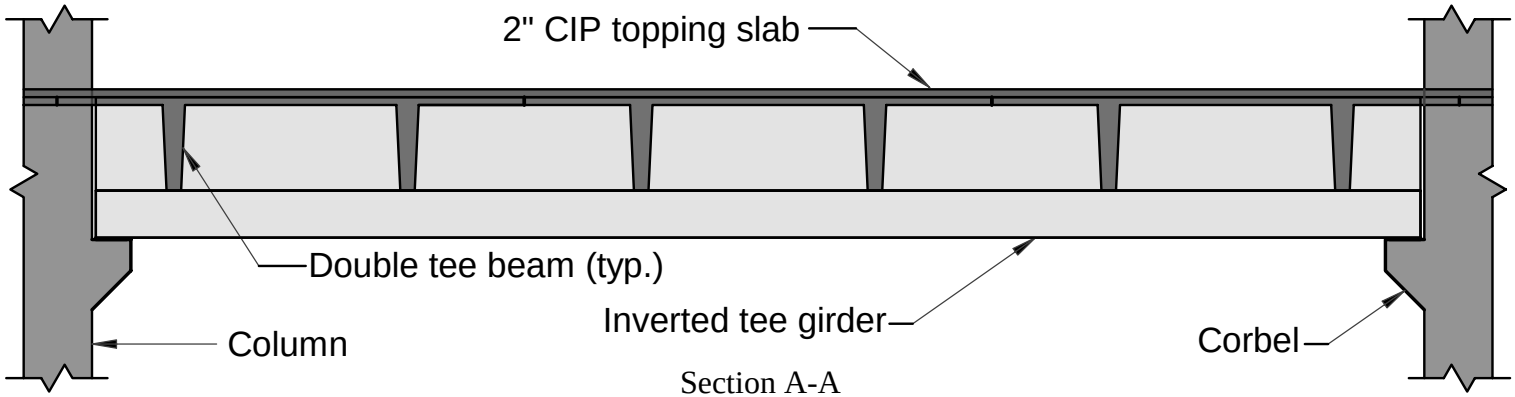

Section A-A

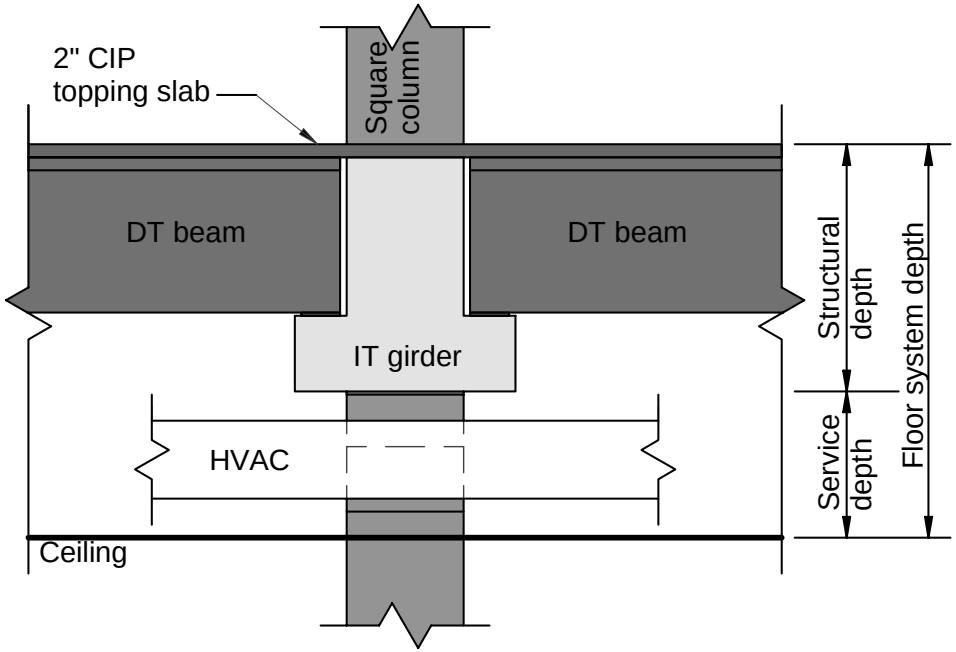

Section B-B

Figure 1.2 Sections through the typical interior bay of the U.S. conventional system with an IT girder

Figure 1.3 Office building constructed with the conventional system

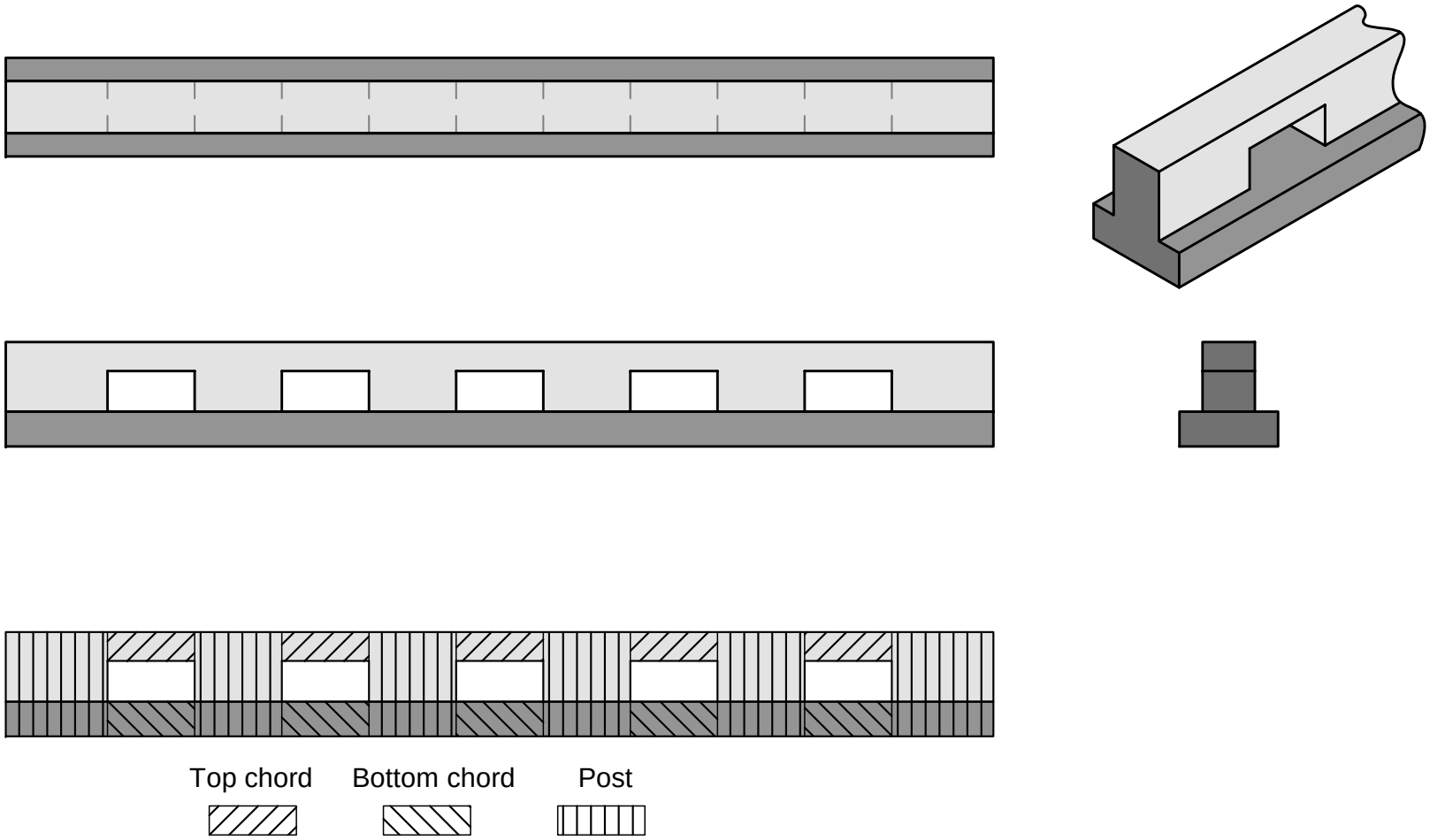

Figure 1.4 Plan, elevations, section and partial isometric of prototype ITO girder

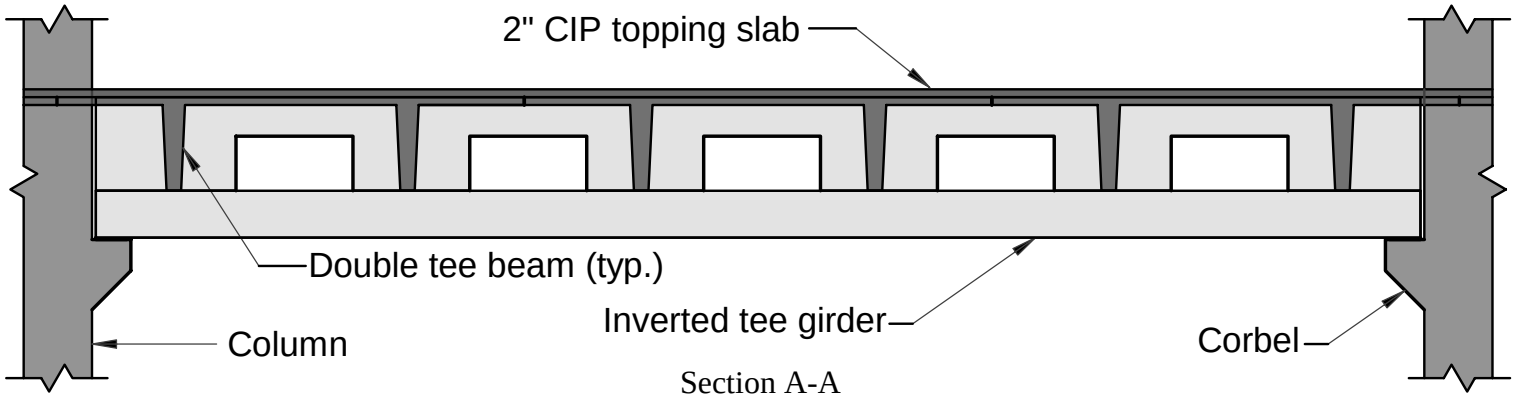

Section A-A

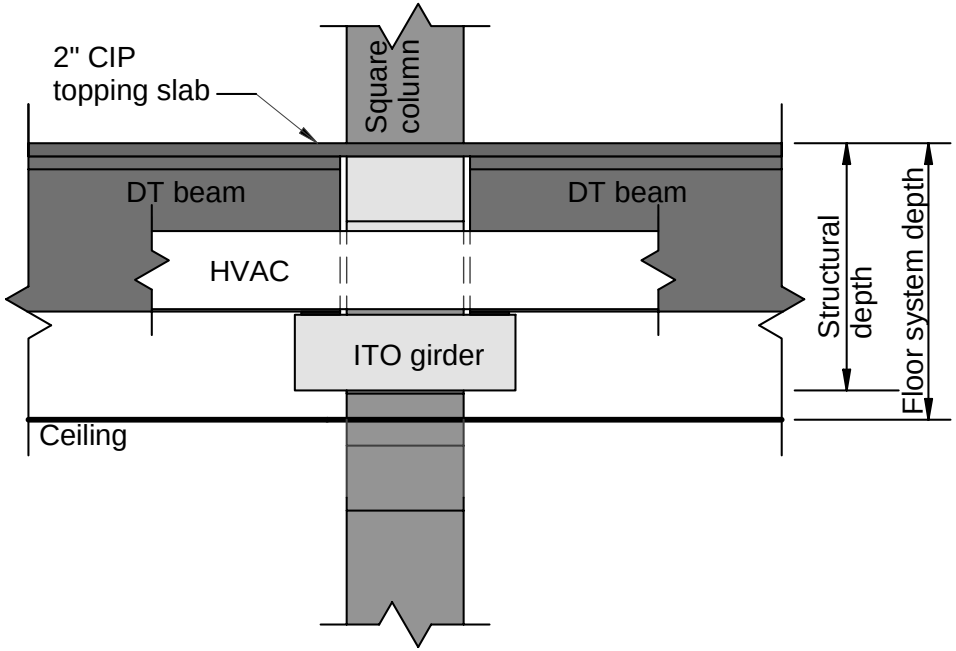

Section B-B

Figure 1.5 Sections through the typical interior bay of the U.S. conventional system with an ITO girder

CHAPTER 2

REVIEW OF EXPERIMENTAL PROGRAM AND ELASTIC FINITE ELEMENT ANALYSES

2.1 INTRODUCTION

This chapter reviews and summarizes the material in Thompson and Pessiki (2001). Section 2.2 presents the background for the work, Section 2.3 summarizes the design of the prototype ITO girder, Section 2.4 describes the experimental program, and Section 2.5 presents the elastic finite element analyses. Section 2.6 compares examines the experimental results and compares them with the elastic finite results and the initial design assumptions. Section 2.7 presents the design implications drawn from this work.

2.2 BACKGROUND

2.2.1 Development at Lehigh University

Improving precast structural floor systems through weight reductions, depth reductions or both, and better accommodation of service systems provides significant improvements in the overall building efficiency. Pessiki, Prior, Sause and Slaughter (1995a) reviewed existing and emerging precast concrete structural systems that are suitable for office building construction. In this context, precast concrete structural systems include the structural floor system plus the vertical load-bearing members such as columns or bearing walls. Pessiki, Prior, Sause, Slaughter and van Zyverden (1995b) conducted an assessment of the systems identified by Pessiki et al. (1995a), based on criteria they developed to evaluate the overall building system's efficiency and performance. This assessment's goal was to identify opportunities for the development of new precast structural systems that improve the efficiency and performance of existing precast structural systems.

Pessiki et al. (1995b) and Slaughter, Sause and Pessiki (1997) identified many opportunities to improve the effectiveness of precast structural floor systems. One of these is reducing the floor system depth by integrating the building service systems within the structural depth. Pessiki, van Zyverden, Sause and Slaughter (1997) proposed three new floor systems that realize this opportunity. Figure 2.1 shows a key component of these proposed floor systems, a structural element they call a stub girder.

This research began with an investigation of the stub girder developed by Pessiki et al. (1997). Before the topping slab's placement, the bottom flange is the only load resisting element between the stubs. After the topping slab is in place, the assumption was that the stub girder acts as a cracked flexural member. Preliminary calculations showed that the stub girder requires a deep bottom flange (ledge) to support the construction loads independently before the composite topping slab has gained its full strength. This results in a structural depth (and floor system depth) approximately equal to the conventional system and negates the gain in efficiency obtained by integration of structure and services.

In a discussion of alternatives for the stub girder, engineers at High Concrete Structures, Inc. (HCSI) suggested incorporating a precast top flange across the stubs. This provides the required compression area to support construction loads without shoring. They said a precast top flange would not greatly increase the difficulty or cost of fabrication, and that any increase in fabrication cost would likely outweigh the cost of shoring. These discussions led to the prototype ITO girder in Figure 1.4. It incorporates openings that are of sufficient size to pass building services through with the idea of a precast compression flange to support the construction loads. This final concept is similar to the Duotek system reviewed in Pessiki et al. (1995a).

2.2.2 Literature Review

Adding an integral top flange across the openings results in the same final configuration as placing the topping slab on the stub girder. In both cases (Figure 1.5 and Figure 2.1(d)) the resulting structural element is a girder with web openings. A review of the previous research on concrete beams with web openings was conducted to see if this design approach would yield better results than the initial approach that assumed the stub girder was a cracked flexural member.

Table 2.1 summarizes the published work found on reinforced and prestressed reinforced concrete beams with web openings. The publications cited in Table 2.1 represent eight experimental programs on reinforced and prestressed concrete beams with web openings. These publications also present the results of finite element analyses, comparisons with experimental results and recommended design rules for concrete beams (prestressed and nonprestressed) with web openings.

The cited researchers concluded that large web openings can be placed in the webs of reinforced and prestressed concrete beams without sacrificing strength or serviceability. A common assumption among the researchers is that the portions of the beam above and below the opening (variously called chords or struts) behave as members of a frame, or like the horizontal members in a Vierendeel truss. The beam's solid sections next to the openings anchor the chords like a Vierendeel truss's vertical members. However, they are not similar to the vertical members of a Vierendeel truss, because they are stiff enough that they do not deform significantly. Most of the researchers cited employ the assumptions typically used in the approximate analysis of a Vierendeel truss to determine the chord forces. The primary difference among the researchers cited is the method used to assign a portion of the shear force to the top and bottom chords.

Section 2.4 in Thompson and Pessiki (2001) reviews the simplified analytical model in Barney, Corley, Hanson, and Parmelee (1977). This model, along with the design recommendations in Barney et al., were used to design the prototype ITO girder. This model and the design recommendations are collectively referred to as the initial design model (IDM) in the remainder of this report.

2.3 DESIGN OF THE PROTOTYPE ITO GIRDER

Figure 2.2 shows the framing plan for a typical interior bay in a representative office building. The span of the double tee beams (DT) and the inverted tee girder (IT) were selected to maximize the efficiency of the precast building system. The uniformly distributed service load (w_s) used for the representative office building's typical interior bay is 200 psf. The service load is the sum of the dead load, w_D = 120 psf, and the live load, w_L = 80 psf. Tables 2.2, 2.3 and 2.4 show the design

material properties for the concrete, mild reinforcement and prestressed reinforcement respectively. These tables also shows the tested values where applicable. Having specified the spans, loads and material properties, the prototype ITO girder was designed according to the IDM. Figure 2.3 shows the resulting girder.

2.4 DESCRIPTION OF THE EXPERIMENTAL PROGRAM

The experimental program's objective is to understand how an IT girder with openings responds to applied loads. In the experimental program, three full-scale ITO girder test specimens and one full-scale IT girder test specimen are loaded to failure to investigate the openings' influence. Among the three ITO specimens, the transverse reinforcement in the top chord and in the posts is varied to investigate these reinforcement requirements. Table 2.5 presents the three variables in the experimental program and their distribution among the four test specimens as a test matrix. Figure 2.4 shows the resulting test specimens.

The primary variable in the test matrix, the placement of multiple large rectangular web openings in an IT girder, assesses the openings' influence on the distribution of forces on the cross-section, cracking, the load-deflection response, the peak load and the failure mode. The labels **Beam** and **Column** in Table 2.5 refer to the variations in the ITO specimens' top chord transverse reinforcement, which Figure 2.4 shows. Figure 2.4 shows the variations in the transverse reinforcement adjacent to the openings (called abutment reinforcement) that Table 2.5 labels **Banded** and **Spread**. This variation in the abutment reinforcement amount and placement investigates the necessity of the prescriptive requirement for transverse reinforcement adjacent to the openings in Barney et al. (1977).

The test specimens are 28.5 ft. long precast, prestressed inverted tee girders with an overall depth of 36 in. and a web width of 18 in. They have the same cross-section dimensions, length, and prestressed and nonprestressed longitudinal reinforcement as the prototype ITO girder, and are designed for the parameters of the typical bay in the representative office building. The test specimens use #4 closed-loop stirrups as transverse reinforcement in the web, the ledge, the posts, and the chords, also the same as the prototype ITO girder. The openings and posts in the ITO specimens in Figure 2.4 are the same size and in the same location as the corresponding openings and posts in the prototype ITO girder, and form the test region of these specimens. Providing three openings instead of five reduces the instrumentation requirements, and is expected to give a good indication of the prototype ITO girder's behavior, because it is symmetric about its longitudinal centerline. The specimens' solid section contains supplemental reinforcement to ensure that the failure occurs in the test region.

Figure 2.5 shows a test specimen on the supports with the loading apparatus in place. Figure 2.6 shows a closer view of the load point and identifies the components that transmit the load from the hydraulic jacks to the ledge's top surface. The test specimens are supported on bearing pads resting on steel supports at each end. The bearing pads have an area equal to that provided by a typical column corbel. The test specimens are loaded on both sides of the web on the ledge's top surface by hydraulic jacks. The loads are at the DT stem locations in the typical bay and are transmitted to the ledge by steel plates on bearing pads with an area equal to a DT stem. The test specimens are

loaded at the four interior DT stem locations in the representative office building, as opposed to the six locations in the typical bay. The two loads closest to the supports were omitted from the test for reasons of economy. Because the DT stem centerline nearest the support in the prototype building is 11 in. from the face of the support, it was thought that this load was primarily carried by shear directly to the support and would have little influence on the specimen's behavior. The shear and moment diagrams caused by the two loadings are similar.

Figure 2.7 shows the instruments' locations and designations on S1. The instruments on the other two ITO specimens and S4 are similar. Each designation refers to a different type of instrument or a different function of the instrument. The instruments labeled LS-xx in Figure 2.7(a) are electrical resistance strain gages placed to measure strains in the longitudinal reinforcement. The top chord strain gages at openings 1 and 2 in Figure 2.7(a) are placed at the same elevation as the top and bottom layers of top chord longitudinal reinforcement, and are used to calculate the top chord's normal force, shear force and moment. The instruments labeled XS-xx in Figure 2.7(b) are electrical resistance strain gages placed to measure strains in the transverse reinforcement. The strain gages on the transverse reinforcement in Figure 2.7(b) are intended to (1) indicate the load at which cracking occurs, (2) provide a basis for comparing the effectiveness of the two abutment reinforcement approaches, (3) provide an estimate of the force in the abutment reinforcement, (4) provide a basis for comparing the effectiveness of the two top chord reinforcement approaches. The instruments designated D-xx in Figure 2.7(c) are linear variable differential transformer (LVDT) displacement transducers that measure the top and bottom surfaces' deflections. These measurements provide data for plotting the deflected shape and comparing the ITO specimens' deflections to each other and to the IT. The instruments designated G-xx in Figure 2.7(d) are linear potentiometers that measure crack opening displacements, which are also referred to as gaps or crack opening displacements in this research. Two rods that transfer the load from the hydraulic jacks to the top surface of the specimen's ledge are instrumented with a full strain gage bridge to serve as load cells.

The data from all the instrumentation, including the load cells, was recorded using a computer-based data acquisition system. The signals from the instruments were amplified as required (strain gages only) and digitized using a 12 bit analog-to-digital converter board in the computer. Each data point is a result of twenty samples taken by the software for the analog-to-digital converter in a fraction of a second. One data point for each instrument was recorded on the computer every six seconds. Pertinent data for monitoring the test was displayed during the test. During the tests, the cracks are marked and photographed. The test specimens were painted white before testing to make the cracks more visible.

HCSI fabricated the test specimens at their plant in Denver, PA. They fabricated the cages (Figure 2.8) and then placed them in the long line casting bed (Figure 2.9). Once the cages were in the forms, the strand was pulled through the cages and tensioned. Foam blocks were tied into place to form the web openings, and sections of PVC pipe were placed to form the openings in the ledge for the loading rods. The concrete was batched and poured from trucks and consolidated with a vibrator. Concrete cylinder and beam specimens were taken from samples of each of the three batches required to pour the four girder specimens, and then left with the girder specimens so they would experience the same curing conditions. The specimens were cast on a Friday afternoon, and prestress transfer occurred the following Monday morning after approximately sixty hours of curing time. The

concrete strength was 6010 psi at the time of transfer. The specimens were lifted out of the forms following the cutting of the strands and placed on flatbeds for transportation and storage (Figure 2.10). At the time they were removed from the forms, it was noted that poor consolidation had caused a large void at midspan in the bottom chord of S3 (Figure 2.11). HCSI repaired this void with a concrete patch. All the specimens were inspected for cracks due to transfer at this time. Cracks were not noted on any specimen except S3.

In subsequent discussions of the ITO girders' behavior, S3 is excluded from examinations of load-deflection response because of the fabrication problem. The local behavior of S3 at the openings away from midspan was unaffected, so in these discussions, reference is made to all three ITO girder specimens.

2.5 ELASTIC FINITE ELEMENT ANALYSIS

Figures 2.12 and 2.13 show the analysis model and the reference coordinate system. The overall model geometry is the same as the test specimens, and represents the test specimens' gross section. The model consists of 6904 solid elements with eight nodes each, and these solid elements' aspect ratio is nowhere greater than two. The model has 9105 nodes with three translational degrees of freedom each, resulting in 27298 degrees of freedom. The material properties required for the analysis are the concrete unit weight, 150 pcf, and modulus of elasticity, 5450 ksi. The vertical (Z) direction restraints are 5 in. in from each end at the nodes within the web width. The model is restrained at each end in the transverse (Y) direction at one node, 5 in. from the end, at the model's bottom surface, in the middle of the cross-section. The model is restrained longitudinally at one node on the bottom surface at approximately midspan, in the middle of the cross-section.

Figure 2.13 shows the loads applied to the model. The girder's self-weight is applied as the acceleration of gravity on the model's distributed mass, which the figure does not explicitly show. The vertical loads labeled ***Q*** in the figure represent the applied load on the girder from two DT stems, one on each side of the web. These loads are applied as a uniform pressure load (***q***) on the elements' face over the width of the ledge as Figure 2.13(c) shows, and over a distance of 6 in. along the length of the ledge, approximately the width of a DT stem. The horizontal loads at the model's ends in Figure 2.13(a) labeled ***P*** are the prestress force applied as an equivalent external load. The prestress force is applied at two elevations as Figure 2.12 shows, at the same elevations as the test specimens' prestressed reinforcement. The prestress force is applied as a series of nodal loads at the locations in the cross-section with circles in Figure 2.13(b). The prestress force is introduced linearly at the model's ends over the first 24 in. to approximate the transfer length assumed for the prestressing strand.

Figure 2.14 shows the longitudinal normal stresses (σ_{xx}) along the length of the model on a vertical section through the model's centerline for prestress plus self-weight plus an applied load of 38.7 kips, which is the service load. The normal stresses are symmetric about the vertical centerline of the model's cross-section, with little variation in magnitude horizontally across a section. Locations of high tensile stress are marked with a ***T*** on the figures. These are the locations at which cracking is expected to occur first.The longitudinal normal stresses at the service load show regions of high tension stress in the top and bottom chords at the corners of opening 1. There are also high tension

stresses at the bottom surface of openings 2 and 3. These stresses lead to cracking, which may affect serviceability and the distribution of forces between the chords. These stresses confirm the assumption of frame behavior at the openings, and show how the expected stresses for a beam are disturbed by the openings' presence.

Figure 2.15 shows the vertical normal stresses (σ_{zz}) in elevation, and their variation through the cross-section depth on vertical sections through the model for prestress plus self-weight plus an applied load of 38.7 kips. This figure shows high concrete tensile stresses at the lower support side and upper span side of the openings. These stresses, combined with the longitudinal normal stresses present at these locations, likely contribute to the observed diagonal cracking in the web at the openings' corners, particularly at opening 1. The vertical normal stresses also indicate the banded approach to providing the abutment reinforcement is the preferred approach. Since these stresses are concentrated at the openings' edges, banding the abutment reinforcement places it where it is most necessary, containing cracks more effectively.

Figure 2.16 shows the chord forces obtained from the FE analysis at the service load, along with the chord forces predicted by the IDM. The comparison shows that the normal forces agree reasonably well between the two approaches. The IDM does not predict well the values of the shear force, moment and inflection point calculated from the FE model. The figure shows an elevation of the ITO girder, with the appropriate loads, and an isolated sketch of the chords at each opening with the forces at the openings' edges. The normal force is at the chord centroid, with the accompanying moment. The line across (and sometimes below) the chord in each sketch represents the line of action of the vector sum of the shear force and the normal force on the chord. The endpoints of this line represent the points at which the resultant force is applied to the ends of the chord with no resulting moment. An open circle on this line represents the chord's inflection point.

2.6 EXPERIMENTAL RESULTS AND COMPARISONS WITH ANALYTICAL RESULTS

Load-Deflection Response

The experimental results show that multiple web openings do not significantly alter an inverted tee girder's load-deflection response when compared with a comparably reinforced girder without openings. Figure 2.17 plots the test specimens' load-deflection response, with the deflection measured at D-33 as the inset shows. This figure also shows that the ITO girders satisfy the ACI 318 Code's deflection limits. The ITO girders exhibit a bilinear load-deflection response with initial and post-cracking stiffness similar to the IT girder's. The similarity of response between the ITO specimens and the IT specimen, up to the ITO specimens' peak load, is also observed along the span at the other points at which the deflection was measured. Finally, it is noted that bearing pad compression at the supports influences the measured midspan deflection and the experimentally determined initial stiffness reported for each test specimen. The support settlement is small and similar in magnitude for all four test specimens. The deflections and initial stiffness can thus be compared among the test specimens without correcting the measured values for the support settlement. Comparing S4's midspan deflection to the theoretical value shows that, allowing for the support settlement, the measured deflection is approximately 3% larger than the theoretical value.

Figures 2.18 and 2.19 compare the test specimens' deflected shapes at selected loads. Along the ITO girders' length, the openings' effect on the deflected shape and the total deflection is observable as an additional deflection at the openings' span side, which is larger than the change across the same distance at the same location in the IT girder. These figures show the deflected shape's scale, the symbols identifying the specimens, and the load at which the deflected shape is plotted on the figure's right side. The ITO specimens' deflected shape is consistent with the double curvature inherent in the frame behavior assumption.

The similar midspan load-deflection response between S1 and S2, observable in Figure 2.17, shows that the banded vs. spread reinforcement variable investigated in the test matrix for the abutment reinforcement does not affect the midspan load-deflection response. Some evidence exists in Figures 2.18 and 2.19 that the banded and spread approaches for the abutment reinforcement affect the deflection across the openings at low applied load levels, comparing the response between S1 and S2. At higher loads, the deflections of S1 and S2 across the openings are nearly identical, suggesting that the cracking is more similar at higher loads.

Because of the large deflections of S3 due to the midspan section, a direct comparison is not possible with the other two ITO specimens. It is unlikely that the amount of top chord reinforcement affects the load-deflection response, because this reinforcement is not active until significant cracking occurs in the top chord.

Concrete Stresses and Cracking

Figure 2.20 shows the cracks on a representative ITO specimen and the cracks on the IT specimen. The ITO specimens' cracking load and crack patterns are significantly different from the IT specimen's, indicating the openings in the ITO specimens alter the distribution of internal forces from the expected pattern for a flexural member. This results in high concrete tensile stresses and horizontal and inclined cracking at the corners of openings 1 and 2 (E1, E3 - E5) at an applied load between 20 and 30 kips. Additional cracks (E8 - E11) were visually observed during the tests at applied loads from 50 kips to 64 kips. The initial cracks in the IT specimen are vertical flexural cracks that occur at midspan at approximately 64 kips. Similar vertical cracking (E12) at approximately the same load occurs near midspan in the ITO specimens.

The vertical cracks at openings 1 and 2 (E4, E8, E13, E14, and E15 on Figure 2.20), occur where the frame behavior assumption predicts an internal tension force due to the moment in the chord. The inclined crack E3 is probably also a result of frame behavior plus a vertical force at the opening's edge. The cracks E12 result from tension in the bottom chord at opening 3, which is also consistent with the frame behavior assumption for an opening with no shear force. At the service load, 38.7 kips, the ***T*** markers in Figure 2.14 show that the FE analysis predicts high tension stresses where these vertical cracks occur. The IDM also predicts high tension stresses at these locations where the moment in the chords causes tension, which increases faster than the compression in the chord due to the normal force.

Both the IDM and the FE analysis predict high tension stresses in the concrete where vertical cracks occurred in the chords at the openings' edges in the test specimens. The FE analysis also predicts high vertical tension stresses at the openings' edges which, alone or combined with the longitudinal tension stresses, cause horizontal and inclined cracking. The absence of vertical cracking in the top

chord at opening 2 is attributable to two effects. First, the compressive stress in the top chord at opening 2 is greater than that at opening 1. Second, the smaller shear force at opening 2 results in a smaller chord moment, and less tension due to the moment than at opening 1. Conversely, at opening 1 the compressive stress due to the axial force is smaller and the tensile stress due to the moment is larger due to the greater shear force, so cracks occur.

Peak Load and Failure Mode

The openings' existence modifies the peak load, the location of the failure zone, the failure mode, and the failure's nature. However, the openings do not prevent the ITO girders from exceeding the factored load, thus satisfying the ACI 318 Code's strength requirements. Figure 2.17 shows that the peak load reached by the S1 and S2 is 85 kips, which is 20% less than the peak load reached by S4 of 108 kips. The peak load reached by S3 is 77 kips, which is 29% less than the peak load reached by S4 and 9% less than the peak load reached by S1 and S2. The openings shift the failure zone from midspan for the IT specimen to the top chord of opening 1 for the ITO specimens. The type of failure limiting the peak load changes also, from a ductile flexural failure due to yielding of the prestressed reinforcement for the IT specimen to a diagonal concrete tension failure in the top chord at opening 1 (Figure 2.21) for the ITO specimens. The ITO specimens' failure was sudden and brittle, in contrast to the ductile failure mode of S4. Figure 2.17 shows this ductility in S4 with the additional displacement after the peak load which accompanies this yielding, at a nearly constant load.

The ITO specimens' brittle chord failure occurs partly because they did not fail at midspan closer to the factored load. Had the ITO specimens not failed by diagonal cracking at opening 1, they could likely have approached the IT specimen's peak load. Therefore, had they failed at midspan at a load close to the factored load of 60 kips, they would not have experienced the chord failure at 85 kips. Typical analysis assumptions, typical design practices, material strengths greater than assumed, and adherence to typical fabrication practices all contributed to the midspan flexural capacity greatly exceeding its required strength.

Comparing the failure mode and load between S1 and S2, the two approaches to providing the abutment reinforcement appear to make no difference in either. The two approaches to providing the top chord transverse reinforcement make no difference in the ITO girders' failure mode, as all three ITO girders reach their peak load when a diagonal crack forms in the top chord at opening 1. The two approaches to providing the top chord transverse reinforcement appear to make a difference in the failure load. The more widely spaced top chord transverse reinforcement in S3 reduces its failure load by 10% compared with that of S1 and S2.

Longitudinal Strains

The top chord longitudinal strains at openings 1 and 2 provide qualitative evidence that the frame behavior assumption at the openings is valid, and quantitative measures of the chord forces for comparison with the IDM and the elastic finite element analysis predictions. Figure 2.22 shows the linear range of the top chord strains for S2. Assuming frame behavior occurs at the openings, the normal strains recorded by these gages contain both an axial strain component which is common to all the gages, and a flexural strain component which is dependent on the gage's distance from the chord's inflection point. The expected overall result for the pattern of recorded strains is a fan shape

like that in Figure 2.22, with the strains closest to the inflection point in the fan's center, and the gages away from the inflection point progressively farther from the fan's center, proportional to their distance from the inflection point.

At opening 1, the strains indicate the inflection point is approximately at the location of gages LS-5 and LS-8 because these gages are at the fan's center. This places the inflection point approximately 3 in. to the span side of the opening's midpoint. At opening 2, the strains indicate the inflection point is approximately at the location of gages LS-24 and LS-20, because these gages are at the fan's center. This places the inflection point for S2 approximately 9.5 in. to the support side of the opening's midpoint based on the location of these gages.

The qualitative pattern of the longitudinal strains is consistent with the frame behavior assumption. A quantitative assessment of the longitudinal strains shows that the inflection point location indicated by the strain pattern does not agree with the IDM's assumption, but is consistent with the FE model predictions in the linear elastic range.

Figure 2.23 compares the midspan longitudinal strains among the test specimens. Their similarity at the top and bottom of the section between the ITO girders and the IT girder, and the similar midspan cracking response, suggests that the midspan opening does not significantly alter the distribution of the internal forces in the midspan region of the ITO girders from that of the IT girder. These observations indicate (1) the midspan region does not need to be designed assuming frame behavior, because it does not appear that it occurs, and (2) if premature chord failure can be prevented, the ITO girder can probably reach its design load and fail in a ductile manner due to midspan reinforcement yielding, similar to an IT girder, at a similar load.

Chord Forces

The initial linear, elastic, uncracked range of the top chord longitudinal strains is used to calculate the chord forces, the inflection point location and the normal force eccentricity from the chord centroid. Calculation of these quantities is limited to this range because cracking changes the section properties, reducing the accuracy of any calculation to the best estimate of the cracking at a particular section. Because the calculations require a pair of readings, the chord force calculations are limited to the smaller linear extent of the two gages at each vertically aligned pair of strain gages. The chord forces are calculated from the strains using the principles of mechanics, with the following assumptions, (1) the pairs of strain gages are vertically aligned, (2) the strain gages measure strains normal to the cross section, (3) the normal strain consists of an axial component and a flexural component, (4) the gages at a section are far enough from the opening's edges so the strain varies linearly through the depth at the section, (5) the section in which the gage is located is uncracked as long as the load-strain relationship is linear.

The normal force, moment, and normal force eccentricity are derived from the data at one vertically aligned pair of strain gages, or at one section. Because the normal force is derived from the average strain from two vertically aligned gages, the normal force results are very good, since the averaging process smooths out the scatter in the data. Because the moment is the difference between the strains, the results are less consistent than those for the normal force, since the subtraction can amplify the scatter in the data. The shear force and the inflection point location are derived from the moments at two sections of the top chord, for example between the section containing LS-6 and the

section containing LS-4. The shear force is the difference between the two moments divided by the distance between the sections, and the inflection point location is a linear interpolation for the point of zero moment between two sections. These results are very dependent on the quality of the moment at the two sections used, and show more scatter than the moments from which they are derived.

Figure 2.24 plots the experimentally determined top chord normal force, N_t, at each of three sections of the top chord (denoted i, j and k on the graph), against the applied load. The average top chord normal force at the three sections is also plotted, along with the predicted values from the IDM and FE analysis. The table in the graph's corner provides a key to identify the plotted values. The table also gives the average value of N_t for the experimentally determined value at each section (i, j, and k), the average value for the three sections, and the average value from the IDM and FE analysis. These values are all normalized by the load associated with each normal force value. The upper graph presents the data for opening 1 and the lower graph, opening 2. For all three ITO specimens, the experimentally determined normal forces at both openings show very little scatter compared with the line representing their average value, and are consistently closer to the value predicted by the FE analysis than they are to the value predicted by the IDM. Both models generally overestimate the experimentally determined normal force. The experimentally determined normal force in the top chord is consistent with the frame behavior assumption, because it is approximately constant across each opening for a given applied load, and increases linearly with the applied load at each opening. The average experimentally determined normal force agrees well with the estimates from the FE analysis, differing by 6.8 % at opening 1 and 0.3% at opening 2. The experimentally determined normal force's average value diverges more from the IDM estimates, differing by 14.3 % at opening 1 and 7.4 % at opening 2, but is still not significantly different.

Figure 2.25 plots the experimentally determined top chord moment, M_t, at each of three sections of the top chord (denoted i, j and k on the graph), against the applied load. The average top chord moment at the three sections is also plotted, along with the predicted values from the IDM and FE analysis. To distinguish which estimate belongs with each experimentally determined force, filled symbols on the lines identical to the open symbols of the data are also plotted on the lines for the IDM and FE estimates. The table in the graph's corner provides a key to identify the plotted values. The table also gives the average value of M_t for the experimentally determined value at each section (i, j, and k), and the average value from the IDM and FE analysis. These values are all normalized by the load associated with each moment value. The upper graph presents the data for opening 1 and the lower graph, opening 2.

For all three ITO specimens, the experimentally determined moments at both openings show some scatter compared with the line representing their average value, and are not consistently aligned with the prediction of either model. The experimentally determined moments in the top chord are consistent with the frame behavior assumption, because they vary approximately linearly across the chord, and increase linearly with the applied load. As expected, these estimates are less consistent than the normal force estimates for all three ITO specimens, although some points of agreement do exist with the models.

Figure 2.26 plots the experimentally determined top chord shear force, V_t, between pairs of the three sections of the top chord (denoted ij, jk and ik on the graph), against the applied load. The average

of top chord shear forces between two sections, (ij, jk, and ik), the predicted values from the IDM and FE analysis, and the average value between pairs of sections are provided in a table on each graph. The values in the table are the top chord shear force divided by the load. The upper graph presents the data for opening 1 and the lower graph, opening 2. The shear force in the top chord predicted by the IDM and FE analysis are plotted as lines on the graph for comparison with the experimentally determined data. For all three ITO specimens, the experimentally determined shear forces at both openings show some scatter compared with the line representing their average value, and the average experimentally determined shear force does not agree consistently with either model. The experimentally determined shear force in the top chord is consistent with the frame behavior assumption, because it is approximately constant across each opening for a given applied load value, and it increases linearly with the applied load at each opening. Because the experimentally determined moments do not consistently agree with either the IDM or FE analysis, the shear forces derived from them are unlikely to be consistently accurate.

2.7 DESIGN IMPLICATIONS

Based on the experimental results and the elastic finite element results, the implications for the ITO girder's design are:

1. Control of deflections is not an area of significant concern for the ITO girder. Up to their failure load, multiple web openings do not significantly alter the ITO girder test specimens' load-deflection response compared with the IT girder.

2. Frame behavior can be assumed for the chords at the openings away from midspan. The ITO girders' deflected shape, top chord strain patterns, crack patterns, normal forces, moments and shear forces all indicate the assumption of frame behavior at these openings is valid.

3. Frame behavior does not need to be assumed at a midspan opening for symmetric loading. The strains and cracking in the midspan region are similar between the ITO girders and the IT girder, which suggests that the midspan opening does not significantly alter the internal force distribution in the ITO girders' midspan region.

4. Excess strength at midspan must be avoided to enforce the desired failure mode, a ductile flexural failure at midspan. Had the ITO girders failed at midspan at a load closer to the factored load of 60 kips, they would not have experienced the chord failure at 85 kips.

5. The banded approach to providing the abutment reinforcement is preferable. The banded approach contains the cracking at the openings' edges more effectively, and the FE analysis shows that the vertical tensile stresses at the openings' edges are contained in a narrow band. The two abutment reinforcement approaches make little difference in the ITO girders' load-deflection response, and no difference in the peak load and failure mode.

6. The top chord should be treated as a beam, rather than a column, when designing the shear reinforcement. The wider top chord transverse reinforcement spacing in S3 likely reduced its peak load carrying capacity, but made no difference in the ITO girders' failure mode.

7. The top chord normal force and inflection point can be predicted by an elastic analysis within the linear elastic range of behavior. The top chord normal force is approximately constant across each opening for a given applied load, and increases linearly with the applied load at each opening. The average experimentally determined normal force agrees well with the estimates from the FE analysis.

These findings show that treating an ITO girder as a flexural member with special detailing regions does not produce satisfactory results. The desired ductile failure mode, prestressed reinforcement yielding and concrete crushing at midspan, does not occur. Instead, an undesirable failure mode, diagonal cracking of the top chord, occurs.

Capacity design provides an alternate way to approach an ITO girder's design. Treating the ITO girder as a structure, the objective is to provide sufficient strength for the undesirable failure modes, shear failure of the chords for example, so they do not occur before the desired failure mode. The capacity design approach also avoids providing the desirable failure mode with unintended additional strength.

Table 2.1 Previous research on concrete beams with web openings

Investigators	**Section**	**Prestressed**	**Results Presented**
Ragan and Warwaruk (1967)	T	Pre	Test results and design recommendations
Barney et al. (1977)	T	Pre	Test results, design recommendations, and design procedure
Savage et al. (1996)	T	Pre	Test results and analysis
Mansur et al. (1985)	R	N	Test results and design procedure
Mansur et al. (1991a)	R	N	Test results
Mansur et al. (1991b)	R	N	Analysis
Mansur et al. (1992)	R	N	Analysis
Tan et al. (1996)	T	N	Test results
Tan and Mansur (1996)	T	N	Design procedure
Kennedy and Abdalla (1992)	R, T, I	Post	Test results and analysis
Abdalla and Kennedy (1995a)	R, T, I	Post	Test results and analysis
Abdalla and Kennedy (1995b)	R, T, I	Post	Test results and analysis

Key to Table 2.1

Section

T: Single tee
R: Rectangle
I: I section

Prestressed

N: Nonprestressed
Pre: Pretensioned
Post: Post-tensioned

Table 2.2 Concrete material properties

Material Property	**Design Value**	**Tested Value**
Compressive strength at release (f'_{ci})	3500 psi	6000 psi
Modulus of elasticity at release (E_{ci})	3590 ksi	–
Compressive strength at 28 days (f'_c)	5000 psi	8200 psi
Modulus of elasticity at 28 days (E_c)	4290 ksi	–

Table 2.3 Mild steel reinforcement material properties

Material Property	**Design Value**	**Tested Value**
Modulus of elasticity (E_s)	29000 ksi	–
Specified yield strength (f_y)	60 ksi	66 ksi (average)

Table 2.4 Design prestressed reinforcement material properties

Material Property - ½" ϕ low-relaxation strands	**Design Value**
Modulus of elasticity of reinforcement (E_p)	28500 ksi
Nominal area (A_p)	0.167 in.^{2}
Specified tensile strength of prestressing tendons (f_{pu})	270 ksi
Specified yield strength of prestressing tendons (f_{py})	243 ksi
Factor for type of prestressing tendon (γ_p)	0.28

Table 2.5 Test matrix

Specimen	Variables					
	Openings		Top Chord Reinforcement		Abutment Reinforcement	
	Yes	No	Beam	Column	Banded	Spread
S1	X		X		X	
S2	X		X			X
S3	X			X	X	
S4		X	N/A	N/A	N/A	N/A

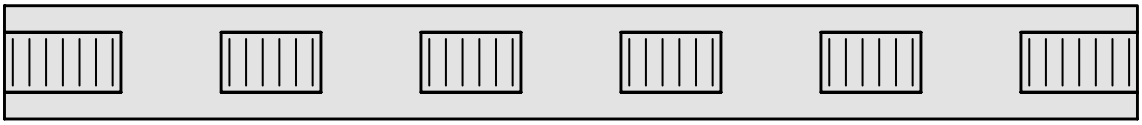

(a)

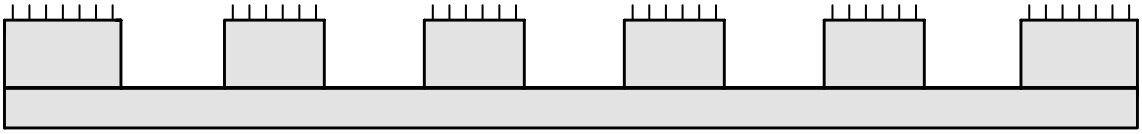

(b)

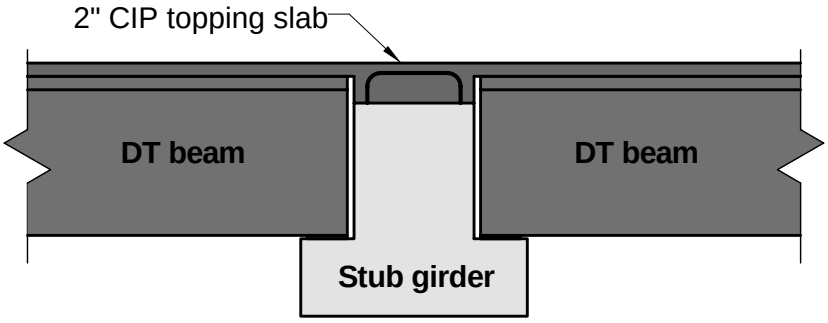

(c)

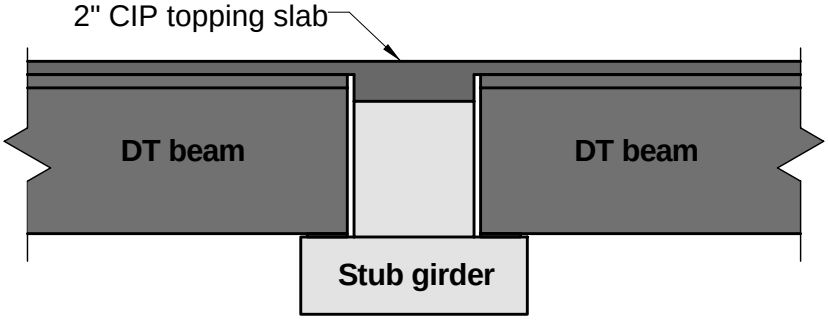

(d)

Figure 2.1 Prestressed concrete stub girder (adapted from Pessiki et al., 1997): (a) plan; (b) elevation; (c) section through a stub, including DT beams and topping; (d) section through an opening, including DT beams and topping

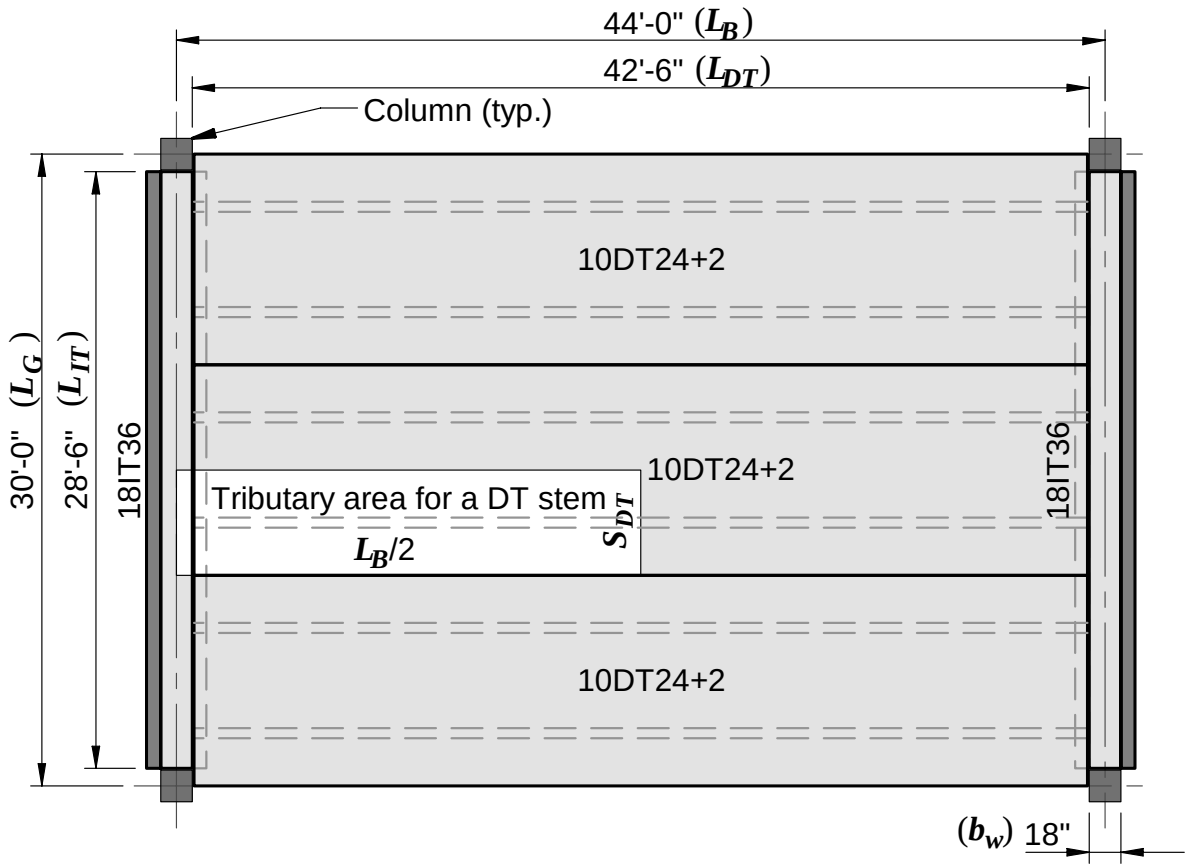

Figure 2.2 Framing plan for the typical interior bay

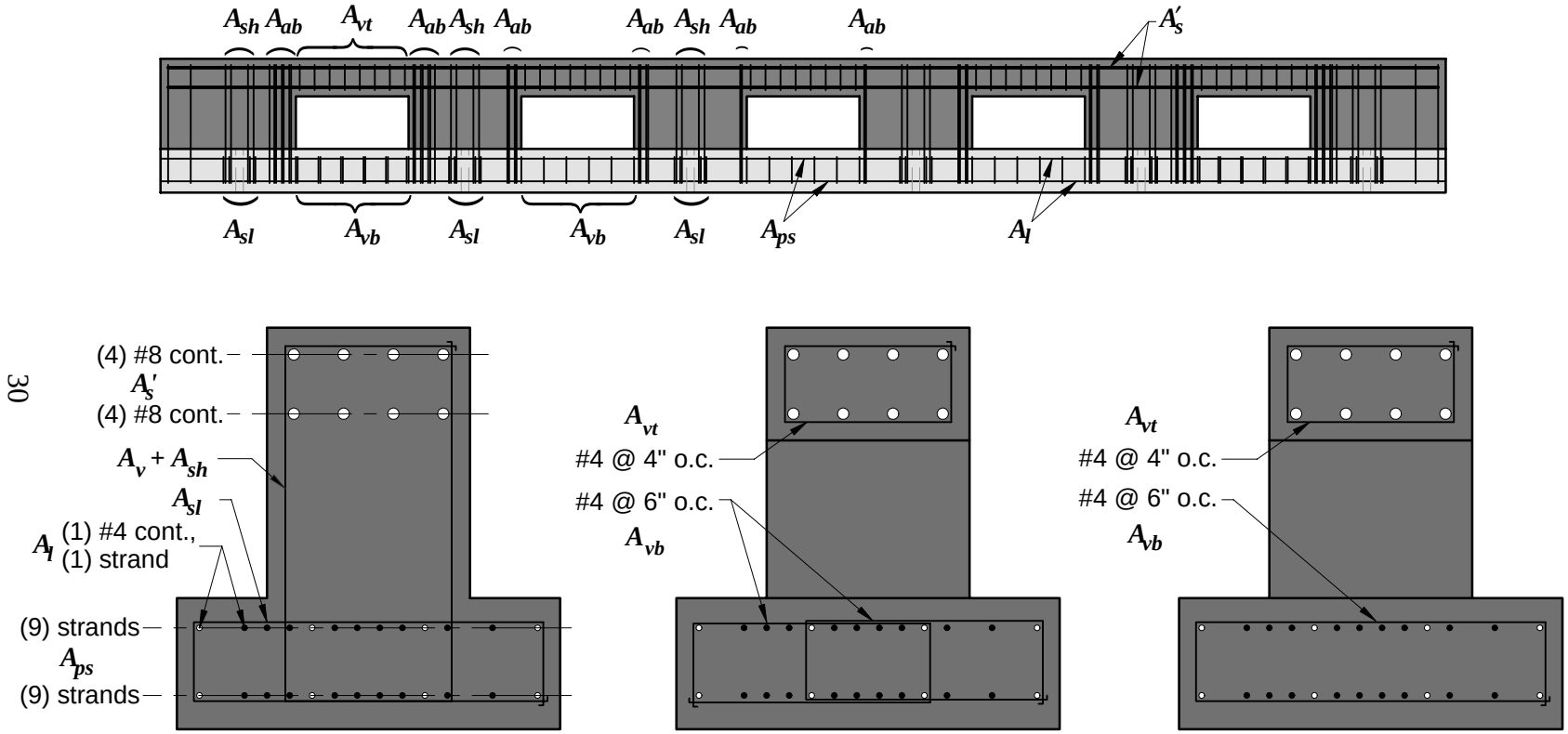

Figure 2.3 Prototype ITO girder with details of reinforcement

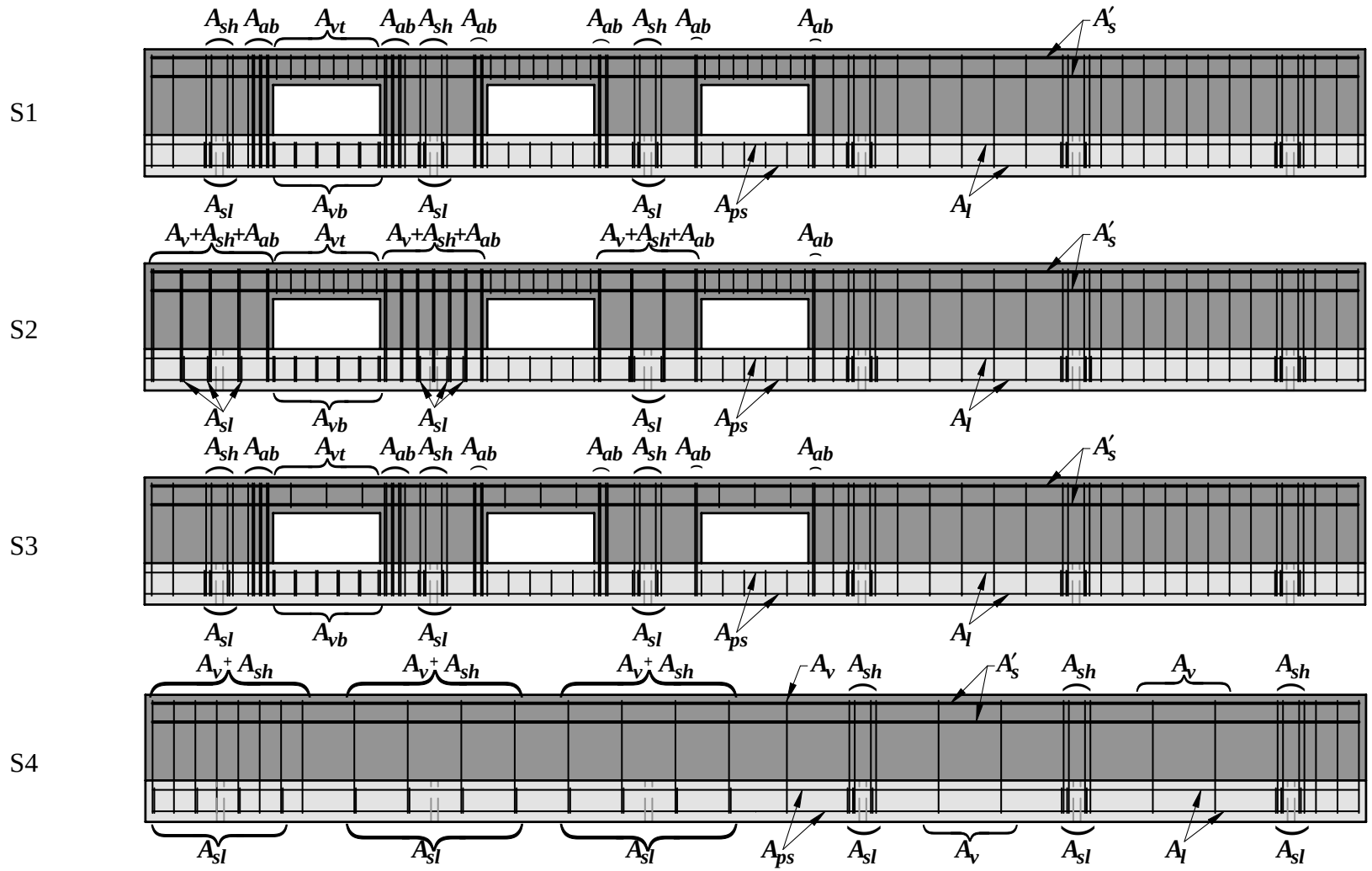

Figure 2.4 Elevations of test specimens showing reinforcement

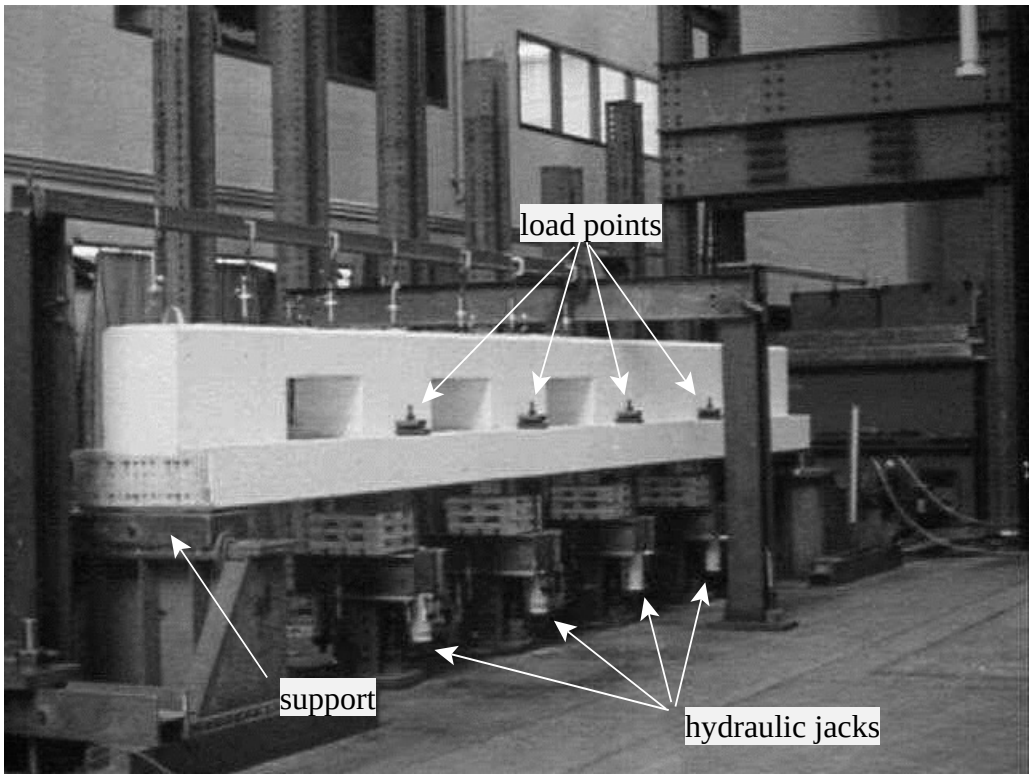

Figure 2.5 Supports and loading apparatus

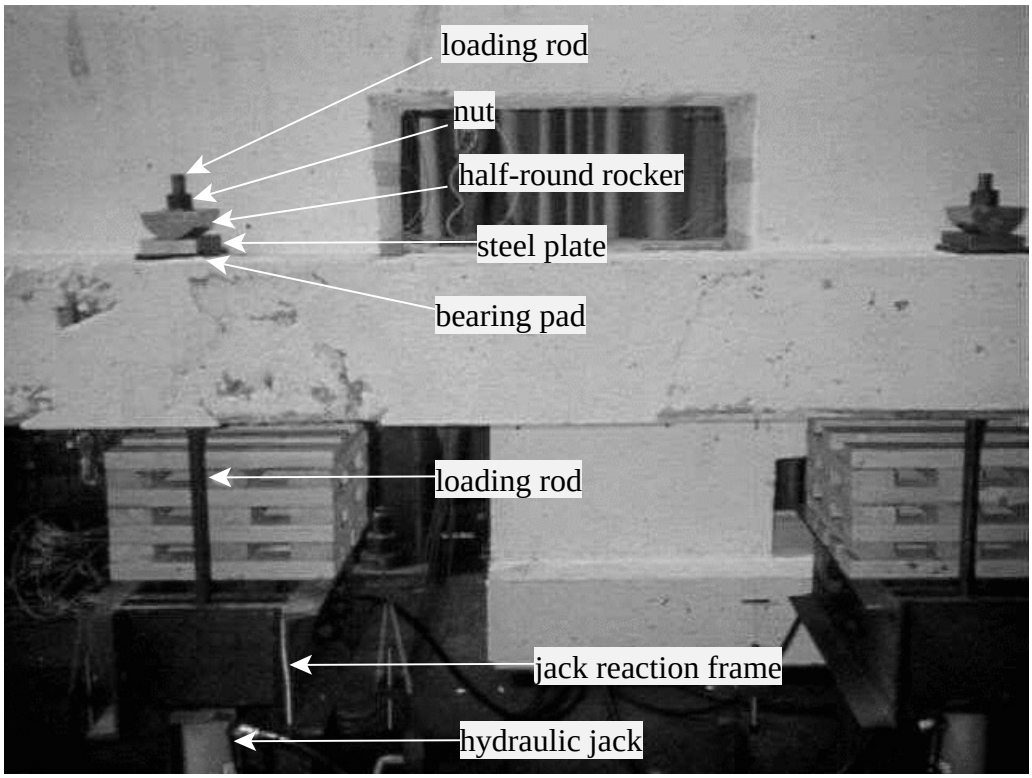

Figure 2.6 Load point

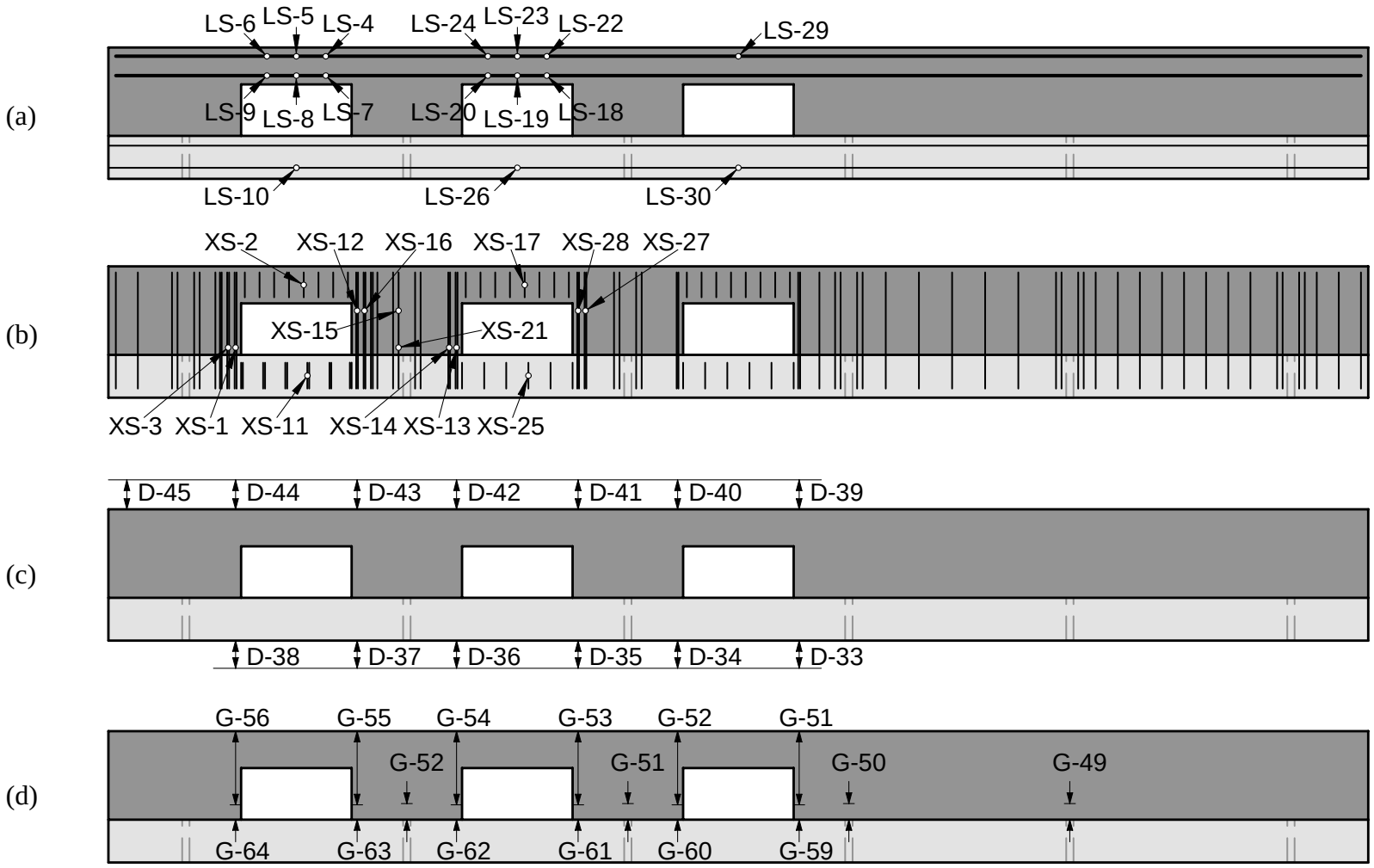

Figure 2.7 Typical instrumentation layout and designations for ITO girder test specimens: (a) longitudinal reinforcement strain gages; (b) transverse reinforcement strain gages; (c) top and bottom surface deflections; (d) crack opening displacements

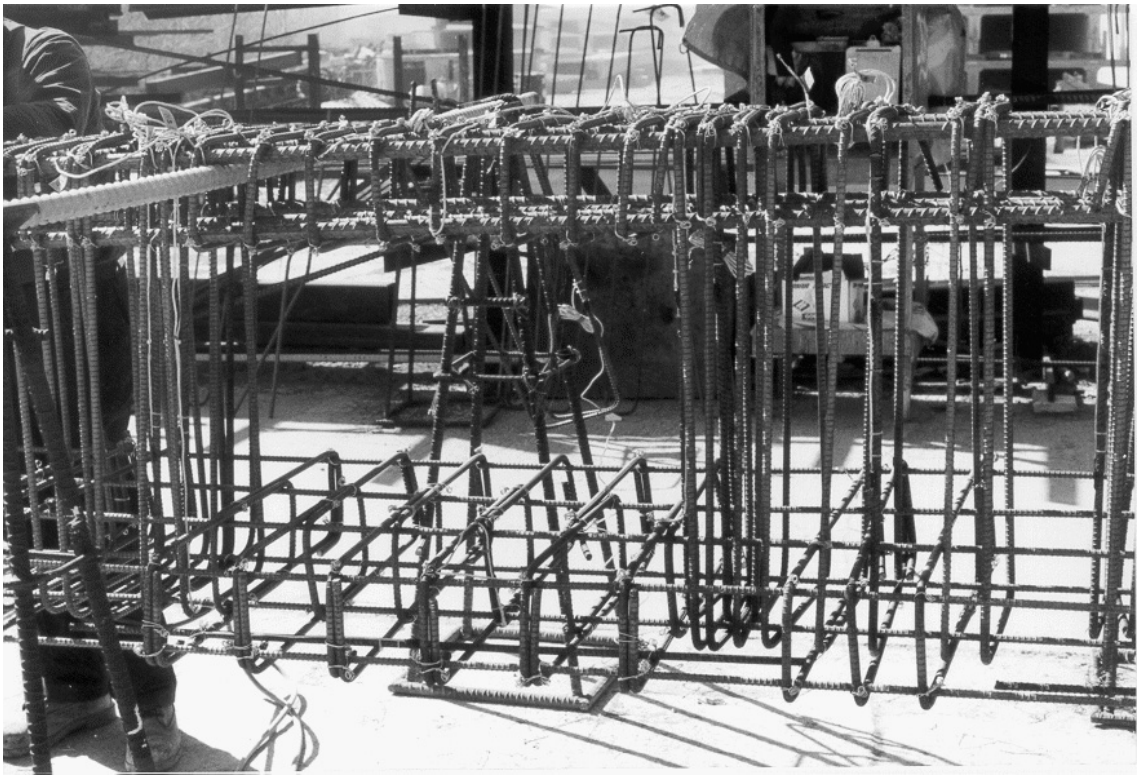

Figure 2.8 Reinforcement cage in fabrication showing instrumented bars, S1, opening 1

Figure 2.9 Fabricated cages in casting bed

Figure 2.10 Specimen after initial curing and transfer of prestress

Figure 2.11 S3 at midspan showing lack of consolidation at midspan

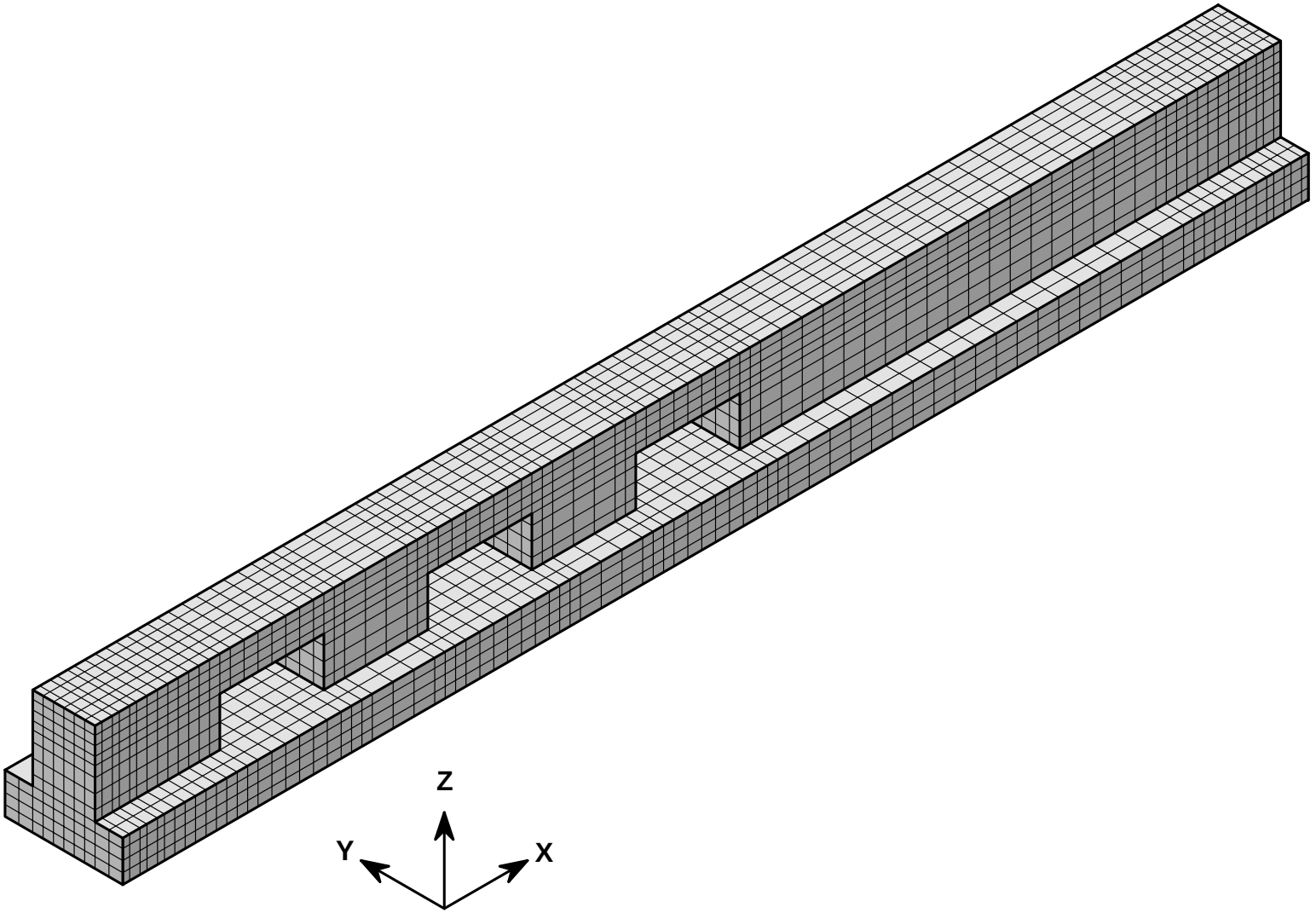

Figure 2.12 Isometric view of the finite element model

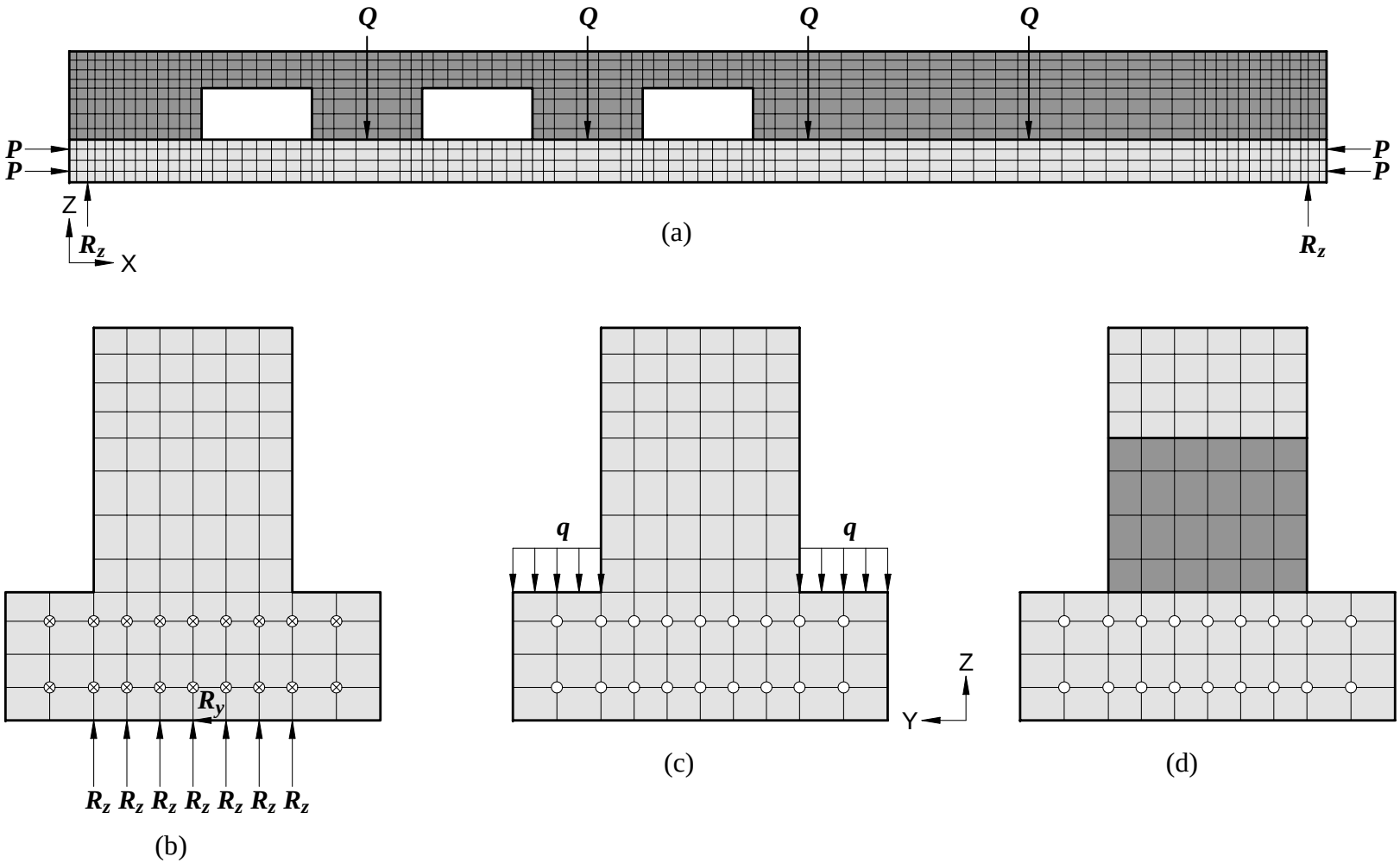

Figure 2.13 Elevation of and sections through the finite element model: (a) elevation; (b) section at support; (c) section at load point; (d) section through an opening

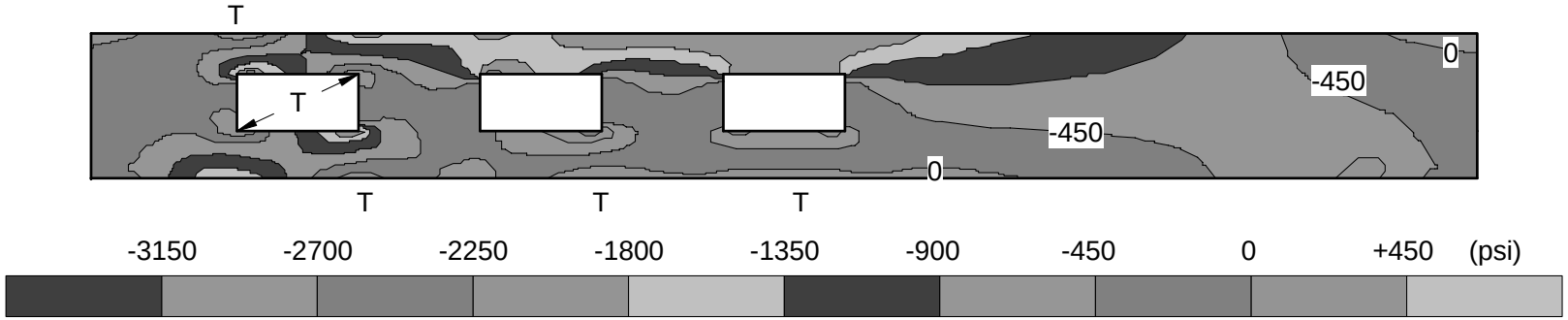

Figure 2.14 Longitudinal normal stresses (σ_{xx}) for load combination: prestress + self-weight + applied load ***Q*** = 38.7 kips (service load)

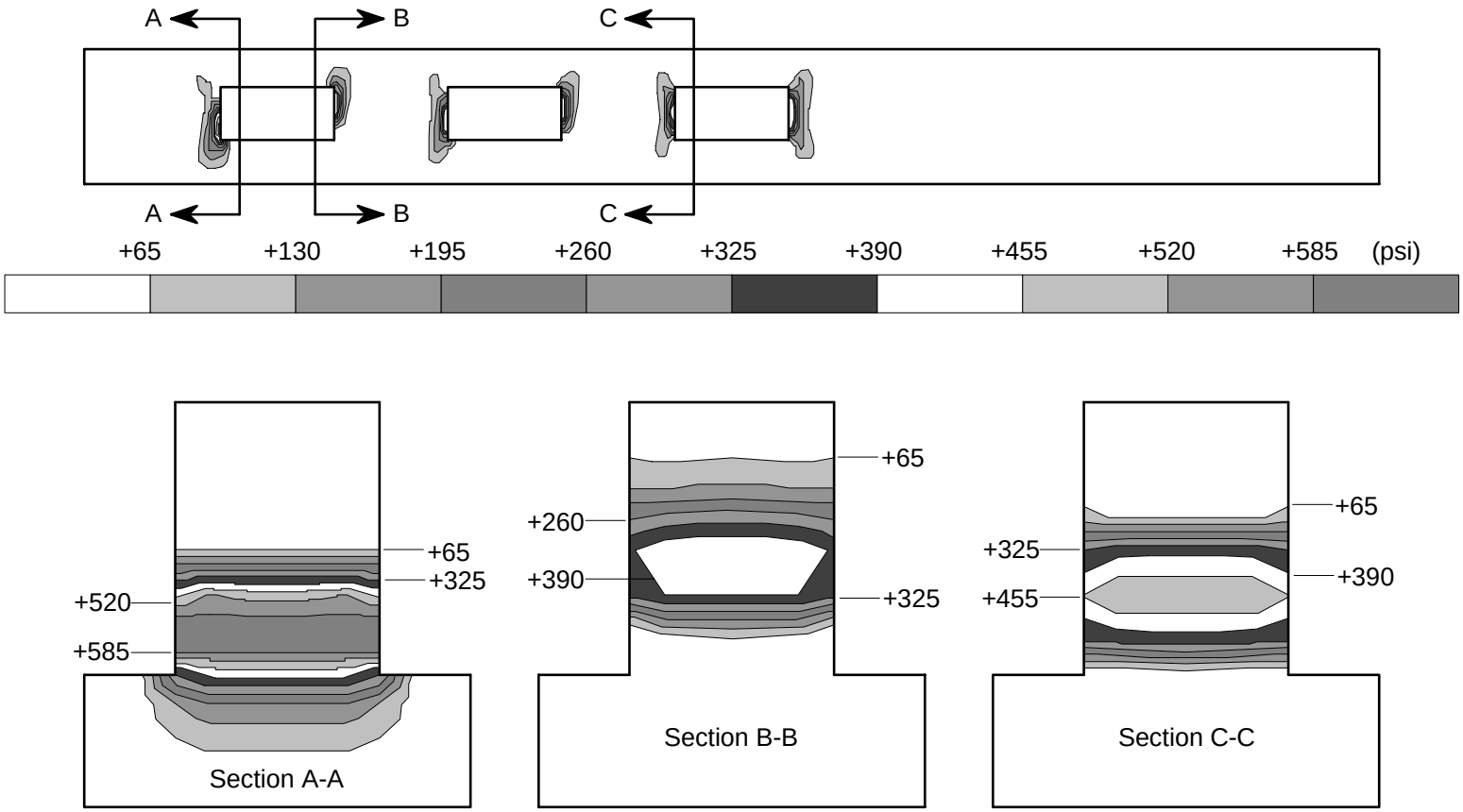

Figure 2.15 Elevation and sections showing vertical normal stresses (σ_{zz}) for load combination: prestress + self-weight + applied load $\boldsymbol{Q}$ = 10 kips

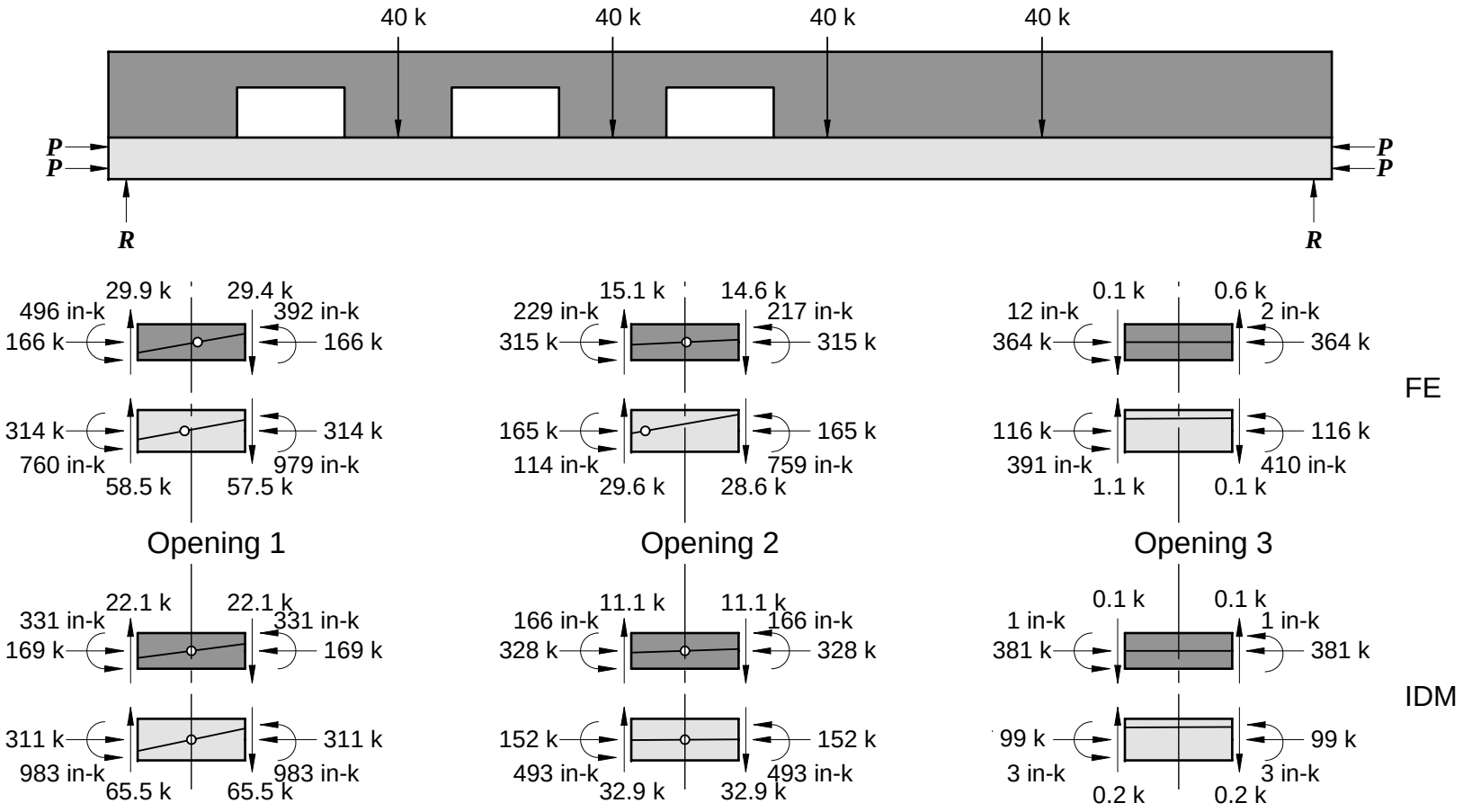

Figure 2.16 Chord forces from FE model compared with IDM for load combination: prestress + self-weight + 40 kips

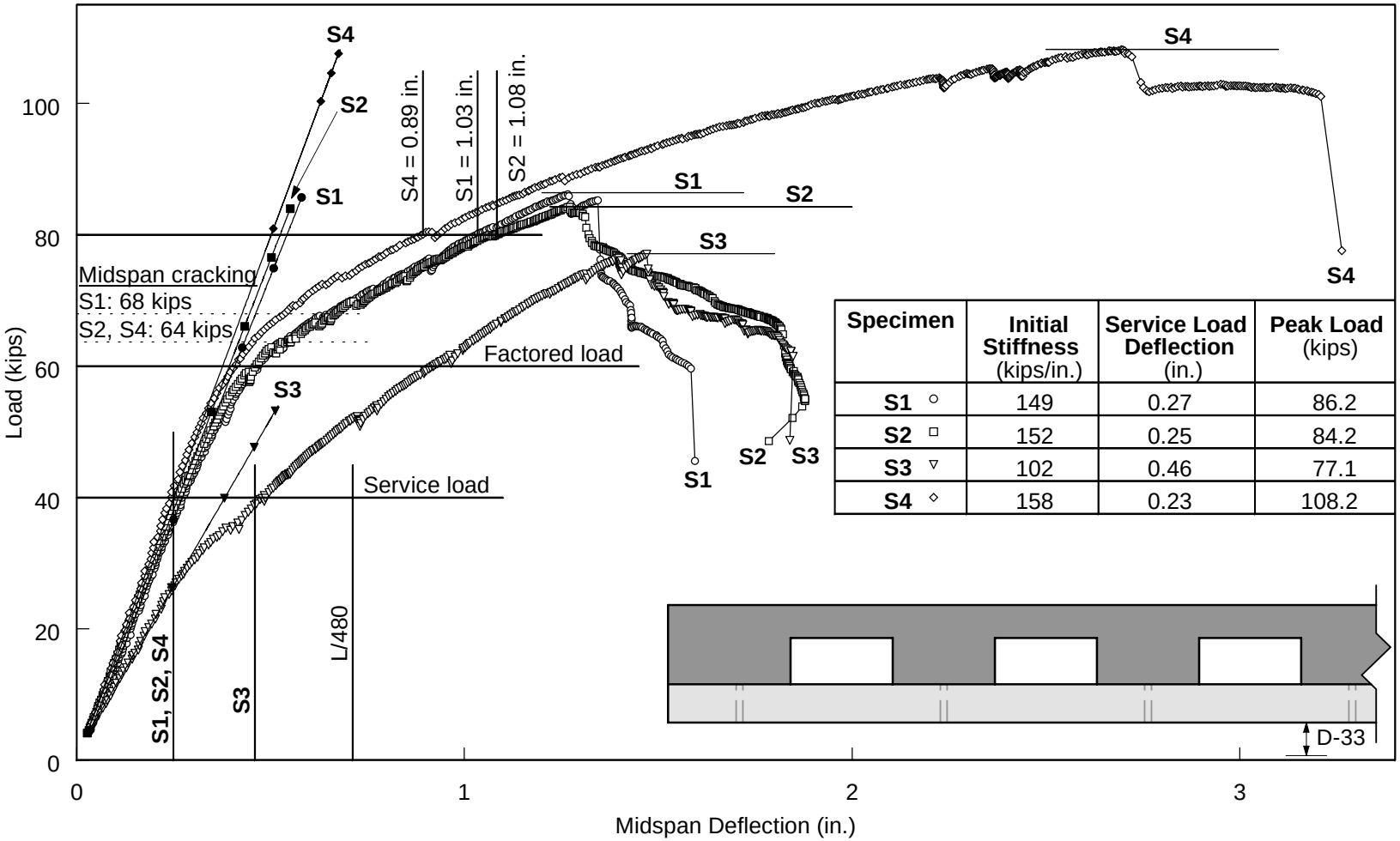

Specimen	Initial Stiffness (kips/in.)	Service Load Deflection (in.)	Peak Load (kips)
S1 ○	149	0.27	86.2
S2 □	152	0.25	84.2
S3 ▽	102	0.46	77.1
S4 ◇	158	0.23	108.2

Figure 2.17 Comparison of overall behavior between ITO specimens and IT specimen

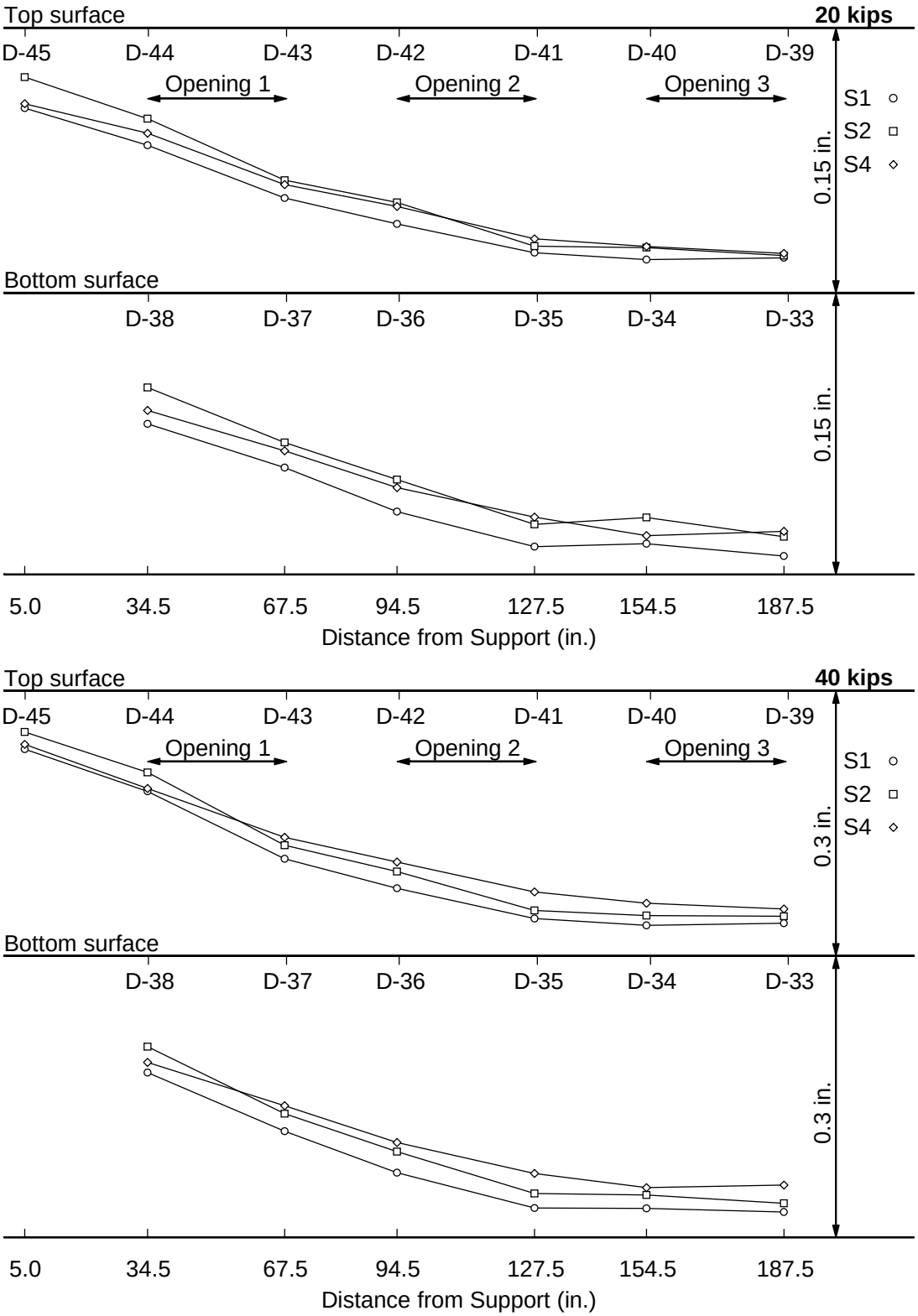

Figure 2.18 Comparison of deflected shape between ITO specimens and IT specimen at 20 kips and 40 kips

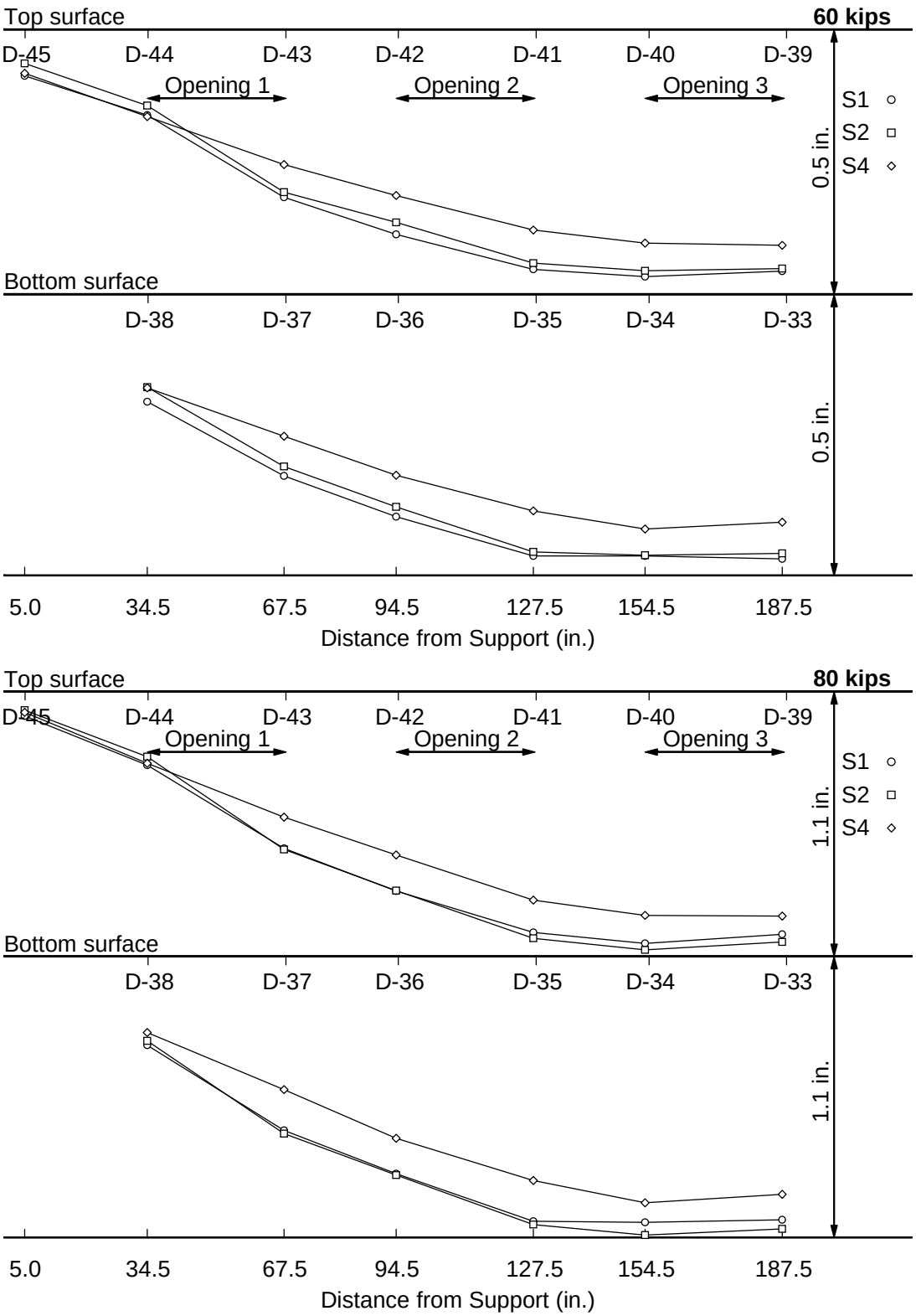

Figure 2.19 Comparison of deflected shape between ITO specimens and IT specimen at 60 kips and 80 kips

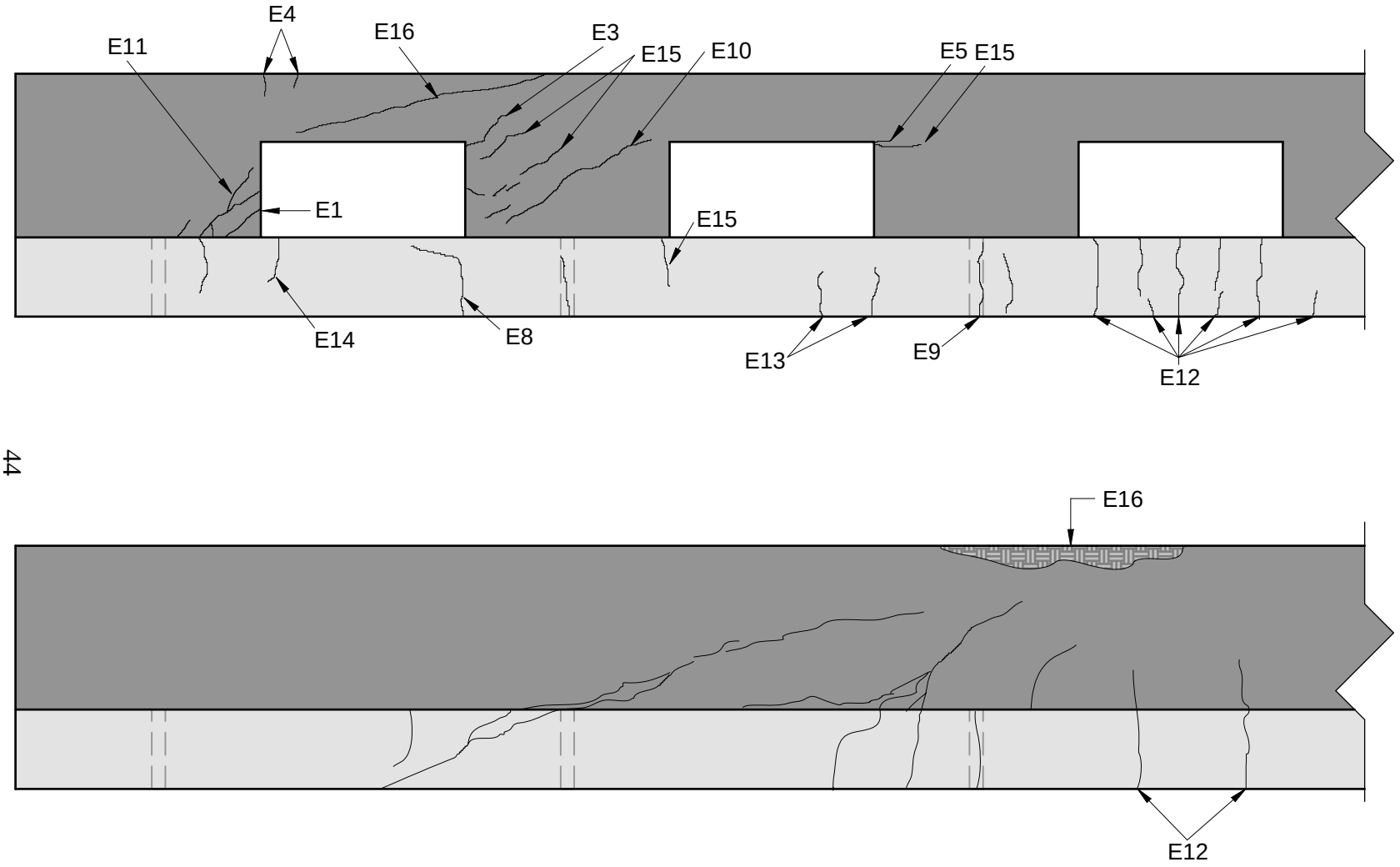

Figure 2.20 Comparison between representative cracks for an ITO specimens and the IT specimen

Figure 2.21 S2 at opening 1 after peak load (support to left in photograph)

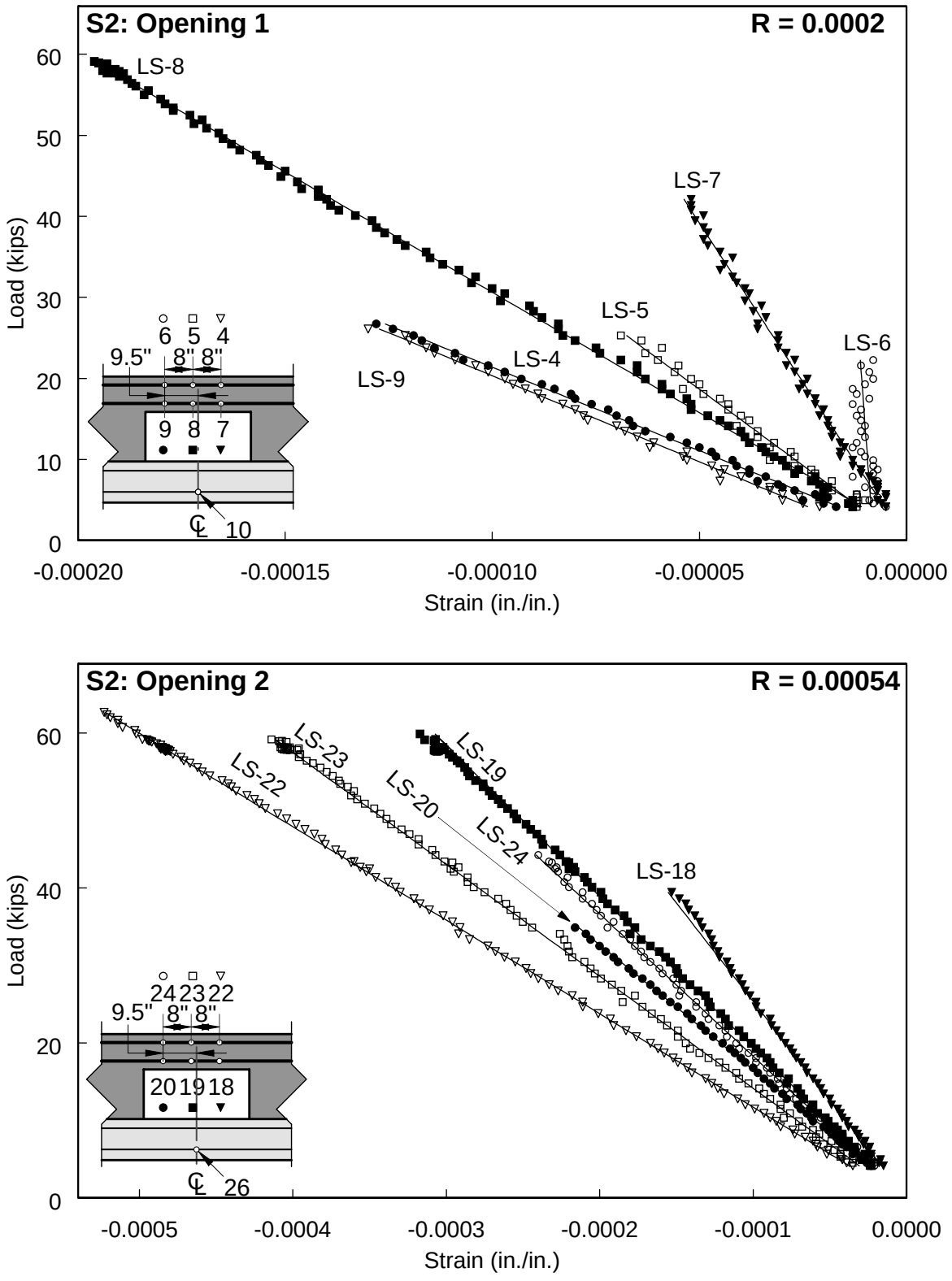

Figure 2.22 S2 - Linear extent of strains in top chord longitudinal reinforcement

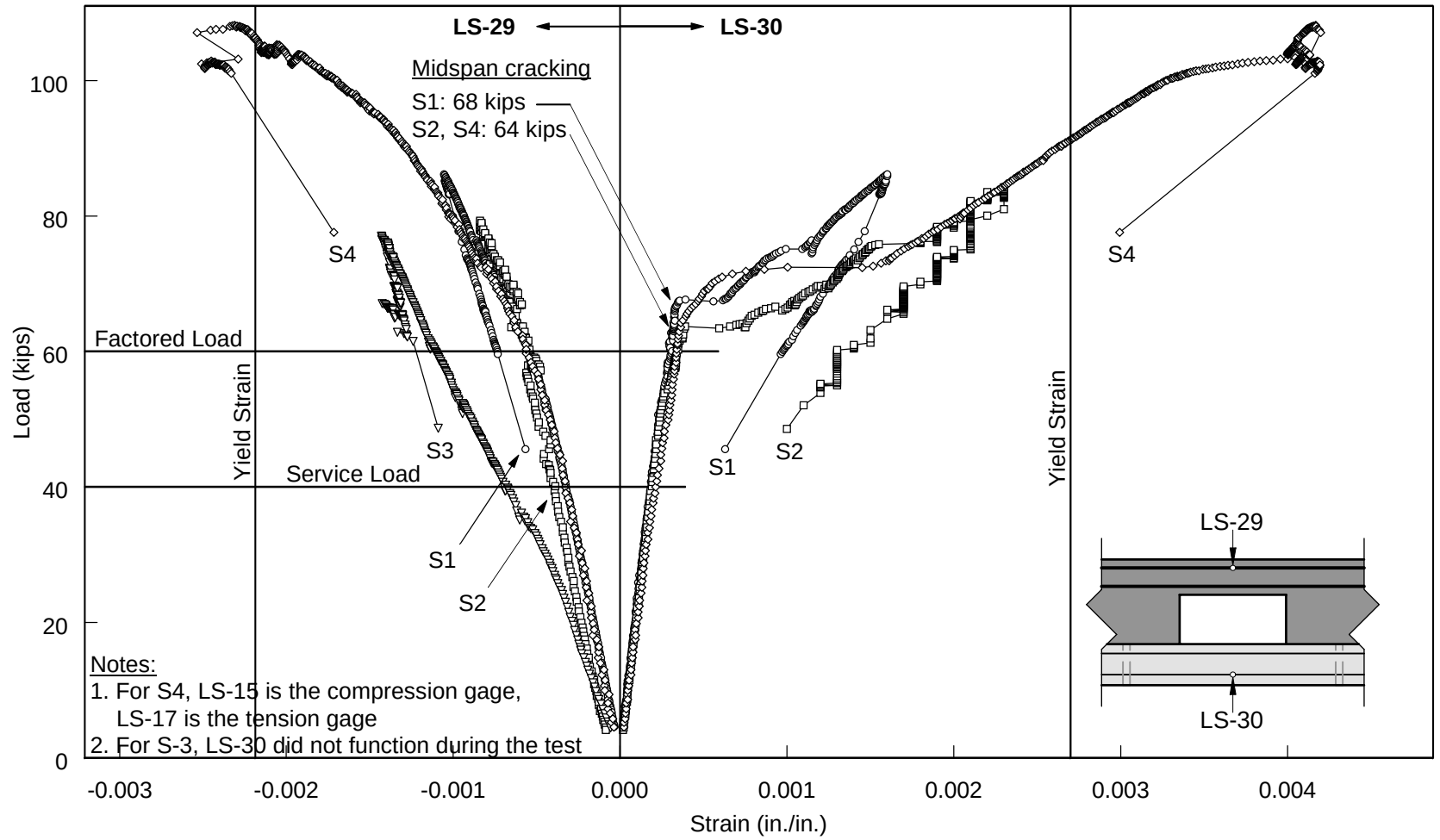

Figure 2.23 Comparison of midspan strains at top and bottom of section between ITO specimens and IT specimen

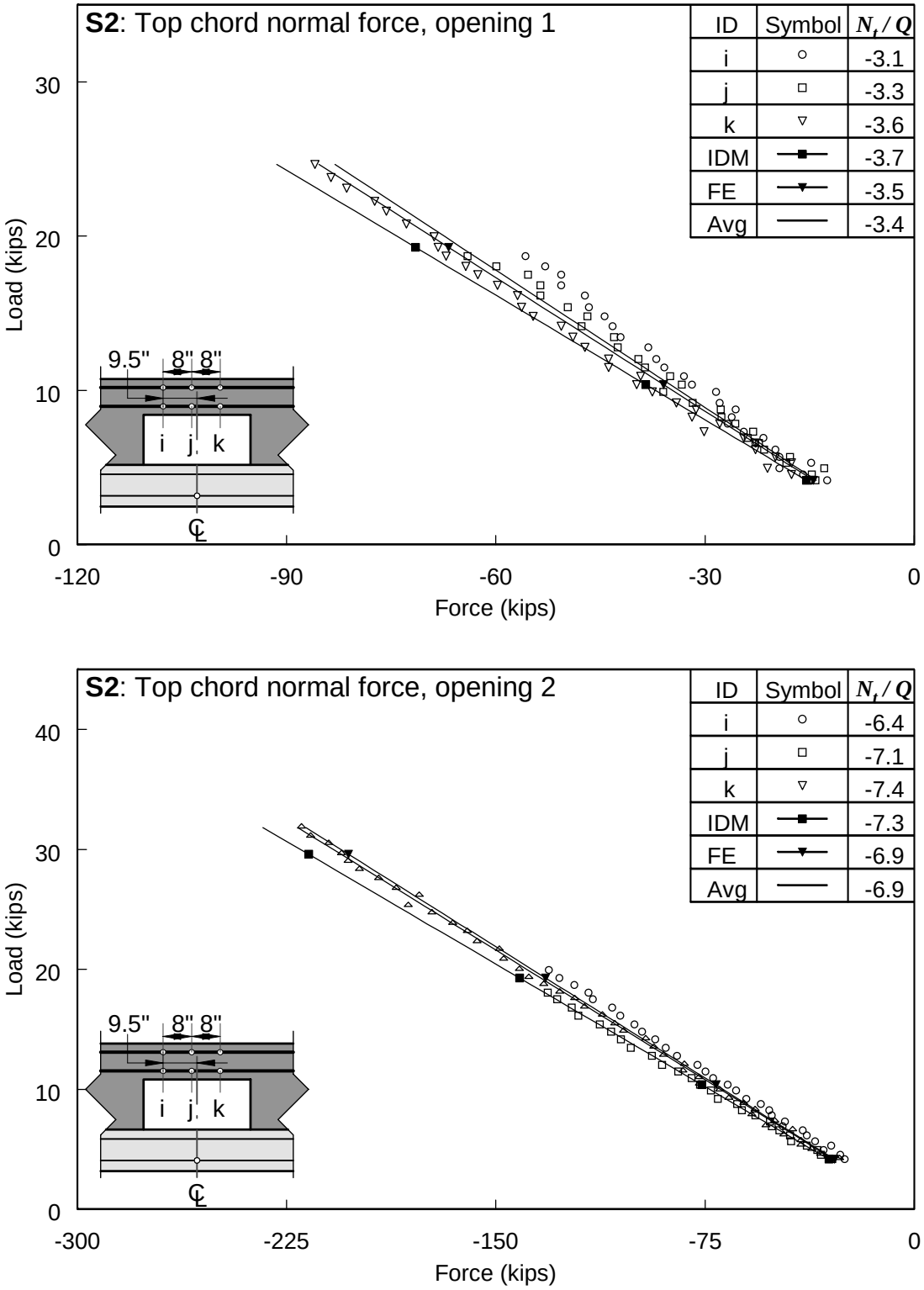

Figure 2.24 S2 - Comparison of experimentally determined top chord normal force with IDM and FE model predictions

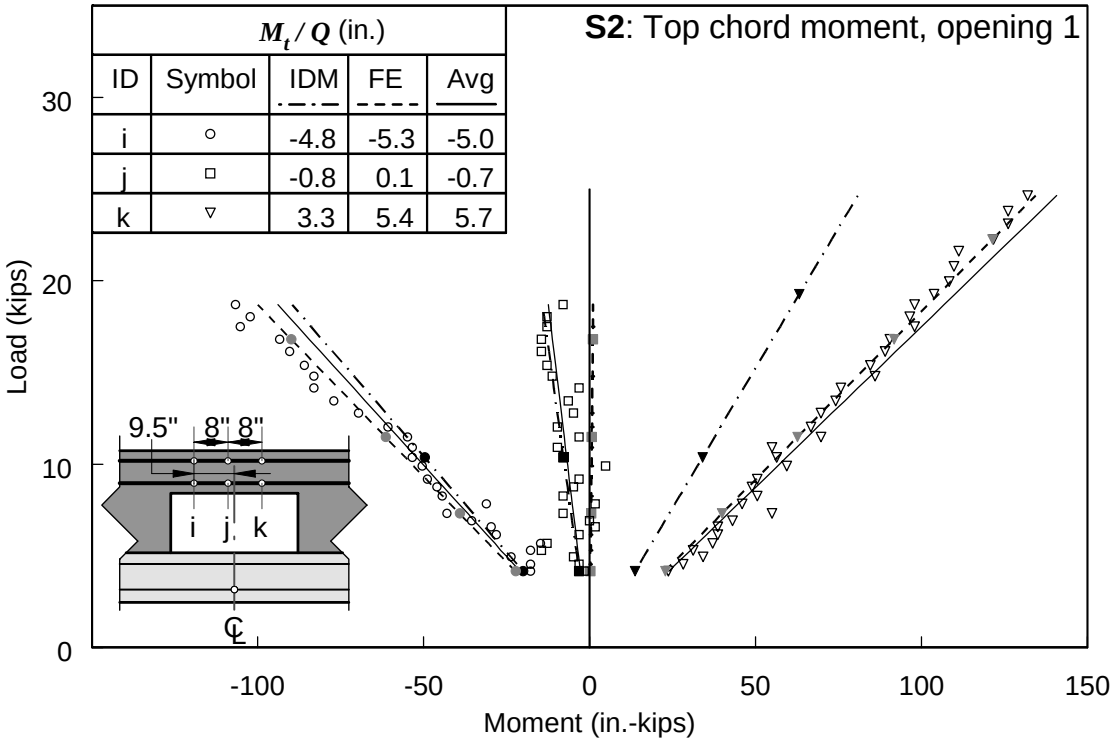

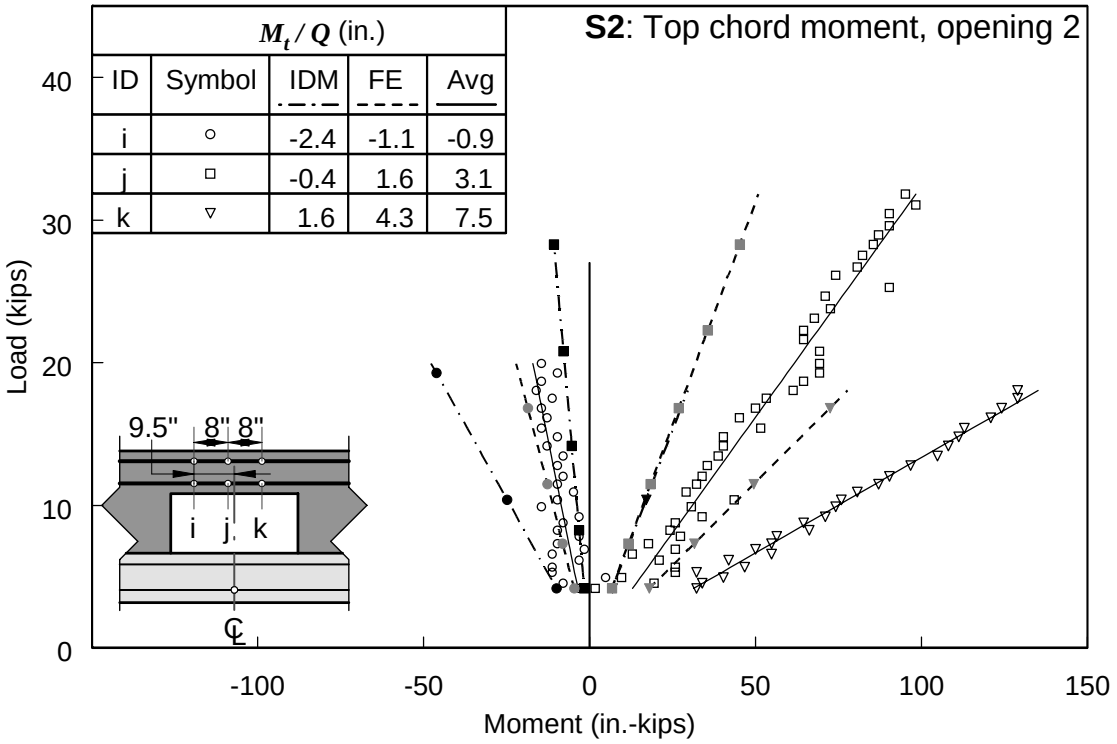

Figure 2.25 S2 - Comparison of experimentally determined moments in the top chord with IDM and FE model predictions

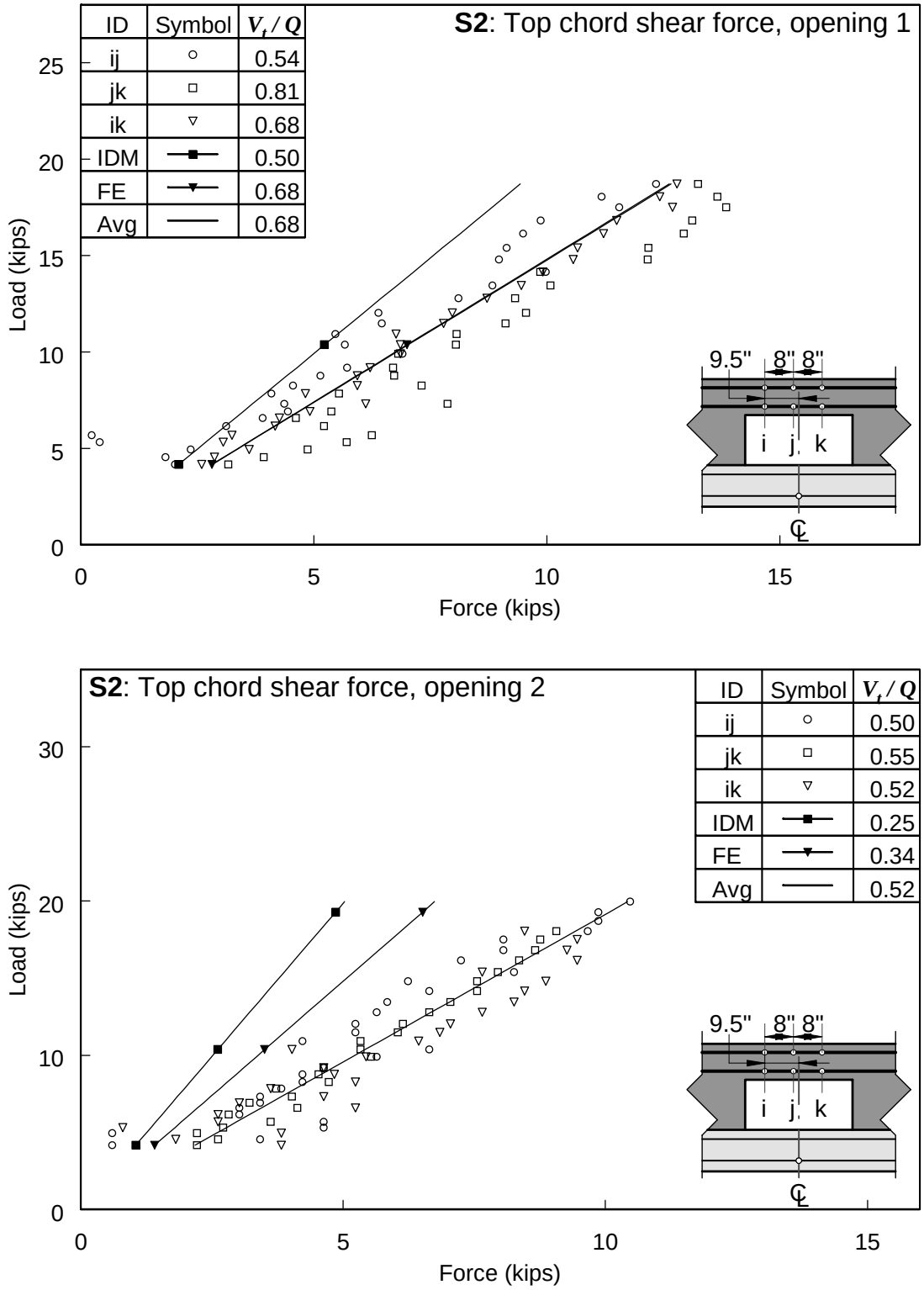

Figure 2.26 S2 - Comparison of experimentally determined shear force in the top chord with IDM and FE model predictions

CHAPTER 3

NONLINEAR FIBER MODEL ANALYSIS

3.1 INTRODUCTION

This chapter presents analysis results from nonlinear fiber element models of the ITO girder. The analyses use the DRAIN-2DX program by Prakash, Powell and Campbell (1993). The primary areas examined with the fiber element models are the ITO girder's chord forces, failure load and failure mode. A suitable fiber element model is first developed through comparison with the experimental results. This model provides further insight into the ITO girder's behavior as cracking occurs. The model is then used to systematically examine the effects of various parameters on the ITO girder's chord forces, failure load and failure mode. These parameter studies provide guidance for developing a design procedure.

The fiber element monitors deformations normal to the cross-section, so it can capture axial and flexural effects and their interaction, and directly provide failure loads for their individual and combined effects. The fiber element also simulates concrete cracking and nonlinear material behavior. The fiber element does not model shear behavior, so the chord forces from the analyses are used in separate calculations to predict shear strength and shear failure.

Section 3.2 describes the test specimen analysis models and validates the models' assumptions through comparison with the experimental results. These analyses show that the fiber element model accurately predicts the experimentally observed failure mode and failure load. This section also examines the ITO girder's behavior further using the analysis results. Section 3.3 presents the parameter study that examines the effects of varying several design parameters on the ITO girder's chord forces, failure load and failure mode. Section 3.4 summarizes the analysis results and presents their design implications.

3.2 TEST SPECIMEN MODEL

3.2.1 Model Description

Figure 3.1 shows the ITO girder and the fiber model in elevation. In the upper sketch, the elements of the fiber model are superimposed on the ITO girder to show their relationship. The lower sketch shows the fiber model more clearly. The filled circles in Figure 3.1 are the nodes and the lines between the points are the elements. The horizontal elements in the model are fiber elements and the vertical elements are beam-column elements. The horizontal elements at the support's elevation are solid section elements located at the solid cross-section centroid. The remaining horizontal elements are the top and bottom chord elements, located at the top and bottom chord's centroids. The vertical elements are located at the openings' edges and provide the connection between the solid sections and the chords.

Figure 3.2 shows the fiber element. The fiber element has an i-end and a j-end, and is divided into four segments, delineated by the points in the figure. The behavior of each segment of an element is monitored at the segment's center cross-section, which is called a slice, and is the shaded area of

the segment in the figure. Each slice is made up of a number of fibers which model the actual cross-section. Each fiber can have nonlinear longitudinal stress-strain relationships with either concrete or steel material properties, which are defined by the material models discussed later in this section. The cross-section strains are monitored at each fiber of the slice. In general, the accuracy of the fiber model increases with the number of segments along the element length, the number of fibers in the cross-section, and the number of points on each material stress-strain curve. This fiber element description is an adaptation of the element's description in Prakash, Powell and Campbell (1993).

The fiber model's solid section elements are 3 in. long, and the chord elements are 1 in. long. Each element has one segment, therefore one slice at its center. The short element length used for the chords allows a slice to be ½ in. from the opening's edge, which provides an accurate value of the chord moment at the opening's edge. Since the primary objective of these analyses is to examine the chord forces and failure loads, the most accurate chord moment consistent with reasonable computation time is desired. An additional reason for small element lengths is to accurately model the chords' self-weight. The small element lengths used for the solid section elements is not necessary for capturing the ITO girder's behavior, but is also used to provide a good approximation of the girder's self-weight. In general the self-weight is a small fraction of the total load on the girder at failure, and could be lumped into the concentrated loads. However, to closely model the test specimens' behavior, accurate modeling of the self-weight was necessary.

The model's beam-column elements have extremely high axial and flexural stiffness and are intended to serve as rigid links which do not yield. The high stiffness is achieved by using large values for $\boldsymbol{I}$ and $\boldsymbol{A}$. The objective was to approximate the rigid abutment in the ITO girder that links the chords and the solid sections. This objective was achieved because both the solid section and chord nodes at each opening's edge displace as if the plane at the opening's edge is rigid.

The connection between the beam-column elements and the fiber elements at the solid section and the top chord is a rigid connection. At the connection between the beam-column elements and the bottom chord, a rigid connection is used for the x and y translational degrees of freedom, and a rotational spring is inserted for the rotational degree of freedom, as Figure 3.1 shows. The rotational spring is inserted to more closely model the elastic shear force distribution from the elastic model. With the fiber model, if a rigid connection is used at all four corners of the opening, the initial shear distribution between the chords is proportional to the chords' moments of inertia, as suggested by Barney et al. (1977). However, the three-dimensional elastic model showed that this is not the correct shear force distribution for this cross-section. The rotational spring was calibrated using the elastic model results to provide the same initial shear force distribution. Fiber models were run with both a rigid and a flexible connection, and there is little difference in the chord forces at failure between these models. If failure loads are the primary area of interest, the rotational springs can be omitted. However, they were included for this investigation.

Nodal restraints provide the supports, and nodal loads simulate the DT stem loads ($\boldsymbol{Q}$), the girder self-weight (not shown), and the prestress force ($\boldsymbol{P}$ and $\boldsymbol{Pe}$ in Figure 3.1). The model simulates the effects of prestressing using equivalent external nodal loads because DRAIN-2DX does not provide for prestressing of fiber elements.

Figure 3.3 shows the model's cross-sections for the solid regions and the opening regions. The diagonally hatched areas in the cross-sections represent the steel reinforcement. As noted previously, the solid region elements (Figure 3.3(a)) are located at the solid cross-section's centroid. The top and bottom chord elements are located at their respective cross-sections' centroids, as Figures 3.1 and 3.3(b) show. The cross-section is divided into 1/4 in. thick fibers through the depth. At the chords' exterior faces, the fibers are 1/8 in. thick so that the outermost fiber's centroid is as close as possible to the outside face. With this discretization, the moment of inertia calculated by DRAIN is within 0.05% of the value calculated from mechanics. The fineness of the discretization and the thin exterior fibers provide greater accuracy in the model's calculated strains.

Figure 3.4(a) shows the fiber model's concrete material model. The dashed line with filled circles in Figure 3.4(a) shows the five points selected to give a piecewise linear representation of the concrete stress-strain behavior. These points are superimposed on a set of stress-strain data measured as part of the experimental program (filled squares) and a numerical model (solid line) for the unconfined concrete compressive stress-strain behavior (Collins and Mitchell (1997)). The agreement between the measured data and the unconfined concrete numerical model's ascending branch indicates the unconfined concrete numerical model provides a good approximation of the concrete's stress-strain behavior. The unconfined concrete numerical model then provides the three points on the stress-strain curve's descending branch. The initial elastic modulus is evaluated at the first point, 0.4 f'c, and the corresponding strain. This value is 5400 ksi, and is approximately 1% in error relative to the value obtained using ACI 318 8.5.1. The model assumes no concrete tensile strength, since the primary objective is to investigate the behavior at ultimate strength, at which point the concrete is assumed fully cracked.

For the chord, the effect of confinement on the concrete's strength and ductility was also investigated. In Figure 3.4, the top chord confined concrete stress-strain curve (dash-dot line) is obtained using the model from Mander, Priestley and Park (1988). The confined concrete model uses the top chord longitudinal and transverse reinforcement from S1. This model was investigated to examine the effects of confinement pressure on the concrete in the top chord.

The confined concrete stress-strain curve in Figure 3.4 shows an increase in both the maximum concrete strength and the concrete's ductility, compared with the unconfined concrete. This additional strength and ductility is unavailable to the ITO girder, however, as the vertical line in the figure shows. This line is the ITO girder (S1) fiber model's maximum strain in the confined concrete core at opening 2. This comparison shows that, at the maximum strain reached in the confined concrete core, the strains are not large enough for this model to significantly affect the flexural behavior.

The unconfined concrete model is used for these and subsequent analyses because it provides a good approximation for the concrete stress-strain behavior. For the fiber model's solid sections, there is not enough reinforcement in both directions to provide any significant confining pressure. In the chords, the comparison discussed above shows there is little influence from the confinement at the chords' predicted strains.

Figure 3.4(b) shows the prestressed reinforcement material model. The dashed line with filled circles in Figure 3.4(b) shows the five points selected to give a piecewise linear representation of the prestressed reinforcement stress-strain behavior. These points are superimposed on a curve (solid

line) representing the stress-strain behavior of low-relaxation prestressing strand (PCI Handbook). The graph also shows a secondary set of stress-strain axes, which are the origin for the strand stresses and strains in the fiber model.

In the actual girder, the strand's stress and strain prior to loading are the values at the secondary axes' origin. Releasing the strand from the casting bed puts a compressive force on the actual girder at the prestressed reinforcement centroid. When loads are applied to the actual girder, the strand accumulates stress and strain and reaches the second filled circle on the graph, the strand's defined yield point. For the fiber models, the strand's material model starts at the graph's secondary axes because equivalent external loads are used to model the prestress force. These equivalent external loads cause the same stresses and strains in the fiber model's concrete as the strand force causes in the actual girder at release, but the strand stresses and strains are not the same. The shifted origin accounts for the initial strand stress which is not present in the fiber model. The fiber model's strand now has to accumulate a strain equal to the difference between its yield stress and the initial stress before yielding, rather than starting from zero stress. The first point is at approximately 75 ksi above the initial stress, which is the difference between the strand's yield stress (taken as 0.9 f_{pu}) and the initial strand stress prior to loading. The selected point gives an initial elastic modulus of 28500 ksi.

The mild steel reinforcement is idealized as an elastic-perfectly plastic material in tension and compression, with the average yield stress values from the experimental program of 64 ksi for the #4 bars and 68 ksi for the #8 bars. The mild steel modulus is taken as 29000 ksi.

3.2.2 Model Verification

To verify the modeling assumptions described in the previous section, fiber models corresponding to S4 and the experimental program's ITO girder test specimens were analyzed, using the unconfined concrete stress-strain relationship throughout the model. The IT fiber model's predicted failure load and mode for a flexural failure of S4 is compared with the experimentally determined failure load and mode to validate the modeling assumptions. The ITO fiber model's chord forces are used to predict the axial-shear failure observed in the experimental program, using separate calculations as previously noted.

The fiber model of S4, similar in all respects to the model described in Section 3.2.1 but without the openings, predicts a midspan flexural failure at an applied load of 108.1 kips, compared with the experimentally measured midspan flexural failure load of 108.2 kips and the flexural failure load of 107.7 kips a plane section analysis predicts. The load-displacement response and midspan strains from the model also compare well with the corresponding experimentally measured values.

Turning next to the shear failure in the ITO test specimens, a fiber model with openings is analyzed to determine the chord forces. The chords' normal forces are used in the calculation of the chords' concrete shear strength, and the chords' shear forces represent the demand. The same fiber model is used for all three ITO test specimens, as the only result the fiber model provides is the chord forces. These are assumed to be independent of the different transverse reinforcement schemes in the experimental program. The different transverse reinforcement in the top chords of S3, compared with S1 and S2, is accounted for in the separate calculation of the shear strength. The failure load is predicted for opening 1, where the failure occurred in the experimental program.

The chords' concrete shear strength is calculated using ACI 318 (11-4). The chords' shear strength provided by the reinforcement is calculated using ACI 318 (11-15). The chords' nominal strength and design strength are then determined. Because the concrete shear strength is a function of the axial force when ACI 318 (11-4) is used, the failure prediction is determined by plotting the fiber model's chord shear force and the chord's calculated nominal strength and design strength against the load. Where the demand and capacity curves intersect is the predicted failure load.

Figure 3.5 plots the model's top chord shear demand (V_u) and top chord shear capacity (ϕV_n and V_n) against the load. Figure 3.5(a) shows that for S1 and S2, (A_{vt} = 0.4 in.^{2} at 4 in. o.c.) the demand intersects the two capacity predictions at 80 kips and 90 kips. These values bracket the observed failure loads for S1 and S2 of 86 and 84 kips, respectively. Figure 3.5(b) shows the demand and capacity curves for S3, (A_{vt} = 0.4 in.^{2} at 10 in. o.c.) intersecting at 61 kips and 70 kips. The nominal strength, V_n, is approximately 9% below the observed failure load for S3 of 77 kips. Both graphs indicate this is the likely mechanism that resulted in the observed failures. In addition to the predicted failure load comparison, the load-displacement response and the strains compare well between the model and the experimentally measured values.

When analyzed to failure, the test specimen ITO fiber model has an axial-flexural failure in the top chord of opening 2. Figure 3.6 plots the fiber model's axial force and moment in both chords at opening 2 on the chords' axial force-moment interaction diagrams. The top chord graph shows that the fiber model forces intersect the nominal strength curve at approximately the load at which the model indicates an axial-flexural failure. This observation serves to further confirm that this fiber model accurately models the strength assumptions of reinforced concrete theory. The bottom chord graph indicates the bottom chord at opening 2 is primarily acting as a tension member at the load at which the model fails. Both graphs also show the design strength curves obtained by applying the ACI 318 Code's strength reduction factors. For the top chord on the span side, the design strength curve is reached at an applied load of 76 kips, still above the factored load of 60 kips, therefore satisfying the ACI 318 Code's strength design criteria.

The accuracy of the predicted failure modes and load for the IT and ITO models shows that the fiber model accurately captures the significant aspects of the test specimens' behavior. Comparisons of the model's deflections and longitudinal strains with the experimental results also show good agreement. The model can be reasonably used to explore the ITO girder's behavior further.

3.2.3 Examination of ITO Behavior

This section examines the fiber model analysis results to gain further insight into the ITO girder's behavior, particularly the chord forces, failure load and failure mode. Two results are presented, one for a fiber element model with four load points, as in the experimental program, and one for a fiber element model with six load points, as would be the case in an actual structure. The most significant difference between a model with four load points and a model with six load points is the chords' axial force magnitude. The axial force increases due to the increase in the moment from the additional loads. This in turn affects the chords' shear forces and moments.

For each opening, a set of three graphs describes the behavior. The results in these graphs are obtained from the fiber element model. The figures are described here for opening 1, and similar figures presented for openings 2 and 3. For all the figures, the quantities are plotted against the

applied load. The applied load that is plotted is the total load at a load point, that is, the load from two DT stems on opposite sides of the web.

For opening 1, Figures 3.7 and 3.8 plot the top and bottom chord normal forces, shear forces and moments for both the four load and six load cases. Both the elastic model and the fiber element model show that the normal and shear forces do not vary with location across the chord, so the plotted value is representative of the entire chord for these quantities. The normal forces from the fiber element model are located at the chord's centroids. The moments are the moments at the opening's edges, with $\boldsymbol{M_i}$ the support side and $\boldsymbol{M_j}$ the span side moments, respectively. These moments are the maximum values in the chords. The individual traces are identified with ***t*** and ***b*** subscripts for the top and bottom chords respectively. Similarly, the four load and six load cases are respectively identified with ***4*** and ***6*** subscripts. In each figure there is also a diagram of the chord forces, with the same designations as the plots.

Each figure also shows the sum of the top and bottom chord force. At any value of the applied load, the top and bottom chord normal forces sum to the equivalent prestress force, and the top and bottom chord shear forces sum to the total shear at the section. At any value of the applied load, the top and bottom chord moments add to the total moment at the section less the sum of the moments due to the axial forces and the effective prestress moment.

For opening 1, Figure 3.9 shows the inflection point location (IP on the figure), the proportion of the shear force resisted by the chord ($\alpha \boldsymbol{V_u}$), and the support and span side uncracked concrete depths for the top and bottom chords for the six load case. The inflection point location is calculated from the chord moments and then divided by half the opening length, so if the value of the IP is 0, it is at the opening's midpoint, if it is -1, it is at the support side, and +1 at the span side. The proportion of the shear force for the top

chord is given by:

$$\alpha V_u = \frac{V_{ut}}{V_{ut} + V_{ub}} \tag{3.1}$$

where the ***t*** and ***b*** subscripts appended to the required shear strength indicate the top and bottom chords respectively. For the bottom chord this value is subtracted from 1. The support and span side uncracked depths are determined from the fiber element model, with the cracked concrete identified by a tensile strain. Once the uncracked depth is calculated, it is divided by the chord height to get the plotted value. So when the uncracked depth is 1, the chord is in compression throughout its depth, and when the uncracked depth is 0, there is no concrete in compression.

Four Loads versus Six Loads

Referring to Figures 3.7, 3.10 and 3.13, the greater total moment at a section in the six load case causes the normal forces to increase relative to the four load case. In the top chord for example, this means at the factored load, the axial compression is greater than for the four load case. In the bottom chord, this means either a smaller value of axial compression or a larger value of axial tension at the factored load.

Again referring to Figures 3.7, 3.10 and 3.13, the differences between the two cases in the shear force is minor in both chords, although the total shear force across the opening does not change. The bottom chord, having a lower compression force with six loads present, cracks at a slightly lower

load, and then to a greater extent than with four loads present. This results in the top chord carrying a greater proportion of the shear force at a lower load after cracking changes the chords' relative stiffness. For the moments at all three openings (Figures 3.8, 3.11 and 3.14), there is little difference between the six load case and the four load case, and the differences are similar to the differences in the shear forces.

The comparison between four loads and six loads is drawn to show that the test specimen behavior did not differ greatly from the expected behavior with six loads present. Because six loads are present, this is the case that must be used in design.

Normal Forces

Figures 3.7(a), 3.10(a) and 3.13(a) show the chords' normal forces vary linearly with the applied load, and increase from opening 1 to opening 3 as the moment increases. Figures 3.9, 3.12 and 3.15 show that cracking occurs in both chords, with the bottom chord cracking at 30 kips at openings 1 and 2, and at 38 kips at opening 3. Comparing the normal forces with the cracking loads, it is also apparent that cracking occurs in the bottom chord while large compressive axial forces are present in the bottom chord at all three openings. These observations show the normal force's linear variation is unaffected by cracking and the chords' accompanying flexural stiffness changes, and that cracking occurs while the net axial force in the bottom chord is compression.

For applied load alone (no prestress force or self-weight) the fiber element model gives the ratio between the top chord normal force and the applied load as 3.5 at opening 1, 6.9 at opening 2, and 8.1 at opening 3. These values agree with the test specimens' and the elastic FE model's ratios. The IDM gives slightly greater ratios while predicting the same overall behavior, because it is also an elastic estimate. From the above comparisons, it appears that the chords' normal forces can be accurately estimated with a linear elastic model over the entire range of loading, and that an elastic finite element model gives a slightly better estimate than the IDM.

Shear Forces

Figures 3.7(b) and 3.10(b) show the chords' shear forces initially vary linearly with the applied load at openings 1 and 2, but are not linear throughout the range of loading. Comparison with the shear proportion in Figures 3.9 and 3.12 shows that the proportion of the shear force resisted by each chord is initially approximately constant and then varies, consistent with the chord force plot. The linear variation and constant proportion exists until approximately the service load. Examining again the bottom chord cracking loads, the end of the initial linear region and constant shear proportion closely follows the onset of cracking at the span side in the bottom chord at both openings.

Comparing the shear force distribution among all three openings, Figures 3.7, 3.10 and 3.13 show that the proportion of the shear force resisted by each chord is approximately the same initially. The similar distribution occurs because while uncracked, the chords' flexural stiffness is the same at both openings. The more extensive cracking at openings 2 and 3, augmented by the more rapidly decreasing compression force in their bottom chords compared with opening 1, leads to the difference in the openings' shear distribution at the model failure load. The final shear force distribution is similar between openings 2 and 3.

At opening 1, in the bottom chord, cracking and the progression of cracking occurs and proceeds on both sides of the opening simultaneously. As cracking progresses in the bottom chord, the shear force increases in both chords, with the top chord's proportion of the total shear force increasing. At opening 2, the span side cracks first, followed by the support side. Both sides have no compression area at failure. From about 50 kips to 70 kips, the magnitude of the bottom chord shear force decreases, indicating redistribution of the shear force between the chords accompanies the change in the proportion carried by each chord. This redistribution occurs following the onset of cracking on the support side in the bottom chord. The proportion of the shear force carried by each chord becomes approximately constant again once the both sides are cracked through their entire depth. As noted in the discussion of the normal forces, the bottom chord axial force is compressive when cracking occurs. At opening 3, the behavior is similar to that at opening 2, with only differences in the loads at which cracking and redistribution occur.

The fiber model shows the ITO girder's shear force redistribution is due to cracking at the openings' edges in the bottom chord, which changes the chords' relative flexural stiffness. In addition to reducing the bottom chord's moment of inertia at a section, the cracking at the openings' edges reduces the chords' rotational restraint at the edges, which also reduces their flexural stiffness. This implies the bottom chords are not rigidly connected to the abutments once cracking occurs, and negates the assumption that the shear force divides in proportion to the chord's moments of inertia.

These observations show that the proportion of the shear force resisted by each chord initially is constant. Once cracking occurs in the bottom chord the shear distribution changes, and is strongly affected by the extent of cracking in the bottom chord. They also show that cracking and redistribution of forces occurs while the net axial force in the bottom chord is compressive. This indicates that the sense of the bottom chord axial force is not an adequate criteria to determine how the shear force is proportioned between the chords. These observations also show that opening 2 and opening 3 behave similarly with respect to cracking and redistribution of shear force between the chords.

Moments

The chord moments are a function of the chord normal and shear forces, and the inflection point location. Their variation is thus complex, particularly at opening 2 as Figure 3.11 shows. For design, the way the moment varies and the sources of the variations are not the most important aspects. Rather, estimation of the maximum chord moment is the most important aspect.

Figure 3.8 shows that at opening 1, the moments at opposite sides of the opening have opposite signs, so the chords are in double curvature. The magnitudes of the total chord moments at each side are similar, with the span side moment larger than the support side moment. The moments vary similarly to the chord's respective shear forces and are always increasing. These observations are consistent with the inflection point locations in Figure 3.9, which are approximately constant and the same in both chords, on the support side of the opening's midpoint as the load increases from 40 kips to failure.

Figure 3.11 shows that at opening 2, the chords are also in double curvature. The magnitudes of the total chord moments at each side are not similar, with the span side total chord moment approximately three times larger than at the support side. Both bottom chord moments vary like the

bottom chord shear force, consistent with the approximately constant bottom chord inflection point location seen in Figure 3.12(b). The top chord span side moment varies like the shear force, and the support side moment varies like the shear force only up to approximately 60 kips, beyond which it begins decreasing. These observations are consistent with the inflection point location in Figure 3.12(a), which shows the top chord inflection point moving toward the support side beyond 60 kips. This movement occurs at the same point as the cracking in the top chord at the span side.

At both sides of opening 2, the bottom chord moments become small and approximately constant above 60 kips. This is consistent with the fully cracked condition above 60 kips seen in the bottom chord in Figure 3.12(b). Beyond that point, the bottom chord moment the fiber model calculates is a difference in steel forces based on a linear strain distribution, not concrete compression and steel tension resultants acting together to form a couple.

In the top chord at opening 2, beyond 60 kips, the support side moments are large and approximately constant, while the span side moments continue to increase. This can be explained by examining the top chord inflection point and compression depth in Figure 3.12. At approximately 60 kips, the top chord on the span side cracks, and the inflection point starts moving toward the support side. This is consistent with the nearly constant moment at the support side, because as the top chord shear force increases, the only way the support side moment can remain approximately constant while the span side moment increases is for the inflection point to move toward the support.

At opening 3, the moments in both chords at each side of the opening have the same sign over the loading range, indicating the chords are in single curvature. In the top chord, the moments continue to increase throughout the loading. These moments arise because the analysis program reports the normal force at the chord's centroid, so they are equivalent to applying the top chord compressive force at a higher elevation in the cross-section. At the end of the loading, the bottom chord moments are approximately zero, because the tension difference between the two layers of reinforcement becomes negligible. Both of these results are consistent with basic reinforced concrete theory.

Figures 3.9, 3.12 and 3.15 show one more important aspect of the ITO girder's behavior. In the top chord at opening 1, the uncracked concrete depth is approximately 50% of the chord's depth. At opening 2, the support side does not crack, and the span side uncracked concrete depth is approximately 60% of the chord depth at failure. This indicates it is unlikely that the tension reinforcement yields, so it will not be possible to use flexural hinging at the opening's edges to control the shear force in the top chord. Further examination of the results shows that the top chord tension reinforcement does not yield at the failure load.

These observations indicate the IDM assumptions for estimating the moment demand are not accurate for this cross-section at either opening 1 or 2, because the assumption that the inflection point is at the opening's midpoint and the chord moments at both sides have the same magnitude and opposite signs is not correct.

The complex interaction between the chord normal and shear forces and chord cracking on the moments at openings 1 and 2 indicates a conservative approach is needed for axial-flexural design. At opening 3, as shown in Section 3.2.2, the midspan opening behaves similarly to a cracked flexural section, so estimation of these moments is not critical for symmetric loading. For

unsymmetric loading, while the maximum moment will still likely occur in the midspan region, shear and increased moments will need to be considered.

Finally, the depth of uncracked concrete in the top chord at failure indicates flexural hinging through yield of the tension reinforcement is not a possible mechanism to control the shear force in the top chord.

Failure Load and Failure Mode

The fiber model's predicted failure load for the test specimens was presented in Section 3.2.2. The objective of this section is to investigate the failure loads for all of the possible failure modes for an ITO girder with the same longitudinal and transverse reinforcement as S1 to provide further insight on the ITO girder's behavior. The possible failure modes at openings 1 and 2 are axial-shear and axial-flexural in either chord. At opening 3, for symmetric loading, the possible chord failure modes are axial-flexural failure, compression failure, and tension failure. There is also the possibility of a cross-section flexural failure.

A fiber model with three openings has only one failure load and failure mode, so to obtain an individual opening's failure loads, a fiber model with only that opening is analyzed. With only one opening in the fiber model, it must fail at that opening and not elsewhere, which allows identification of the individual opening's failure modes. The chord forces at each opening when it is isolated are the same as when all of the openings are present, so this provides a valid approach to determining each opening's failure loads.

The fiber model predicts the axial-flexural failure loads directly for each opening. However, the fiber model can only predict an axial-flexural failure in one chord at an opening, unless both chords happen to fail at the same load. Based on the discussion of the behavior in the preceding sections, it is not possible to strengthen one chord to force the failure in the other because this alters the distribution of forces and the problem.

As explained earlier, the fiber model does not predict the axial-shear failure mode directly. The approach in Section 3.2.2 gives the axial-shear failure load prediction, using the chord's axial forces to calculate $\boldsymbol{V_c}$, and the chord's transverse reinforcement to calculate $\boldsymbol{V_s}$. The chord's nominal shear strength, $\phi \boldsymbol{V_n}$, is calculated from these quantities and compared with the shear demand from the fiber model.

Table 3.1 shows the predicted failure loads for the different possible failure modes for the ITO girder at openings 1 and 2 for both the four load and six load cases. Looking at the "4 Loads" column in Table 3.1, which represents the test specimen loading, the fiber model results show that had the axial-shear failure not occurred at opening 1 in the test specimens, they would likely have had an axial-flexural failure at opening 2, below the midspan capacity. This is still not the desired failure mode for the ITO girder and further underscores the necessity of controlling the strength in all failure modes to force the desired failure mode.

Table 3.1 also compares the predicted failure load of an IT girder based on a plane section analysis with the predicted midspan opening failure load from an ITO fiber model for the same cross-section, and these values agree well. (While not shown in Table 3.1, an IT fiber model was also run, and gave nearly identical results as these two approaches in all cases). Additionally, the ITO fiber model

shows that at the midspan opening, the strain distribution is linear through the depth. The fiber model only requires that each chord independently have a linear strain distribution through the depth to satisfy the plane section assumption, so the linear strain distribution through the full girder depth at the midspan opening indicates this section acts as if it were a cracked flexural cross-section. This is consistent with the observed similarity in the midspan strains between the IT and ITO test specimens that Figure 2.23 shows. This provides further evidence that for symmetric loading, the midspan opening region can be designed for flexure as if the opening does not exist.

Table 3.1 further shows that the six load case consistently fails at a lower load at openings 1 and 2 than the four load model. The chord forces in the previous section show that the shear force is slightly greater at a given load at both openings for the six load model. This is due to the larger tension/smaller compression force in the bottom chord in the six load model, which allows cracking at lower loads, reducing the bottom chord's stiffness and its share of the shear force. The slightly larger shear force produces a larger moment along with the increased top chord axial force. These effects together result in the lower failure load in all the failure modes.

These observations show that the strength in all failure modes must be considered to obtain the desired failure mode. Further, if the failure loads for the chord failure modes exceed the midspan opening failure load, an ITO girder can reach approximately the same failure load as the identical IT girder. Finally, these observations show that the midspan region does not need to be designed assuming frame behavior, because it does not appear that it occurs for symmetric loading.

3.3 PARAMETER STUDY

This section describes a fiber model study of several design parameters. The objective is to determine each design parameter's effect on the ITO girder's chord forces, failure load and failure mode, and their implications for design. The design parameters studied are the top chord reinforcement area, top chord depth, prestressed reinforcement area, and composite action with a topping slab. The effect of each parameter is examined separately, by holding the remaining parameters constant. Table 3.2 summarizes the parameters' initial values, which are the same as those in S1. The material properties are the same as those used in Section 3.2. The six load case is used throughout the parameter study.

For each parameter, a table summarizes its effect on the predicted failure loads and failure modes. The Ref column in each table gives the failure loads for the test specimen model of S1 with six loads (i.e., the values from the "6 Loads" column in Table 3.1). The remaining columns give the parameter's failure loads. The tables have the same format as Table 3.1, and the description in the previous section explains how the failure loads were determined.

One or more graphs, similar to Figures 3.9 and 3.12, are also used to examine the effects of each parameter on the chord forces. These graphs are explained in Section 3.2.3. One additional plot is added to each graph, and that is a normalized value of the chord's axial force. This value is added so the point at which the chord switches from net compression to net tension can be compared with other events in the chord. The normalized normal force is obtained by dividing the chord's normal

force by the effective prestress force. For the top chord on some graphs, the normal force plot is truncated at -1 to keep the range of the graph from -1 to +1.

3.3.1 Top Chord Longitudinal Reinforcement Area

The objective of varying the top chord longitudinal reinforcement area was to see if the top chord could be made to hinge at both ends, providing a means to limit the top chord shear force. The test specimens had four # 8 bars (A'_s = 3.16 in.^{2}) in two layers placed symmetrically about the top chord centroid. To examine the effect of varying the top chord longitudinal reinforcement area, the initial top chord reinforcement was successively reduced to 50% (TCS-1), 25% (TCS-2) and 10% (TCS-3) of the original area. Table 3.3 shows the predicted failure loads for each potential failure mode.

Table 3.3 shows that the most significant effect of reducing the top chord longitudinal reinforcement area is the reduction in the top chords' axial-flexural strength. The table also shows that reducing the top chord longitudinal reinforcement area does not affect the failure modes' order of occurrence. The chord failure modes occur either below or approximately at the same load as the midspan failure mode. At opening 3, reducing the top chord longitudinal reinforcement area has only a small influence on the ITO girder's failure load, no different than would be expected from a reduction in compression reinforcement in a solid girder.

Reducing the top chord longitudinal reinforcement area results in a small increase in the top chord axial-shear failure load at opening 1. This occurs because as the top chord longitudinal reinforcement area is reduced, its flexural stiffness decreases slightly. This in turn means the top chord attracts less shear force (relative to the reference model), so it takes a higher load to reach a shear force that predicts failure. This is because the chord shear capacity for all four models is identical. The concrete shear capacity is the same because the axial force is the same, and all four models use the same transverse reinforcement (see Table 3.2) so the shear reinforcement capacity is also the same.

Figures 3.18 and 3.19 show the normalized chord forces and uncracked concrete depths at openings 1 and 2 for TCS-3, where the top chord longitudinal reinforcement area has been reduced to 10% of the initial area. Comparing these figures with Figures 3.16 and 3.17 for the reference model shows there is little difference in the overall behavior between these two models. The top chord uncracked concrete depths show that at both openings 1 and 2, it is unlikely the steel will yield and allow the chord to hinge. Thus forming a flexural hinge is not a viable option for limiting the top chord shear force.

3.3.2 Top Chord Depth

The objective of varying the top chord depth is to see if a less deep top chord, attracting less shear, provides a ductile failure or a means to control the top chord shear force. Varying the top chord depth also examines this parameter's effect on the midspan opening failure load. As Table 3.2 shows, the test specimens' had a 10 in. deep top chord, with 4 # 8 bars as longitudinal reinforcement in two layers centered at 2.375 in. from each face. To examine the effect of varying the top chord depth, the original depth was successively reduced from 10 in. to 8 in., 6 in. and 4 in. Table 3.4 shows the predicted failure loads for each potential failure mode.

Varying the top chord depth requires moving the bottom layer of top chord reinforcement up in the cross-section as the chord depth is reduced. This causes the reinforcement layers to get closer together, reduces the structural depth on the opening's span side, and causes the total reinforcement area to move upward in the section. To compare the variations with the reference model, the first model, TCD-1, has a 10 in. deep top chord, with the reinforcement at 1.25 in. from each face. This allows a comparison of the effect of a different reinforcement depth, ***d***, with the reference model. Subsequent models use the 1.25 in. distance from each face with reduced chord depths. The comparison is then between TCD-1 and the subsequent models.

Comparing the Ref and TCD-1 columns in Table 3.4 shows that increasing the structural depth from 7.625 in. to 8.75 in. results in an increase in the top chord axial-flexural failure mode at both openings. For this case, increasing the structural depth strengthens the opening's span side. Figures 3.20 and 3.21 show the top chord inflection point is on the support side of the opening's midpoint, so the increase in strength occurs at the section with the larger demand, increasing the failure load. The axial-shear failure loads also increase at both openings for TCD-1 compared with the reference model. This is because the structural depth is incorporated in the concrete shear strength estimate, and directly increases this value. Comparing Figures 3.20 and 3.21 with the reference model shows the top chord shear force increases slightly in TCD-1 compared with the reference model. The small increase in the plane section analysis and ITO fiber model failure loads at opening 3 is due to the bottom layer of top chord longitudinal reinforcement moving downward in the section. The equivalent rectangular stress block depth for this cross-section is 5.8 in., so the bottom layer of top chord reinforcement is in tension. As the reinforcement moves downward in the section, the strain at the lower elevation is larger, so the force contribution from that layer of steel increases.

Comparing Figures 3.20 and 3.21 for TCD-1 with Figures 3.22 through 3.25 for TCD-3 and TCD-4, several differences in the chord forces are apparent. Reducing the top chord depth reduces its flexural stiffness relative to the bottom chord, so the proportion of the shear force carried by the top chord, both initially and at failure, decreases as the top chord depth decreases. Consequently, the bottom chord shear force increases. This in turn reduces the top chord moments and increases the bottom chord moments. At both openings, there is little change in the bottom chord cracking loads, while top chord cracking is almost eliminated. The normal forces decrease slightly as the distance between the top and bottom chord centroids increases. The top chord's capacities for both axial-shear and axial-flexural failure also change with the change in chord depth. Since both capacities are dependent on the structural depth, they both decrease as the chord depth decreases. These changes in both capacity and demand alter the order of the failure modes and the failure modes the model predicts.

The results of these changes in both demand and capacity are evident in Table 3.4. Comparing TCD-1 through TCD-3, the top chord axial-flexural failure load decreases at both openings as the depth decreases. In TCD-4 at opening 1, the top chord does not have an axial-flexural failure because the moments have decreased sufficiently. The axial-flexural failure instead shifts to the bottom chord, which is carrying almost the entire shear force. At opening 1, the top chord axial-shear failure initially increases as the shear demand decreases, then the axial-shear failure shifts to the bottom chord as the depth is reduced further.

Decreasing the top chord depth significantly affects the shear force distribution, the predicted failure loads and failure modes, and the order in which they occur. While the order of predicted failure modes changes, all of the chord failure modes except the axial-flexural failure at opening 1 for the 10 in. and 8 in. deep chords have a lower failure load than the midspan failure load. This shows that reducing the top chord depth does not provide the desired failure mode. It also shows that the shear force distribution is strongly influenced by the top chord depth, both before and after the bottom chord cracks, and that this parameter can be used to limit the top chord shear force. However, these studies show that there is no direct and simple way to predict the maximum or the final shear force distribution between the chords.

At opening 3, for all of the models except TCD-4, the failure load predicted by a plane section analysis and the ITO fiber model with only a midspan opening are approximately the same. This is the same behavior observed in all of the parameter studies, that absent a chord failure, the ITO fiber model reaches approximately the plane section analysis flexural strength. For TCD-4, the failure load at the midspan opening is less that the corresponding plane section failure load. This is also the only model where the top chord depth is less than the required equivalent stress block depth for an IT girder at failure. This leads to the conclusion that the minimum top chord depth for the midspan opening must be at least the depth of the equivalent rectangular stress block for an IT girder, if this is the desired failure mode. This does not preclude varying the opening depths along the span if desired, as long as sufficient strength can be provided and uniformity of the opening size and reinforcement placement is not an overriding factor for fabrication efficiency.

3.3.3 Top Chord Longitudinal Reinforcement Area and Depth

One objective of varying both of the previous parameters was to attempt to cause flexural hinging in the top chord at both sides of an opening, limiting the top chord shear force. If this can be accomplished, the design procedure no longer relies on an assumption for the shear force distribution, and likely provides a safer and more predictable design.

Neither parameter individually provides the desired result. Decreasing the top chord longitudinal reinforcement area decreases the axial-flexural capacity, but because of the axial force magnitude, the capacity is reached by concrete crushing rather than steel yielding. Decreasing the top chord depth significantly decreases the top chord shear force, but again does not result in flexural hinges in the chord.

Can a flexural hinge form if both the top chord longitudinal reinforcement area and depth are reduced simultaneously? The results of the previous two parameter studies indicate this will not occur. Decreasing the top chord longitudinal reinforcement area to 10% of the initial area with a 10 in. deep top chord does not result in flexural hinging. Increasing the structural depth for the same reinforcement area and a 10 in. top chord depth (TCD-1) also does not result in flexural hinging. Further reducing the top chord depth reduces the top chord shear force, therefore the top chord moment, and reduces the lever arm between the tension and compression resultants in the chord is reduced. The combination of these factors makes it less likely the tension reinforcement will yield rather than more likely.

The effect of both reductions on the midspan failure load would also be minimal. Table 3.3 shows that there is very little decrease in the midspan failure load as the top chord longitudinal

reinforcement area is reduced. Table 3.4 shows that with a top chord depth at least as deep as the required equivalent rectangular stress block depth for a solid section, reducing the top chord depth has very little effect on the failure load.

3.3.4 Prestressed Reinforcement Area Reductions

The objective of the prestressed reinforcement area reductions is to attempt to bring the midspan flexural failure load below the chord failure loads, and closer to the factored load for which the girder was designed. This seems a more rational approach than adding more chord reinforcement to increase the chord failure loads above the midspan flexural failure load, particularly if the midspan flexural failure load already exceeds the required capacity by a significant amount, as was the case in the experimental program. The solid girder in the experimental program, S4, failed at midspan at an applied load of 108 kips, which is 80% greater than the target failure load of 60 kips, the factored load. Based on the results of these fiber model analyses, S1, S2 and S3 would likely have reached a similar load had the chord failure not occurred.

For the ITO girder, a midspan failure due to tension reinforcement yielding at the midspan opening is the desired failure mode. Assuming the chord forces can be quantified accurately enough to predict the chord failure loads, the overall objective of the design approach pursued in this research is to have the chord failure loads exceed the midspan failure load. The performance of the ITO girders in the experimental program shows these test specimens had excess midspan capacity, as they failed at an applied load of approximately 85 kips, which is 42% greater than the factored load of 60 kips. This excess midspan contributed to the observed brittle failure. Reducing the midspan capacity by reducing the prestressed reinforcement area offers the potential to bring the midspan failure load under the chord failure loads, resulting in a more predictable and ductile failure mode for the ITO girder.

As Table 3.2 shows, the test specimens had nine ½ in. diameter “special” strands in two layers placed approximately symmetrically about the bottom chord centroid. To examine the effect of reducing the strand area, the number of strands in each layer was successively reduced, from 9 strands to 8, then 7, then 6 strands in each layer.

As with the top chord depth, reducing the number of strands requires additional adjustments. As the number of strands in each layer decreases, either the prestress force decreases while the strand stress remains constant, or the prestress force remains constant and the strand stress increases. This parameter investigation uses both approaches.

In the PAf series of fiber models, the prestress strand effective stress is held constant at the same level as in the test specimens while the strand area is reduced. This reduces the prestress force and the accompanying moment for the equivalent loads that model the effects of prestressing. Table 3.5 shows the failure loads for the various failure modes for this approach.

In the PA6 series of fiber models, the prestress force and moment are kept approximately the same as the reference model’s while the strand area decreases. In this approach, as the strand area decreases, the initial strand stress increases. This means the model starts at a higher stress on the strand stress-strain curve, so it takes less load for the strand to accumulate sufficient stress to yield. For this approach, the prestress force and moment are selected to cause the tension stress at the

bottom fiber at midspan at service loads for a solid cross-section to equal $6\sqrt{f'_c}$, consistent with ACI 318 18.4.2(c))). Since the reference model has an appreciably higher prestress force, a transition model is required in this parameter variation. The PA6-1 model has nine strands, like the reference model, but a reduced prestress force consistent with the requirement outlined above. This model is compared with the reference model, and then subsequent models with fewer strands are compared with PA6-1. Table 3.6 shows the failure loads for the various failure modes for this approach.

Both Tables 3.5 and 3.6 show the expected result, that reducing the area of prestressed reinforcement reduces the ITO fiber model's midspan opening failure load. In both cases, the failure load at the midspan opening is still approximately the same as the plane section analysis failure load. The similarity in the failure loads between the two series indicates the reinforcement area controls the behavior, not the strand stress or prestress force, again as expected.

For the PAf series (Table 3.5) the top chord axial-flexural failure loads at opening 1 are all greater than the midspan failure load, which is the desired result, but not really a change from previous models. At opening 2 however, where previously the top chord axial-flexural failure load was generally below the midspan failure load, when the number of strands in each layer is reduced to six, the failure load exceeds the midspan opening failure load. For the PA6 series (Table 3.6) the top chord axial-flexural failure loads at opening 1 become greater than the midspan failure load when the number of strands is eight or less in each layer. At opening 2, like the PAf series, this result is not seen until the number of strands in each layer is reduced to six. For both series of models, the top chord axial-shear failure loads at opening 1 are still lower than the midspan failure load, and decrease as the strand area is reduced.

Comparing Figures 3.26 and 3.27 (PAf -3) with the reference model figures, several differences in the chord forces are apparent. At both openings 1 and 2, the chords' axial forces still vary linearly with the applied load, but are reduced compared with the reference model. This is directly attributable to the decreased prestress force. At both openings, the bottom chord cracking load also decreases, initiating changes in the proportion of the shear force carried by each chord at a lower load, and resulting in the top chord carrying a greater proportion of the shear force at failure. This is also a result of the decreased prestress force, which provides less precompression to the tension regions of the chords. This change is responsible for most of the reduction in the axial-shear failure loads observed in Table 3.5. The reduction in the axial force also reduces the concrete shear capacity at both openings. At opening 1, the bottom chord has a smaller uncracked concrete depth at failure as a result of the decrease in the strand area and prestress force. At opening 2, the bottom chord becomes fully cracked at a lower load as a result of these changes. The top chord cracking load also decreases compared with the reference model, but the uncracked concrete depth at failure is similar to the reference model's.

Comparing Figures 3.28 and 3.29 (PA6 -4) with the reference model figures, similar differences between these models and the reference model occur as observed for the PAf series. At both openings 1 and 2, the chords' axial forces still vary linearly with the applied load, but are again reduced compared with the reference model, which is a function of the decreased prestress force. At both openings, the bottom chord cracking load again decreases, with the same results as for the PAf series. The cracking load is slightly higher for PA6-4 than for PAf-3 because the prestress force is slightly higher, 376 kips compared with 332 kips. At opening 1, the bottom chord has a smaller

uncracked concrete depth at failure as a result of the decrease in the strand area and prestress force. At opening 2, the bottom chord becomes fully cracked at a lower load as a result of these changes. The top chord cracking load also decreases compared with the reference model, but the uncracked concrete depth at failure is similar to the reference model's.

Varying the strand area shows that at opening 1, the shear force distribution can be controlled by controlling the prestress force. A greater prestress force delays cracking in the bottom chord, and maintains the initial shear force distribution to higher loads. At opening 2, at or near failure, the shear force distribution is relatively independent of the prestress force because the bottom chord has a net tensile force.

The overall result of reducing the strand area for both approaches is a reduction in the failure load for all of the failure modes. For the least area of prestressed reinforcement examined, the top chord axial-flexural failures at both openings have greater failure loads than the midspan failure load, which is the desired result. The axial-shear failure modes are still predicted at a lower load than the midspan failure load, but if the shear demand can be controlled, then sufficient transverse reinforcement can be provided to raise the axial-shear failure loads above the midspan failure load. This parameter also reinforces the idea that reducing the midspan strength is necessary to attempt to control the failure mode.

3.3.5 Composite Topping Slab

The objective of adding a composite topping slab is to assess its effects on the ITO girder's chord forces, failure load and failure mode. A composite topping slab significantly increases an IT girder's flexural strength, and will likely have a similar affect on the midspan opening's failure load. This increase in strength is exactly opposite the desired effect, which is to keep the midspan failure load below the chord failure loads and control the failure mode. This is particularly critical if precast concrete fabricators follow HCSI's standard practice of designing their composite girders without considering the additional strength.

Figure 3.30 shows the topped ITO girder. For the model, it is assumed a 2 in. thick topping slab with the same concrete strength as the girder is applied to the floor system. The topping slab is 4 in. deep directly over the girder, and 2 in. deep over the double tee beams. The effective width is assumed as 50 in., in accordance with ACI 318 8.10.2. Because the primary area of interest is failure loads and failure modes, the composite section is loaded without considering the construction sequence. This is consistent with standard strength design approaches for composite beams. The ITO girder is the same as the reference model with the topping slab added, consistent with not relying on the topping slab in design.

Table 3.7 compares the failure loads for the various modes between the composite model and the reference model. As expected, the midspan opening's failure load increases significantly with the added topping slab. The ITO fiber model's predictions still closely match the plane section analysis value, so the modeling assumptions still appear reasonable. Unexpectedly, the failure loads for axial-flexural failure at both openings 1 and 2 increase with the addition of the topping slab, and at both openings they are now above the failure load at midspan. The axial-shear failure load at opening 1 decreases significantly due to the additional shear force attracted by the stiffer top chord. Similarly, at opening 2, where the non-composite model does not have an axial-shear failure, the composite

model fails in this mode. Both failures occur below the midspan failure load, which is not a change from the reference model, but the difference between the axial-shear failure and the midspan flexural failure has increased.

Figures 3.31 and 3.32 show the normalized chord forces for the composite model at openings 1 and 2. Comparing these with the reference model figures, several differences are apparent. In the top chord, the normal force is not significantly different than the reference model's. The top chord shear force proportion at failure has increased to nearly 100% for the composite model at both openings, compared with 62% at opening 1 and 87% at opening 2 in the reference model. The top chord on the span side is cracked more deeply than the reference model, while the support side is approximately the same. At opening 1, the inflection point has moved more toward the support side than in the reference model. At opening 2, above approximately 80 kips, the composite model's top chord is in single curvature, so no inflection point is plotted. All of this indicates the moment demand has increased considerably over the reference model, particularly at the span side.

Figure 3.33 shows the composite model's normal forces and moments plotted on an interaction diagram. This diagram, when compared with Figure 3.6 for the reference model, shows that the interaction surface has gotten larger at both the support side and the span side. This is due to the increased top chord depth with the topping slab present. On the span side, not only has the top chord depth increased, but the structural depth has increased also. On the span side, only the top chord depth increases. The top chord depth change alters the plastic centroid location, about which the moments are calculated, and results in the increased strength observed in the figure.

Figure 3.33 (a) shows that at opening 1, the load at the point at which the fiber model's forces cross the interaction surface is 156 kips, and failure follows shortly after at 169 kips. The diagram also shows that the support side forces have just reached the failure surface when the model fails. Figure 3.33(b) shows that at opening 2, the chord moments have the same sign at failure, as indicated by the inflection point in Figure 3.32. This figure also shows that opening 2 crosses the interaction surface at an applied load of approximately 128 kips, compared with the fiber model's failure load of 130 kips. Note that the chord forces in the two graphs in Figure 3.33 are obtained by running separate fiber models with each opening isolated.

Adding a topping slab to an ITO girder that is not designed for composite action increases the chords' axial-flexural failure loads to a load greater than the (also increased) midspan opening failure load. This is the desired behavior, and occurs because the topping slab shifts the plastic centroid location in the chord's cross-section, which results in an increase in its moment capacity. The axial-shear failure load decreases at opening 1, widening the difference between this failure mode and the midspan opening's failure load, which is an undesirable behavior. The increased top chord stiffness also triggers an axial-shear failure at opening 2 which was not present in the reference model. The failure loads for these two failure modes are calculated using the least depth and width, which occurs at the opening's support side. These conservative estimates lead to the low axial-shear failure load predictions. This presents the same problem discussed at the end of the previous section, that is, if the shear demand can be controlled, then sufficient transverse reinforcement can be provided to raise the axial-shear failure loads above the midspan failure load.

3.4 DESIGN IMPLICATIONS

The examination of the ITO girder's behavior provides the following implications for an ITO girder's design:

1. The chord's normal force varies linearly with the applied load, and this linear variation is unaffected by the chords' cracking and accompanying stiffness changes. These observations, along with the evidence from the experimental program and the elastic finite element analyses, indicate the normal forces can be accurately estimated with a linear elastic model and can be used for ultimate strength design.

2. Cracking in the bottom chord changes the distribution of the shear force between the top and bottom chords. This observation shows that an elastic estimate of the chord shear forces is not sufficiently accurate for design.

3. Cracking occurs in the bottom chord at both openings 1 and 2 while the chord's axial force is compressive. This observation indicates that the sign of the chord's axial force is not sufficient as a criterion for apportioning the shear force between the chords.

4. The chord moments are a function of the chord normal and shear forces and the inflection point location, and therefore a function of the extent of cracking in the chords. The bottom chord cracking controls the shear distribution, and the top chord cracking influences the top chord inflection point location. These observations indicate an elastic analysis similar to the assumptions made for the analysis of a Vierendeel truss is inadequate for estimating the chord moments. They also indicate a conservative approach for the chord's axial-flexural design is needed.

5. The depth of the uncracked concrete at openings 1 and 2 shows that it is unlikely the chord reinforcement will yield. This indicates flexural hinging of the top chord at both ends of the opening is not a viable mechanism to control the top chord shear force.

6. The failure load at the midspan opening for a symmetrically loaded ITO girder is nearly identical with the failure load determined from a plane section analysis of an IT girder with the identical cross-section. This observation shows that if the failure loads for the other possible failure modes exceed the midspan opening failure load, an ITO girder can reach approximately the same load as the identical IT girder. This also indicates the logical place to start the ITO girder design is with an IT girder.

7. The fiber model results show that a properly reinforced opening can be located within the strand development length. Because strand slip can result in a sudden failure, the bottom chord at an opening within the strand development length should not be designed for an excessive amount of shear force, which leads to large moments and extensive cracking.

The parameter study provides the following implications for an ITO girder's design:

1. The top chord longitudinal reinforcement area variations show that this parameter does not significantly affect the ITO girder's overall behavior or its failure modes' order of occurrence. Additionally, varying this parameter shows it is unlikely the top chord will yield

its reinforcement and hinge, so this is not a viable approach to limiting the top chord shear force.

2. The top chord depth variations show that this parameter has a significant influence on the chord forces and the chord strength. While the order of predicted failure modes changes, all of the chord failure modes except the axial-flexural failure at opening 1 for the 10 in. and 8 in. deep chords have a lower failure load than the midspan failure load. This shows that reducing the top chord depth does not provide the desired midspan opening ductile failure mode.

3. The top chord depth variations show that as long as the midspan top chord depth is at least as deep as the required equivalent rectangular stress block depth for the comparable solid cross-section, the ITO girder reaches the same failure load.

4. The prestressed reinforcement area variations show that controlling the midspan opening strength is the key to controlling the girder's overall failure mode. Considering all other longitudinal reinforcement in the section and reducing the prestressed reinforcement to the minimum required for flexural strength provides the lowest midspan opening failure load.

5. The prestressed reinforcement area variations also show that a larger prestress force delays the onset of bottom chord cracking and thus provides some measure of control over the chord forces. A larger prestress force provides more precompression for the bottom chord's tension regions, delaying cracking and force redistribution to a higher load.

6. Adding a composite topping slab to an ITO girder designed as non-composite increases its midspan opening failure load, and causes the axial-flexural failure load at openings 1 and 2 to be above the midspan failure load. The axial-shear failures occur at lower loads than the midspan opening failure load due to the increased proportion of the shear force resisted by the top chord. These results show that the effect of a topping slab must be considered in the design process. Either the topping slab must be purposely made non-composite with the ITO girder, or the design must consider the topping slab from the start and provisions must be made to ensure the requisite amount of composite action occurs.

All of the above indicates the ITO girder must be treated as a structure in its design. Sufficient strength must be provided in undesirable failure modes so that the entire girder reaches failure at the load corresponding to the desired failure mode. This also implies that overstrength cannot be allowed in the desirable failure modes if control of the failure mode is desired. There are two possible ways to approach the prevention of undesirable failures. Either the undesirable failure mode's capacity can be made large enough that it does not occur, or the demand for the undesirable failure mode can be limited so it does not occur. Both approaches have the same limitation, which is that for the chords, both the capacity and demand are functions of the applied load.

The test specimen fiber model provides several insights on the ITO girder's behavior at failure. The parameter studies also give insight on the girder's behavior and the effect of varying the several parameters. However, some of the results provide contradictory advice, and the effects of several changes together need to be assessed. This assessment occurs as part of the process of developing the design procedure, where both the top chord reinforcement area and the strand area may be reduced simultaneously.

Table 3.1 Test Specimens – Predicted Failure Loads (kips)

Opening	Failure Mode		Chord	Model Designation	
				4 Loads	6 Loads
1	N+M		Top	115.3	106.3
			Bot	–	–
	N + V	ϕV_n	Top	80	77
		V_n		90	86
		ϕV_n	Bot	–	–
		V_n		–	–
2	N+M		Top	99.4	93.5
			Bot	–	–
	N + V	ϕV_n	Top	–	–
		V_n		–	–
		ϕV_n	Bot	–	–
		V_n		–	–
3	Plane Sections Analysis			107.7	100.1
	ITO Fiber Model			108.1	100.5

Table 3.2 Initial Parameter Values: S1

Parameters Held Constant		
Ledge reinforcement area @ depth from top of section	Upper Layer	0.80 in.^{2} @ 26.625 in.
	Lower Layer	0.80 in.^{2} @ 32.625 in.
Top chord shear reinforcement area @ spacing	Opening 1	0.4 in.^{2} @ 4 in.
	Opening 2	0.4 in.^{2} @ 4 in.
	Opening 3	0.4 in.^{2} @ 4 in.
Bottom chord shear reinforcement area @ spacing	Opening 1	0.8 in.^{2} @ 6 in.
	Opening 2	0.4 in.^{2} @ 6 in.
	Opening 3	0.4 in.^{2} @ 6 in.
Parameters Varied		
Top chord depth	All Openings	10 in.
Top chord longitudinal reinforcement area @ depth from top of section	Upper Layer	3.16 in.^{2} @ 2.375 in.
	Lower Layer	3.16 in.^{2} @ 7.625 in.
Prestressed reinforcement area @ depth from top of section	Upper Layer	1.50 in.^{2} @ 26.625 in.
	Lower Layer	1.50 in.^{2} @ 32.625 in.
Effective prestress force		504 kips
Equivalent prestress moment		4742 in.-kips
Effective strand stress		162.2 ksi

Table 3.3 Top Chord Longitudinal Reinforcement Area Variations – Predicted Failure Loads (kips)

Opening	Failure Mode		Chord	Model Designation			
				Ref	TCS-1	TCS-2	TCS-3
				Longitudinal Steel Area (in.^{2})			
				3.16	1.58	0.79	0.32
1	N+M		Top	106.3	99.3	94.8	91.1
			Bot	–	–	–	–
	N + V	ϕV_n	Top	77	78	78	80
		V_n		86	88	90	–
		ϕV_n	Bot	–	–	–	–
		V_n		–	–	–	–
2	N+M		Top	93.5	88.8	86.1	84.5
			Bot	–	–	–	–
	N + V	ϕV_n	Top	–	–	–	–
		V_n		–	–	–	–
		ϕV_n	Bot	–	–	–	–
		V_n		–	–	–	–
3	Plane Section Analysis			100.1	99.5	98.5	97.8
	ITO Fiber Model			100.5	99.1	98.3	97.7

Table 3.4 Top Chord Depth Variations – Predicted Failure Loads (kips)

Opening	Failure Mode		Chord	Model Designation				
				Ref	TCD-1	TCD-2	TCD-3	TCD-4
				Top Chord Depth (in.)				
				10	10	8	6	4
1	N+M		Top	106.3	119.8	108.2	96.9	–
			Bot	–	–	–	–	86.0
	N + V	ϕV_n	Top	77	80	84	–	–
		V_n		86	90	94	–	–
		ϕV_n	Bot	–	–	102	70	58
		V_n		–	–	–	86	70
2	N+M		Top	93.5	100.8	92.1	83.0	79.0
			Bot	–	–	–	–	
	N + V	ϕV_n	Top	–	–	–	–	
		V_n		–	–	–	–	
		ϕV_n	Bot	–	–	–	–	
		V_n		–	–	–	–	
3	Plane Section Analysis			100.1	102.2	102.1	102.8	104.4
	ITO Fiber Model			100.5	102.8	102.3	102.5	99.5

Table 3.5 Prestressed Strand Area Variations – Strand Stress Constant (Paf) – Predicted Failure Loads (kips)

Opening	Failure Mode		Chord	Model Designation			
				Ref	PAf-1	PAf-2	PAf-3
				Strand Area (in.^{2})			
				3.00	2.67	2.34	2.00
				Effective Prestress Force (kips)			
				504	446	389	332
				Equiv. Prestress Moment (in.-kip)			
				4742	4207	3673	3141
1	N+M		Top	106.3	100.6	94.3	87.7
			Bot	–	–	–	–
	N + V	ϕV_n	Top	77	70	66	60
		V_n		86	80	72	66
		ϕV_n	Bot	–	–	–	–
		V_n		–	–	–	–
2	N+M		Top	93.5	88.1	81.8	74.9
			Bot	–	–	–	–
	N + V	ϕV_n	Top	–	–	–	–
		V_n		–	–	–	–
		ϕV_n	Bot	–	–	–	–
		V_n		–	–	–	–
3	Plane Sections Analysis			100.1	92.4	83.3	74.0
	ITO Fiber Model			100.5	91.8	82.7	73.5

Table 3.6 Prestressed Strand Area Variations – Prestress Force Constant (PA6) – Predicted Failure Loads (kips)

Opening	Failure Mode		Chord	Model Designation				
				Ref	PA6-1	PA6-2	PA6-3	PA6-4
				Strand Area (in.^{2})				
				3.00	3.00	2.67	2.34	2.00
				Effective Prestress (ksi)				
				162	121	137	157	184
				Effective Prestress Force				
				504	376	376	376	376
1	N+M		Top	106.3	95.5	94.3	93.1	91.1
			Bot	–	–	–	–	–
	N + V	ϕV_n	Top	77	66	64	64	64
		V_n		86	74	72	72	70
		ϕV_n	Bot	–	–	–	–	–
		V_n		–	–	–	–	–
2	N+M		Top	93.5	86.0	84.2	81.2	76.2
			Bot	–	–	–	–	–
	N + V	ϕV_n	Top	–	–	–	–	–
		V_n		–	–	–	–	–
		ϕV_n	Bot	–	–	–	–	–
		V_n		–	–	–	–	–
3	Plane Sections Analysis			100.1	100.6	92.1	83.3	74.1
	ITO Fiber Model			100.5	99.9	91.5	82.7	73.6

Table 3.7 Composite Topping Slab – Predicted Failure Loads (kips)

Opening	Failure Mode		Chord	Model Designation	
				Ref	Composite
1	N+M		Top	106.3	169.3
			Bot	–	–
	N + V	ϕV_n	Top	77	46
		V_n		86	58
		ϕV_n	Bot	–	–
		V_n		–	–
2	N+M		Top	93.5	130
			Bot	–	–
	N + V	ϕV_n	Top	–	79
		V_n		–	101
		ϕV_n	Bot	–	–
		V_n		–	–
3	Plane Sections Analysis			100.1	127.4
	ITO Fiber Model			100.5	123.5

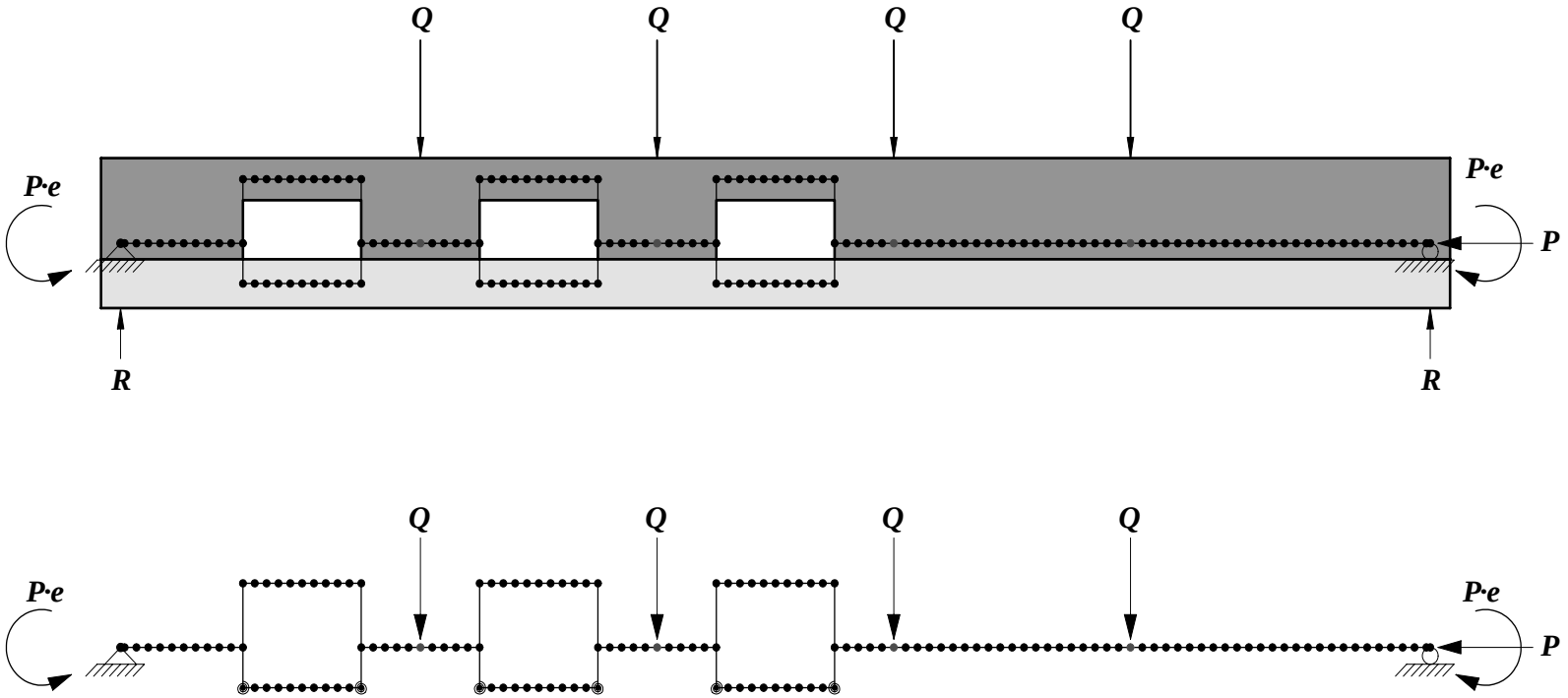

Figure 3.1 ITO and fiber model elevations

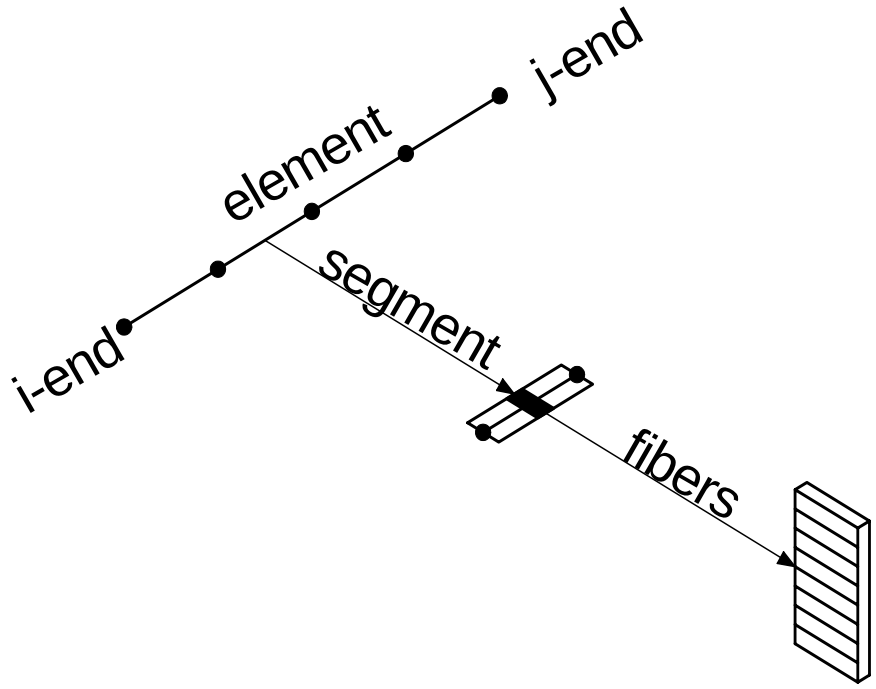

Figure 3.2 DRAIN-2DX fiber element

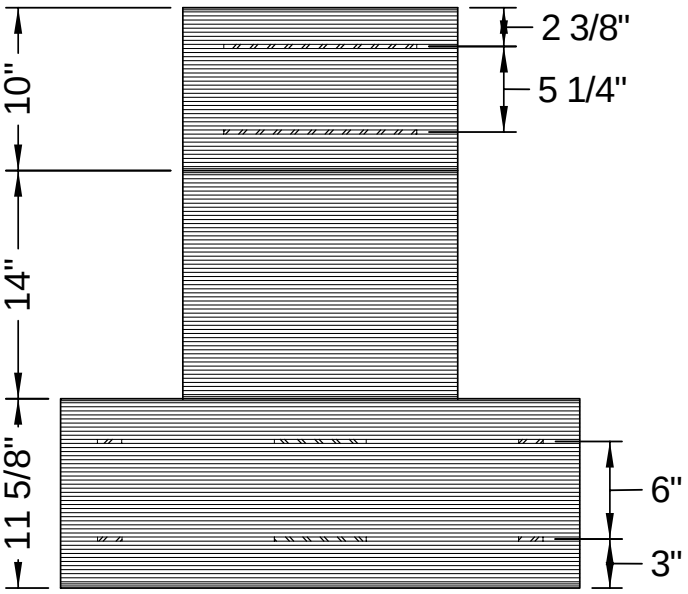

(a)

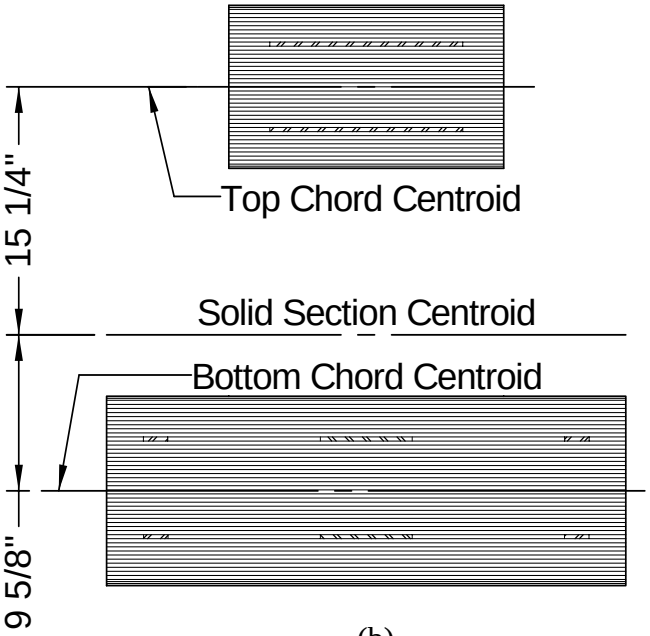

(b)

Figure 3.3 Fiber model cross-sections: (a) solid regions; (b) opening regions

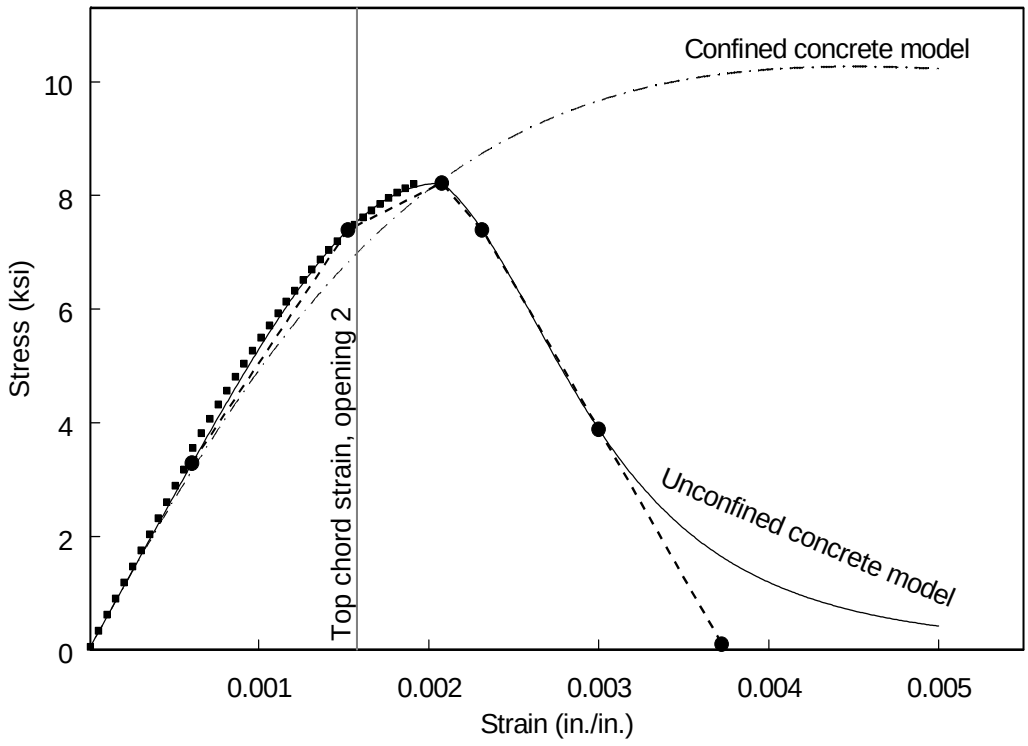

(a)

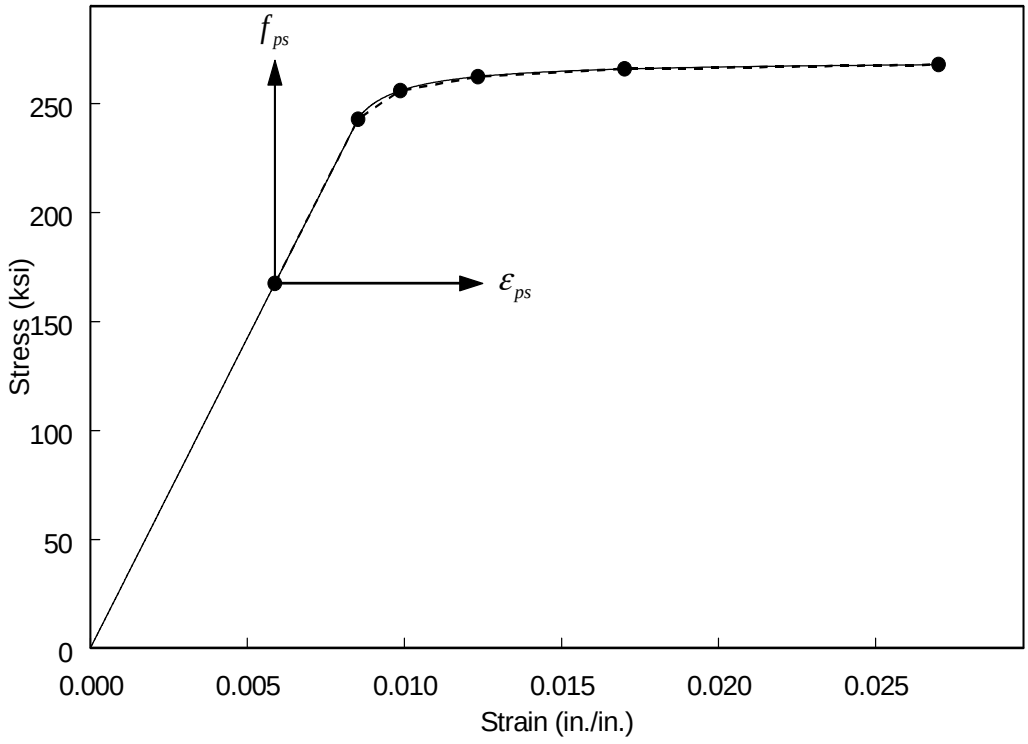

(b)

Figure 3.4 Fiber model material models: (a) concrete stress-strain curve; (b) prestressed reinforcement stress-strain curve

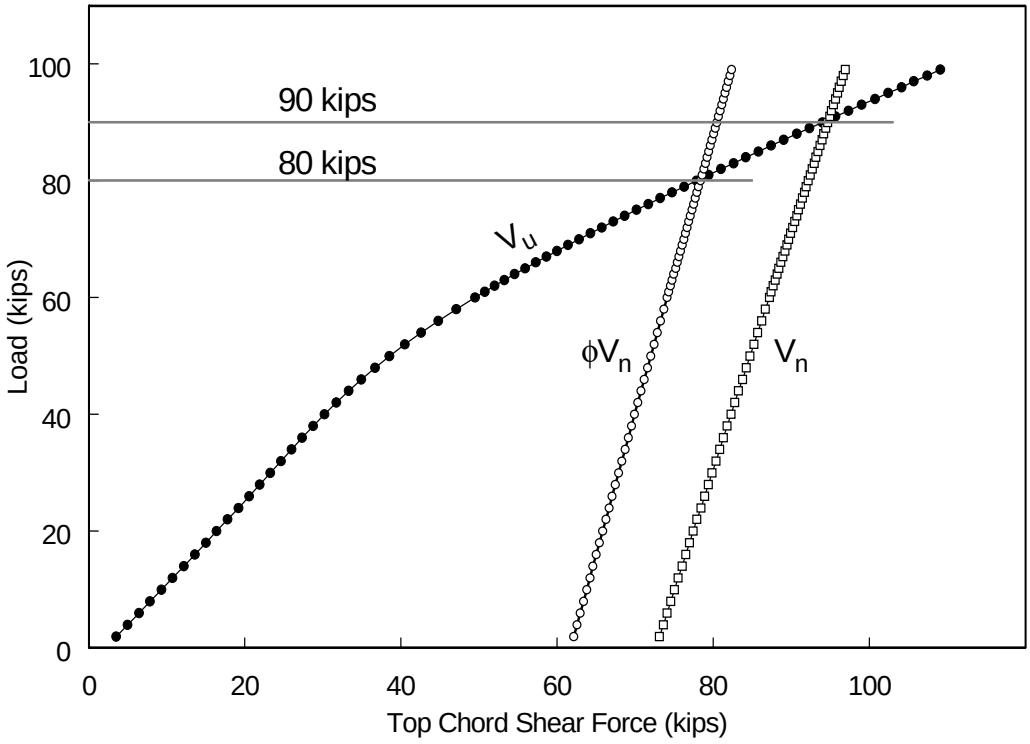

(a)

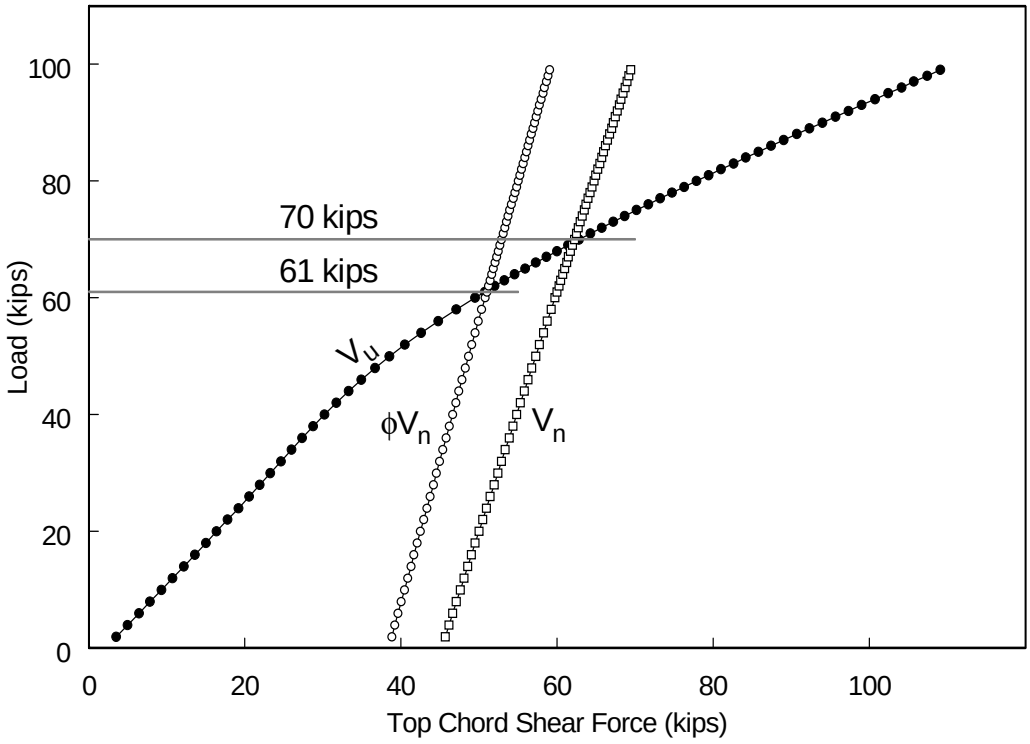

(b)

Figure 3.5 Predicted top chord failure load at opening 1 due to combined axial force and shear force: (a) S1 and S2; (b) S3

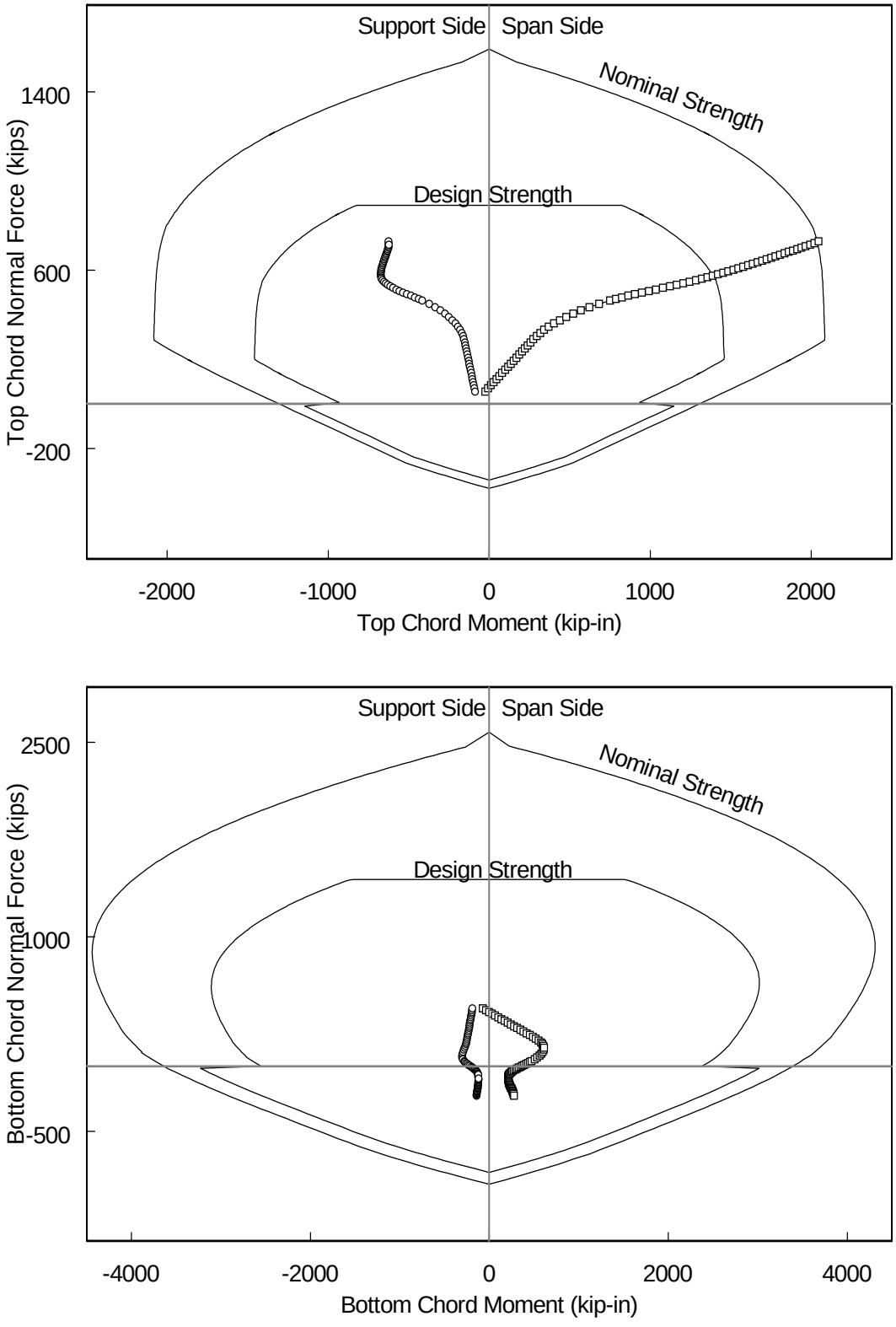

Figure 3.6 Axial-flexural response and axial force-moment interaction diagram at opening 2

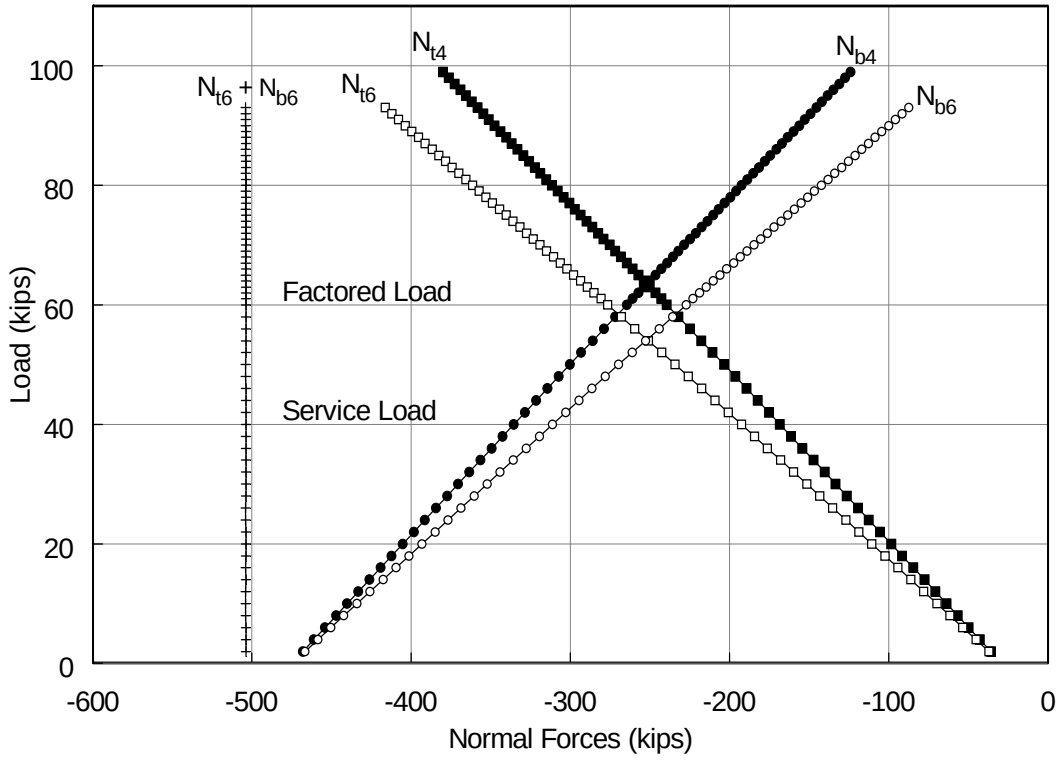

(a)

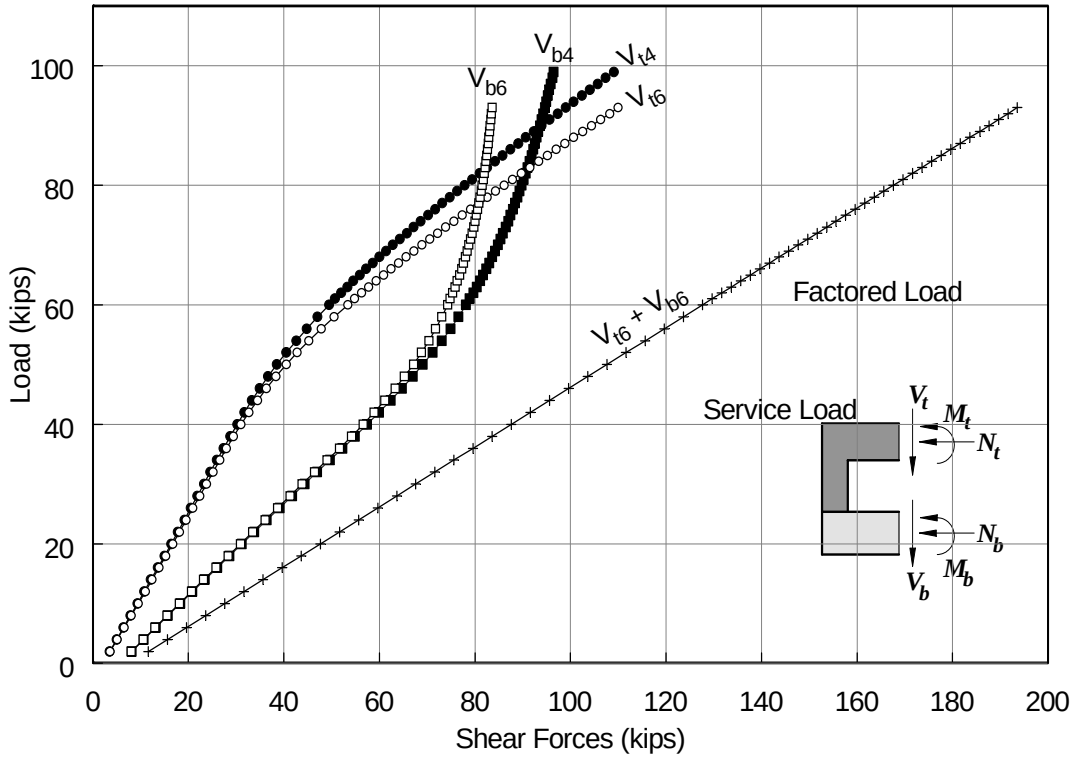

(b)

Figure 3.7 Opening 1 normal and shear forces: (a) normal forces; (b) shear forces

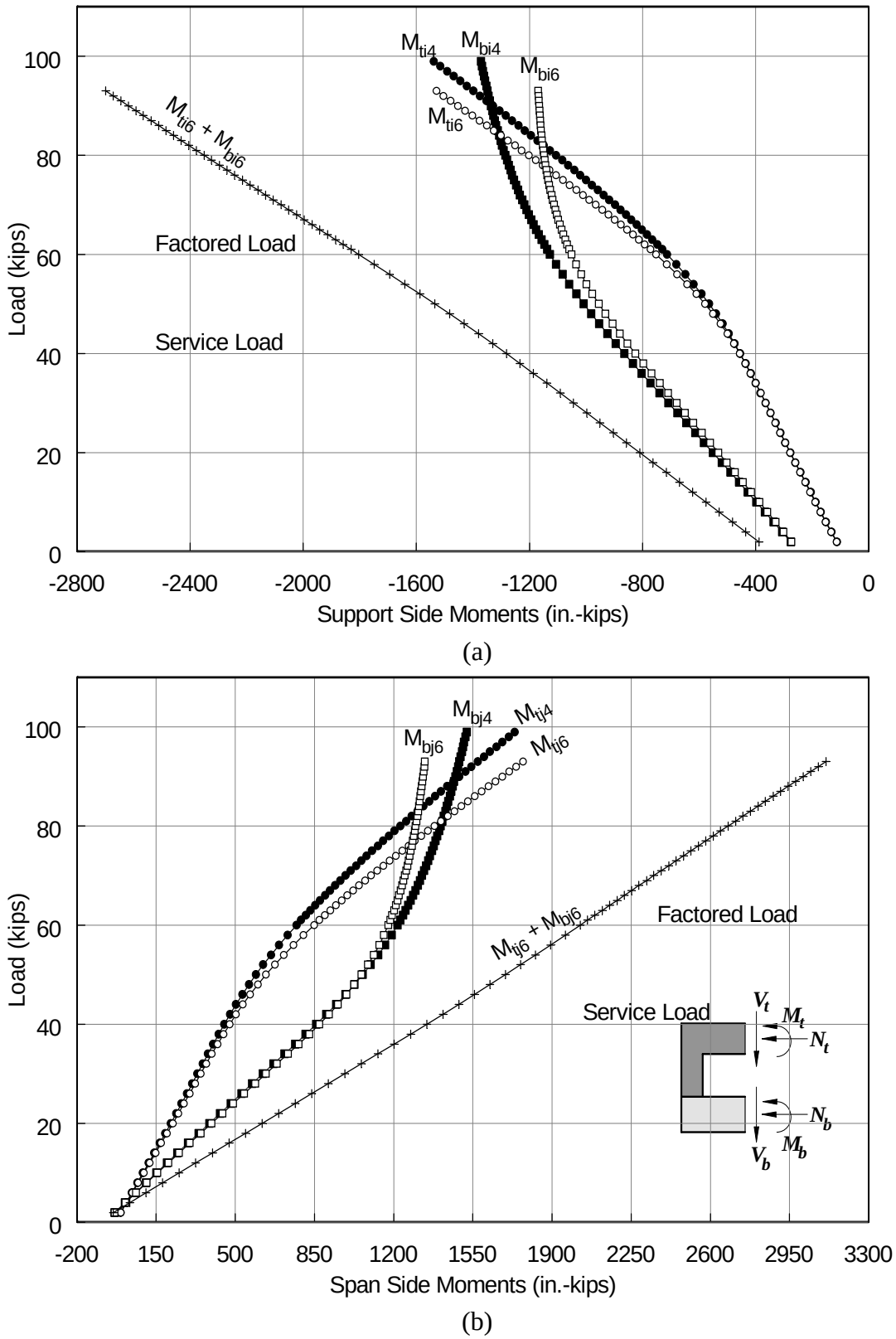

Figure 3.8 Opening 1 chord moments: (a) support side; (b) span side

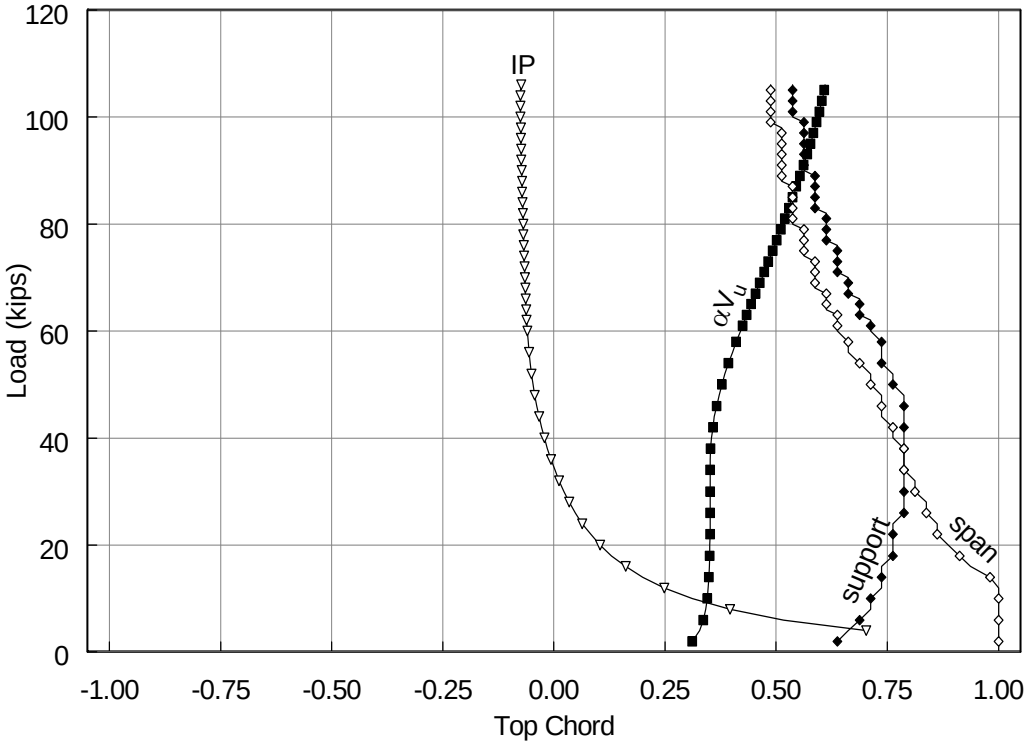

(a)

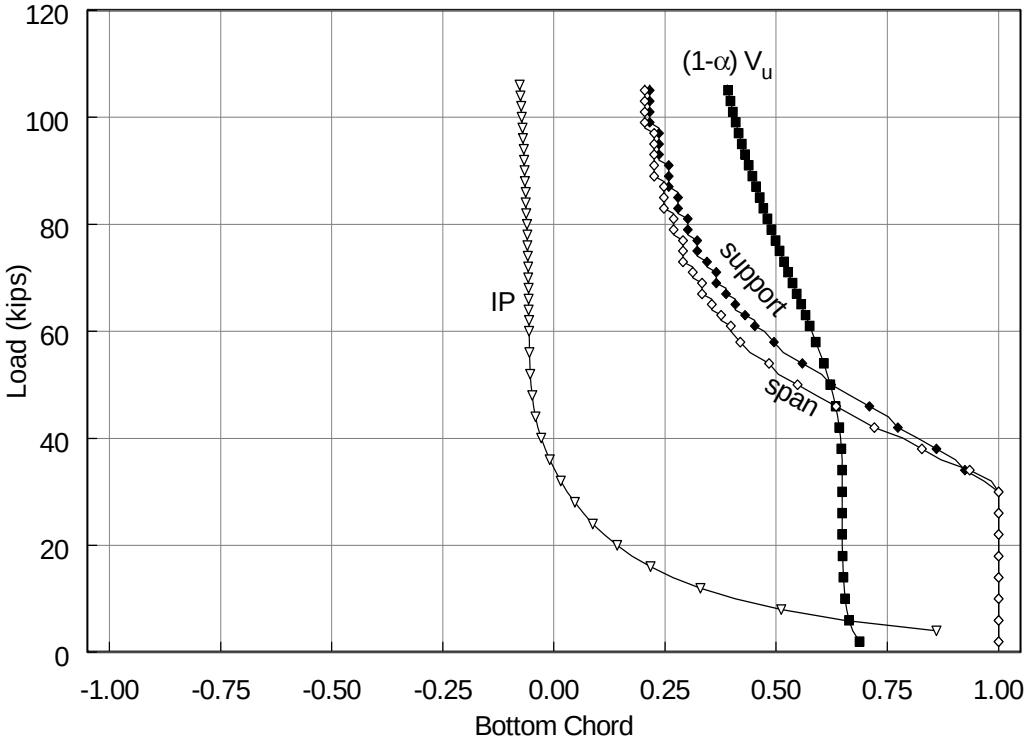

(b)

Figure 3.9 Opening 1 normalized chord parameters for the six load case: (a) top chord; (b) bottom chord

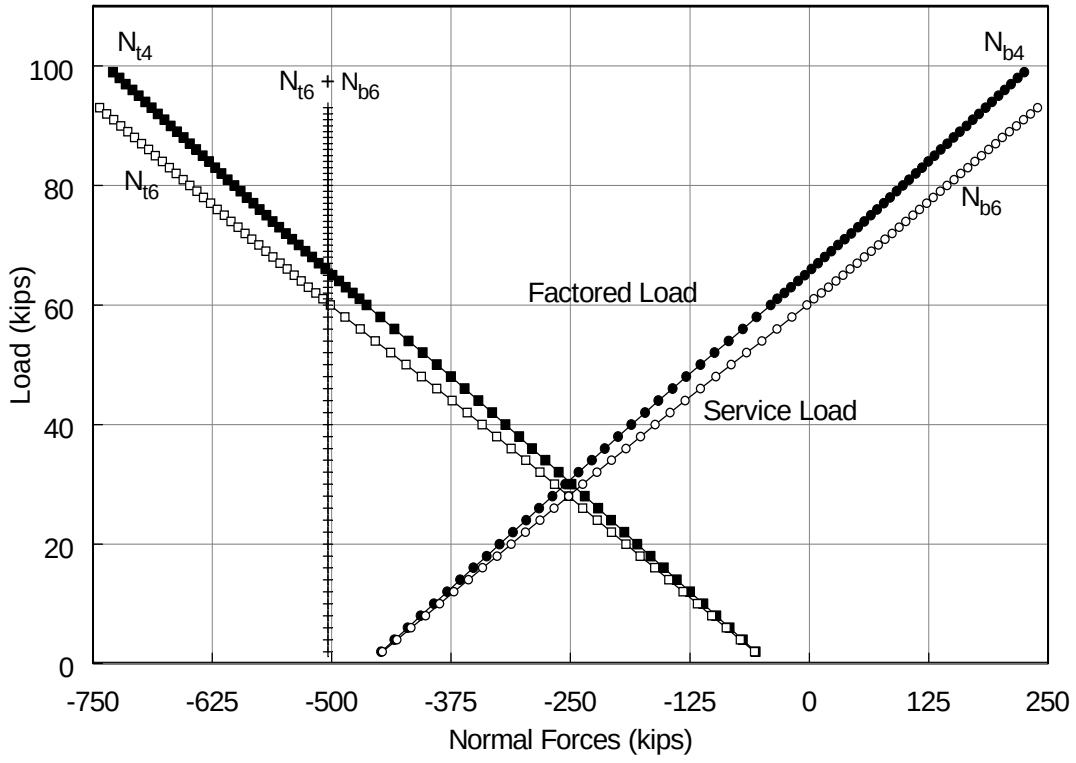

(a)

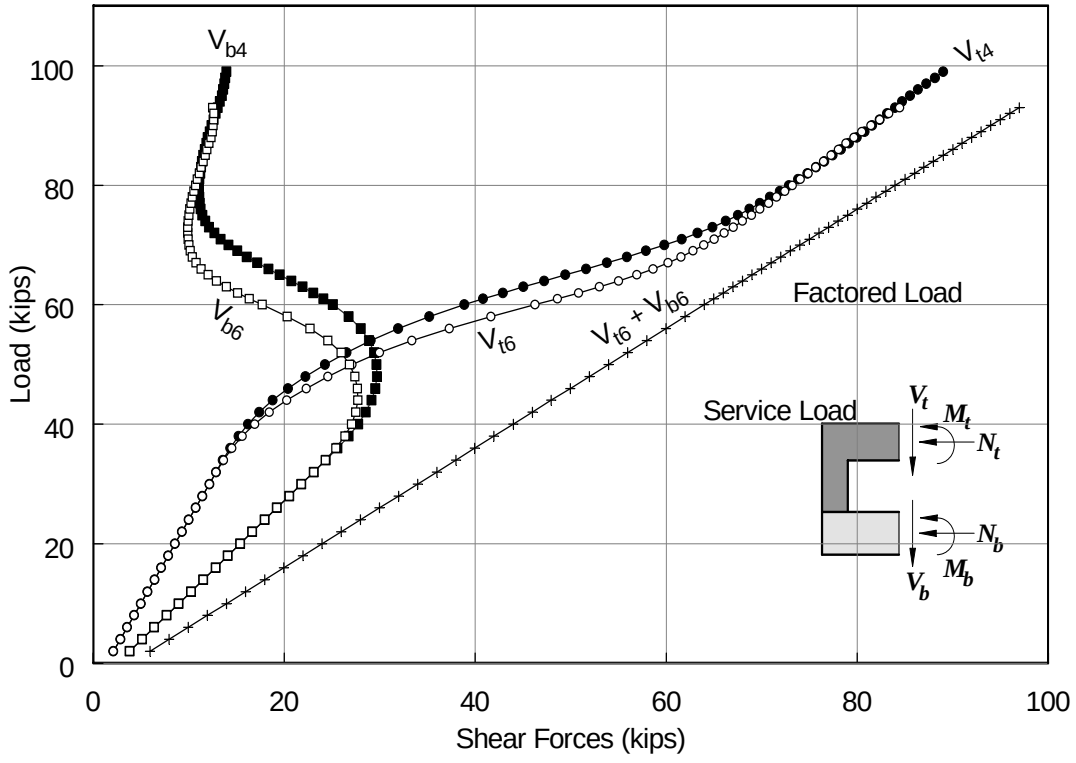

(b)

Figure 3.10 Opening 2 normal and shear forces: (a) normal forces; (b) shear forces

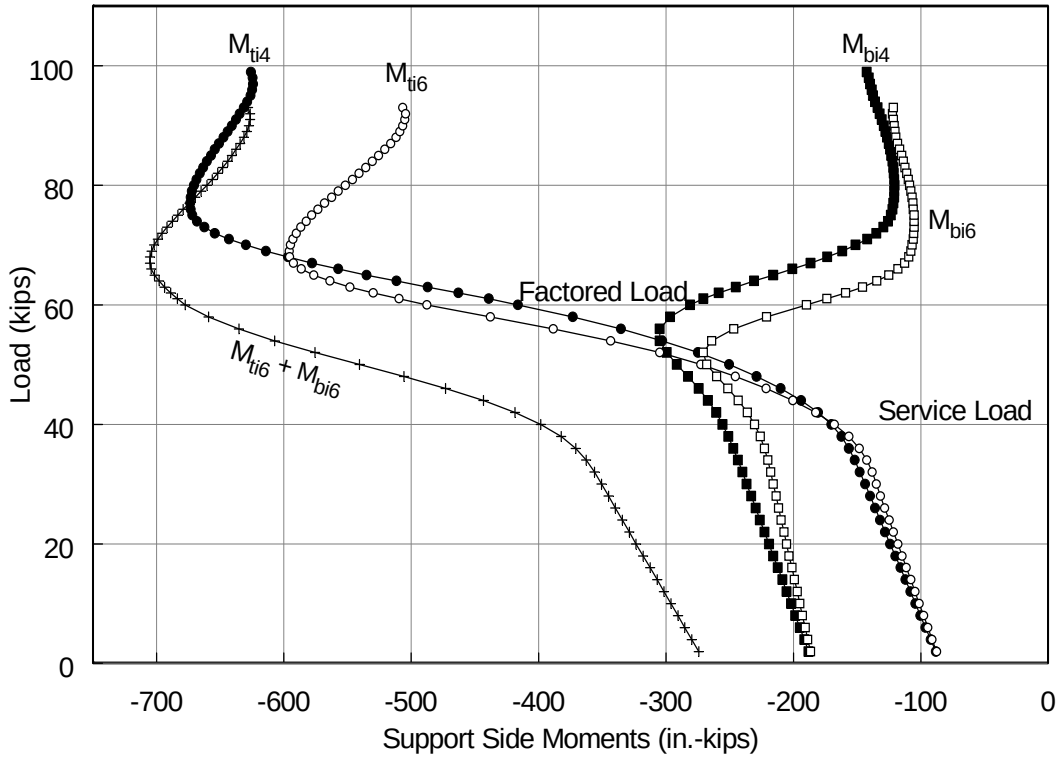

(a)

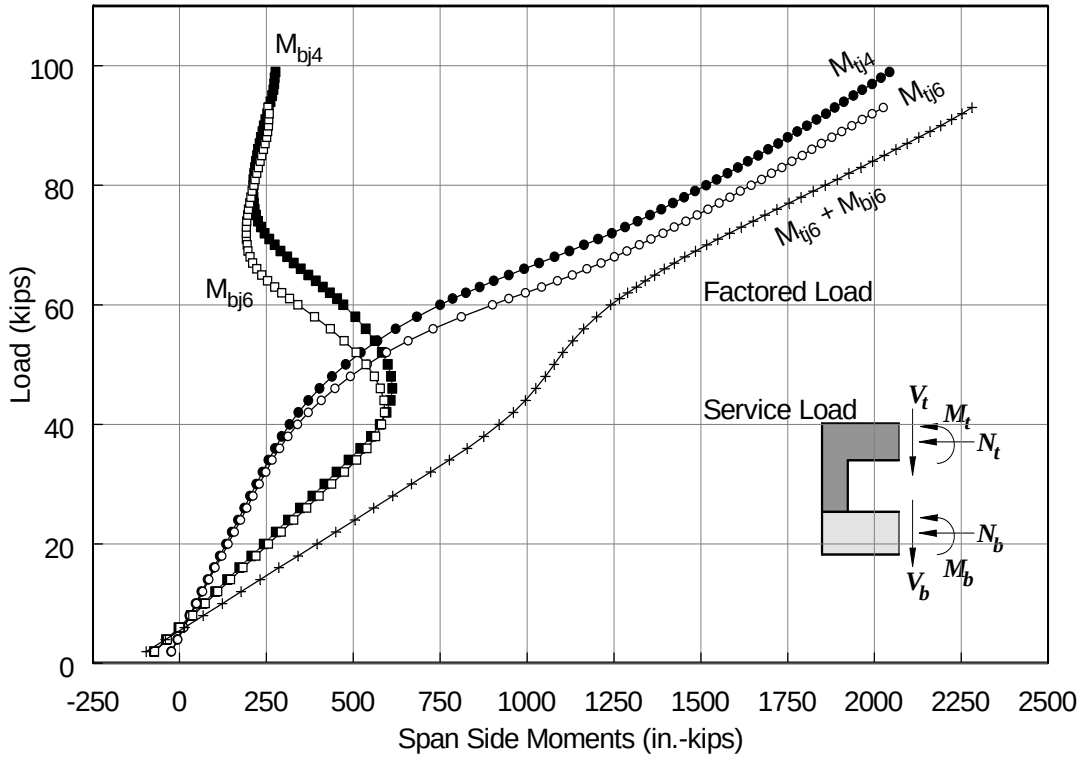

(b)

Figure 3.11 Opening 2 chord moments: (a) support side; (b) span side

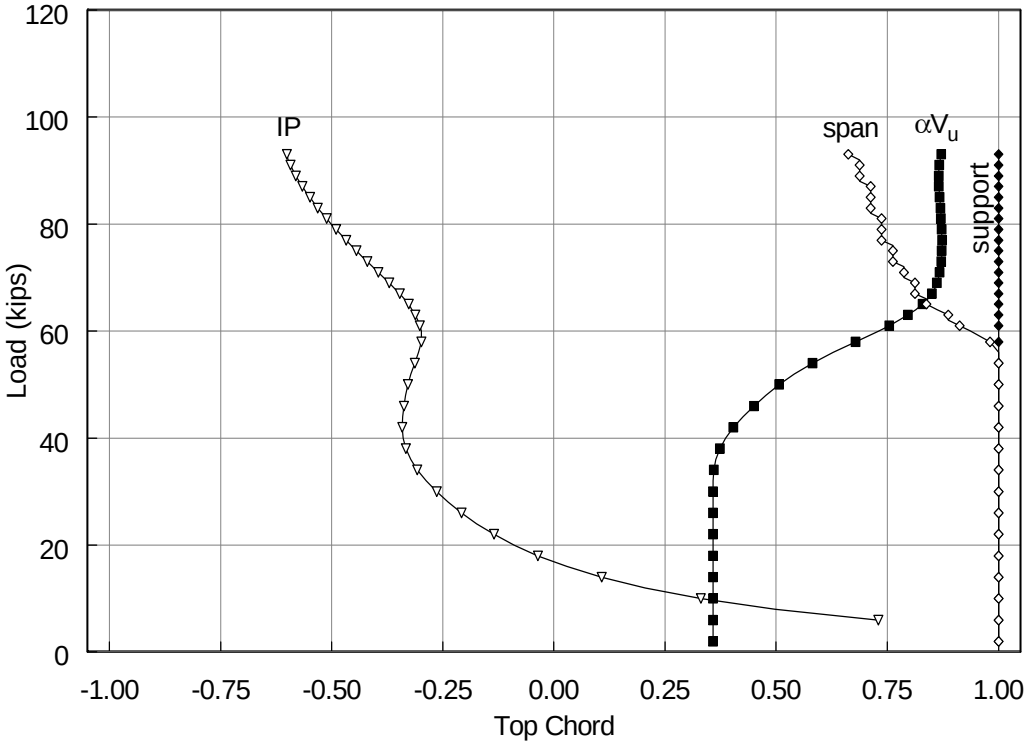

(a)

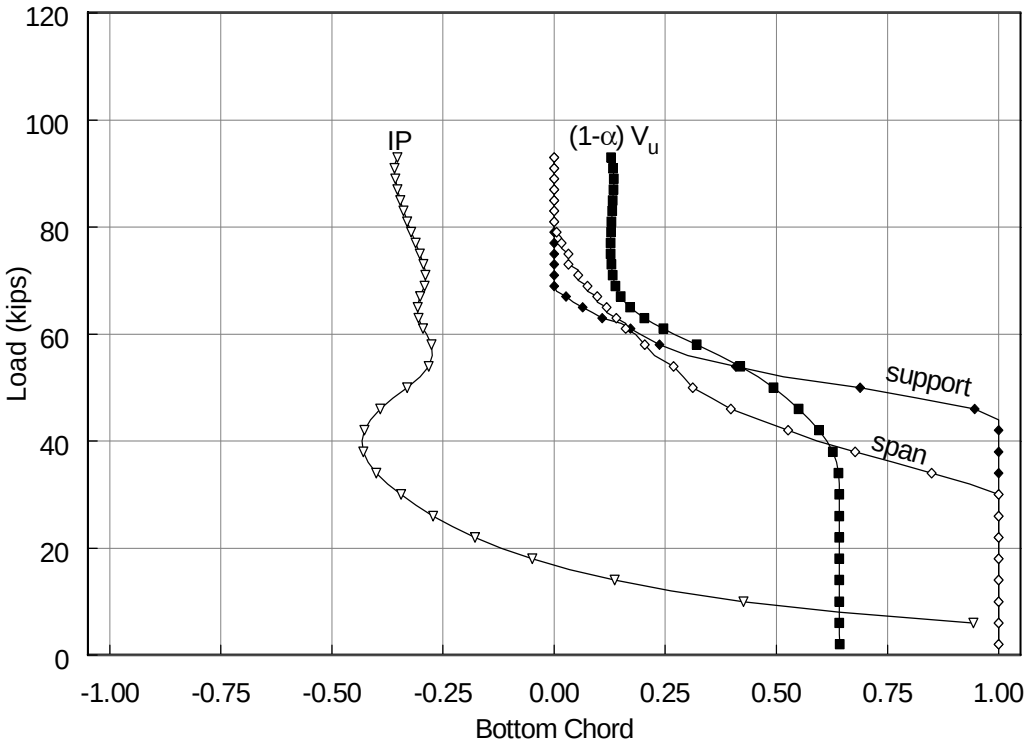

(b)

Figure 3.12 Opening 2 normalized chord parameters for the six load case: (a) top chord; (b) bottom chord

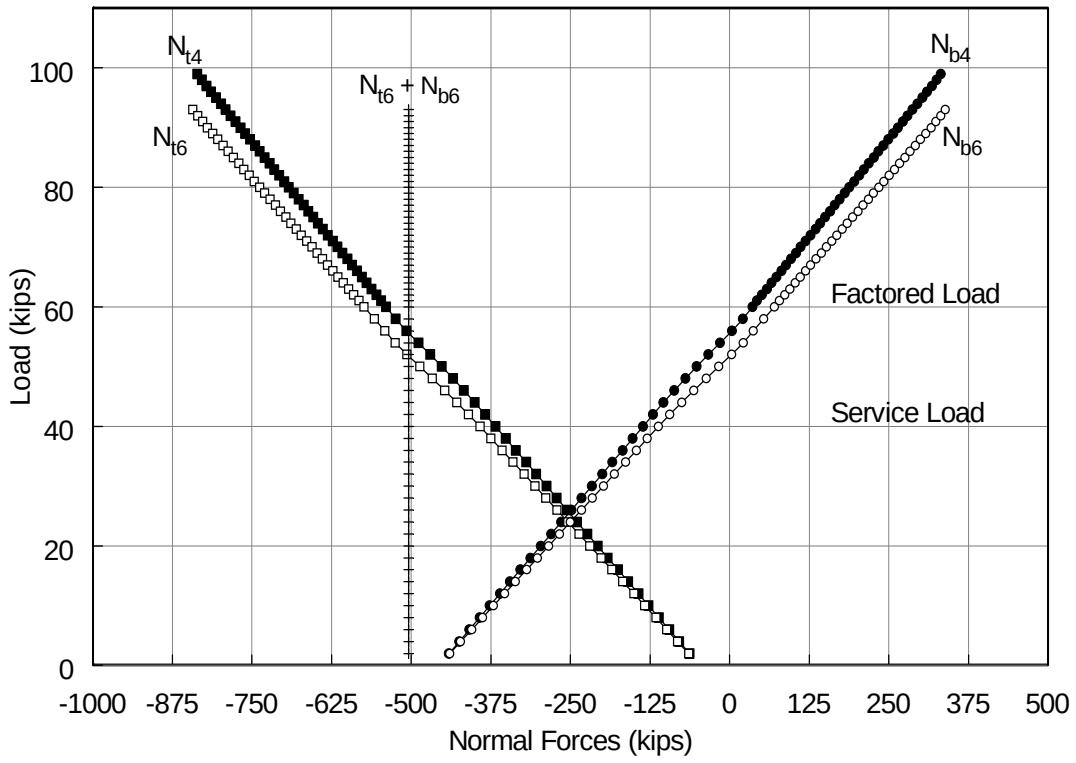

(a)

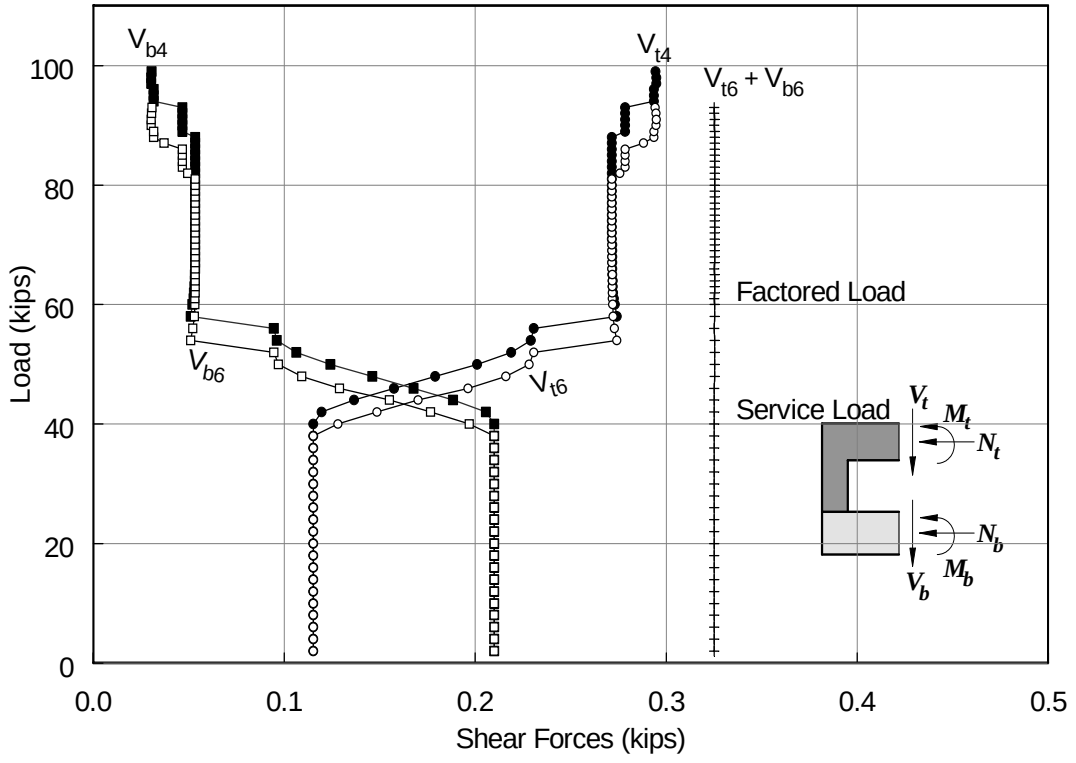

(b)

Figure 3.13 Opening 3 normal and shear forces: (a) normal force; (b) shear force

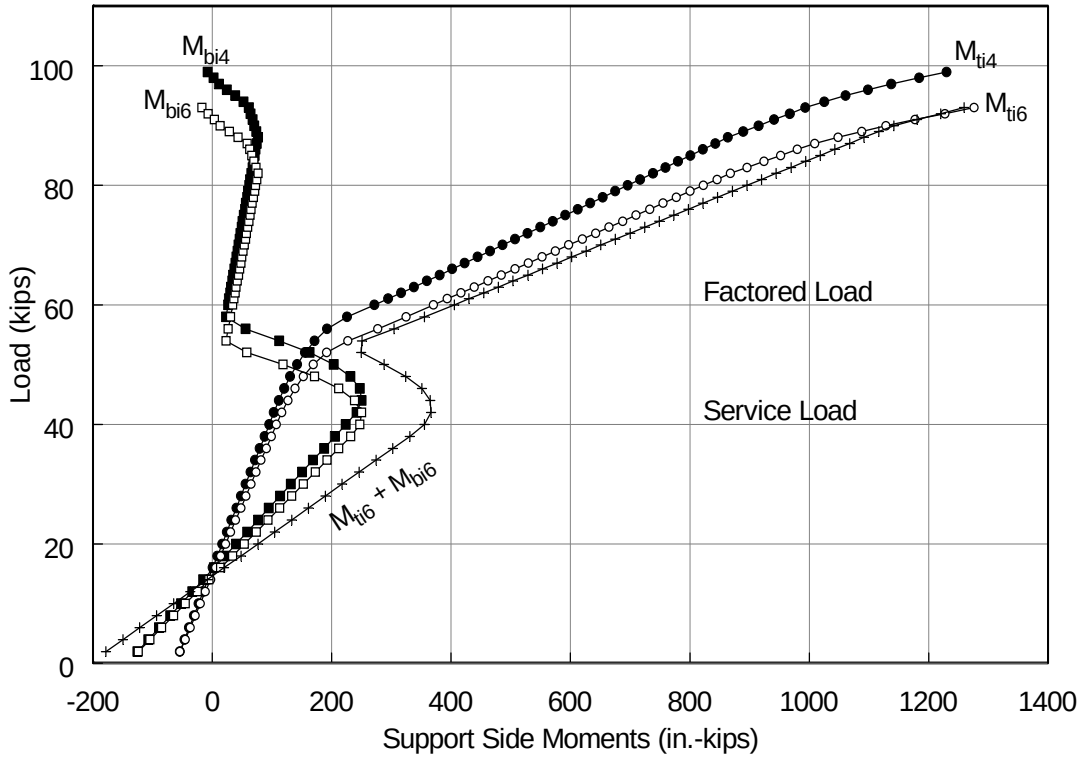

(a)

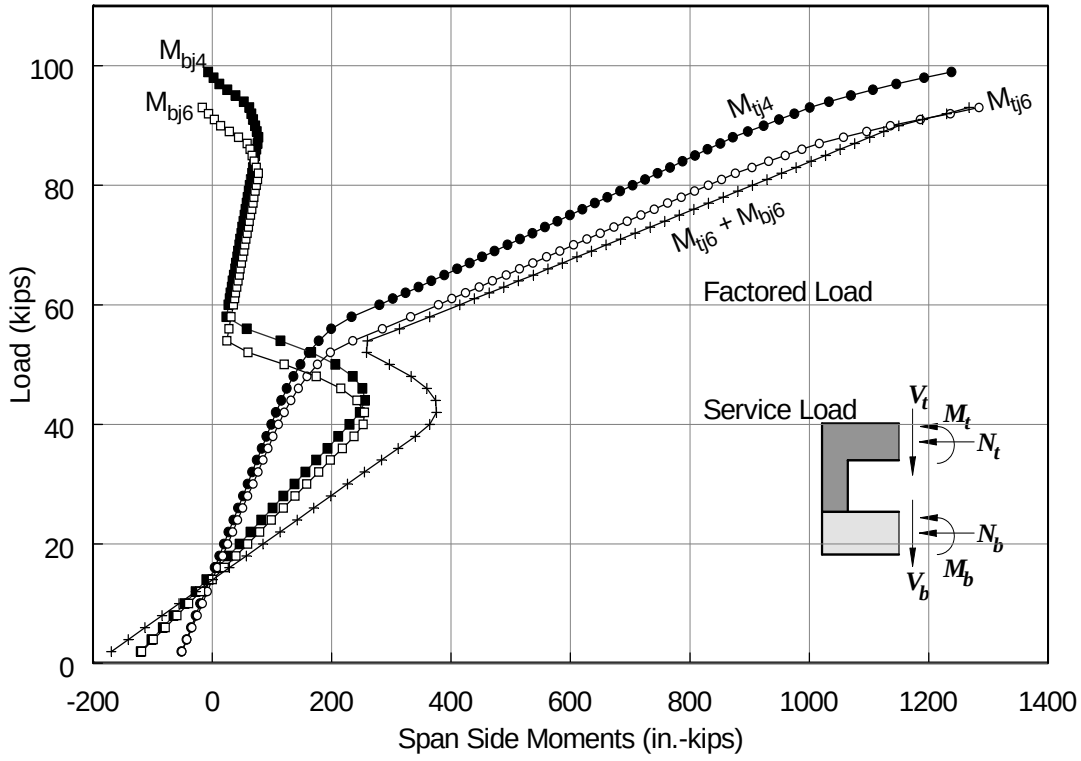

(b)

Figure 3.14 Opening 3 chord moments: (a) support side; (b) span side

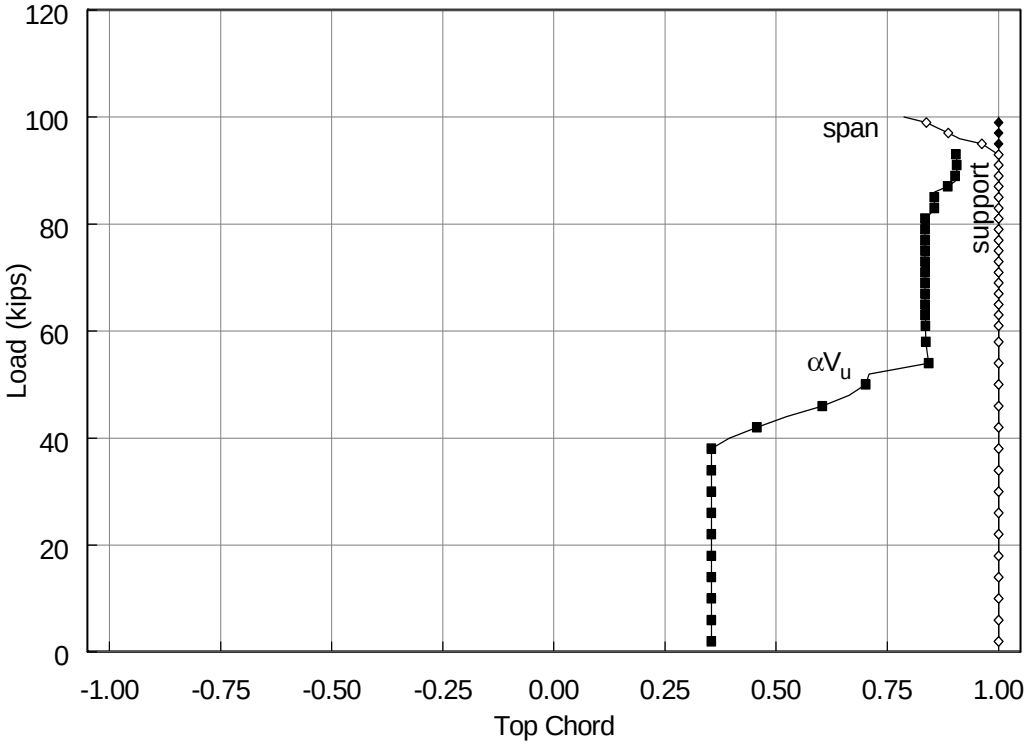

(a)

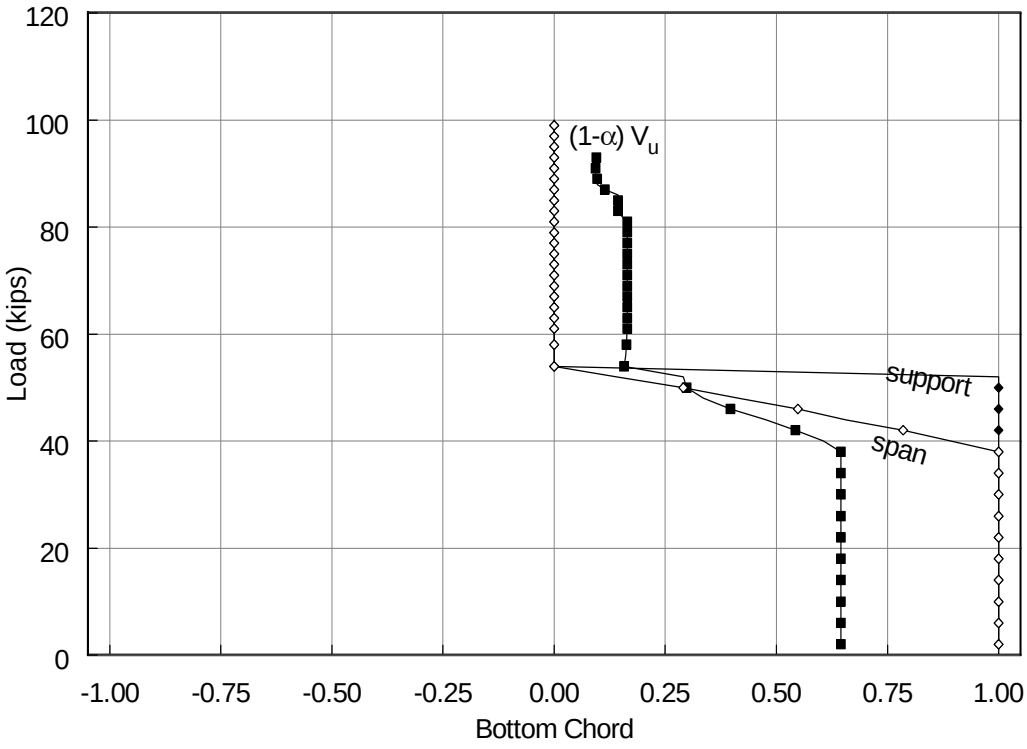

(b)

Figure 3.15 Opening 3 normalized chord forces for the six load case: (a) top chord; (b) bottom chord

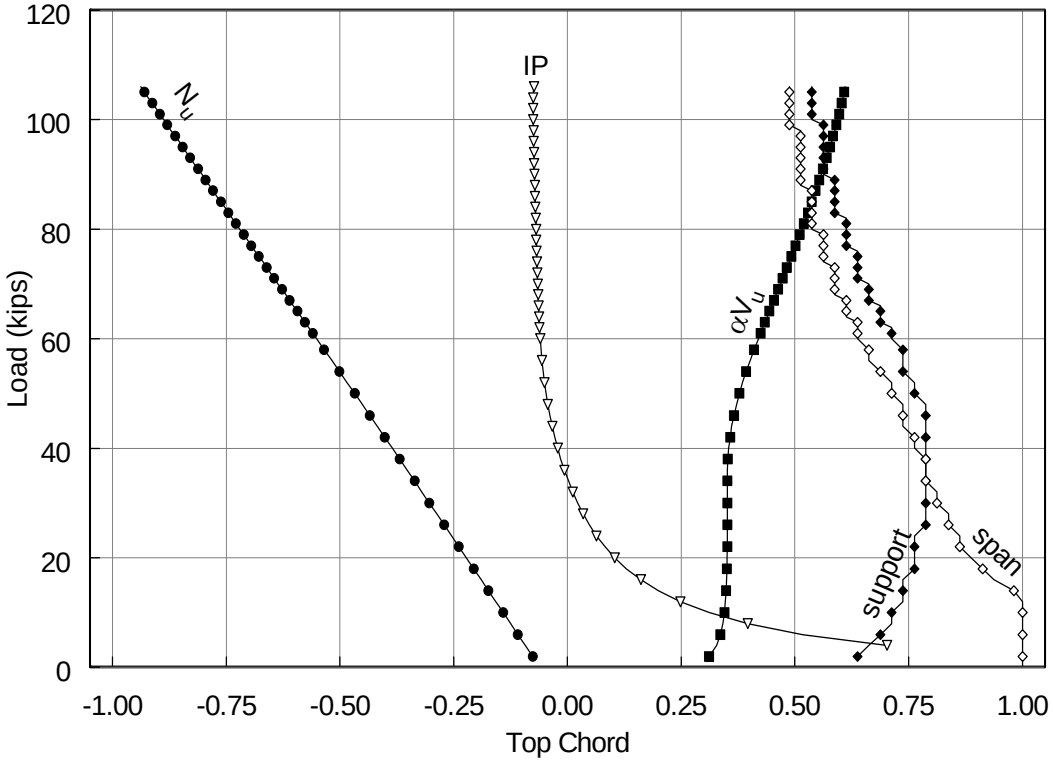

(a)

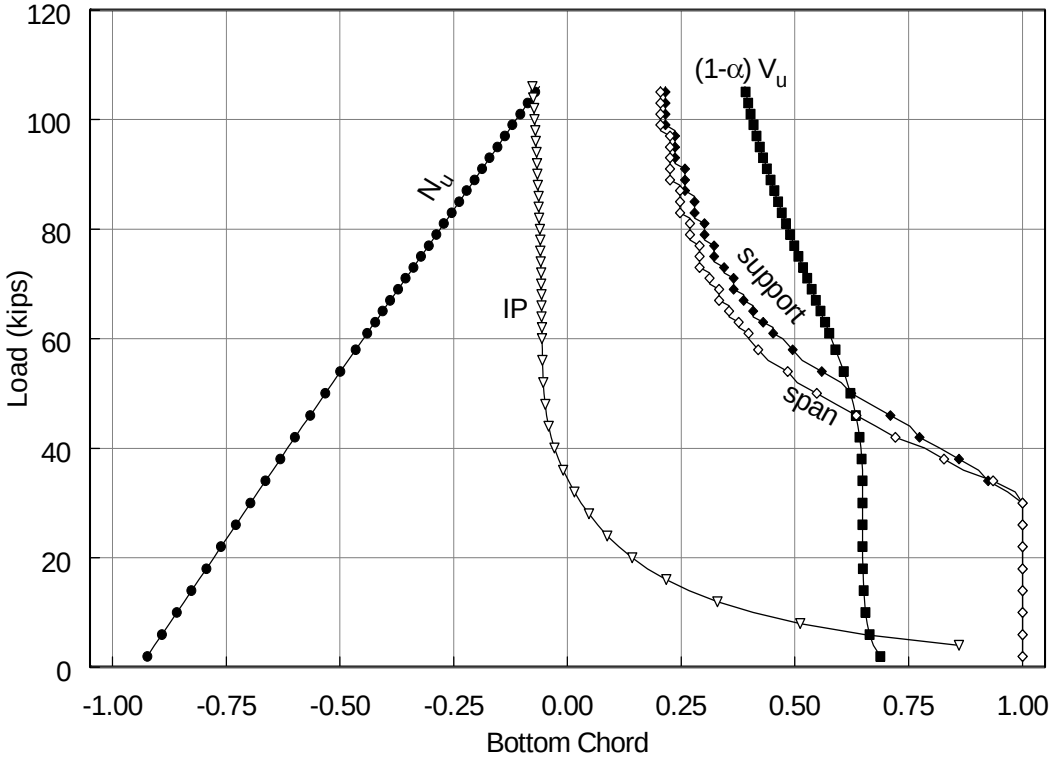

(b)

Figure 3.16 Opening 1 normalized chord parameters: Reference

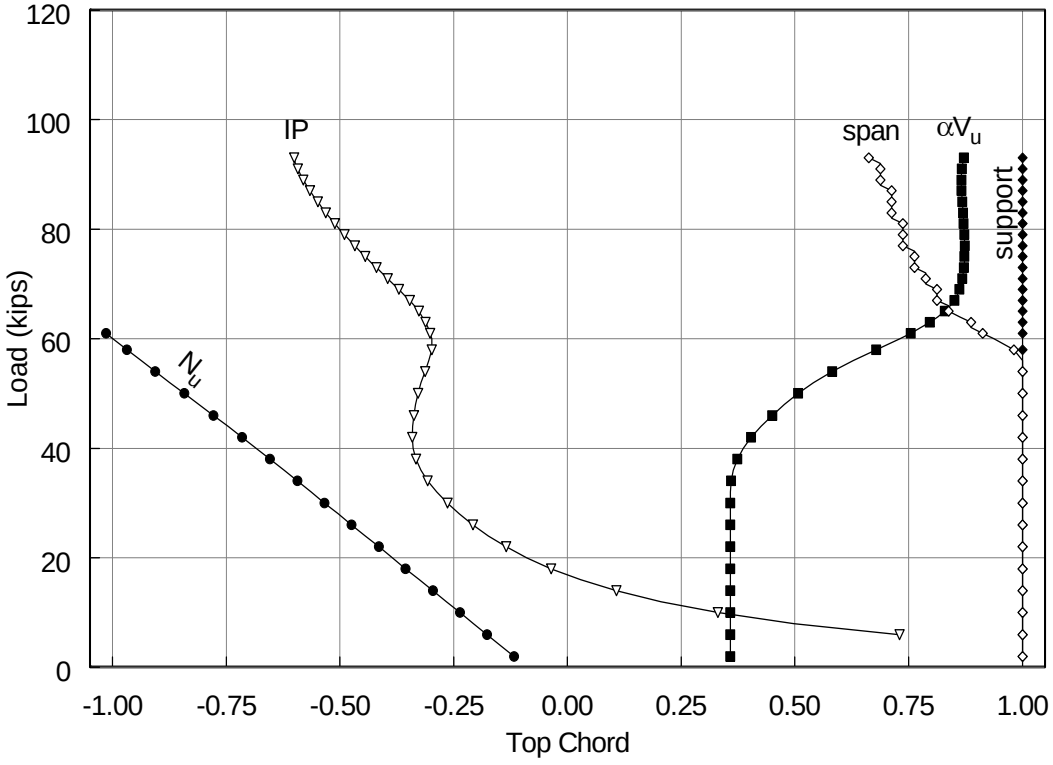

(a)

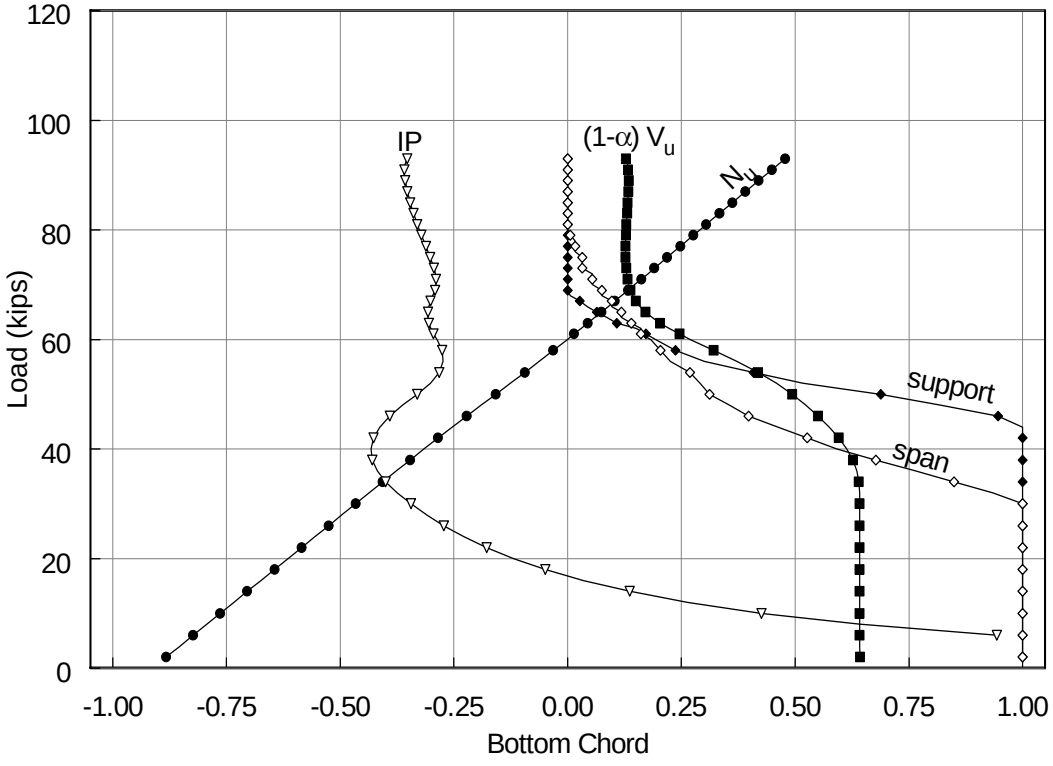

(b)

Figure 3.17 Opening 2 normalized chord parameters: Reference

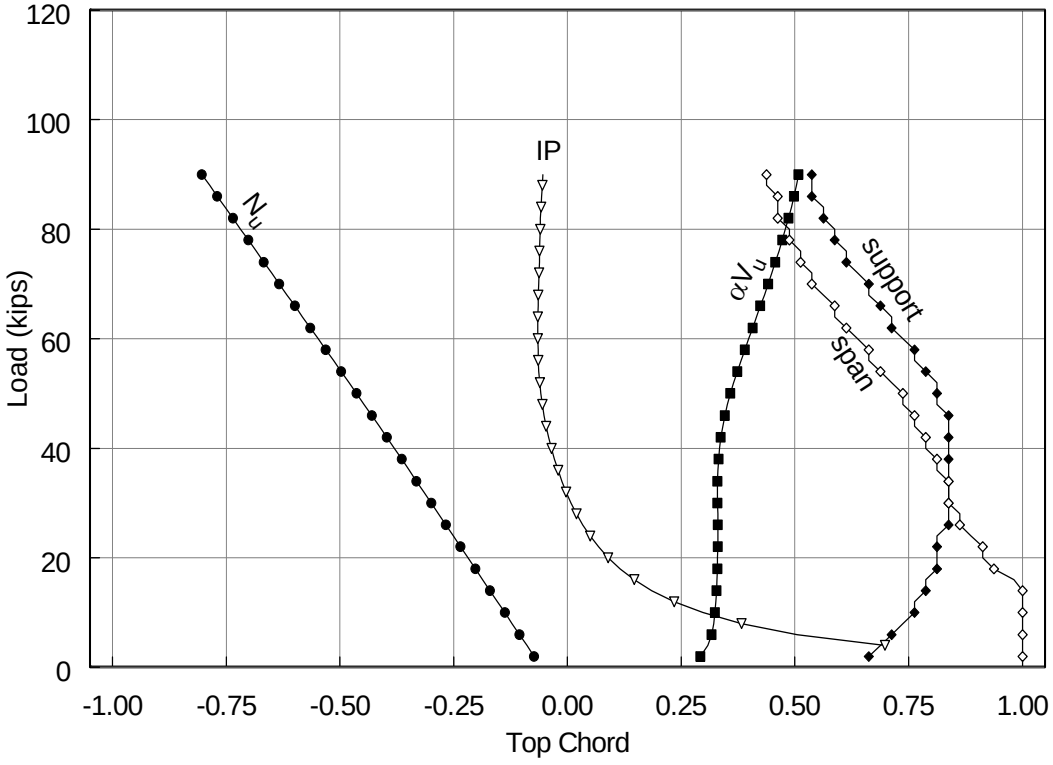

(a)

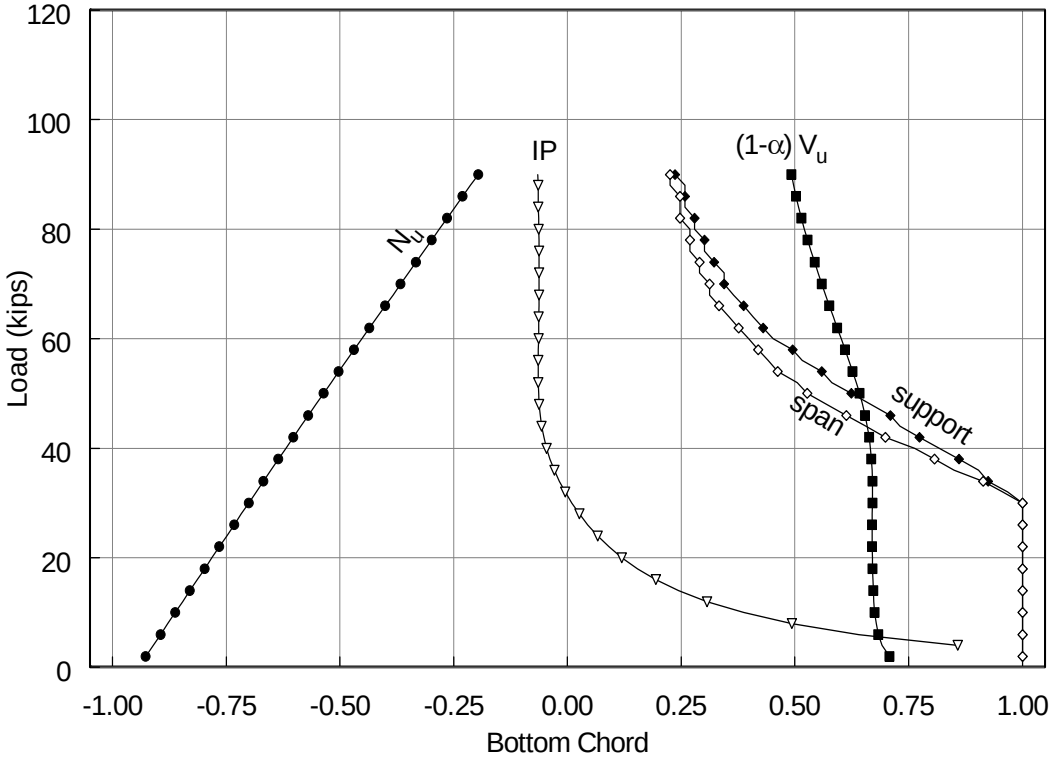

(b)

Figure 3.18 Opening 1 normalized chord parameters: TCS-3

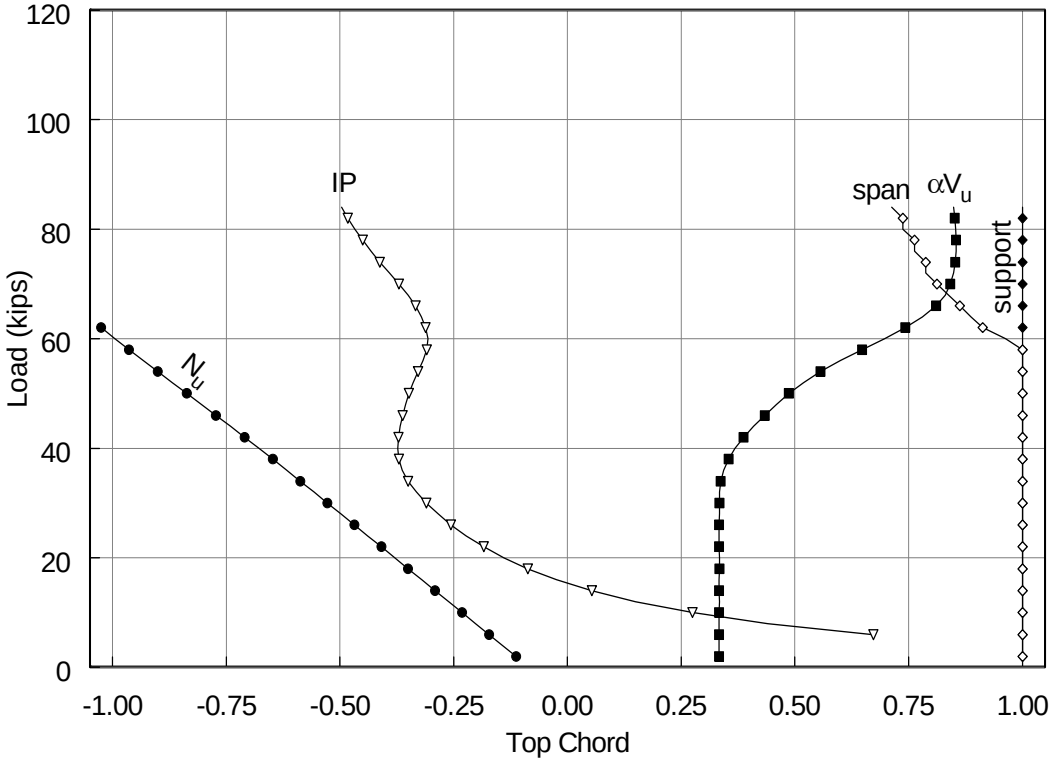

(a)

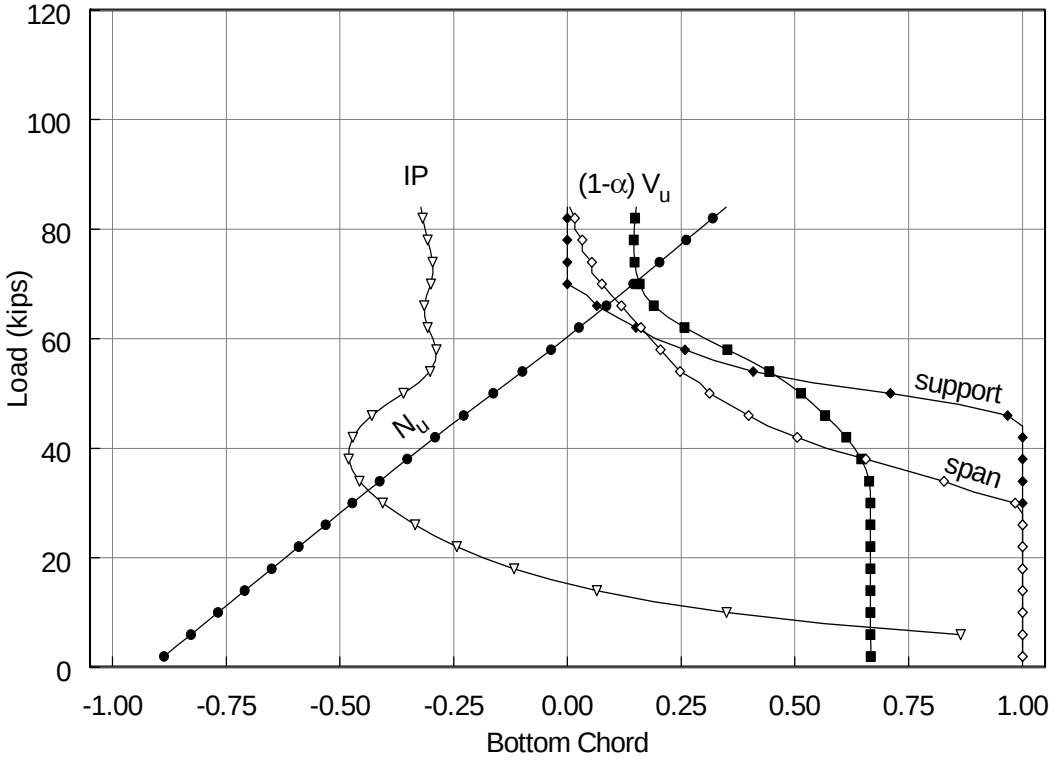

(b)

Figure 3.19 Opening 2 normalized chord parameters: TCS-3

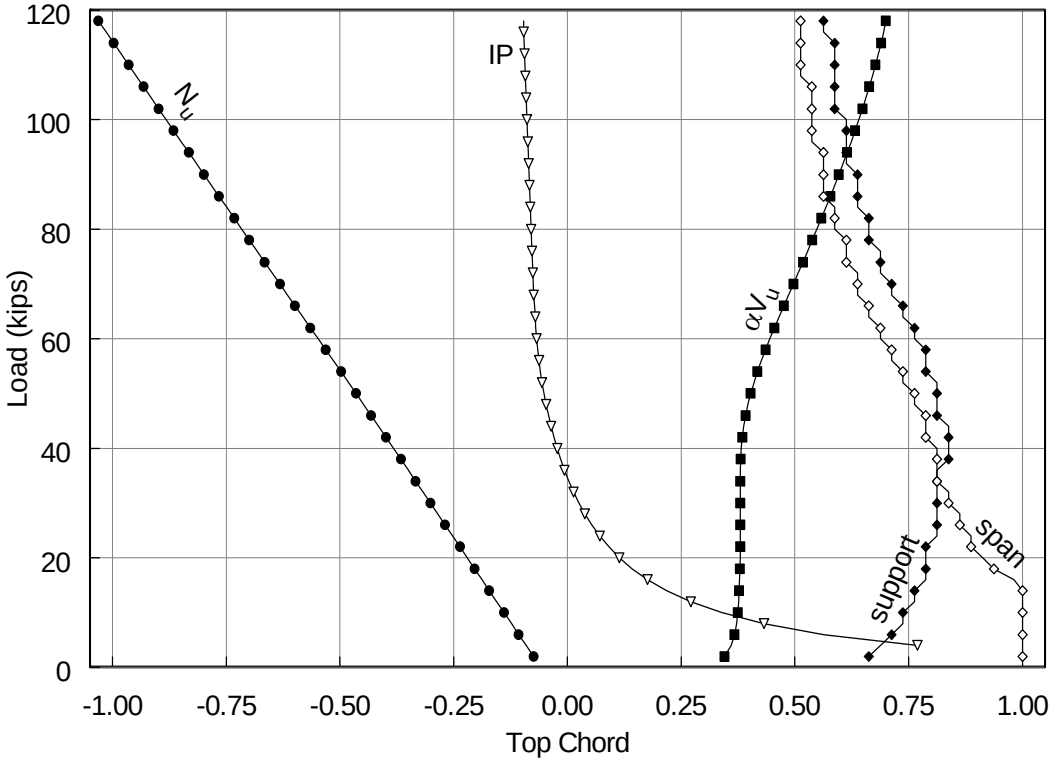

(a)

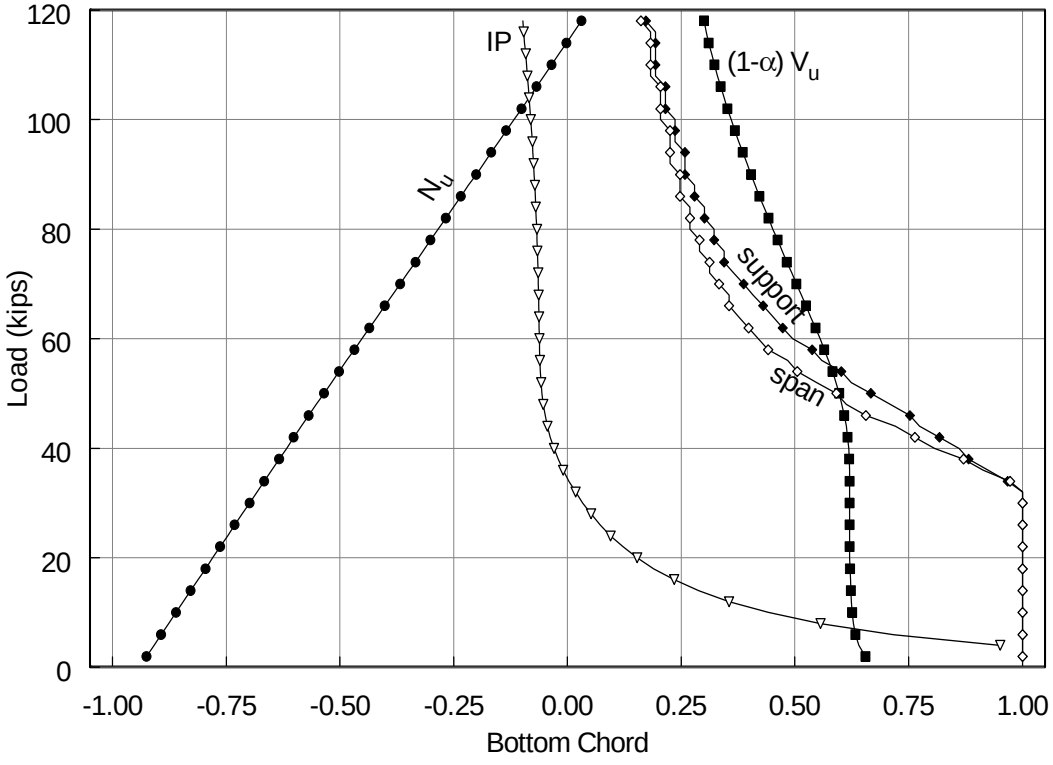

(b)

Figure 3.20 Opening 1 normalized chord parameters: TCD-1

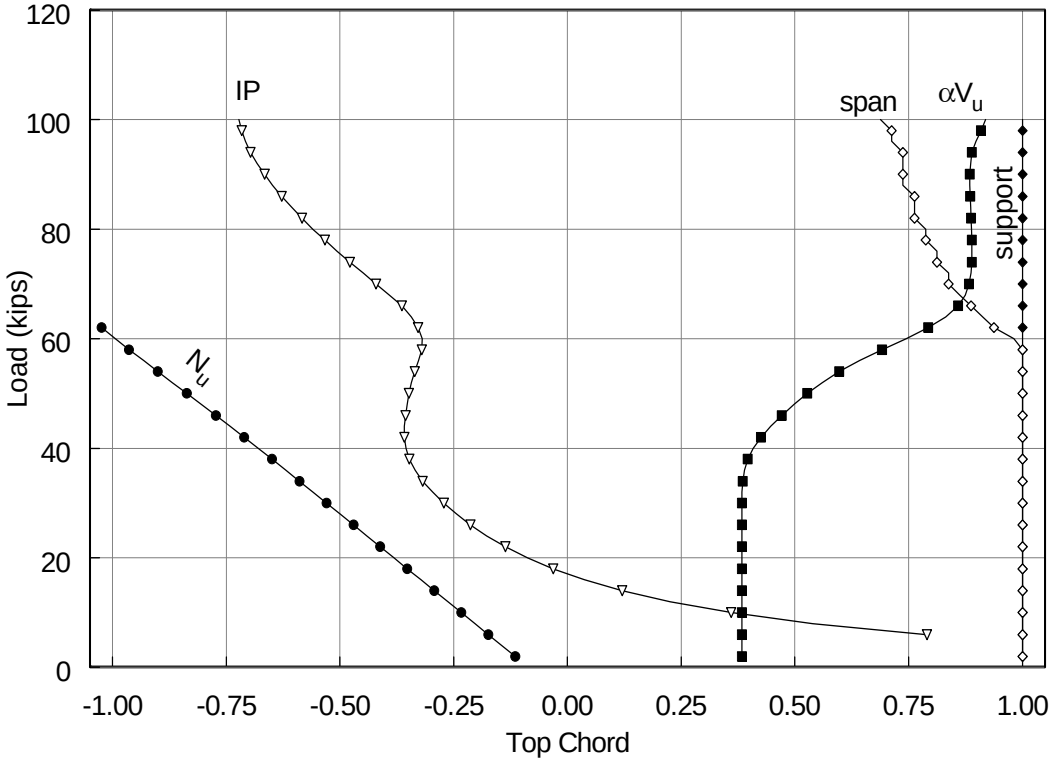

(a)

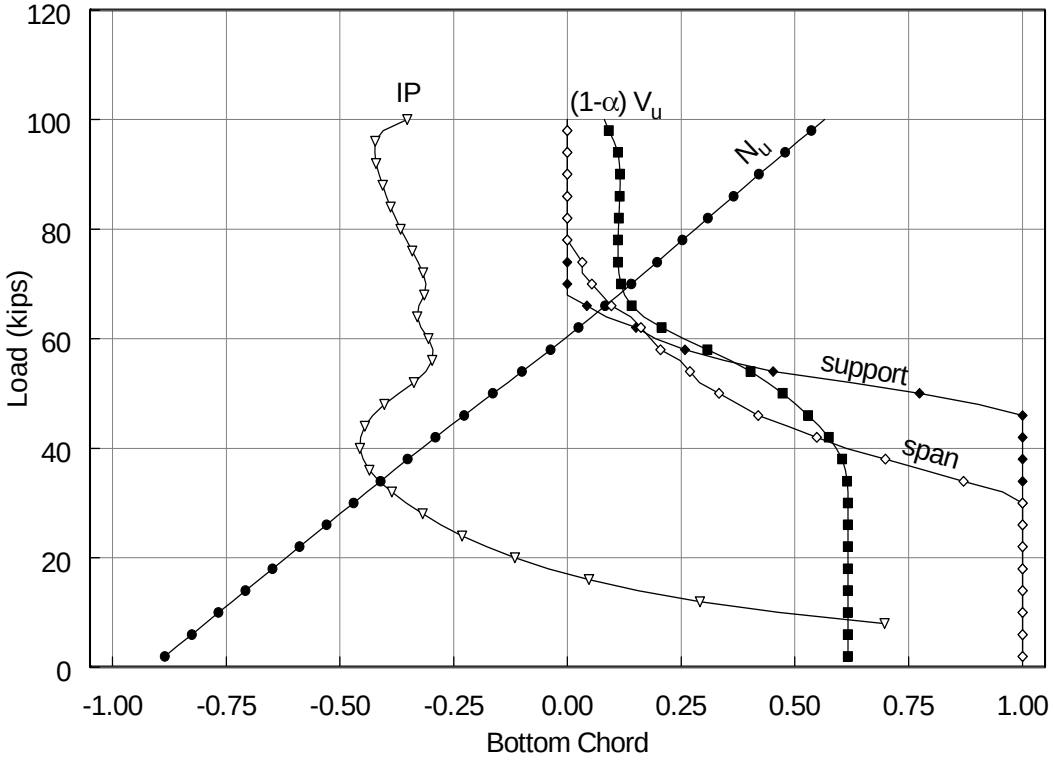

(b)

Figure 3.21 Opening 2 normalized chord parameters: TCD-1

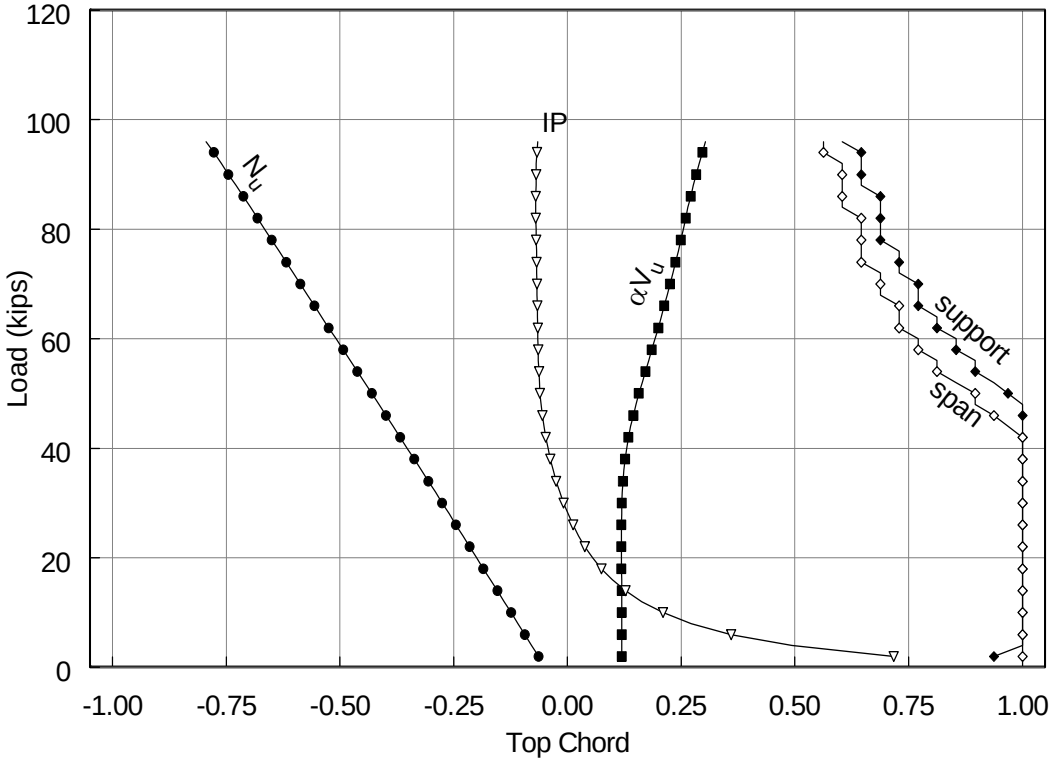

(a)

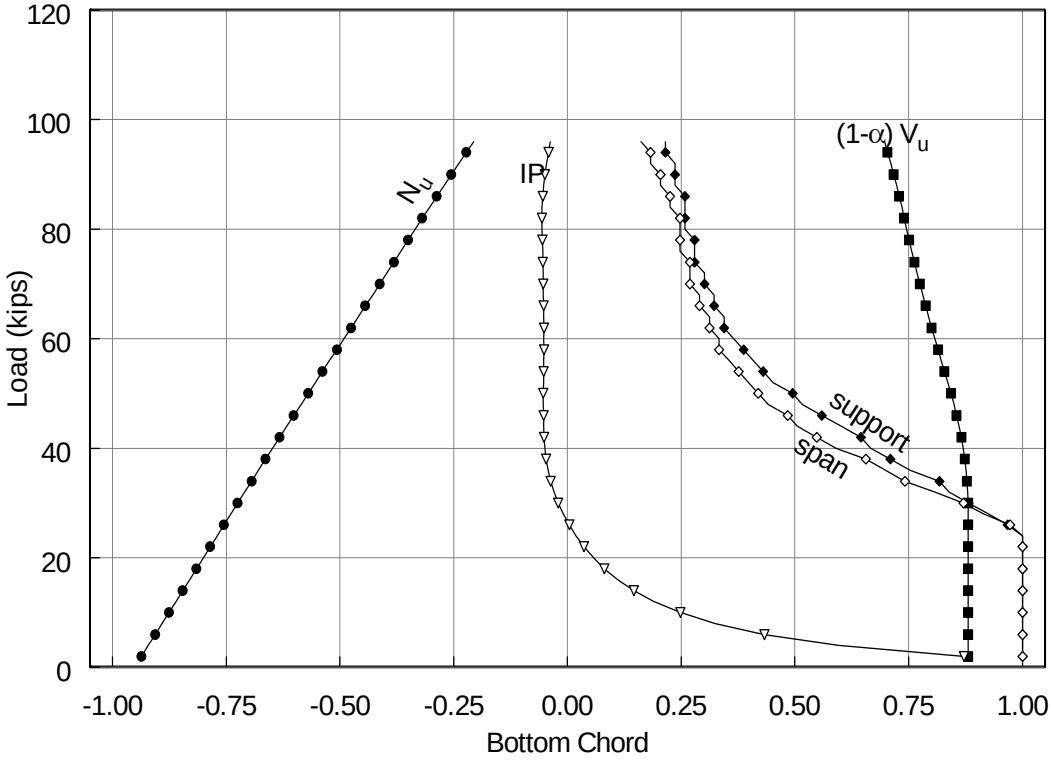

(b)

Figure 3.22 Opening 1 normalized chord parameters: TCD-3

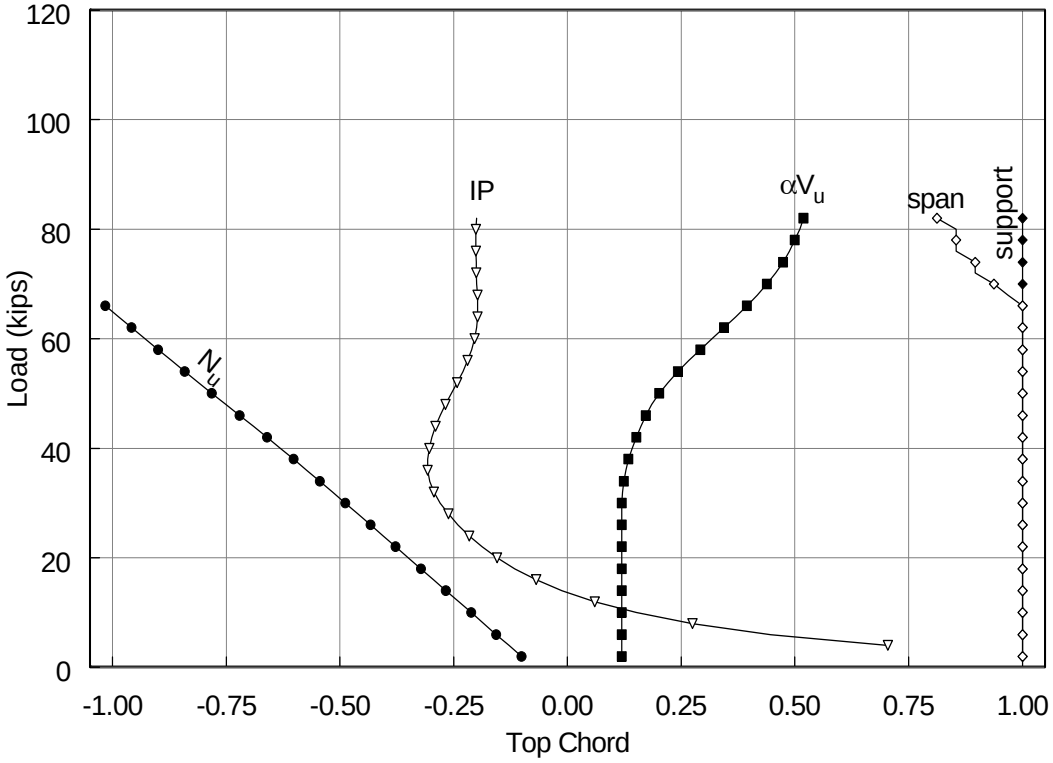

(a)

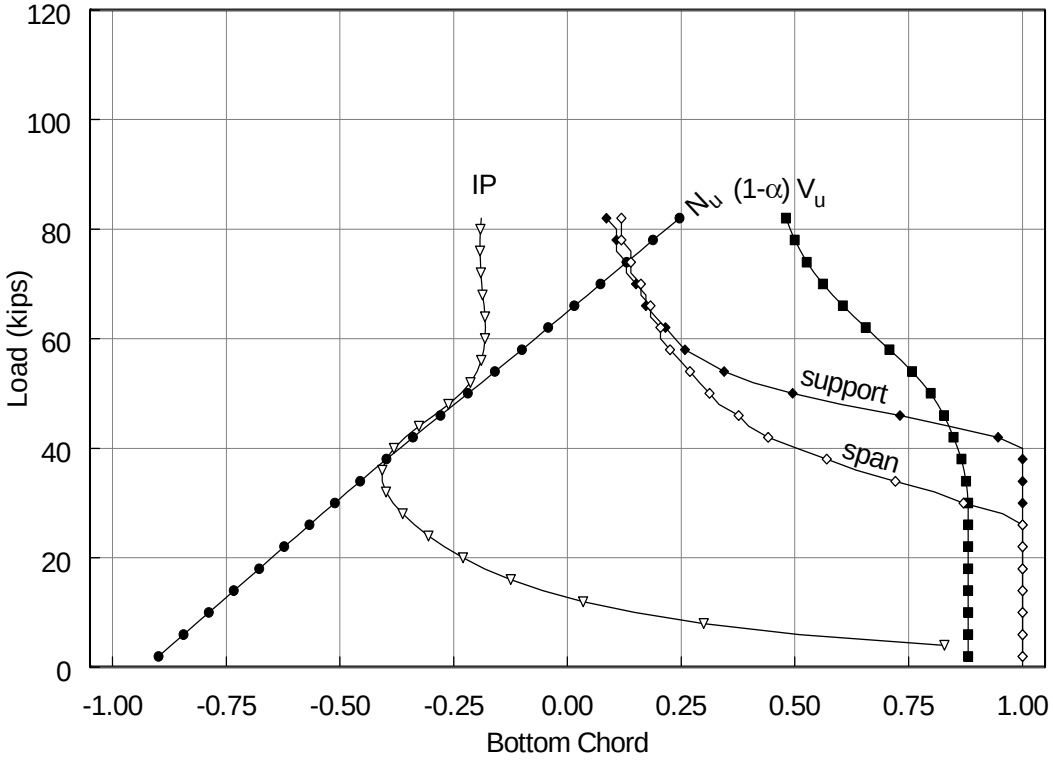

(b)

Figure 3.23 Opening 2 normalized chord parameters: TCD-3

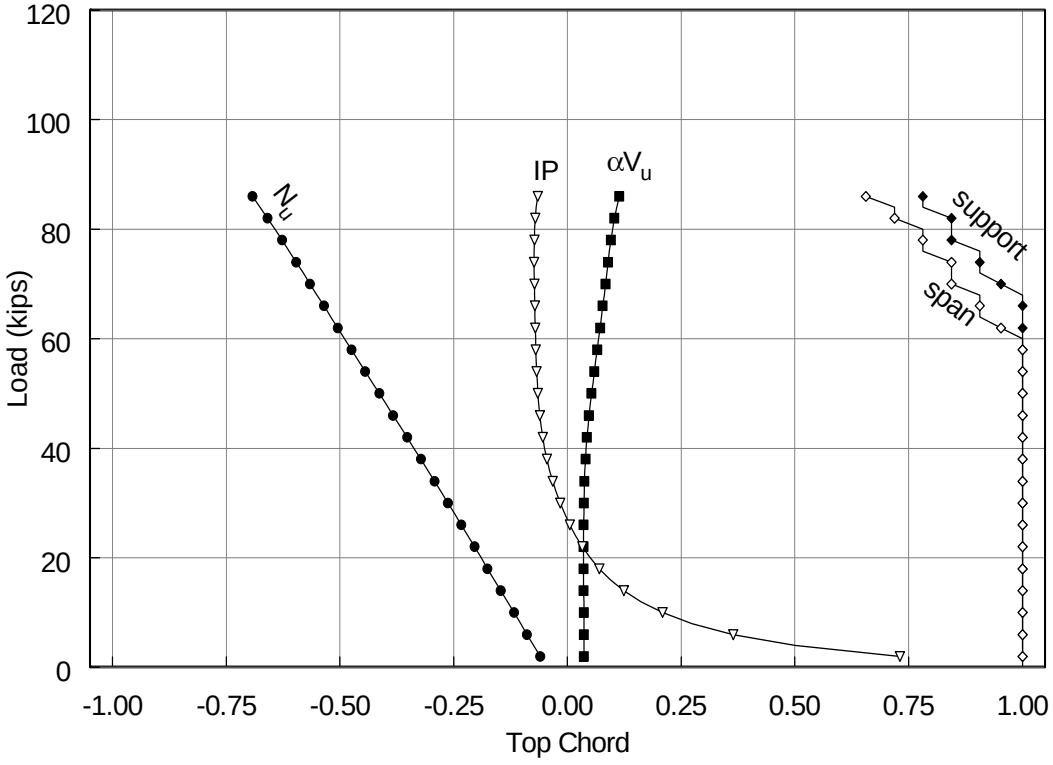

(a)

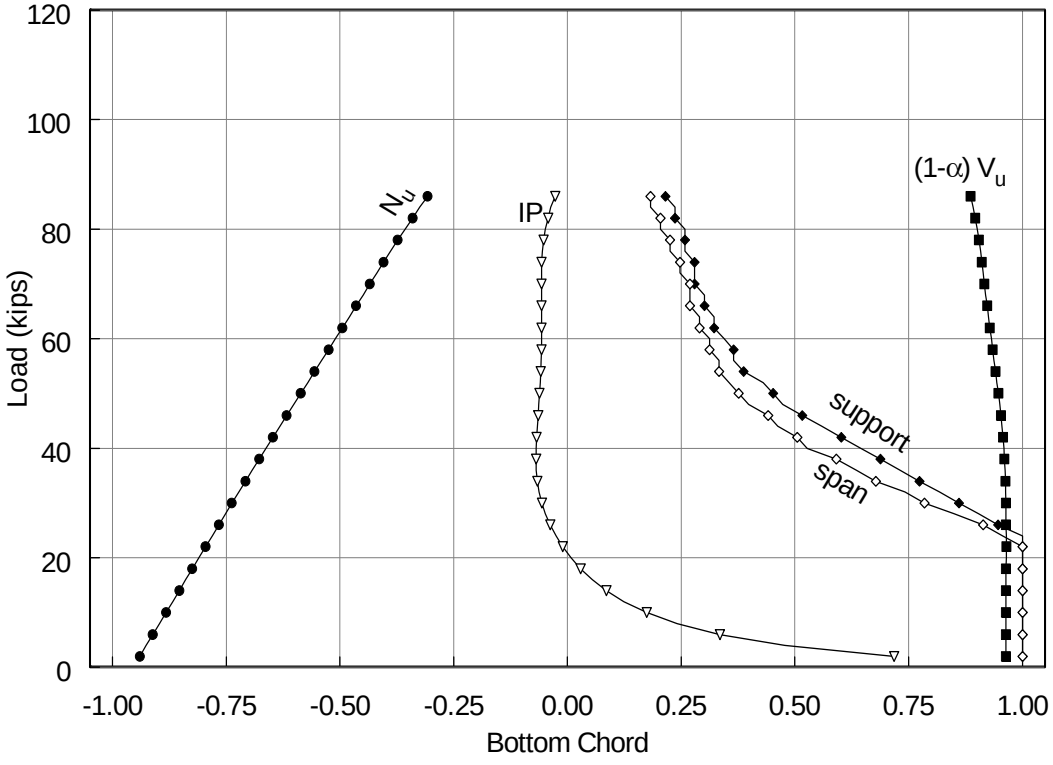

(b)

Figure 3.24 Opening 1 normalized chord parameters: TCD-4

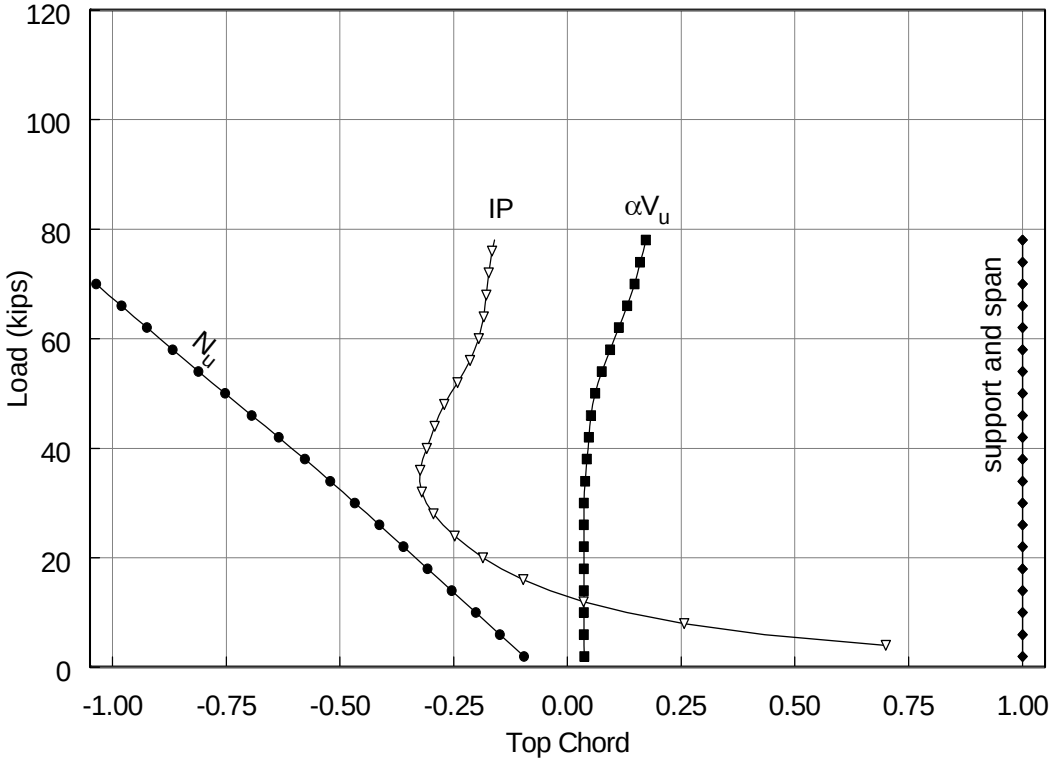

(a)

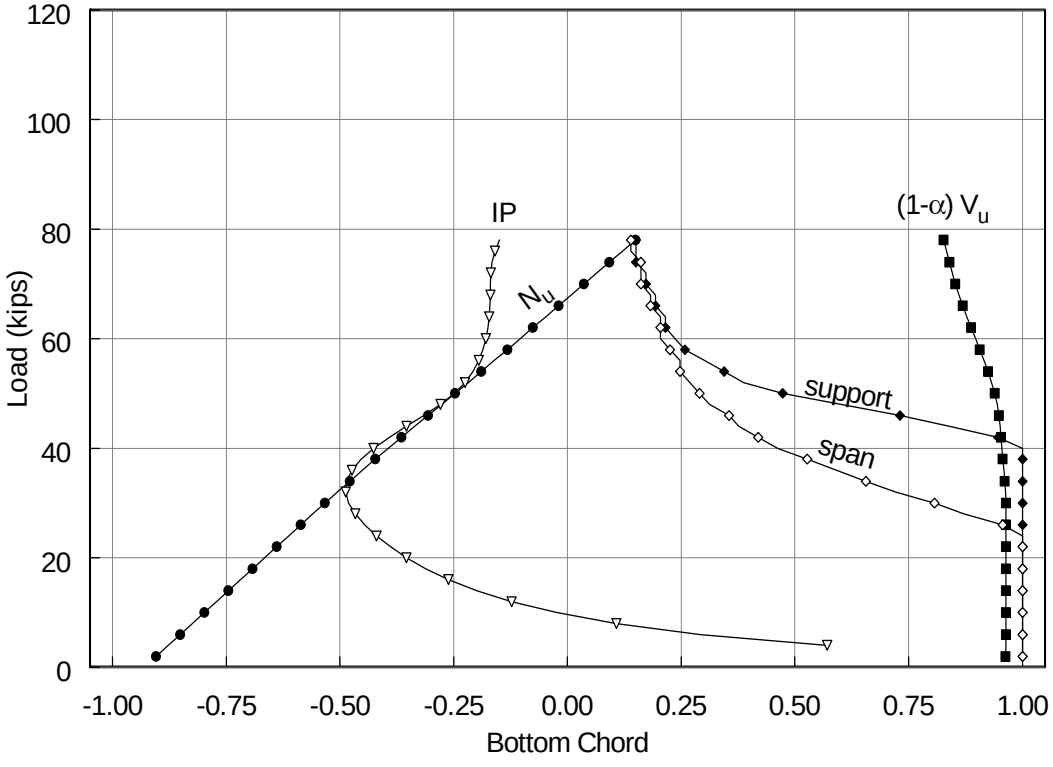

(b)

Figure 3.25 Opening 2 normalized chord parameters: TCD-4

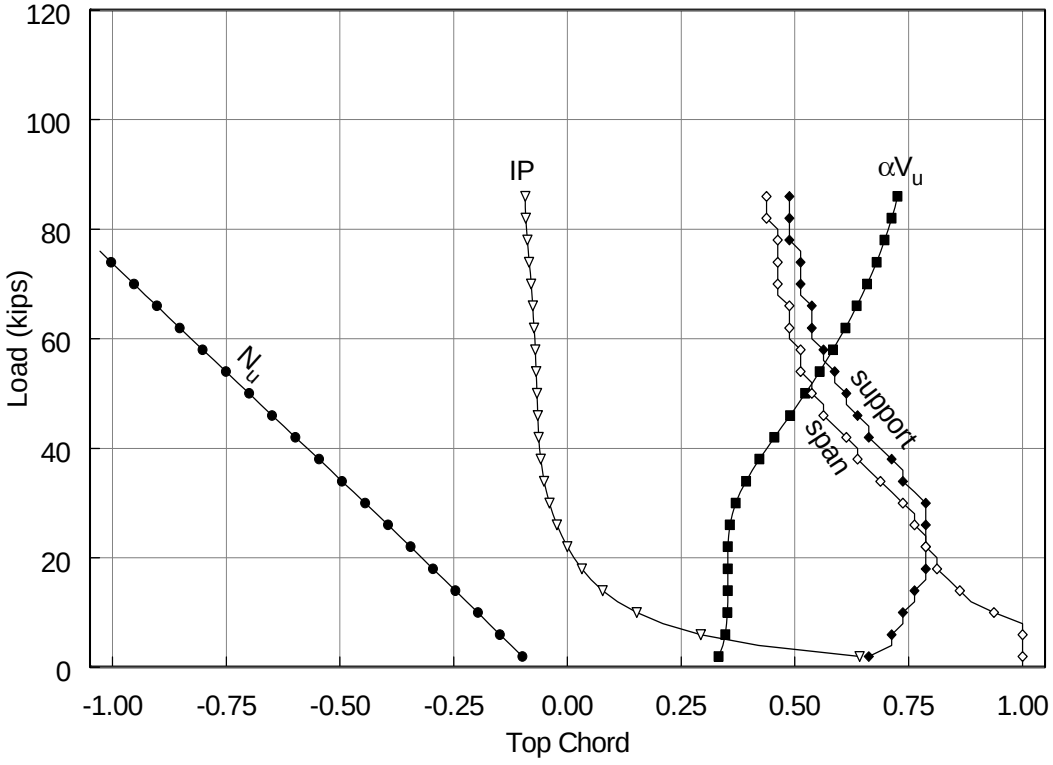

(a)

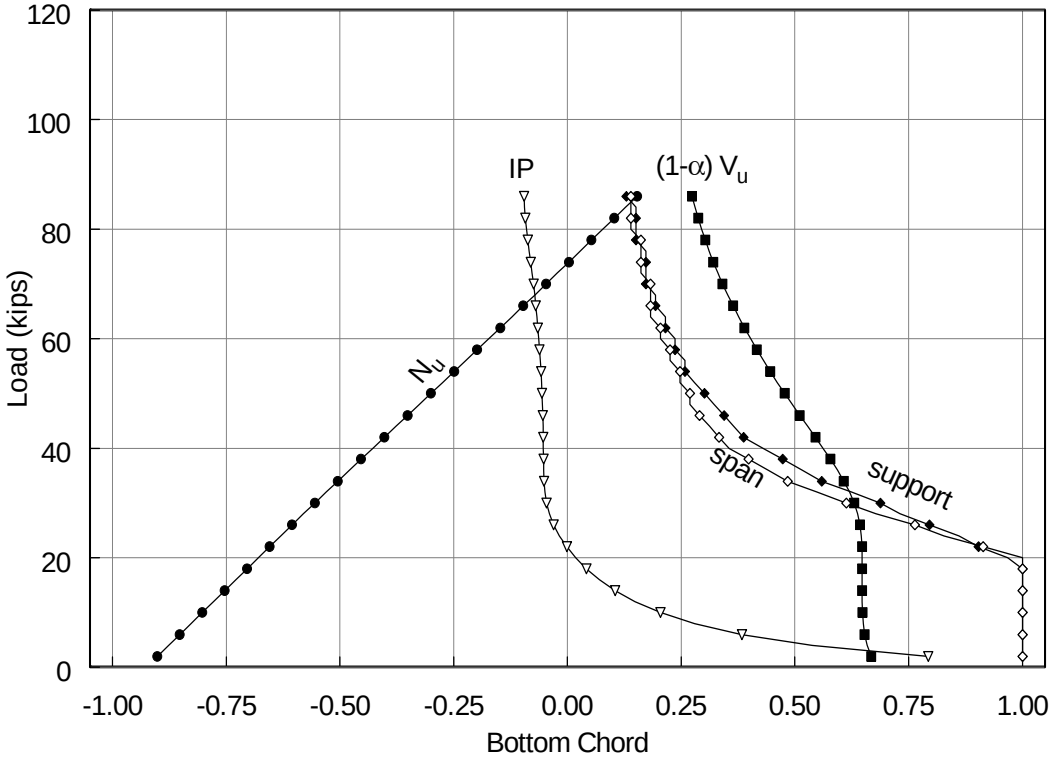

(b)

Figure 3.26 Opening 1 normalized chord parameters: PAf-3

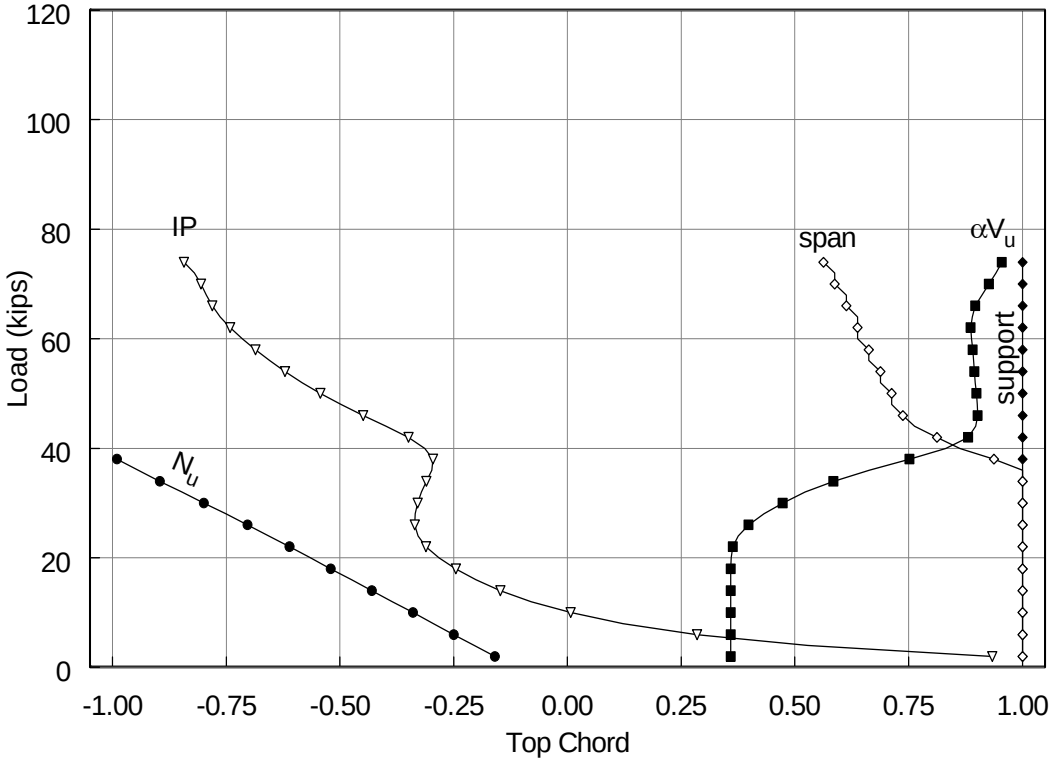

(a)

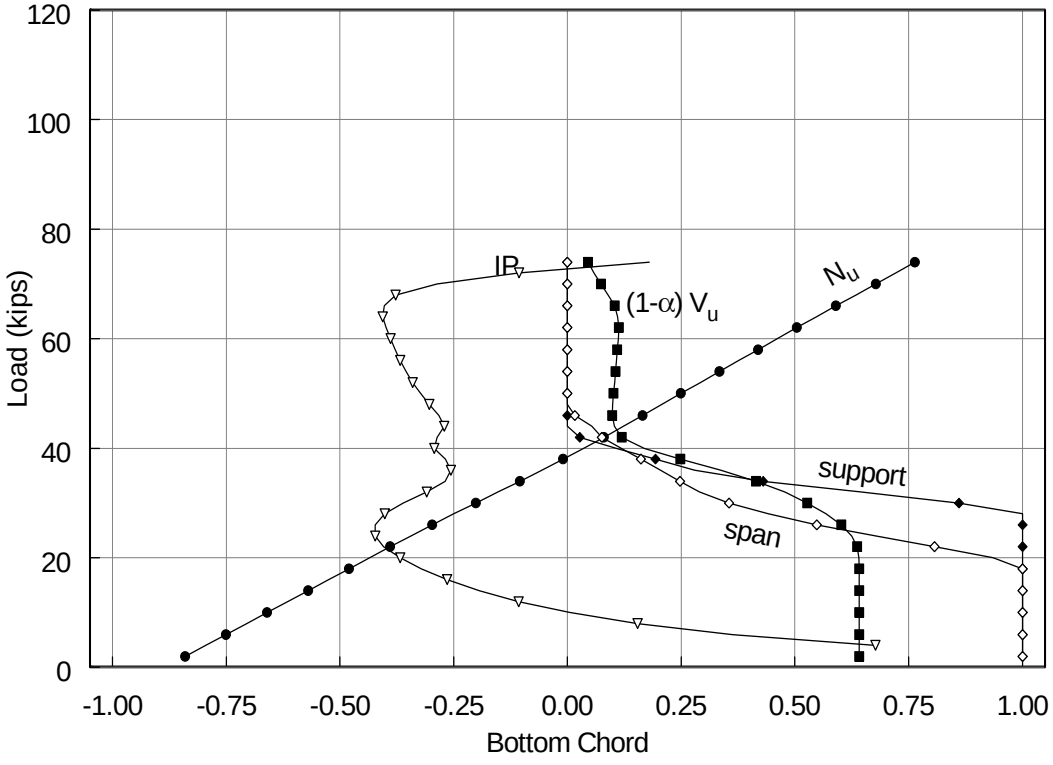

(b)

Figure 3.27 Opening 2 normalized chord parameters: PAf-3

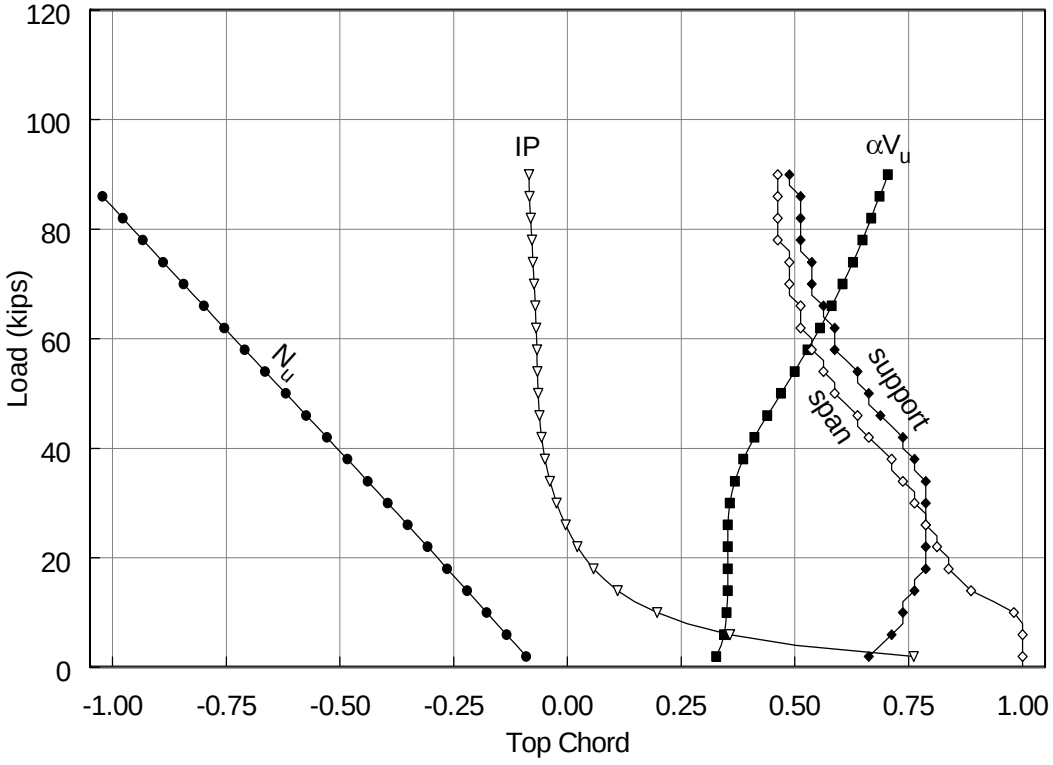

(a)

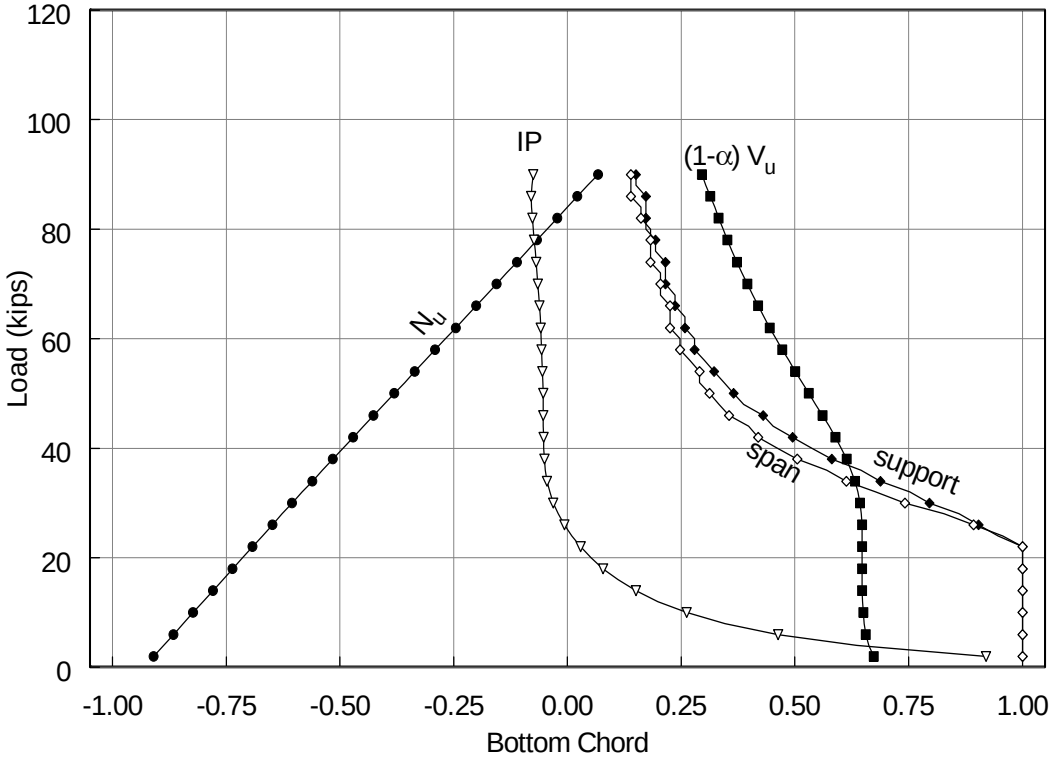

(b)

Figure 3.28 Opening 1 normalized chord parameters: PA6-4

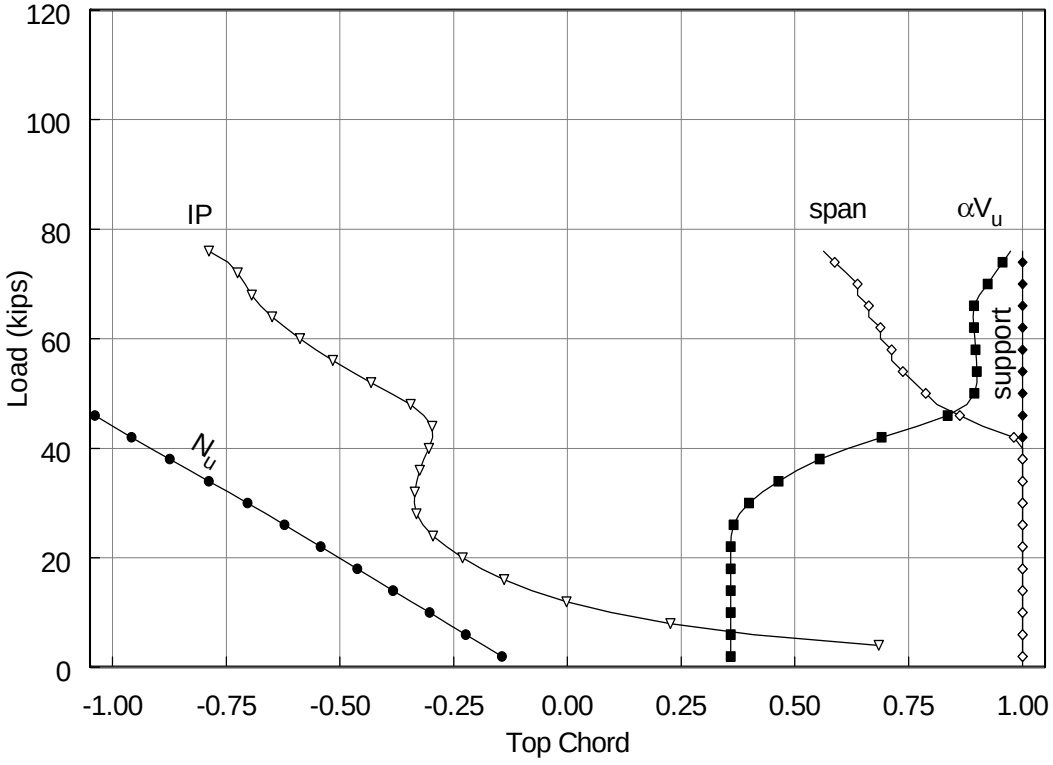

(a)

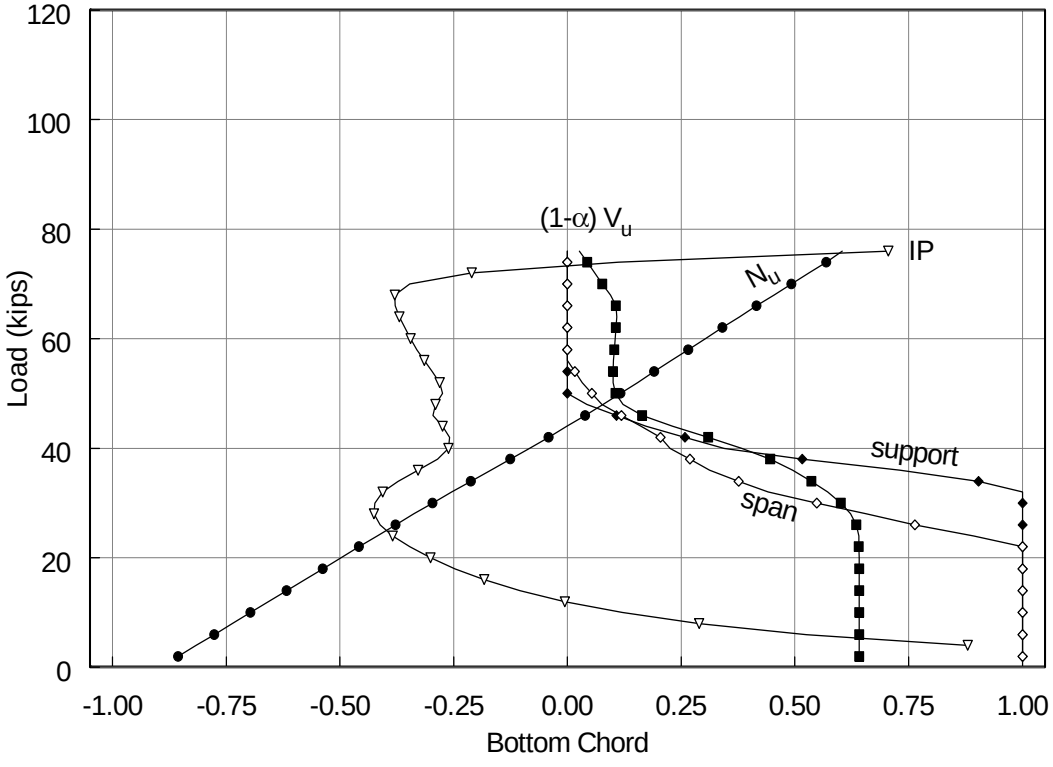

(b)

Figure 3.29 Opening 2 normalized chord parameters: PA6-4

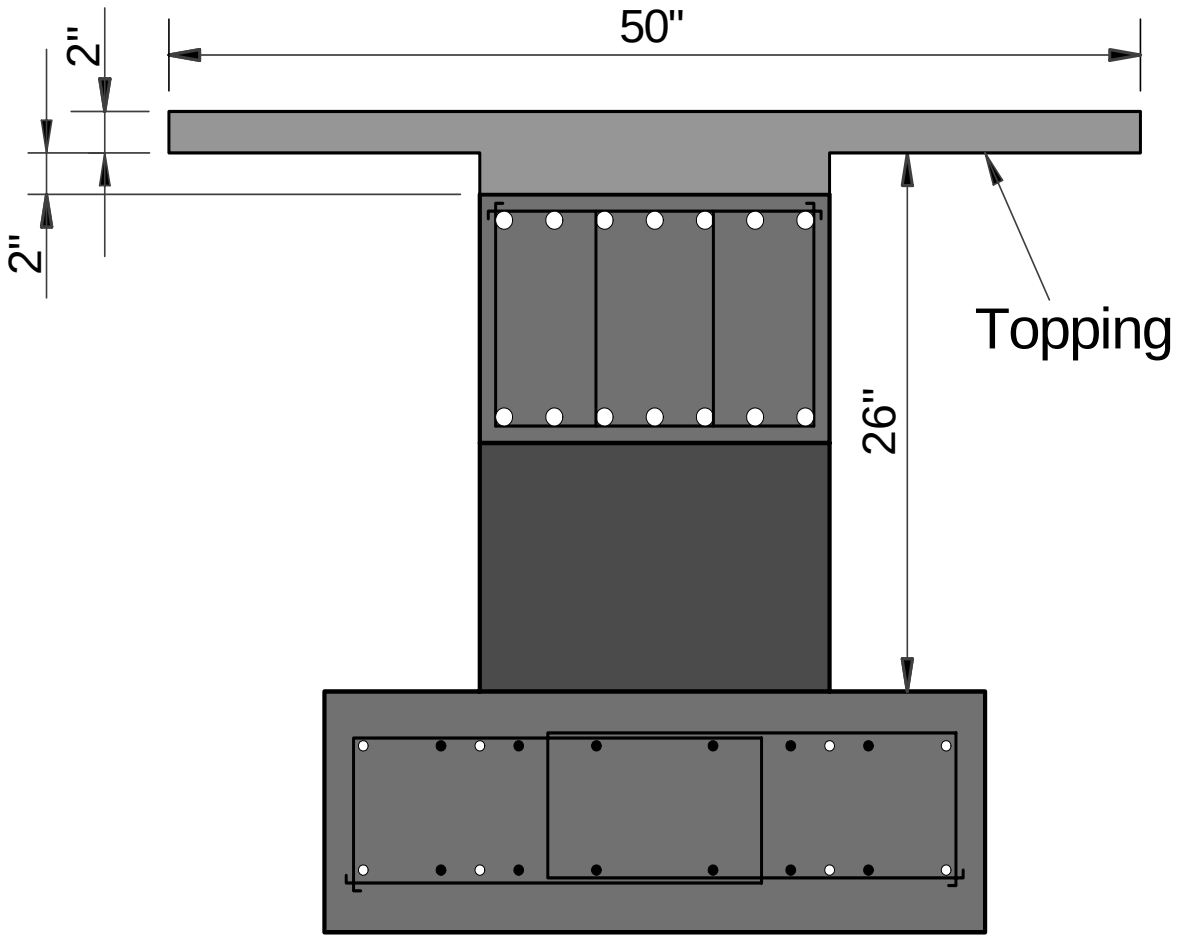

Figure 3.30 Topped ITO girder cross-section

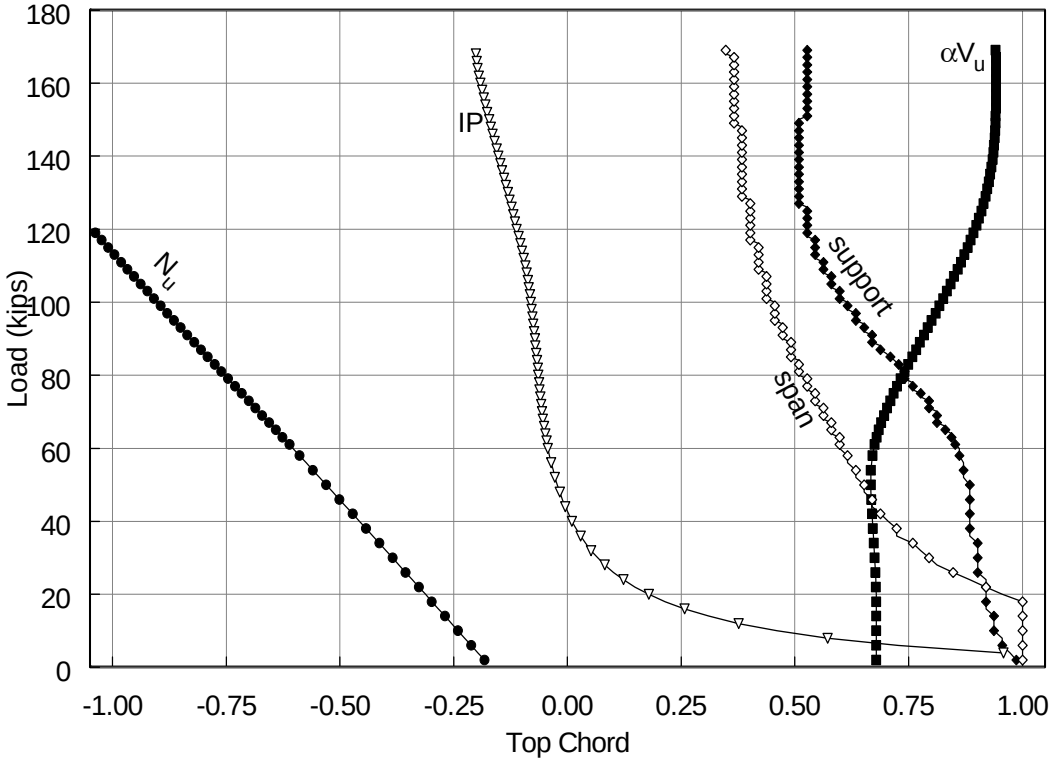

(a)

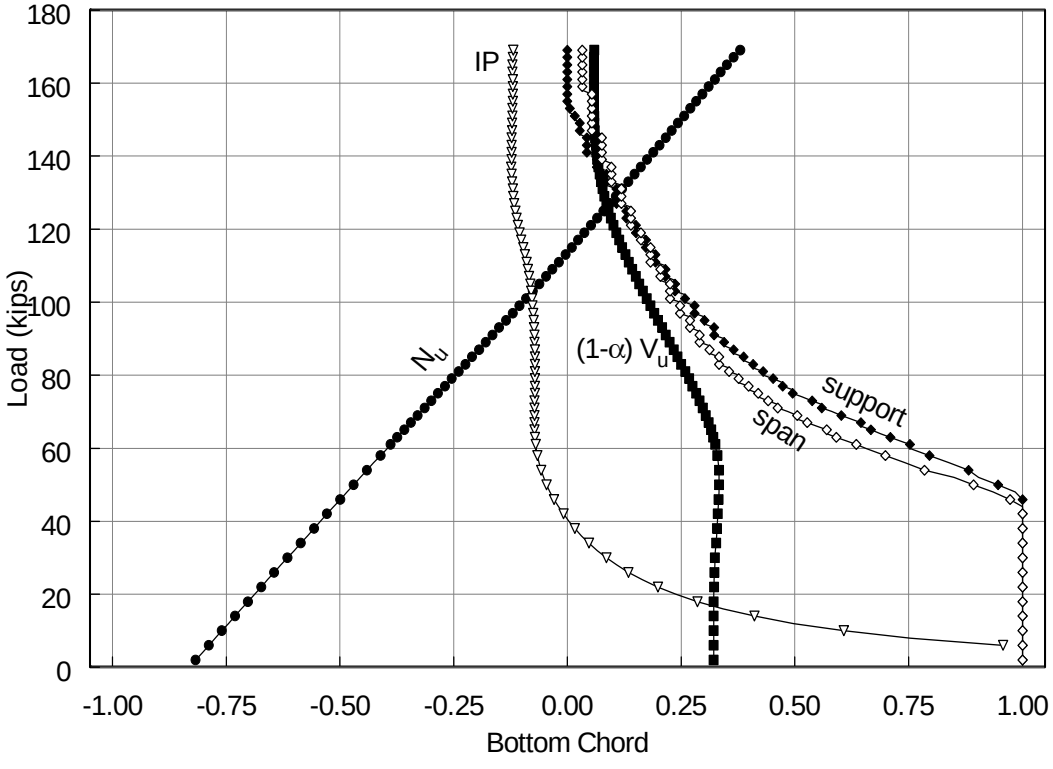

(b)

Figure 3.31 Opening 1 normalized chord parameters: Topped ITO

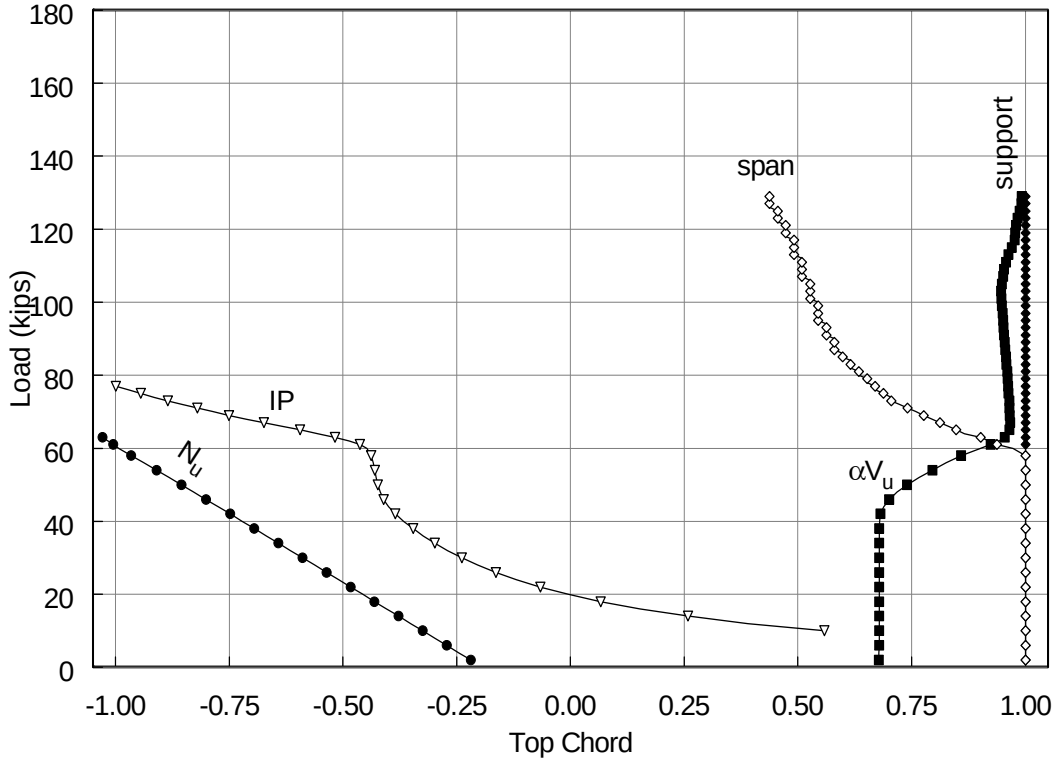

(a)

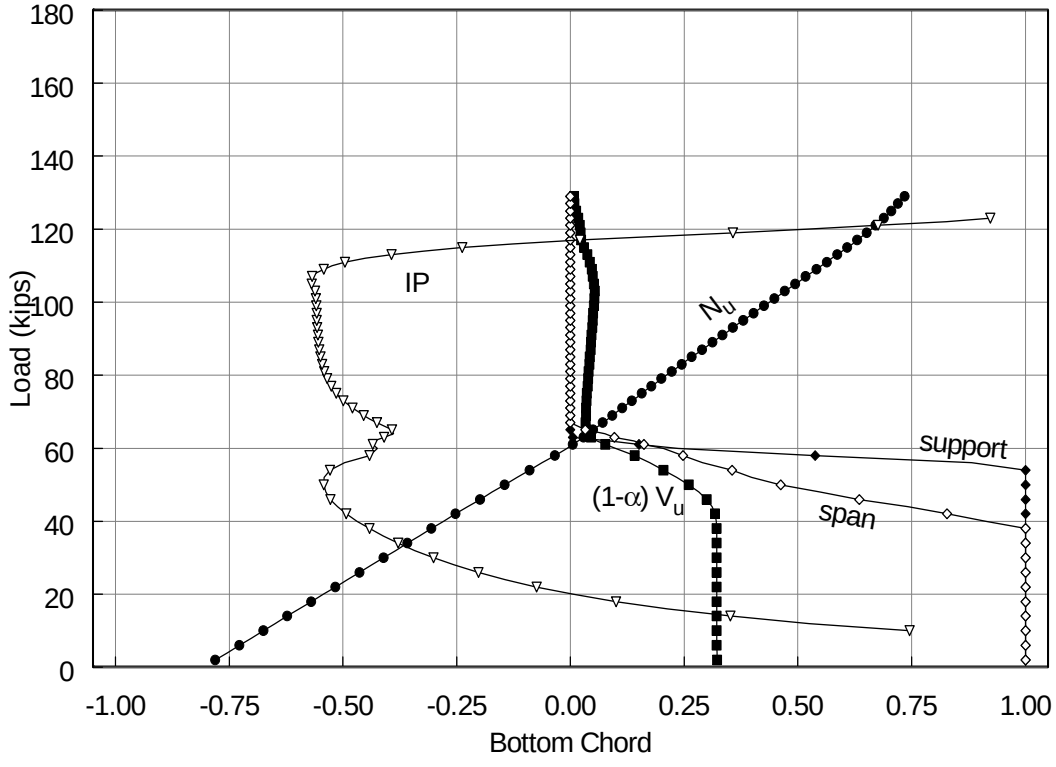

(b)

Figure 3.32 Opening 2 normalized chord parameters: Topped ITO

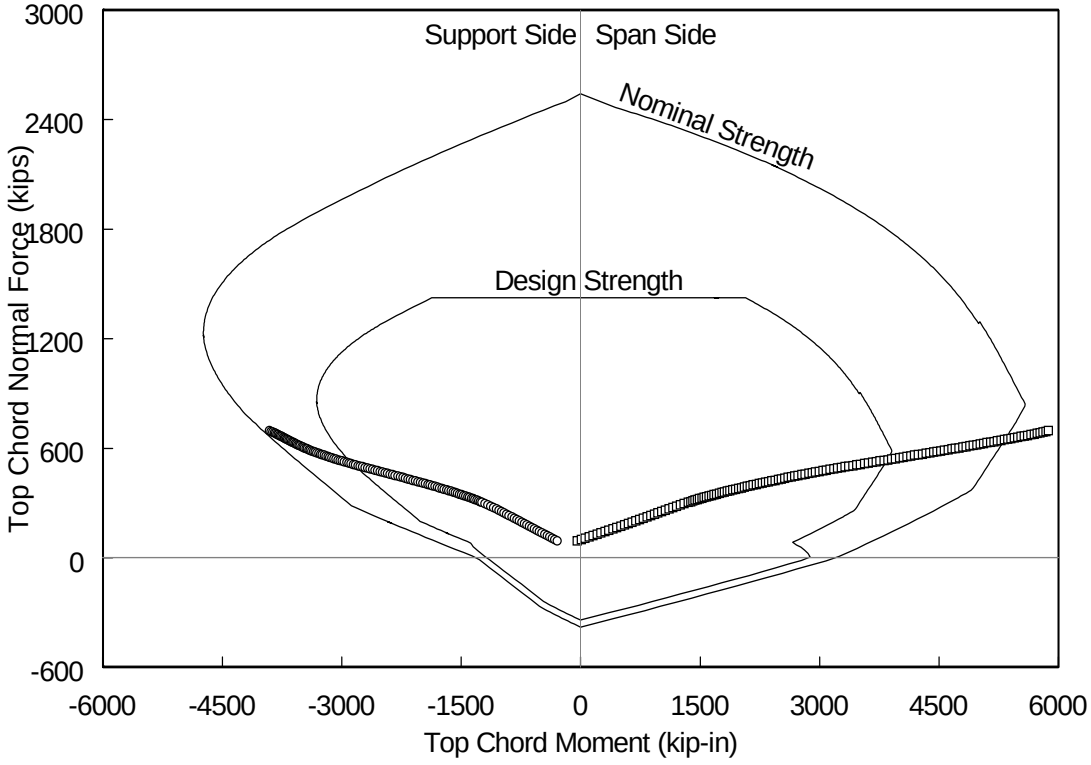

(a)

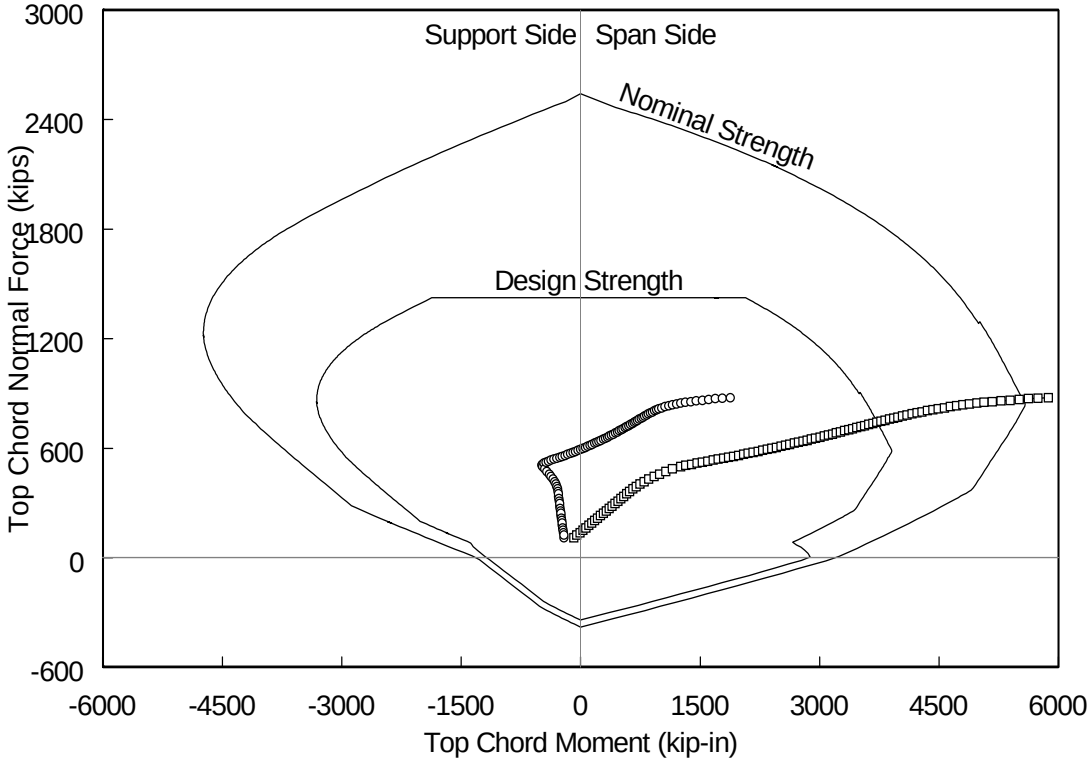

(b)

Figure 3.33 Composite model interaction diagrams: (a) opening 1; (b) opening 2

CHAPTER 4

CONTROL OF SHEAR DISTRIBUTION

4.1 INTRODUCTION

The fiber model analyses in Chapter 3 indicate the top chord longitudinal reinforcement does not yield and form a flexural hinge at the ends of the openings. The most direct approach to providing a ductile means to control the top chord shear force is thus unavailable for this cross-section. As noted in Chapter 3, the chords' capacity and demand are functions of the applied load and the extent of cracking in the chords, making it difficult to predict either with certainty without a nonlinear model such as that used in Chapter 3. A means to control the shear force demand, and therefore be able to predict the axial-flexural demand more accurately is necessary to develop a design procedure that does not require nonlinear modeling.

Truss models were explored in this research as an alternative approach to traditional design methods for the ITO girder. While these efforts did not result in a design procedure for the ITO girder, the truss models suggest an alternative way to control the shear demand, which is the subject of this chapter. Section 4.2 presents two strut-and-tie models for a beam with one opening that provide insight on the function of the various types of reinforcement required at an opening. Specifically, these models show that the abutment reinforcement transfers the shear force to the top chord and from the bottom chord.

Section 4.3 compares the test specimens' abutment reinforcement strains and the fiber model forces. This comparison shows that there is evidence the test specimens' abutment reinforcement acted as postulated in Section 4.2. The abutment reinforcement thus can be used to control the chords' shear demand, allowing a more accurate prediction of both the chords' shear demand and their axial-flexural demand. This in turn allows development of the design procedure without the necessity of nonlinear modeling.

Section 4.4 examines the implications of allowing the abutment reinforcement to yield as an approach to controlling the chords' shear force demand. In typical reinforced concrete beam design, yielding of the transverse reinforcement ends the resistance at a section, and is followed by failure. This is an undesirable failure mode for the ITO girder, and must be prevented. Section 4.5 presents the design implications from examining strut-and-tie models for the ITO girder.

4.2 STRUT-AND-TIE MODELS FOR A BEAM WITH ONE OPENING

Figure 4.1 and Figure 4.2 show two different approaches to strut-and-tie models for a beam with one opening that offer insight for constructing truss models for the ITO girder. Figure 4.1 shows a strut-and-tie model for a T-beam with an opening near the top (Cook and Mitchell (1988)). Figure 4.2 shows a strut-and-tie model for a rectangular beam with an opening near the bottom (Schlaich, Shafer and Jennewein (1987)).

Figure 4.1(a) shows the stress fields in the T-beam, and Figure 4.1(b) shows the strut-and-tie idealization, with the open circles representing the joints in a truss. In the figures, the dashed lines

represent the diagonal compression elements, solid lines represent the tension elements, and the shaded triangle at the support in Figure 4.1(a) is a nodal zone. Figure 4.1(b) collapses the stress fields of Figure 4.1(a) to line element representations intersecting at discrete points.

Cook and Mitchell present the strut-and-tie model to illustrate the way an opening alters the internal forces in a uniformly loaded beam. This model assumes the diagonal compression field to the opening's right transfers the vertical force to the bottom chord. Diagonal compression elements and longitudinal and vertical tension elements then transfer the vertical and horizontal forces across the bottom chord. Cook and Mitchell also show how strut-and-tie models reveal the reinforcement's function. They provide a tension tie at the opening's support side to drag the shear force back up to the top of the section. This uses the full depth of the section to resist the shear force and allows it to be transmitted to the support by diagonal compression. They only provide transverse reinforcement in the bottom chord in this model, because they assume that the top chord carries only compression.

Figure 4.2(a) shows the B and D-regions into which Schlaich et al. divided the beam, with inclined hatching identifying the D-regions and horizontal hatching identifying the B-regions. Figure 4.2(b) shows the strut-and-tie models for the regions surrounding the opening. Dashed and solid lines, respectively, represent the compression and tension elements in the strut-and-tie model. Going from (a) to (b), Schlaich et al. extend the B-region in the top chord into the adjacent D-regions to simplify the discussion. Figure 4.2(c) shows the resulting reinforcement. In this strut-and-tie model, Schlaich et al. assume the top chord resists the entire shear force. The vertical tension element T_6 transfers the shear force to the top chord, where diagonal compression and longitudinal compression and tension elements provide the resistance. At the opening's left side, diagonal compression transfers the shear force to the bottom of T_5. This tension tie then lifts the force back up to the section's top and redistributes it to the entire section. Presumably from this point to the support they used a standard strut-and-tie model to design the horizontal and vertical reinforcement.

Schlaich et al. (1987) provide the tension tie T_6 in the beam with the banded reinforcement on the opening's right side (Figure 4.2(c)). The three stirrups to the opening's left, shown with heavy lines, provides the tension tie T_5 in the beam. Presumably both bands are placed at the centroid of the corresponding tension forces in the strut-and-tie model, although they provide no details. Schlaich et al. provide transverse reinforcement in both the top and bottom chords, though they assume that the bottom chord carries only tension forces.

The strut-and-tie models show two different ways to transfer the forces around an opening. In the Cook and Mitchell example, the bottom chord carries the vertical forces, and in the Schlaich et al. example, the top chord carries them. This is likely due to the differences in the chord areas in the two examples. However, both models recognize the necessity of transverse web reinforcement next to the openings to transfer the vertical forces from the entire section to the chords, and from the chords back to the entire section. Both also recognize the necessity of providing transverse chord reinforcement and longitudinal chord reinforcement.

4.3 COMPARISON OF ABUTMENT REINFORCEMENT STRAINS AND FIBER MODEL CHORD SHEAR FORCES

Figures 4.3 through 4.6 compare the test specimen's abutment strains with the corresponding fiber model chord forces. In each figure, the top graph plots the abutment strains vs. the applied load, and the bottom graph plots the fiber model's chord shear force vs. the applied load.

Figure 4.3 compares the response of the span side abutment reinforcement for the test specimens at opening 1 with the fiber model's top chord shear force at opening 1. Comparing the general shape of the two figures, both are bilinear, at least up to the test specimens' factored load. Beyond that point there is some variation in the response among the test specimens, and their response differs from the fiber model's. With the insight gained from the fiber model, it appears from the abutment strains that the top chord at opening 1 for test specimens S1 and S3 begins to redistribute some of its shear force to the bottom chord beyond approximately 70 kips. For S2, the wider spacing of the abutment reinforcement makes it difficult to draw any conclusions.

Figure 4.4 compares the response of the support side abutment reinforcement for the test specimens at opening 1 with the fiber model's bottom chord shear force at opening 1. These two graphs do not show the same level of similarity as the span side graphs, but some resemblance is apparent. The abutment strains are generally bilinear, with a downward curvature after the initial linear region. The fiber model's shear force is initially linear, and beyond the service load has an upward curvature. It is this second region that shows some similarity with the abutment strains. The abutment strains for S1 and S3 show an upward curvature also, starting between the service load and the factored load, and continuing to approximately 75 kips. Again, relying on the insights from the fiber model, this suggests that the bottom chord is redistributing shear force to the top chord in this region. The downward curvature that follows this region is consistent with the upward curvature at the upper load range for the span side reinforcement in Figure 4.3.

Figure 4.5 compares the response of the span side abutment reinforcement for the test specimens at opening 2 with the fiber model's top chord shear force at opening 2. These graphs show a distinct similarity throughout the loading range shown between all three test specimens and the fiber model's shear force. Test specimen S2 agrees more closely with the other two test specimens, likely because the abutment reinforcement at the span side of opening 2 is isolated from the adjacent reinforcement, unlike at opening 1.

Figure 4.6 compares the response of the support side abutment reinforcement for the test specimens at opening 2 with the fiber model's bottom chord shear force at opening 2. Like the span side reinforcement, the initial linear region followed by downward curvature in the abutment strains is not evident in the fiber model's chord forces. However, the similarity between the two graphs beyond the factored load for the abutment strains and from a point between the service and factored loads for the fiber model's shear force is unmistakable. This suggests that the test specimens redistributed their bottom chord shear force to the top chord just above the factored load. The lack of a distinct jump in the fiber model's shear force just above the factored load, compared with the test specimens' abutment strains, is likely due to the lack of concrete tensile strength in the fiber model. Without tensile strength, the concrete cracks very gradually in the fiber model, one fiber at a time, where in the test specimens, once the tensile strength is exceeded, the crack opens rapidly.

These comparisons show that the abutment reinforcement was likely acting as postulated in Section 4.2. They further show that a redistribution of forces between the top and bottom chords occurred in the test specimens, causing the top chord to resist a greater portion of the shear force than assumed in the design using the IDM to predict the chord forces. This increased top chord shear force compared with the design value likely caused the observed failure.

4.4 EXAMINATION OF ABUTMENT REINFORCEMENT YIELDING

From the evidence in the preceding sections, allowing the abutment reinforcement to yield appears to be a viable approach to controlling the chords' shear forces. The abutment reinforcement is then acting as a structural fuse to limit the chords' shear forces, much as a flexural hinge is used to limit forces. If the deformations associated with yielding the abutment reinforcement are controlled, then this approach provides a ductile failure mode for the ITO girder. If yielding the abutment reinforcement results in uncontrolled deformations at the sides of the openings, it is possible the ITO girder will form a mechanism at the opening, resulting in an undesirable sudden failure. The objective of this section is to demonstrate that this is not the case as long as the abutment reinforcement on both sides of the opening does not yield.

Figure 4.7(a) shows a portion of S1 with the cracks present prior to the peak load. The figure shows the crack at the opening's upper span side corner extending to the girder's top surface. If the span side abutment reinforcement yields, the deformation of the part of the girder on the span side of the crack is restrained by the bottom chord's flexural stiffness.

Figure 4.7(b) is the same as 4.7(a), except now the crack at the opening's lower support side is assumed to extend to the girder's bottom surface. If this occurs and the abutment reinforcement on both sides of the opening yields, the part of the girder on the span side of the cracks can deform in an uncontrolled manner as the reinforcement elongates at a constant load.

Figure 4.7(b) shows that yielding the abutment reinforcement at both sides of the opening may result in uncontrolled deformations, and must be prevented. While yielding of the abutment reinforcement on only one side results in controlled deformations, the failure depicted in Figure 9.7(a) must also be avoided (because of its brittle nature). The ability of this region to accommodate – with proper reinforcement details – the inelastic elongation of the yielding abutment reinforcement in a ductile manner needs experimental verification.

4.5 DESIGN IMPLICATIONS

The strut-and-tie models show a plausible path for the transfer of forces from the load points to the supports. This load path shows the function of the abutment reinforcement, the top and bottom chord transverse reinforcement, and the symmetrically distributed longitudinal chord reinforcement. It also shows the necessity for closely spaced transverse reinforcement at the abutments and in the chords, to anchor the truss elements and distribute the loads.

The strut-and-tie models also show that providing abutment reinforcement for the full shear force at the section is unnecessary. Instead, providing abutment reinforcement on each side of each

opening in proportion to the top and bottom chord shear forces provides a mechanism, yielding, with which to control and limit these forces. The chords can then be designed not for an assumed force, but for the force the selected abutment reinforcement can transfer at its yield strength. The examination of abutment reinforcement yielding shows that yielding results in contained deformations as long as both sides are not allowed to yield simultaneously.

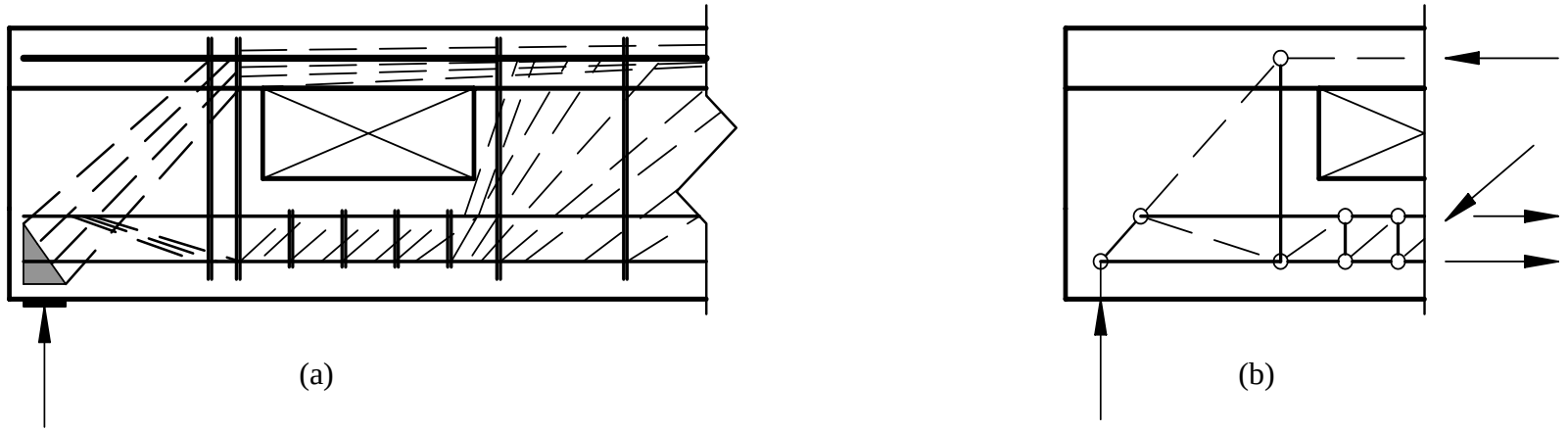

Figure 4.1 Strut-and-tie model for a T-beam with an opening near the top (adapted from Cook and Mitchell (1988))

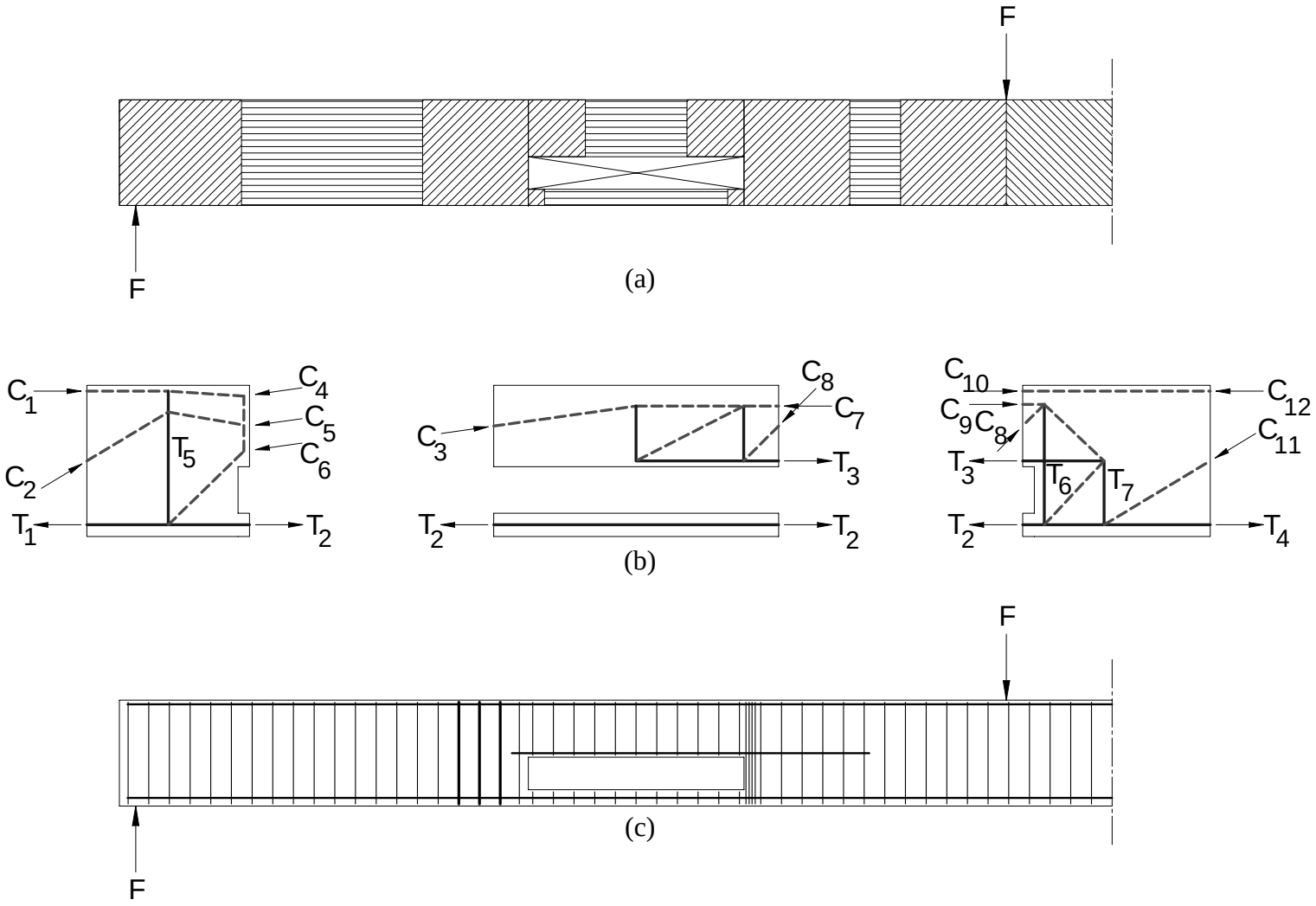

Figure 4.2 Strut-and-tie model for a rectangular beam with an opening near the bottom (adapted from Schlaich et al. (1987)): (a) B and D-regions; (b) strut-and-tie model; (c) beam with reinforcement

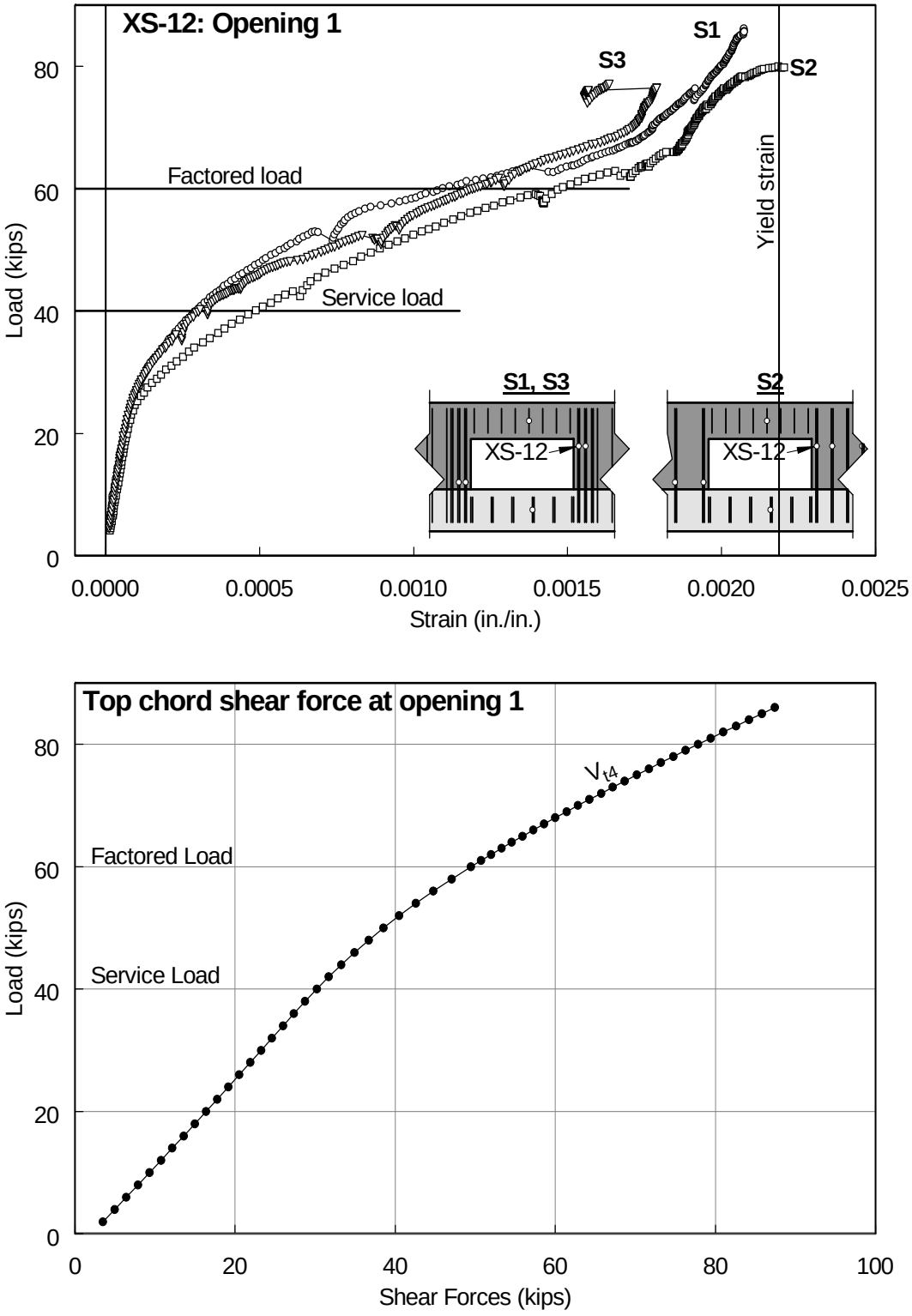

Figure 4.3 Test specimen abutment strains vs. fiber model chord shear force: Top chord at opening 1

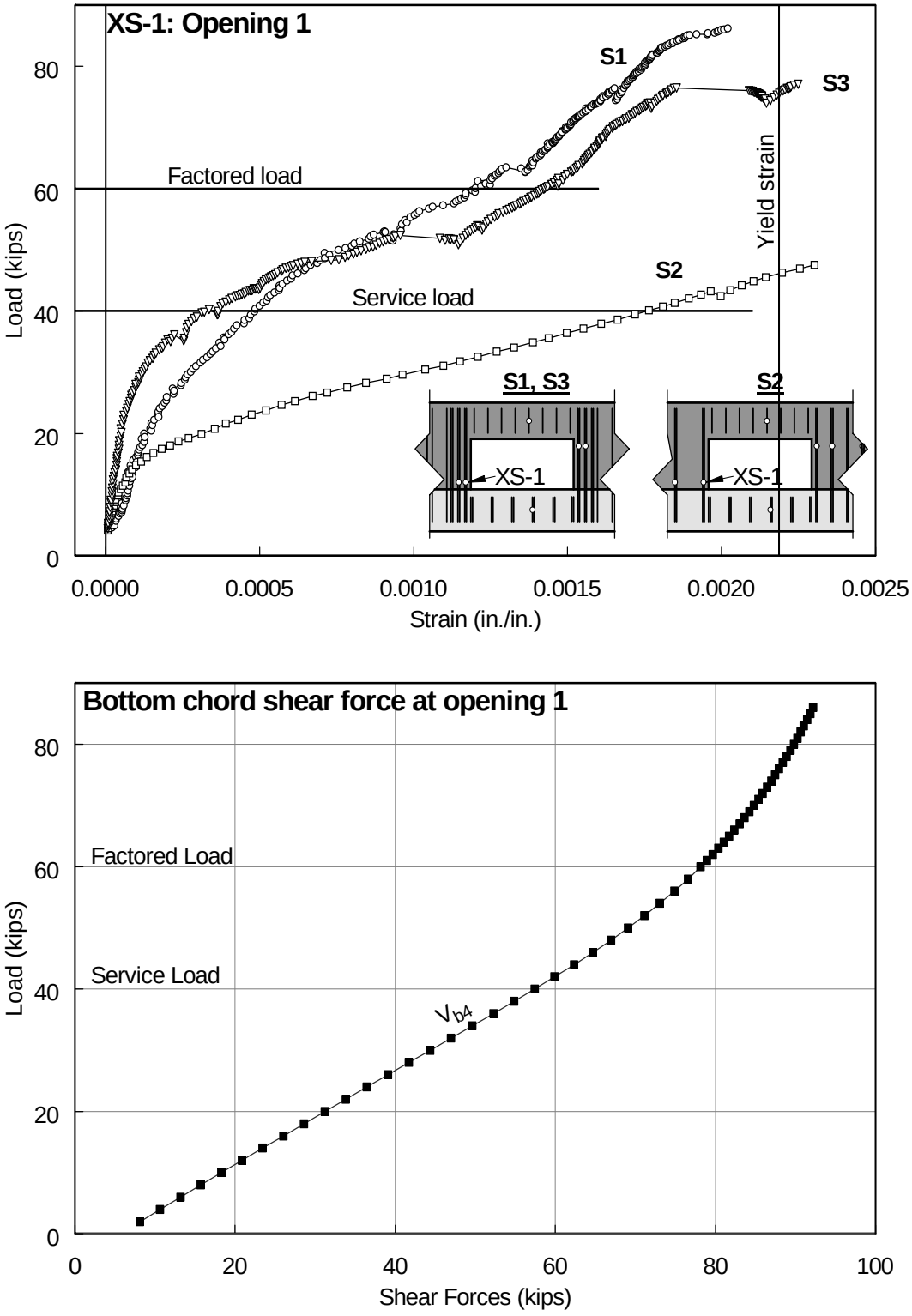

Figure 4.4 Test specimen abutment strains vs. fiber model chord shear force: Bottom chord at opening 1

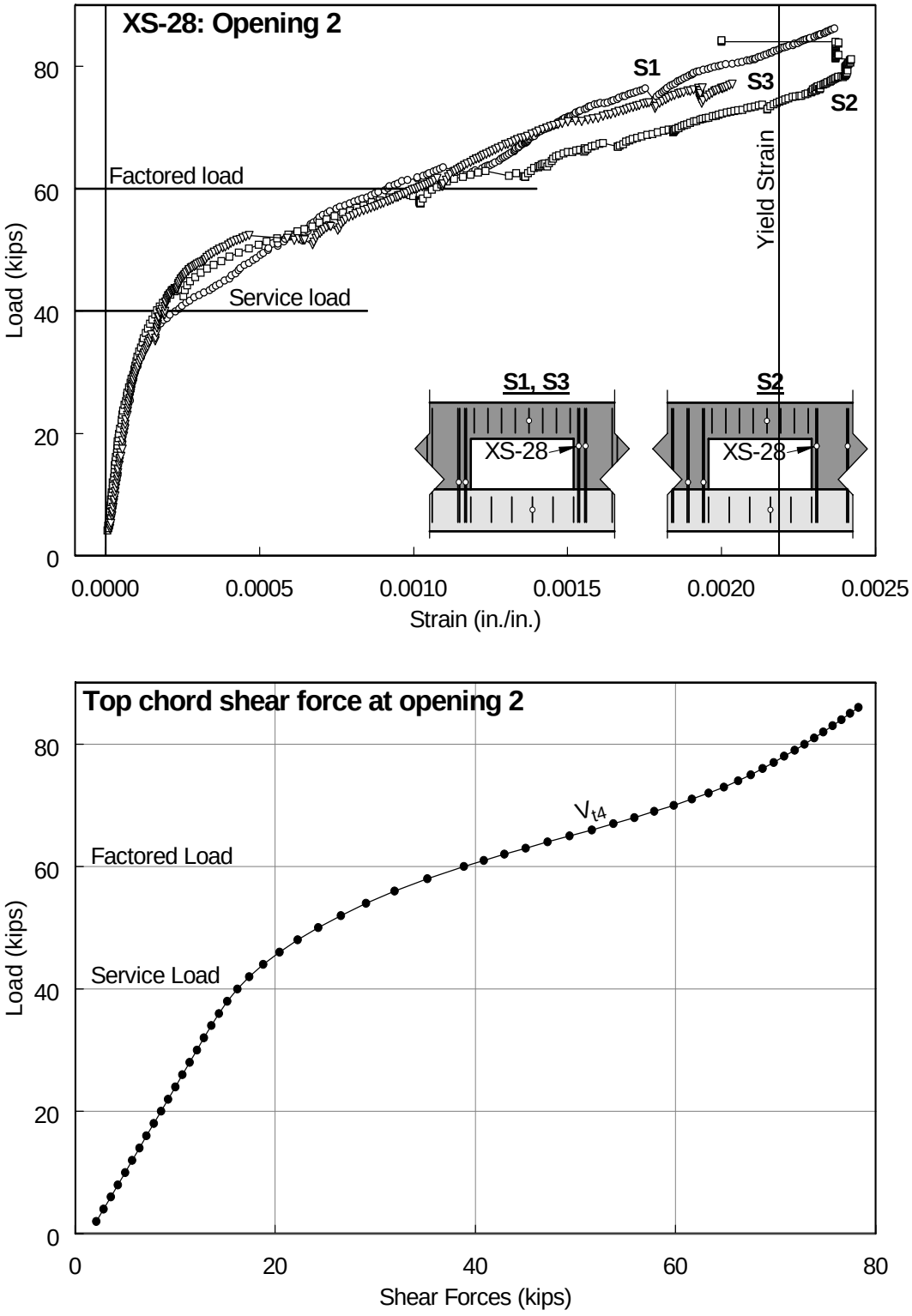

Figure 4.5 Test specimen abutment strains vs. fiber model chord shear force: Top chord at opening 2

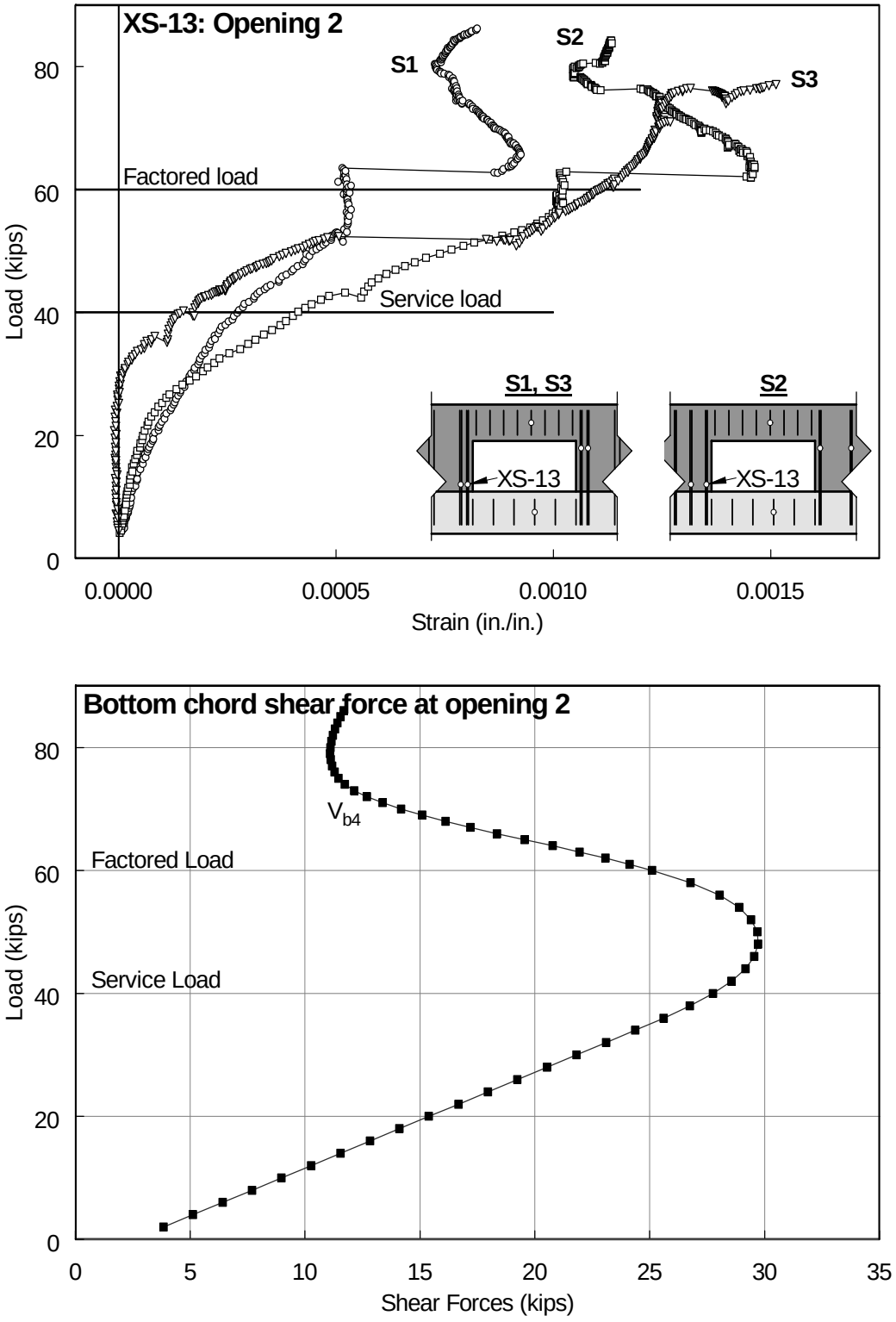

Figure 4.6 Test specimen abutment strains vs. fiber model chord shear force: Bottom chord at opening 2

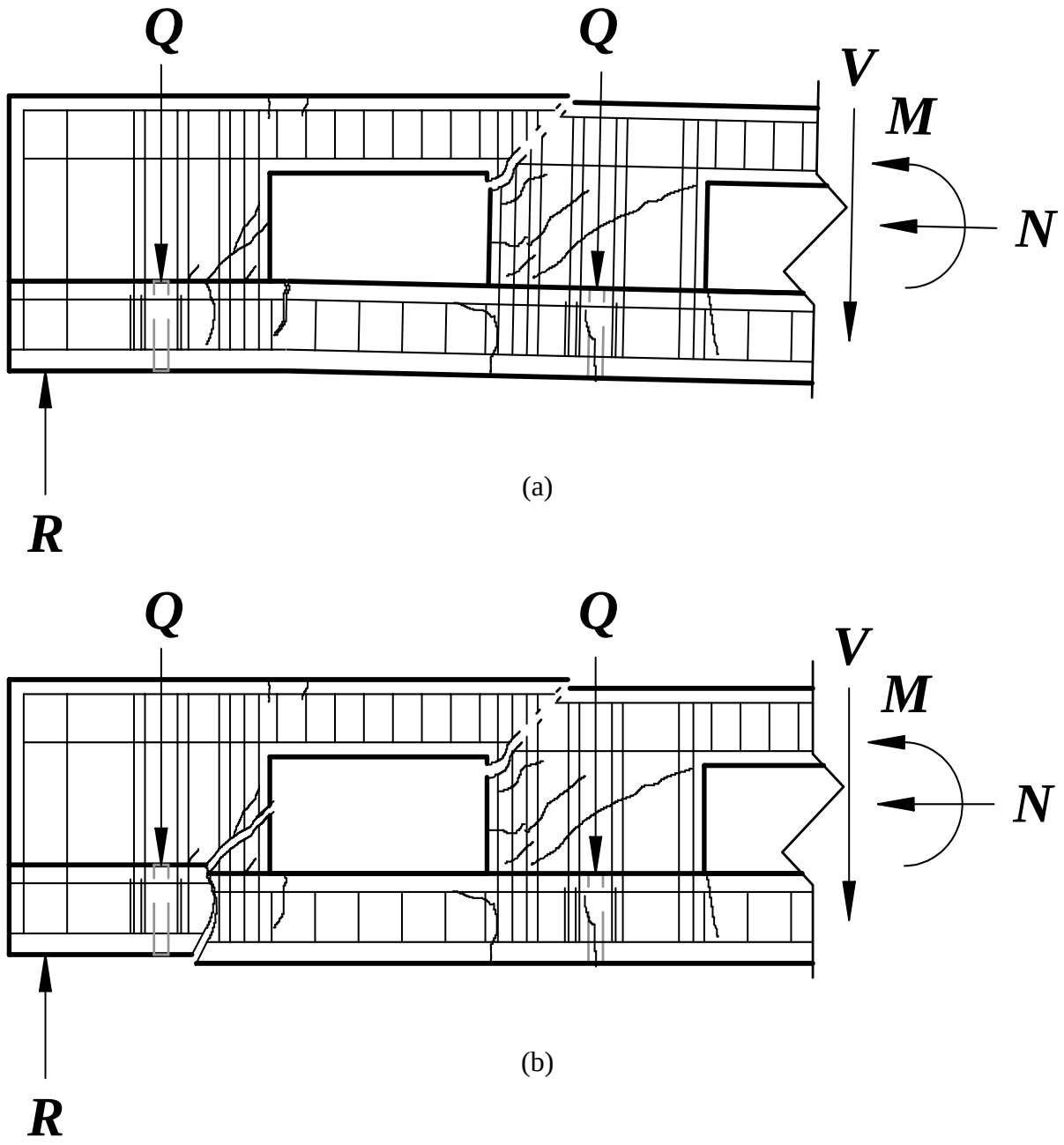

Figure 4.7 Examination of abutment reinforcement yielding: (a) yielded on one side; (b) yielded on both sides

CHAPTER 5

DESIGN PROCEDURE

5.1 INTRODUCTION

This chapter presents a design procedure for the ITO girder. This design procedure is currently restricted to girders reinforced with closed-loop stirrups. Use of welded wire fabric must be investigated experimentally before being adopted. Section 5.2 presents the design recommendations developed from the experimental and analytical work. Section 5.3 presents the steps in the design procedure. This section also presents the rationale for each step, based on the experimental and analytical results. Sections 5.4 through 5.7 present a design example, which shows how the various provisions of the design procedure affect the final cross-section. Section 5.8 presents a verification of the design procedure, which is accomplished by analyzing the resulting design with a fiber model. Section 5.9 discusses the effects of a topping slab on the ITO girder. Section 5.10 discusses the effects of live load on half the span.

5.2 DESIGN RECOMMENDATIONS

1. The prestressed reinforcement should be placed in two layers, symmetric about the bottom chord centroid. This provides beneficial precompression for the tension zones that occur at the bottom chord's support side top surface and its span side bottom surface. This delays cracking and the redistribution of forces that accompanies cracking.

2. When specifying the prestressed reinforcement, the designer must include all the longitudinal reinforcement in the cross-section. Controlling the strength in the various failure modes is essential to controlling the ITO girder's failure mode.

3. Divide the shear force at an opening in proportion to the chords' concrete shear capacity. This approach accounts for the effects of the axial force and the cross-section dimensions directly, and provides a reasonable approximation of the chord shear demand once cracking has occurred.

4. Assume the span side abutment reinforcement transfers the shear force to the top chord, and the support side abutment reinforcement transfers the shear force from the bottom chord. Proportion the abutment reinforcement to transfer the shear force to the chords consistent with the proportions determined in recommendation 3. This prevents the chords from attracting more shear than the amount that they are designed to resist. Provide a minimum of one closed loop stirrup on each side of each opening. Provide sufficient abutment reinforcement at both sides of an opening so that both sides cannot yield at the factored load.

5. Provide the minimum shear reinforcement in all chords at all openings. For shear reinforcement spacing, if the chord is in compression, use the spacing requirements for prestressed members. If the chord is in tension, use the spacing requirements for ordinary reinforced concrete members.

6. Assume that the chord moments are the lesser of:

   a) the maximum chord shear force multiplied by the opening length;

   b) the maximum chord moment that can occur at the section.

   This recommendation is conservative, but the results of this investigation show that the inflection point location varies, and that the chords can go into single curvature, warranting this approach. The lesser moment is used to reduce the conservatism.

7. Check that the ratio of each chord's design strength to its required strength exceeds the ratio of the midspan nominal flexural strength to the factored moment. This recommendation ensures that a midspan flexural failure will occur before a chord failing due to either combined axial-shear effects or axial-flexural effects. A capacity design factor should be considered when comparing these ratios. This factor, greater than one, provides additional assurance that the ductile midspan failure mode occurs at a load below the chord failure loads. This factor is discussed further in Step 5 in the design procedure.

8. If a topping slab will be placed as part of the floor system, it must be considered in the design process. If composite action is expected, then the design must ensure, through proper detailing, either the desired composite action occurs or no composite action occurs, and continue accordingly.

9. The effect of live load on only half the span should be considered for a midspan opening for a symmetrically loaded member. The minimum amount of abutment reinforcement should be provided at both sides of the opening, minimum shear reinforcement should be provided in both chords, and minimum flexural reinforcement provided in the top chord.

5.3 DESIGN PROCEDURE

Figure 5.1 shows a flowchart that outlines the design procedure. The flowchart shows the steps in the design procedure, and the remainder of this section explains them in detail. Figure 5.2 shows the ITO girder that results from the application of the design procedure to the typical interior bay in Chapter 2.

5.3.1 Step 1: Design an IT girder for the specified span, loads, and design material properties.

(a) determine the required prestressed reinforcement area to satisfy the ACI 318 Code's flexural strength requirements, placing the required reinforcement symmetrically about the ledge centroid ($\boldsymbol{A_{ps}}$ in Figure 5.2(b));

(b) determine the required ledge longitudinal reinforcement in accordance with PCI Handbook 4.5.3 and place it at the same elevations in the ledge as the prestressed reinforcement ($\boldsymbol{A_l}$ in Figure 5.2(b));

When the openings are placed in the IT girder, the ledge becomes the bottom chord. Placing the prestressed reinforcement and ledge reinforcement symmetrically about the ledge centroid provides

beneficial precompression at both faces of the bottom chord for the ITO girder that is designed based on this IT girder. It also provides flexural reinforcement at both faces without having to add additional reinforcement solely for this purpose.

(c) determine $\boldsymbol{P_e}$ so that the tension stress at the extreme fiber stress in tension in the precompressed tensile zone at service loads equals $6\sqrt{f'_c}$, consistent with ACI 318 18.4.2(c);

Setting $\boldsymbol{P_e}$ at the level recommended above, along with the symmetric reinforcement placement, delays the onset of cracking in the bottom chord, and thus the redistribution of forces that occurs as cracking occurs.

(d) calculate $\boldsymbol{P_i}$ and $\boldsymbol{P_j}$ from $\boldsymbol{P_e}$ based on typical assumptions for prestress losses per ACI 318 18.6;

(e) check the permissible stresses in concrete (ACI 318 18.4) and prestressing tendons (ACI 318 18.5);

(f) provide tension reinforcement in the tensile zone as required per ACI 318 18.4.1 and PCI Handbook 4.2.2.2 (the upper reinforcement layer labeled $\boldsymbol{A'_s}$ in Figure 5.2(b));

The checks in Steps (d) through (f) serve as a reference point for the ITO girder design. The reinforcement determined in Step (f) also serves as a tentative amount of top chord reinforcement.

(g) reevaluate the flexural strength, including all longitudinal reinforcement, and reduce the amount of prestressed reinforcement if possible to minimize the overstrength in this failure mode;

The check in Step (g) ensures that the midspan design flexural strength is as close as possible to the required flexural strength to avoid excess capacity for this failure mode. Excess strength at midspan can result in chord failure modes occurring at a lower load than the midspan flexural failure load. In the experimental program, the midspan region had significant excess strength, which contributed to the observed brittle chord failure.

(h) check that the reinforcement provided satisfies the limits for reinforcement of flexural members, ACI 318 18.8;

(i) determine the required hanger and ledge transverse reinforcement at the load points, bearing reinforcement and shear reinforcement.

The reinforcement determined in Step (i) is required for both the IT and ITO girder. As the openings do not affect this reinforcement, it is not examined in detail here.

5.3.2 Step 2: Specify the openings' size, location, and preliminary top chord reinforcement.

(a) assume a top chord depth greater than or equal to the equivalent rectangular stress block from the flexural analysis in Step 1;

The fiber models showed that with a top chord depth at least as great as the equivalent rectangular stress block depth, the midspan opening region can reach the same failure load as a solid section.

(b) take the bottom chord depth as equal to the ledge depth;

With an assumed top and bottom chord depth, the opening's depth and vertical location are fixed.

(c) provide the larger of the reinforcement from Step 1(f) and the minimum required flexural reinforcement from ACI 318 10.5.1 as the top chord reinforcement at both top chord faces;

Longitudinal reinforcement is placed at both faces because the chord moments have the opposite sense at each end of the opening.

(d) center openings between the DT stems along the ITO girder's length;

The experimental results show that strand slip is not a concern for this cross-section and opening geometry, so openings are placed regularly along the girder's length, including within the strand development length. This provides maximum flexibility for the location of the building's service systems. Placing the openings between the DT stems along the ITO girder's length allows building services to be placed in the space between the DT stems and continue uninterrupted across the girder line.

For other cross-sections and opening geometries, if openings are placed within the strand development length, the force the strand can develop at the support side of the opening must be checked. If the strand cannot develop sufficient force to resist the tension from the chord moment, additional mild reinforcement must be specified. The designer also needs to investigate further if the opening is within the prestress transfer length. If the prestress force is not adequately developed, the chords' axial forces will not be the same as predicted by an elastic analysis, and therefore not reliable for use in designing the chords for strength.

(e) assume an opening length consistent with the recommendations in Barney et al. (1977).

The opening length is determined indirectly by applying the recommendations from Barney et al. for the posts' length-to-height ratio.

5.3.3 Step 3: Check the chords' nominal concrete stresses at transfer and service loads.

The chord forces used to check the nominal concrete stresses are determined with an elastic frame model. The frame model is similar to the fiber model (Figure 3.1), with the chords placed at their respective centroids relative to the solid section centroid. Rigid links connect the posts to the chords. The elastic chord forces at transfer and service load are used to check the chords' concrete stresses per ACI 18.4. Because there will be minimal cracking at service loads, as seen in the experimental program, these forces provide reasonable values for checking the nominal stresses. An elastic finite element model like that used previously would also provide good results, and provide the stresses directly, eliminating the need to calculate them from the forces.

5.3.4 Step 4: Determine the chord forces for strength design.

(a) take the chords' elastic axial forces at the factored load as the normal forces for strength design of the chords;

The elastic force is used because it has been shown that the elastically determined axial force agrees well with both the experimental data and the fiber model analyses. The fiber model analyses show that the axial force is a function of the applied load only, and is independent of cracking. The elastic

axial force at the factored load is used in the remainder of the design procedure to determine the proportion of the shear force resisted by each chord and to predict the chord's moment capacity.

(b) estimate the proportion of the shear force at the opening resisted by each chord, based on their concrete shear strength at the factored load;

Proportioning the shear this way accounts for the influence of the chord axial force, including its sense, and the chord dimensions, since both equations incorporate the web width and the structural depth. Each chord's concrete shear strength is estimated using the provisions of ACI 318 11.4.2.2 when it is in compression, and ACI 318 11.3.2.3 when it is in tension. The resulting proportions are consistent with the values from the fiber model analyses.

The following expressions are used to determine the concrete shear capacity, based on the sense of the axial force:

Net compression:
$$V_c = 4\sqrt{f_c'}\sqrt{1+\frac{1}{4\sqrt{f_c'}}\frac{N_u}{A_g}}\,b_w d \qquad (5.1)$$

Net tension (ACI 318 (11-8)):
$$V_c = 2\left(1+\frac{N_u}{500A_g}\right)\sqrt{f_c'}\,b_w d \qquad (5.2)$$

where $\boldsymbol{N_u}$ is the chord axial force, positive in Equation (5.1) for compression and negative in Equation (5.2) for tension, $\boldsymbol{A_g}$ is the chord's gross area, $\boldsymbol{b_w}$ is the chord width, and $\boldsymbol{d}$ is the depth to the tension reinforcement. These values of $\boldsymbol{V_c}$ are then used to determine the chord's shear proportion as follows:

Proportion of shear force resisted by the top chord:
$$\alpha_t = \frac{V_{ct}}{V_{ct}+V_{cb}} \qquad (5.3)$$

where $\boldsymbol{V_{ct}}$ is the top chord concrete shear capacity and $\boldsymbol{V_{cb}}$ is the bottom chord shear capacity. The bottom chord shear proportion is:
$$\alpha_b = 1-\alpha_t \qquad (5.4)$$

(c) calculate the chord shear forces based on the proportions from Step 4(b);

The chord shear forces are calculated as the product of each chord's shear proportion and the total shear at the opening at the factored load, $\boldsymbol{V_u}$ as shown below:

Top chord shear force:
$$V_{ut} = \alpha_t V_u \qquad (5.5)$$

Bottom chord shear force:
$$V_{ub} = \alpha_b V_u \qquad (5.6)$$

(d) determine the required abutment reinforcement at each side of the opening based on the chord shear forces determined in Step 4(c);

Span side abutment reinforcement area:
$$A_{ab} = \frac{V_{ut}}{f_y} \qquad (5.7)$$

Support side abutment reinforcement area:
$$A_{ab} = \frac{V_{ub}}{f_y} \qquad (5.8)$$

where $\boldsymbol{A_{ab}}$ is the required area of abutment reinforcement, $\boldsymbol{V_{ut}}$ and $\boldsymbol{V_{ub}}$ are the chord shear forces, and $\boldsymbol{f_y}$ is the reinforcement yield stress. A strength reduction factor is not used in sizing the abutment

reinforcement, because additional strength allows additional shear force to reach the chord, and the abutment reinforcement is meant to serve as a fuse for the shear force. Once the required area is determined, an actual area is calculated based on available bar sizes. A minimum of one closed loop stirrup is recommended for the abutment reinforcement. A separate check in Step 5 ensures that sufficient abutment reinforcement is provided at both sides of the opening to satisfy the ACI 318 Code's requirement that the design strength exceed the required strength.

(e) set the chord factored shear force equal to the value of the actual abutment reinforcement area times the steel yield strength;

Using the abutment reinforcement's yield strength to determine the factored shear force for each chord ensures the chord is provided with a design strength equal to the maximum force it must resist. The top and bottom chord shear forces, $\boldsymbol{V_{ut}}$ and $\boldsymbol{V_{ub}}$, resulting from this step are now greater than or equal to the values from step 4(c). The sum of the top and bottom chord shear forces will generally exceed the shear force at the opening, $\boldsymbol{V_u}$.

(f) determine the chord moments.

The chord moments are taken as the lesser of the chord required shear strength times the opening length and the maximum chord moment that can occur at the opening. Both approaches are conservative, but since the inflection point cannot at this point be located with any certainty, this seems a reasonable approach. The lesser moment is used to attempt to reduce the conservatism. Figure 5.3 shows a section cut from the ITO girder. Referring to the figure, taking moments about the point $\boldsymbol{O}$ with positive moments counterclockwise, assuming the distance on each side of the point is negligible, gives the following,

$$\Sigma M_O = 0 : -\left(M - P_e \cdot e\right) + M_t + M_b - N_t \cdot c_t + N_b \cdot c_b = 0 \qquad (5.9)$$

Where $\boldsymbol{M}$ is the total moment at the section, $\boldsymbol{P_e \cdot e}$ is the equivalent moment due to the prestress force, $\boldsymbol{M_t}$ and $\boldsymbol{M_b}$ are the top and bottom chord moments, $\boldsymbol{N_t}$ and $\boldsymbol{N_b}$ are the top and bottom chord axial forces, and $\boldsymbol{c_t}$ and $\boldsymbol{c_b}$ are the distances between the point of application of the effective prestress force and the chords' centroids. Because of the assumption that the distance to either side of the point is negligible, the shear forces $\boldsymbol{V_t}$ and $\boldsymbol{V_b}$ do not enter into the moment equation. Solving Equation (5.6) for the sum $\boldsymbol{M_t + M_b}$ gives the maximum chord moment that can occur in either chord at the opening, assuming the moment in the other chord is zero.

5.3.5 Step 5: Check abutment reinforcement failure.

An additional design requirement, which will be called the abutment reinforcement failure mode check, is that the abutment reinforcement does not yield at both sides of the opening before the girder reaches its nominal flexural strength at midspan. This prevents uncontrolled deformations at the openings. An additional check is also provided to ensure the abutment reinforcement satisfies the ACI 318 Code strength requirements. The following equations show the requirements.

Failure mode check:
$$\frac{\left(\left(A_{ab}\right)_{span} + \left(A_{ab}\right)_{\text{sup port}}\right) f_y}{V_u} \geq \left(\frac{M_n}{M_u}\right)_{midspan} \geq FMF \qquad (5.10)$$

Strength check:
$$\frac{\left(\left(A_{ab}\right)_{span}+\left(A_{ab}\right)_{\sup port}\right)f_y}{V_u}\geq\frac{1}{\phi} \tag{5.11}$$

where the numerator on the left side of each inequality is the total force the abutment reinforcement on both sides of an opening can resist, and the denominator is the total shear force at the opening. The right-hand side quantities are those at midspan in the first inequality, and ϕ in the second inequality is 0.85. If the inequality is not satisfied, additional stirrup legs are added at the opening until it is. In general, stirrup legs are added to try to preserve as closely as possible the original shear proportions. Adding additional stirrup legs requires the recalculation of the chords' required shear force and moments.

To ensure the desired ductile midspan failure mode occurs, the designer should investigate the necessity of including a failure mode factor (FMF in Equation 5.10) on the right-hand side of the inequality. If the ratio of the nominal midspan flexural capacity to the demand is close to 1.1, then the FMF, greater than 1.1, overrides the strength ratio. Using the FMF as a limit rather than applying a capacity design factor to the midspan strength ratio eliminates making the criterion stricter than necessary. The ratio of the nominal midspan flexural capacity to the demand is always greater than or equal to 1.1, and may provide sufficient protection against chord failures and material overstrength. The value of the FMF is within the designer's discretion.

5.3.6 Step 6: Design the chords for strength

a) determine the required chord shear reinforcement;

When the chord is in compression, the concrete shear capacity is determined as the lesser of $\boldsymbol{V_{ci}}$ (ACI 318 (11-10)) and $\boldsymbol{V_{cw}}$ (ACI 318 (11-12)). All other pertinent ACI 318 Code equations were investigated, and with this design procedure, ACI 318 (11-10) consistently gives the least estimate of the concrete shear capacity. This is primarily due to the conservative estimate used for the chord moment. When the chord is in tension, the concrete shear capacity is determined from ACI 318 (11-8). The shear reinforcement spacing applies the provisions of ACI 318 11.5.4 for prestressed members when the chord is in compression, and applies that section's requirements for ordinary reinforced concrete members when the chord is in tension. The required shear reinforcement is determined using ACI 318 (11-15), and checked against the minimum shear reinforcement requirements of ACI 318 11.5.5.

For the chord shear failure, the failure mode requirement is that the ratio of the design shear strength to the required shear strength should exceed the ratio of the midspan nominal flexural strength to the midspan required strength. This prevents a chord shear failure prior to a midspan flexural failure.

This requirement is stated as:
$$\frac{\phi V_n}{V_u}\geq\left(\frac{M_n}{M_u}\right)_{midspan}\geq FMF \tag{5.12}$$

where the numerator on the left side of the inequality is the chord's design shear strength, and the denominator is the chord's required shear strength. The right-hand side quantities are those at midspan. If the inequality is not satisfied, additional stirrups may be added or the spacing reduced.

As in Step 5, depending on the midspan strength ratio, a failure mode factor may be necessary to ensure the desired ductile failure mode.

b) design the chord's longitudinal reinforcement to resist axial load and flexure.

The elastic axial force at the factored load is treated as the axial force demand and located on an interaction diagram. The allowable moment at that axial force is determined from the interaction diagram and compared with the chord moment. Reinforcement is provided as necessary to resist the chord moment.

In general, for the bottom chord, this is a check that must be satisfied because the bottom chord has a significant area of steel. For the top chord, an area of steel must be specified that satisfies the strength requirements.

The failure mode requirement for both chords is that the ratio of the chord's design flexural strength to its required flexural strength should exceed the ratio of the midspan design flexural strength to the midspan required strength. This prevents a chord axial-flexural failure before a midspan flexural failure.

This requirement is stated as:

$$\left(\frac{\phi M_n}{M_u}\right)_{chord} \geq \left(\frac{\phi M_n}{M_u}\right)_{midspan} \geq FMF \qquad (5.13)$$

where the numerator on the left side of the inequality is the chord's design flexural strength, and the denominator is the chord's required flexural strength. The right-hand side quantities are those at midspan. If the inequality is not satisfied, additional reinforcement is added. For flexure, the design strength rather than the nominal strength at midspan is used in the comparison. This is done because the chord moments are conservative, and requiring the ratio to meet the stricter standard results in excessive amounts of reinforcement. Additionally, an axial-flexural chord failure is more ductile than a shear failure, so a lesser standard is applied. If a failure mode factor is deemed necessary, it should be consistent with the failure mode factors used in previous steps.

After determining the required top chord longitudinal reinforcement at each opening, the greater amount is run continuously throughout the girder's length. As the top chord reinforcement is increased, the midspan flexural strength also increases and must be recalculated to ensure the failure ratio is still satisfied. If it becomes difficult to satisfy the failure ratio, running the same steel continuously for the entire girder length may not be possible.

If the bottom chord does not satisfy the strength requirements, additional mild reinforcement may be placed in the bottom chord or the top chord depth may be increased. Increasing the top chord depth decreases the bottom chord shear demand, and thus the moment demand. If additional mild reinforcement is added to the bottom chord, and it is run continuously, the same problem occurs as in the top chord. This may also require that the bottom chord reinforcement not be continuous for the entire girder length.

5.4 DESIGN EXAMPLE - TRIAL 1

This section and the following three sections (5.5 through 5.7) present a design example, applying the recommended design procedure to the IT girder in the typical bay from Chapter 2, providing intermediate results at each step. These sections examine four trial cross-sections. In each section, the design procedure is followed until a requirement cannot be satisfied. The trial cross-section is revised, and the design procedure repeated. Section 5.7 steps through the design of the cross-section that satisfies the design procedure's requirements. The details of the unsuccessful trials are presented to show the effects the various requirements have on the final design.

Figure 5.2 shows the ITO girder that results from the successful application of the design procedure. Table 5.1 compares this ITO girder with S1 from the experimental program. Comparing the girders in Table 5.1, it is apparent that two very different girders result from the two different design processes.

For all four trials, the parameters are the same. The girder span is 27 ft.-8 in., accounting for the supports, with six loads at 5 ft. on-center placed symmetrically along the length. The superimposed uniformly distributed dead load is 20 psf, and the live load is 80 psf. The design uses a concrete strength of 8000 psi, a mild steel yield strength of 60 ksi, and ½ in. diameter, 270 ksi low-relaxation prestressing strands.

5.4.1 Trial 1, Step 1: Design an IT girder for the specified span, loads, and design material properties.

(a) Seven ½ in. diameter "special" strands in two layers (A_{ps} in Figure 5.2) give a design strength of ϕM_n = 15085 in.-kip, which provides sufficient strength to satisfy the flexural strength requirements with a midspan moment M_u = 14935 in.-kip;

(b) two # 4 bars on each side of the ledge at the top and bottom satisfy the ledge reinforcement requirement (A_l in Figure 5.2);

(c) a prestress force of 389 kips is required, giving a strand stress after long-term losses of 167 ksi;

(d) P_i = 408 kips, P_j = 421 kips, with associated strand stresses f_{pi} = 175 ksi and f_{pj} = 180 ksi;

(e) the permissible stress requirements are satisfied;

(f) four # 4 bars (0.8 in.^{2}) are necessary to resist the tension stresses at transfer;

(g) reevaluating the flexural strength considering the ledge reinforcement and the compression reinforcement, six ½ in. diameter "special" strands in two layers give a design strength of ϕM_n = 15415 in.-kip;

(h) the reinforcement limits are satisfied.

5.4.2 Trial 1, Step 2: Specify the opening's size, location and preliminary top chord reinforcement.

(a) The equivalent rectangular stress block depth from the previous step is a = 4.77 in., so a top chord depth of 6 in. is selected;

(b) the bottom chord depth is 11.625 in;

(c) the chord's minimum flexural reinforcement is 0.4 in.^{2}, which is less than the reinforcement required to resist the transfer stresses, so 0.8 in.^{2} is the tentative top chord reinforcement, placed at both faces of the top chord. Recalculating the midspan moment capacity with the increased compression reinforcement gives a design strength of ϕM_n = 15423 in.-kip. No further reduction in the strand area is possible;

(d) five openings are placed at 5 ft. on-center, with the center of the first opening at 46 in. from the member's end;

(e) an opening length of 30 in. is selected, which satisfies the recommendations in Barney et al. (1977).

5.4.3 Trial 1, Step 3: Check the nominal concrete stresses in the chords at transfer and service loads.

The trial cross-section stresses exceed the allowable service load stresses at the bottom face of the bottom chord on the span side of both openings 1 and 2, ending Trial 1.

5.5 DESIGN EXAMPLE - TRIAL 2

The top chord depth is increased to 8 in. for Trial 2, decreasing the assumed shear force in the bottom chord and reducing the moments and tensile stresses. Since Steps 1 and 2 treat the IT cross-section and the opening size and placement, the results of these steps do not change, with the exception of Step 2(c). The increase in the top chord depth increases the minimum flexural reinforcement area to 0.6 in.^{2}, which is the same as the area required to resist the tension stresses at transfer, so Trial 2 starts at Step 3. A revised elastic frame model is run to determine the elastic chord forces.

5.5.1 Trial 2, Step 3: Check the nominal concrete stresses in the chords at transfer and service loads.

The trial cross-section satisfies the nominal stress limits.

5.5.2 Trial 2, Step 4: Determine the chord forces for strength design.

(a) Opening 1: At the factored load, the chords' axial forces are: N_{ut} = 261 kips (C) and N_{ub} = 118 kips (C);

Opening 2: At the factored load, the chords' axial forces are: N_{ut} = 472 kips (C) and N_{ub} = 91 kips (T);

(b) Opening 1: The chords' nominal concrete shear strengths are: V_{ct} = 107 kips and V_{cb} = 142 kips. The top chord is thus assumed to carry 43% of the factored shear force, and the bottom chord 57%;

Opening 2: The chords' nominal concrete shear strengths are: $\boldsymbol{V_{ct}}$ = 139 kips and $\boldsymbol{V_{cb}}$ = 28 kips. The top chord is thus assumed to carry 83% of the factored shear force, and the bottom chord 17%;

(c) Opening 1: $\boldsymbol{V_{ut}}$ = 56 kips and $\boldsymbol{V_{ub}}$ = 74 kips;

Opening 2: $\boldsymbol{V_{ut}}$ = 55 kips and $\boldsymbol{V_{ub}}$ = 11 kips;

(d) Opening 1: The span side requires five # 4 stirrup legs, and the support side six;

Opening 2: The span side requires five # 4 stirrup legs, and the support side two, dictated by the recommended minimum;

(e) Opening 1: Based on the abutment reinforcement, $\boldsymbol{V_{ut}}$ = 60 kips and $\boldsymbol{V_{ub}}$ = 72 kips;

Opening 2: Based on the abutment reinforcement, $\boldsymbol{V_{ut}}$ = 60 kips and $\boldsymbol{V_{ub}}$ = 24 kips;

(f) Opening 1: The maximum chord moment is 2355 in.-kips. For the top chord the required shear force times the opening length is 1800 in.-kips, so $\boldsymbol{M_{ut}}$ = 1800 in.-kips. For the bottom chord, the required shear force times the opening length is 2160 in.-kips, so $\boldsymbol{M_{ub}}$ = 2160 in.-kips;

Opening 2: The maximum chord moment is 1842 in.-kips. For the top chord the required shear force times the opening length is 1800 in.-kips, so $\boldsymbol{M_{ut}}$ = 1800 in.-kips. For the bottom chord, the required shear force times the opening length is 720 in-kips, so $\boldsymbol{M_{ub}}$ = 720 in.-kips.

5.5.3 Trial 2, Step 5: Check abutment reinforcement failure.

Opening 1: Checking the failure mode requirement shows that the abutment reinforcement provided is not sufficient. Adding one stirrup leg to each side satisfies the failure mode requirement, giving six #4 stirrups on the span side and seven on the support side.

Initial abutment reinforcement: $$\frac{60\ kips + 72\ kips}{130\ kips} = 1.01 < \frac{17107}{14935} = 1.15$$

Final abutment reinforcement: $$\frac{72\ kips + 84\ kips}{130\ kips} = 1.20 > 1.15$$

The revised abutment reinforcement means the chord shear forces and moments at opening 1 must be revised.

Opening 2: Checking the failure mode requirement shows that the abutment reinforcement provided is sufficient.

Final abutment reinforcement: $$\frac{60\ kips + 24\ kips}{66\ kips} = 1.27 \geq \frac{17107}{14935} = 1.15$$

5.5.4 Trial 2, Step 4 (repeated): Determine the chord forces for strength design.

(e) Opening 1: Based on the abutment reinforcement, $\boldsymbol{V_{ut}}$ = 72 kips and $\boldsymbol{V_{ub}}$ = 84 kips;

(f) Opening 1: The maximum chord moment is 2355 in.-kips. For the top chord the required shear force times the opening length is 2160 in.-kips, so $\boldsymbol{M_{ut}}$ = 2160 in.-kips. For the bottom

chord, the required shear force times the opening length is 2520 in.-kips, so M_{ub} = 2355 in.-kips.

The abutment reinforcement failure mode check does not need to be repeated.

5.5.5 Trial 2, Step 6: Design the chords for strength

(a) Opening 1: For the top chord, V_{ct} = 21 kips, which requires stirrups with an area of 0.8 in.^{2} at 6 in. on-center. For the bottom chord, V_{cb} = 39 kips, which requires stirrups with an area of 0.8 in.^{2} at 5 in. on-center.;

Opening 2: For the top chord, V_{ct} = 23 kips, which requires stirrups with an area of 0.8 in.^{2} at 5 in. on-center. For the bottom chord, V_{cb} = 28 kips, which requires stirrups with an area of 0.4 in.^{2} at 4 in. on-center;

(b) Opening 2: Limiting the longitudinal reinforcement to $0.75\rho_b$, sufficient longitudinal reinforcement cannot be specified to satisfy flexural strength requirements, ending Trial 2.

5.6 DESIGN EXAMPLE - TRIAL 3

The top chord depth was increased to 10 in. for Trial 3, and this trial ended the same way as trial 2, that is, sufficient longitudinal reinforcement could not be provided in the top chord to satisfy flexural strength without exceeding $0.75\rho_b$. This trial's details are omitted because there is little difference from Trial 2.

5.7 DESIGN EXAMPLE - TRIAL 4

The top chord depth is increased to 12 in. for Trial 4. This increases the shear force in the top chord, but it also provides a larger lever arm for flexure because the depth to the tension reinforcement increases with the top chord depth. Since Steps 1 and 2 treat the IT cross-section and the opening size and placement, the results of these steps do not change, with the exception of Step 2(c). The increase in the top chord depth increases the minimum flexural reinforcement area to 1.0 in.^{2}, which is the greater than the area required to resist the tension stresses at transfer. Trial 4 starts at Step 3, and again, a revised elastic frame model is run to determine the elastic chord forces.

5.7.1 Trial 4, Step 3: Check the nominal concrete stresses in the chords at transfer and service loads.

The trial cross-section satisfies the nominal stress limits.

5.7.2 Trial 4, Step 4: Determine the chord forces for strength design.

(a) Opening 1: At the factored load, the chords' axial forces are: N_{ut} = 277 kips (C) and N_{ub} = 91 kips (C);

Opening 2: At the factored load, the chords' axial forces are: N_{ut} = 502 kips (C) and N_{ub} = 134 kips (T);

(b) Opening 1: The chords' nominal concrete shear strengths are: V_{ct} = 148 kips and V_{cb} = 135 kips. The top chord is thus assumed to carry 52% of the factored shear force, and the bottom chord 48%;

Opening 2: The chords' nominal concrete shear strengths are: V_{ct} = 190 kips and V_{cb} = 17 kips. The top chord is thus assumed to carry 92% of the factored shear force, and the bottom chord 8%;

(c) Opening 1: V_{ut} = 69 kips and V_{ub} = 62 kips;

Opening 2: V_{ut} = 61 kips and V_{ub} = 5 kips;

(d) Opening 1: The span side requires seven # 4 stirrup legs, and the support side six;

Opening 2: The span side requires five # 4 stirrup legs, and the support side two, dictated by the recommended minimum;

(e) Opening 1: Based on the abutment reinforcement, V_{ut} = 84 kips and V_{ub} = 72 kips;

Opening 2: Based on the abutment reinforcement, V_{ut} = 60 kips and V_{ub} = 24 kips;

(f) Opening 1: The maximum chord moment is 2579 in.-kips. For the top chord the required shear force times the opening length is 2520 in.-kips, so M_{ut} = 2520 in.-kips. For the bottom chord, the required shear force times the opening length is 2160 in.-kips, so M_{ub} = 2160 in.-kips;

Opening 2: The maximum chord moment is 2124 in.-kips. For the top chord the required shear force times the opening length is 1800 in.-kips, so M_{ut} = 1800 in.-kips. For the bottom chord, the required shear force times the opening length is 720 in-kips, so M_{ub} = 720 in.-kips.

5.7.3 Trial 4, Step 5: Check abutment reinforcement failure.

For this trial, the abutment reinforcement failure mode check was performed simultaneously with the chord force determination in Step 4. The results in Step 4 satisfy this check at both openings.

5.7.4 Trial 4, Step 6: Design the chords for strength.

(a) Opening 1: For the top chord, V_{ct} = 35 kips, which requires stirrups with an area of 0.8 in.^{2} at 6 in. on-center. For the bottom chord, V_{cb} = 36 kips, which requires stirrups with an area of 0.8 in.^{2} at 6 in. on-center.;

Opening 2: For the top chord, V_{ct} = 55 kips, which requires stirrups with an area of 0.4 in.^{2} at 9 in. on-center. For the bottom chord, V_{cb} = 18 kips, which requires stirrups with an area of 0.4 in.^{2} at 4 in. on-center;

(b) A top chord reinforcement area of 4.2 in.^{2} (A'_s in Figure 5.2(b)) is required for flexural strength, satisfying both the ACI 318 Codes's strength requirements and the failure mode requirements at both openings. This reinforcement is provided as seven # 7 bars at each face of the top chord. The bottom chord reinforcement is sufficient to satisfy both requirements without additional reinforcement.

5.7.5 Trial 4: Summary

Figure 5.2 and Table 5.1 show the final design that results from the design process. The top chord depth increases 2 in. relative to the test specimens, the prestressed reinforcement area decreases by 33%, and the top chord longitudinal reinforcement area increases 32%. The chord shear reinforcement increases significantly in the top chord at opening 1, and either stays the same or decreases everywhere else. The net result of these changes is a 33% decrease in the midspan failure load. This brings the failure load closer to the factored load, and makes it possible to have chord failure loads that are greater than the midspan failure load without excessive transverse reinforcement.

Satisfying the failure mode requirement for several failure modes at opening 1 was not possible with continuous top chord reinforcement, so the top chord reinforcement at midspan was reduced to the minimum flexural reinforcement initially specified, 1.0 in.^{2}. This reduces the ratio of the midspan nominal strength to required strength to a level where all the failure modes satisfy the failure mode requirements.

5.8 MODEL VERIFICATION

A fiber model of the ITO girder in Figure 5.2, implementing the abutment reinforcement fuses, was analyzed. It indicates flexural failure at the midspan opening at a load of 71.4 kips, compared with the predicted plane section analysis failure load of 71.9 kips. The model indicates neither an axial-flexural failure nor an axial-shear failure occurs in the chords at openings 1 and 2 at or below the midspan failure load.

A confined concrete model was again investigated for the final design, to see what the effects of confinement are. For the reinforcement selected, the confining pressure decreases compared with the model in Section 3.2 for the test specimens. This is due to wider stirrup spacing and increased chord depth, both of which increase the ineffective concrete area. Again, as for the test specimens in Section 3.2, there is an increase in the concrete strength and ductility, but the chords do not take advantage of this increase because the strains do not get large enough. For design, using the maximum confined concrete strength and the corresponding maximum concrete strain in place of the cylinder strength and the ACI 318 Code's limit of 0.003 in./in. for the ultimate concrete strain to predict the axial-flexural strength in the interaction diagram results in only a small increase in the flexural capacity from the confinement.

Table 5.2 shows the fiber model chord forces at the factored load, and compares them with the chord forces from the elastic analysis and the design procedure. The elastic normal forces are used in the design procedure, so they are the same for both. The normal forces from the fiber model agree well with the elastic normal forces, as expected.

The elastic chord forces are included for comparison with the fiber model forces to show that an elastic approach, like that proposed by Barney et al. (1977), does not give a reasonable set of design forces for this cross-section. Comparing the elastic analysis shear forces with the fiber model results, the elastic results are unconservative for all of the shear force estimates. This leads directly to the

result that the elastic analysis top chord moments are unconservative, and the bottom chord moments are conservative, because of the reversal of the shear forces.

Table 5.2 presents two shear forces for the design procedure. The first value is based on the chords' relative concrete shear capacity, and the second value is based on the abutment reinforcement provided.

At opening 1, the design procedure predicts a top chord shear force of 69 kips, while the limiting value based on the abutment reinforcement is 84 kips. The fiber model reaches a top chord shear force of 84 kips, which indicates the top chord at the factored load attracts a greater portion of the shear force than the design procedure predicts. This also shows that the abutment reinforcement fuse works as designed to limit the top chord shear force. The design procedure predicts a bottom chord shear force of 62 kips, while the fiber model only reaches a shear force of 43 kips. This is a result of the top chord attracting a greater portion of the shear force than the design procedure predicts. However, the design shear force of 72 kips, based on the abutment reinforcement, exceeds the fiber model shear force, providing a conservative design.

At opening 2, the design procedure predicts a top chord shear force of 61 kips, and the fiber model reaches a top chord shear force of 60 kips, limited by the abutment reinforcement fuse. The bottom chord is predicted to resist a shear force of 5 kips at the factored load, and the fiber model shows the bottom chord resists a shear force of 4 kips at the factored load. Again, this division of the shear force is partly due to the abutment reinforcement acting as designed. Even without the abutment reinforcement fuse, the division of shear predicted by the design procedure is very close to the fiber model result.

At both openings 1 and 2, only the span side abutment reinforcement yields, so the vertical deformations are well controlled.

Table 5.2 presents two values for the fiber model and the elastic analysis chord moments. The first value is the opening's support side moment, and the second value is the span side moment. For the design procedure, only the required strength is presented. This comparison shows that the design procedure estimates are conservative in all cases except the top chord at opening 2. Here, the design procedure moment is approximately 9% less than the fiber model moment. The fiber model moment exceeds the required moment (maximum shear force times opening length) because the top chord at opening 2 is in single curvature at the factored load, negating the assumption from which the required moment was calculated. This difference is small but unconservative, suggesting that using the maximum chord moment may be necessary (2124 in-kips) for the top chord flexural design at opening 2.

5.9 TOPPING SLAB EFFECTS

If a topping slab is placed as part of the floor system, and it develops composite action, the midspan flexural failure load increases. This means the failure mode requirement is likely not satisfied for any of the chord failure modes, so a chord failure may occur before a midspan failure. However, because the shear fuses are present and the failure mode requirements are enforced for the untopped

ITO girder, whichever failure mode is reached first will still exceed the factored load, satisfying the ACI 318 Code's strength requirements.

For the ITO girder considered here, addition of the same topping slab as in Chapter 3 increases the midspan failure load from 72 kips to 90 kips. A fiber model of this configuration indicates a failure at opening 1 at 93 kips, and at opening 2 at 91 kips. While appearing to give a margin of safety, these values are in fact meaningless. Because the abutment reinforcement is sized for the untopped girder, and the failure mode requirement enforced, there is a total shear capacity at opening 1 of 78 kips, and at opening 2 of 84 kips. This means that beyond these loads, uncontrolled deformations occur because the abutment reinforcement on both sides of the opening has yielded.

This appears to leave it to the designer's judgement whether or not to include the topping slab in the design. The untopped girder will satisfactorily resist loads up to and beyond the factored load, and will fail at a load approximately 30% greater than the factored load through yielding of the abutment reinforcement at opening 1. It is not necessary, under the ACI 318 Code, to design a structural member to fail in a ductile fashion at a load 30% greater than the design load, which is already a severe overload.

These results show that there is not a safety issue in a topping slab exhibiting composite action for the ITO girder. The certainty of how the girder will fail is lost, however, if the composite action is not considered. The recommended approach is to either ensure that composite action occurs, and account for it in the design, or ensure that it does not occur and design an untopped girder. This approach will yield an economical girder in both cases, and provide a certainty on how failure will occur.

5.10 UNBALANCED LIVE LOAD

The ITO girder should be checked for the effects of unbalanced live load. The most severe case for the midspan opening is live load on half the span. For the ITO girder considered in this study, this gives a shear across the midspan opening of 21 kips. Placing the minimum abutment reinforcement at both sides of the opening satisfies the abutment reinforcement requirements for strength and satisfies the failure mode requirement. Since the bottom chord will be in tension at the factored load, the top chord can be assumed to carry the entire shear force. Minimum shear reinforcement is placed in the top chord, and the axial force is greater than at opening 2, so the midspan opening's shear capacity is greater than at opening 2, with a demand approximately one-third of that at opening 2 for live load on the entire span. The midspan opening thus satisfies strength requirements.

Table 5.1 Comparison of Test Specimen S1 with Design Procedure ITO

			S1	Design Procedure
Top Chord Depth (in.)			10 in.	12 in.
A_{ps}			3.0 in.^{2}	2.0 in.^{2}
P_e			487.7 kips	378.2 kips
f_{pe}			162.2 ksi	188.7 ksi
A_l			0.8 in.^{2}	0.8 in.^{2}
A'_s		Opening 1	3.16 in.^{2}	4.2 in.^{2}
		Opening 2	3.16 in.^{2}	4.2 in.^{2}
		Opening 3	3.16 in.^{2}	1.0 in.^{2}
A_{vt}		Opening 1	0.4 in.^{2} @ 4 in.	0.8 in.^{2} @ 6 in.
		Opening 2	0.4 in.^{2} @ 4 in.	0.4 in.^{2} @ 9 in.
		Opening 3	0.4 in.^{2} @ 4 in.	0.4 in.^{2} @ 9 in.
A_{vb}		Opening 1	0.8 in.^{2} @ 6 in.	0.8 in.^{2} @ 6 in.
		Opening 2	0.4 in.^{2} @ 6 in.	0.4 in.^{2} @ 4 in.
		Opening 3	0.4 in.^{2} @ 6 in.	0.4 in.^{2} @ 4 in.
A_{ab}	Opening	Side		
	1	Support	2.8 in.^{2}	1.2 in.^{2}
		Span	2.8 in.^{2}	1.4 in.^{2}
	2	Support	1.6 in.^{2}	0.4 in.^{2}
		Span	1.6 in.^{2}	1.0 in.^{2}
	3	Support	0.8 in.^{2}	0.4 in.^{2}
		Span	0.8 in.^{2}	0.4 in.^{2}

Table 5.2 Comparison of Elastic Analysis, Design Procedure and Fiber Model - Chord Forces

	Opening/Chord		Elastic Analysis	Design Procedure	Fiber Model
N_u (kip)	1	Top	-277		-284
		Bot	-91		-85
	2	Top	-502		-486
		Bot	134		118
	3	Top	-578		-547
		Bot	210		179
V_u (kip)	1	Top	48	69 / 84†	84
		Bot	83	62 / 72†	43
	2	Top	24	61 / 60†	60
		Bot	42	5 / 24†	4
M_u (in.-kip)	1	Top	-603 / 829‡	2520	-1111 / 1416‡
		Bot	-1037 / 1422‡	2160	-603 / 698‡
	2	Top	-71 / 647‡	1800	179 / 1986‡
		Bot	-122 / 1111‡	720	-21 / 90‡

† The first value is the predicted shear force from the design procedure, based on the concrete shear capacity. The second value is the shear force for which the chords were designed, based on the area of abutment reinforcement.
‡ The first value is the support side moment, the second value is the span side moment.

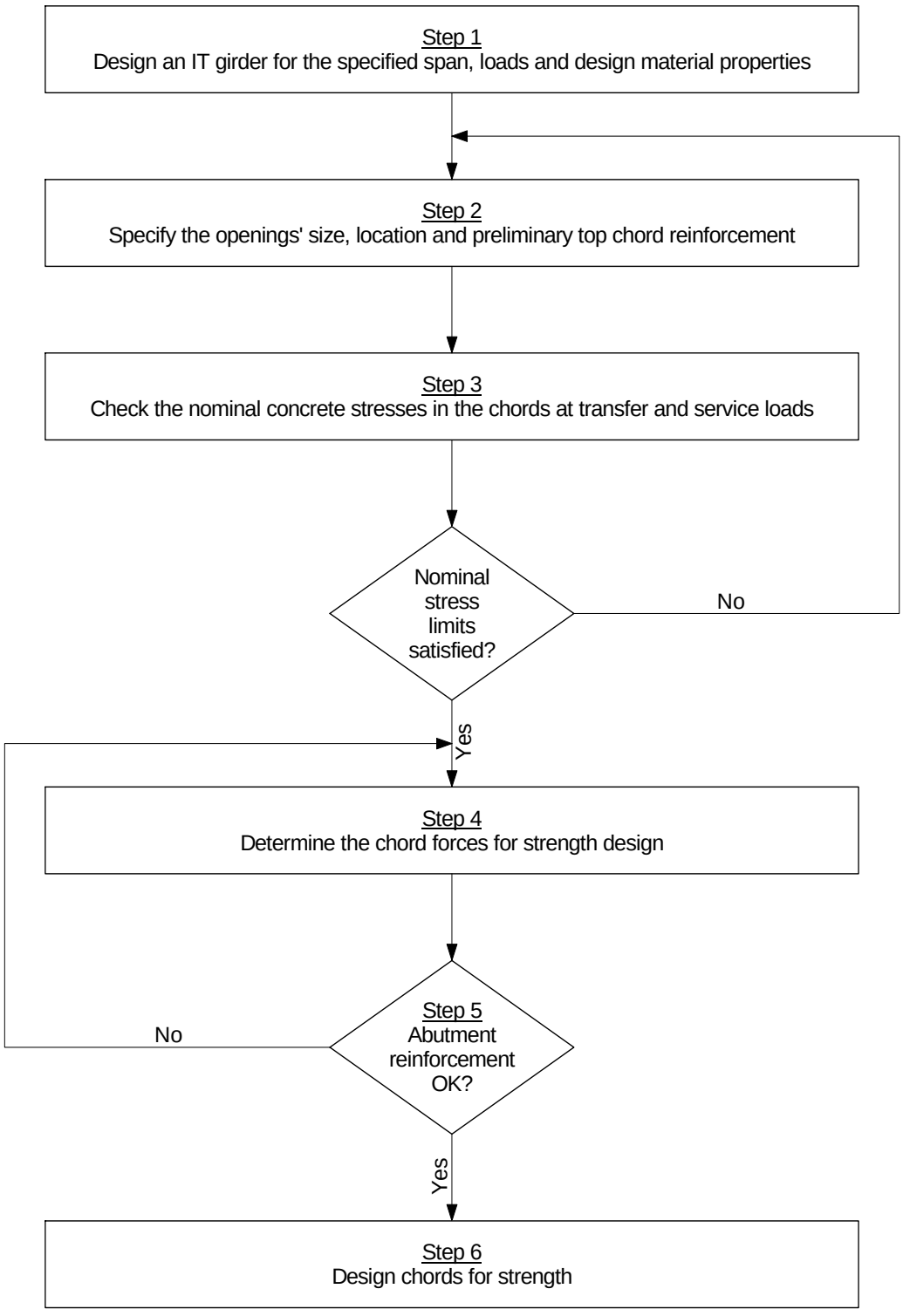

Figure 5.1 Design procedure flowchart

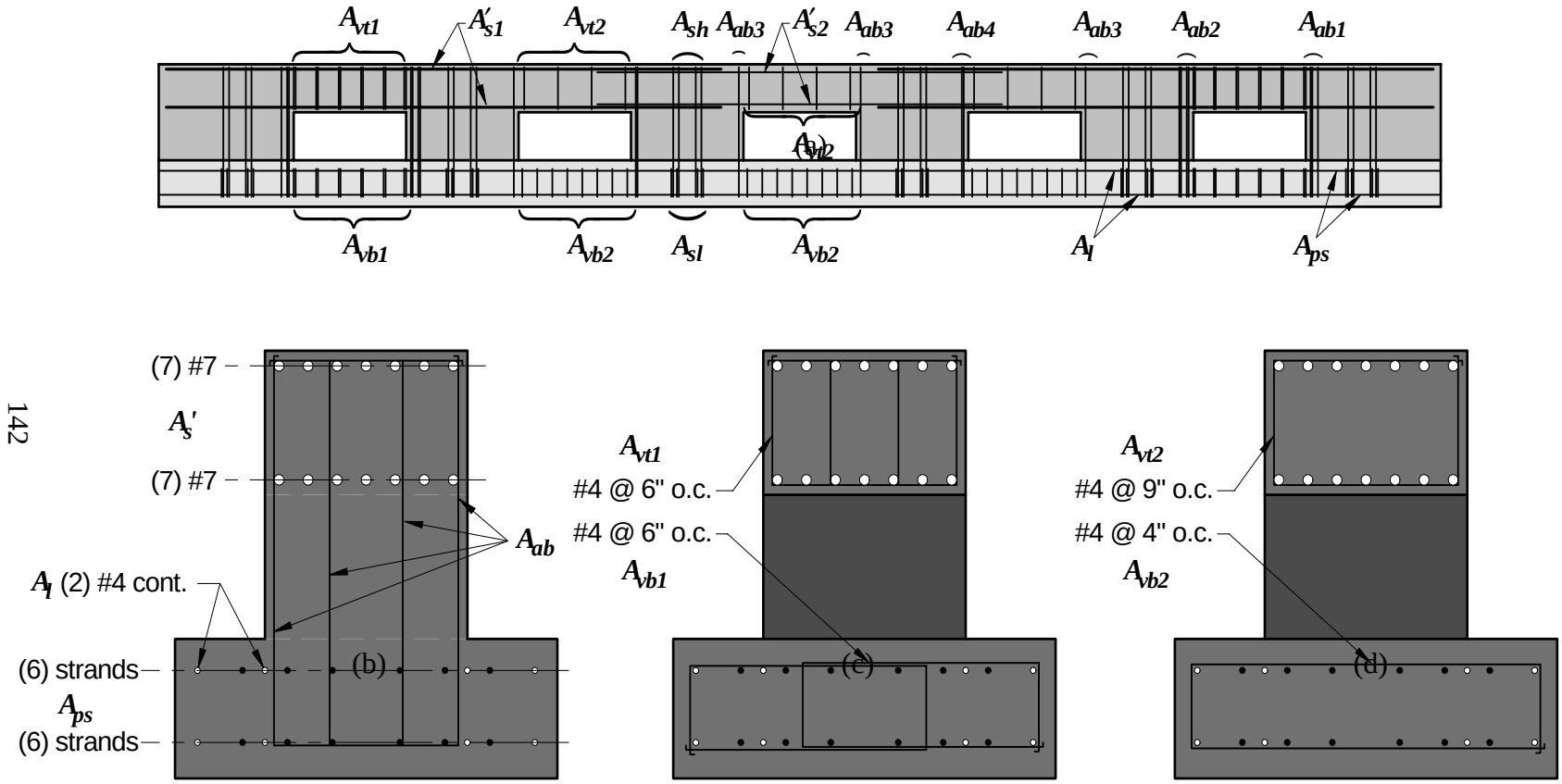

Figure 5.2 Prototype ITO girder elevation and sections

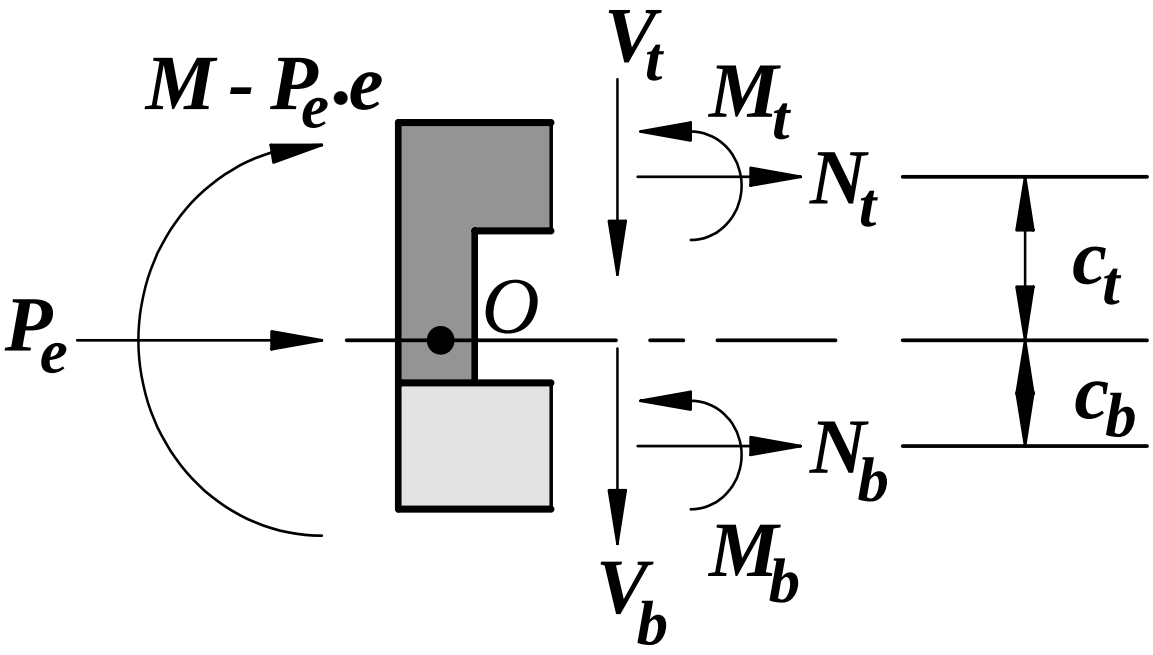

Figure 5.3 Section at an opening for calculating maximum chord moments

[This page intentionally blank]

CHAPTER 6

SUMMARY, CONCLUSIONS AND FUTURE WORK

6.1 INTRODUCTION

Large web openings in a precast, prestressed IT girder allow the passage of building services across the girder line within the floor system's structural depth, reducing the floor-to-floor height and the overall height of a building. The objectives of this research were to understand how the openings alter the behavior of an IT girder with large web openings (ITO girder) at the service load and the ultimate strength limit states, and to develop a design procedure for this structural member.

Section 6.2 summarizes the results of this research. Section 6.3 presents the conclusions drawn from the work. Section 6.4 presents suggested future work to learn more about the ITO girder's behavior, refine the design procedure, and study the economics of its use.

6.2 SUMMARY

A prototype ITO girder was designed based on the available literature on concrete beams with web openings. Three full-scale ITO girders and an IT girder were tested to evaluate and compare their behavior. Variables in the tests included the transverse reinforcement details between the openings and above the openings. Linear elastic finite element analyses, nonlinear finite element analyses (fiber models) and strut-and-tie models were used to investigate the ITO girder's behavior.

An inverted tee girder with large web openings can provide satisfactory service load performance and adequate strength. At the service load, the ITO specimens' overall behavior was similar to the behavior of the comparably longitudinally reinforced IT specimen. The similarity in behavior continued to the point at which the ITO specimens failed, at a load approximately 27% less than the IT specimen. The ITO specimens failed when a diagonal crack occurred in the top chord at the opening nearest the support. This prevented them from reaching their flexural strength at midspan and failing in a more ductile manner.

The amount of transverse reinforcement and its distribution in the posts was not found to affect the test specimens' peak load. It was found to affect the width of the cracks that formed between openings. The amount of transverse reinforcement in the top chord did affect the girder's peak load capacity, and the extent of the cracks that occurred.

The ITO specimens' behavior confirms the findings of previous researchers that a beam with large web openings exhibits frame behavior at the openings. The results also show that the findings of the previous research, primarily on double tee beams, are not completely applicable to this cross-section. The recommendations of the previous research did not result in an accurate failure load or failure mode prediction for the ITO specimens. The opening location along the span was found to affect the cracking at the opening significantly. This is due to the relative shear force and moment values at the opening.

The finite element analyses and the experimental program show that the proportion of the shear force resisted by each chord is dependent on their relative stiffness. The fiber model analyses show that the proportion of the shear force resisted by each chord changes as cracking occurs in the chords. These results also show that the relative stiffness is not only dependent on the moments of inertia, but also depends on the rigidity of the connection between the chords and the girder web. Once cracking occurs, these supports are not sufficiently rigid at the opening edges to allow the assumption of a fully fixed end condition for computing the relative stiffness.

The fiber model shows that the midspan opening failure load for a symmetrically loaded ITO girder is nearly identical with the failure load determined from a plane section analysis of an IT girder with the identical cross-section. This observation shows that if the failure loads for the other possible failure modes exceed the midspan opening failure load, an ITO girder can reach approximately the same load as the identical IT girder.

This research shows that treating an ITO girder as a flexural member with regions requiring special detailing does not produce completely satisfactory results. The desired ductile failure mode, prestressed reinforcement yielding at midspan, does not occur. Instead, an undesirable failure mode, diagonal cracking in the top chord, occurs. Capacity design provides an alternate way to approach the ITO girder's design. This approach's objective is to provide sufficient strength for the undesirable failure modes so they do not occur before the desired failure mode. To implement a capacity design approach, the demand must be known with certainty.

The test and fiber model results show that the chords' shear forces and moments are highly dependent on the extent of cracking in the chords, while the chords' axial forces depend primarily on the total moment at a section and the distance between the chords' centroids. The bottom chord cracking controls the shear distribution between the top and bottom chords, and the top chord cracking influences the top chord inflection point location. The chords' moments vary with the chord's normal and shear forces and the inflection point location, and therefore are a function of how much cracking occurs in the chords. These observations indicate an elastic analysis similar to the assumptions made for the analysis of a Vierendeel truss is inadequate for estimating the chord shear forces and moments. They also indicate a conservative approach for the chord's axial-flexural design is needed.

The fiber model analyses also show that cracking occurs in the bottom chord at both openings 1 and 2 while the chord's axial force is compressive. This observation shows that the sign of the chord's axial force is not sufficient as a criterion for apportioning the shear force between the chords. The experimental and fiber model results also show that, for this cross-section, a properly reinforced opening can be located within the strand development length. Because strand slip can result in a sudden failure, the bottom chord at an opening within the strand development length should not be designed for an excessive amount of shear force, which leads to large moments and extensive cracking.

The fiber model shows that the depth of the uncracked concrete in the top chords at openings 1 and 2 makes it unlikely the chord reinforcement will yield. This indicates flexural hinging of the top chord at both ends of the opening is not a viable mechanism to control the top chord shear force. The strut-and-tie models reveal the function of the ITO girder's various types of reinforcement and show that the abutment reinforcement on an opening's span side transfers shear force to the top chord, and

on an opening's support side, transfers shear force from the bottom chord to the section. Once the abutment reinforcement's function in the transfer of forces to the chords is understood, it is apparent that this reinforcement can be used to limit the chord forces to known values through controlled yielding. Once the chord forces are known and limited, the chords can be designed to provide adequate strength, allowing the ITO girder to fail in the desired failure mode.

A design procedure is presented that provides a means to quantify and limit the chord forces for strength design, using the abutment reinforcement to control the chord forces. The design procedure provides recommendations on the sizing of the various types of reinforcement required for the ITO girder. It also provides a method to ensure that a ductile midspan failure occurs prior to a brittle failure like those observed in the experimental program.

6.3 CONCLUSIONS

Placing multiple large web openings in an IT girder does not compromise the resulting ITO girder's strength or serviceability. The proposed design procedure provides a relatively simple approach to the design of an ITO girder that should ensure a ductile midspan failure.

The following conclusions focus on the experimentally observed differences between the ITO girders and the IT girder.

1. Up to their failure load, multiple web openings did not significantly alter the ITO girder specimens' load-deflection response compared with the IT girder.

The ITO girders have a bilinear load-deflection response similar to the IT girder, and the ITO girders' initial stiffness (as characterized by the midspan deflection) is approximately 95% of the IT girder's initial stiffness. The ITO girders' stiffness after midspan bottom chord cracking is approximately the same as the IT girder's post-cracking stiffness. Along the ITO girders' length the openings affect on the deflected shape and the total deflection is observable as an additional deflection at each opening's span side, which is larger than the change across the same distance at the same location in the IT girder.

2. The openings in the ITO girders alter the distribution of internal forces from the expected pattern for a flexural member.

The observed cracking at the corners of openings 1 and 2, both in the web adjacent to the openings and in the chords, indicates high concrete tensile stresses at these locations. This cracking occurs at a load approximately half that at which initial vertical flexural cracking occurs in the IT girder.

3. The peak load, the failure zone location, the type of failure, and the failure's ductility are all modified by the openings' presence.

The peak load carried by S1 and S2 is 27% less than the peak load carried by the IT girder, and the peak load carried by S3 is 40% less. The openings shift the failure zone from midspan for the IT girder to the top chord of opening 1 for the ITO girders. The type of failure limiting the peak load changes also, from a ductile flexural failure due to the prestressed reinforcement yielding for the IT girder to a brittle failure due to a diagonal crack in the top chord for the ITO girders.

The following conclusions focus on the ITO girder's experimentally observed behavior relative to the ACI 318 Code criteria.

4. An IT girder with multiple large web openings can be designed to satisfy the strength requirements of the ACI 318 Code.

The ITO girders in the experimental program reached a load 42% greater than the load necessary to satisfy the ACI 318 Code strength requirements. However, the test specimens' actual concrete strength (64% greater than the design value), their large area of compression reinforcement, and the unaccounted for tension reinforcement (the ledge reinforcement), all contributed to the test specimens' observed strength. These factors caused the test specimens to exhibit a greater than intended strength, and contributed to the observed chord failure by preventing a flexural failure at a lower load.

5. The ITO girders tested in the experimental program do not fail in a ductile manner, and thus do not completely satisfy the safety intentions of the ACI 318 Code.

The test specimens satisfy the minimum reinforcement requirements and reinforcement limits in the ACI 318 Code for both flexure and shear. These requirements are intended to ensure a ductile failure, which did not occur. The design procedure recommended by Barney et al., including the application of these criteria, thus is not sufficient to guarantee a ductile failure for this cross-section.

6. An ITO girder can be designed to have acceptable service load behavior with respect to deflections, cracking and concrete stresses.

The ITO girders' maximum service load deflection due to the total applied load was less than the maximum recommended value for live load deflection in Table 9.5(b) of the ACI 318 Code for roof or floor construction supporting of attached to nonstructural elements likely to be damaged by large deflections. No cracks were visually observed below the service load level in any ITO girder test specimens, although the response of some instruments indicates the existence of cracks below the service load level. The largest measured crack widths at the service load level are less than the accepted guidance on maximum crack widths for interior exposure in R10.6.4 of the ACI 318 Code. The permissible stress limits are assumed satisfied by the absence of cracking at the transfer stage and the small amount of observed cracking at the service load level. The stress levels in the test specimens are also deemed acceptable because they do not, in the tests, impair the performance of the girder (ACI 318 18.4.3).

The following conclusions focus on the two reinforcement variations' influence on the ITO girder's experimentally observed behavior.

7. The banded and spread approaches to providing the abutment reinforcement make little difference in the ITO girders' load-deflection response, peak load, and failure mode.

The banded approach contains the cracking at the openings' corners more effectively than the spread approach, particularly at opening 1, and some evidence exists that the spread approach results in greater deflection across the openings at low applied load levels. The different approaches to the abutment reinforcement did not alter the ITO girder's load-deflection response, as this was nearly

identical for S1 and S2. The different abutment reinforcement approaches did not affect the peak load carried by the ITO girders as evidenced by the 2% difference in the peak loads of S1 and S2. The different abutment reinforcement approaches also did not affect the failure mode, as all three ITO girders reached their peak load when a diagonal crack formed in the top chord at opening 1.

8. The two approaches to providing the top chord transverse reinforcement make no difference in the ITO girders' failure mode.

All three ITO girders reached their peak load when a diagonal crack formed in the top chord at opening 1.

9. The two approaches to providing the top chord transverse reinforcement make a difference in the failure load.

The more widely spaced top chord transverse reinforcement in S3 reduces its failure load by 10% compared with that of S1 and S2.

The following conclusions focus on the ITO girder's behavior and the design implications drawn from the behavior. Evidence for the conclusions comes from the experimental results, elastic finite element analysis, fiber model analysis, and the qualitative truss model.

10. The experimental results, the three-dimensional elastic finite element analysis and the fiber model analysis all show that the ITO girder's chords resist axial force, shear force and moment, like frame members.

The experimental evidence, including the deflected shape, the top chord longitudinal strains' pattern, and the pattern of vertical cracking in the chords all support the conclusion that the ITO girder exhibits frame behavior in the chords. The deflected shape shows evidence of double curvature when compared with the IT girder's deflected shape. The top chord longitudinal strain pattern is consistent with combined axial, shear and flexural forces in the top chord. The observed vertical cracks at the openings' edges are consistent with the frame moments in both the top and bottom chords.

11. An elastic estimate of the chords' axial forces is sufficiently accurate for strength design.

The chord's axial forces are primarily a function of the cross-section moment, the prestress moment, and the distance between the chords. For a given top chord depth, the chords' axial forces vary linearly with the applied load, and this linear variation is unaffected by the chords' cracking and accompanying stiffness changes. The close agreement between the axial forces from the experimental program, the three-dimensional linear elastic finite element analysis, the nonlinear fiber model analysis, and a linear frame analysis all support this conclusion. These observations indicate the chords' axial forces at the factored load can be accurately estimated with a linear elastic model and can be used for ultimate strength design.

12. The distribution of the shear force between the chords at an opening is primarily a function of the extent of cracking in the bottom chord.

The fiber model shows that when the bottom chord is uncracked, the proportion of the shear force carried by each chord is approximately constant, and is relatively close to the elastic distribution.

Once the bottom chord cracks, the proportion of the shear force it resists begins decreasing. If the bottom chord becomes fully cracked, it resists almost no shear.

13. An elastic estimate of the chords' shear forces is not sufficiently accurate for strength design.

The experimental program's observed chord failures indicate the top chord was carrying significantly more shear than the elastic estimate used in design. The fiber model shows that cracking occurs at the opening's edges in the bottom chord while the bottom chord axial force is compression, because of the chord moments caused by the frame behavior. The fiber model also shows that the shear force distribution between the chords once cracking occurs differs significantly from the initial elastic distribution. This difference is significant enough that the fiber model shear force predicts the test specimens axial-shear failure.

14. The assumption of an inflection point at the midpoint of the openings is not applicable to an inverted tee cross-section.

In the initial linear range, where the data appear consistent across an opening (S1, opening 2, S2 opening 1, and S3 opening 1) over the data's linear extent, the measured top chord longitudinal strains indicate an inflection point exists close to the midpoint of opening 1 and approximately 6 in. to 9 in. to the support side of the midpoint of opening 2. The three-dimensional elastic finite element model and the ITO fiber model (prior to cracking) predict similar inflection point locations. Once cracking occurs, the inflection point can vary further.

15. An elastic estimate of the chord moments is not sufficiently accurate for strength design.

The chord moments are a function of the chord normal and shear forces and the inflection point location, and therefore a function of the extent of cracking in the chords. The bottom chord cracking controls the shear distribution, and the top chord cracking influences the top chord inflection point location. These observations indicate an elastic analysis similar to the assumptions made for the analysis of a Vierendeel truss is inadequate for estimating the chord moments. They also indicate a conservative approach for the chord's axial-flexural design is needed.

16. Flexural hinging of the top chord at both ends of the opening is not a viable mechanism to control the top chord shear force.

The fiber model shows that, due to the compressive force in the top chord, the depth of the uncracked concrete at openings 1 and 2 is generally 50% or more of the top chord depth. This makes it unlikely the chord reinforcement will yield.

17. The strut-and-tie models and the fiber models show that yielding of the abutment reinforcement could provide a mechanism to control the shear force in both chords. The ability of the abutment region to accommodate – with proper reinforcement details – the inelastic elongation of the yielding abutment reinforcement in a ductile manner needs experimental verification.

The strut-and-tie models show a plausible path for the transfer of forces from the load points to the supports. This load path shows the function of the span side abutment reinforcement is to transfer a portion of the solid cross-section's vertical force to the top chord. It also shows the function of the support side abutment reinforcement is to transfer vertical forces from the bottom chord to the cross-

section. The fiber model shows that providing abutment reinforcement on each side of each opening in proportion to the top and bottom chords' shear forces provides a mechanism, yielding, with which to control and limit these forces. The chords can then be designed not for an assumed force, but for the force the selected abutment reinforcement can transfer at its yield strength.

18. The abutment reinforcement must be proportioned so that both sides of the opening do not yield below the factored load.

If the abutment reinforcement yields on both sides of the opening, large uncontrolled deformations will occur. If only one side yields below the factored load, the deformations are controlled by the stiffness of the opening and the other side's abutment reinforcement.

19. The abutment reinforcement should be placed as close to the opening's edges as cover requirements and fabrication practices allow.

The abutment reinforcement prescribed by the IDM is needed to resist the vertical tensile stresses at the openings' corners. The elastic finite element analysis shows that at transfer these stresses are over half the measured average value of f_r for the concrete, and continue to increase with the applied load. The elastic finite element analysis also shows that these vertical tensile stresses are confined to a narrow region at the openings' edges, supporting the experimental observation that the banded reinforcement contains the cracks at the openings' corners more effectively than the spread reinforcement. Also, in order to allow the truss behavior at the openings' edges to occur, the abutment reinforcement needs to be closely spaced to provide sufficient anchorage for the diagonal compression forces it is assumed to anchor.

20. For symmetric loading, the ITO girders' midspan region may be designed as if no opening is present.

In the experimental program, the similarity of the midspan strains between the ITO girders and the IT girder, along with the similar cracking response at midspan, suggests that the midspan opening does not significantly alter the internal force distribution in the ITO girders' midspan region from that of the IT girder. The ITO fiber model shows that the failure load at the midspan opening for a symmetrically loaded ITO is nearly identical to the failure load determined from a plane section analysis of an IT girder with the identical cross-section. This observation holds as long as the midspan top chord depth is at least as deep as the required equivalent rectangular stress block depth for the comparable solid cross-section. These observations show that if the failure loads for the other possible failure modes exceed the midspan opening failure load, an ITO girder can reach approximately the same load as the identical IT girder. Further, this shows that the midspan region does not need to be designed assuming frame behavior, because it does not appear that it occurs. This also indicates the logical place to start the ITO girder design is with an IT girder.

21. Openings can be located within the strand development length if this region is properly designed.

The experimental results show that, for this cross-section, an opening can be located within the strand development length without compromising the ITO girder's strength. Because strand slip can result in a sudden failure, the bottom chord at an opening within the strand development length

should not be designed for an excessive amount of shear force, which leads to large moments and extensive cracking.

22. To ensure a ductile midspan failure, the strength in all possible failure modes must be controlled.

Controlling the strength in the various failure modes, including the midspan failure mode, is essential to controlling the ITO girder's failure mode. To limit the midspan flexural strength, when specifying the prestressed reinforcement the designer must include all the longitudinal reinforcement in the cross-section. Providing sufficient strength to ensure the chord failure modes occur at a greater load than a midspan failure is accomplished by comparing the ratio of the chord failure modes nominal strength to the required strength and ensuring this ratio does not exceed the ratio for midspan flexural failure.

23. Dividing the shear force between the top and bottom chords in proportion to the chords' concrete shear capacity provides a reasonable approximation of the chord shear demand once cracking has occurred.

This approach accounts for the effects of the axial force and the cross-section dimensions directly.

24. If a topping slab will be placed as part of the floor system, it must be considered in the design process.

If composite action is expected, then the design must ensure, through proper detailing, either the desired composite action occurs or no composite action occurs, and continue accordingly.

25. The effect of live load on only half the span should be considered for a midspan opening for a symmetrically loaded member.

The minimum amount of abutment reinforcement should be provided at both sides of the opening, minimum shear reinforcement should be provided in both chords, and minimum flexural reinforcement provided in the top chord.

26. Placing the prestressed reinforcement in two layers, symmetric about the bottom chord centroid, is beneficial to the ITO girder's performance.

This provides beneficial precompression for the tension zones that occur at the bottom chord's support side top surface and its span side bottom surface. This delays cracking and the redistribution of forces that accompanies cracking.

6.4 FUTURE WORK

Testing full-scale non-composite ITO girders designed with the proposed design procedure is necessary to validate the design procedure and show that it provides the desired ductile failure mode for an untopped ITO girder. The ability of the abutment region to accommodate – with proper reinforcement details – the inelastic elongation of the yielding abutment reinforcement in a ductile manner needs experimental verification. Additionally, testing full-scale ITO girders that incorporate a composite topping slab, without ensuring composite action, would validate the conclusion in this

research that adding a topping slab without considering its effect in design is an acceptable procedure.

Further investigation of including a topping slab's effects on the ITO girder's behavior and ultimate strength would help determine whether the additional design effort is warranted. Is the resulting ITO girder more predictable in its ultimate strength behavior? Do the additional design and fabrication costs provide a more economical overall result? Some of the questions that could be investigated are (a) what is the minimum required top chord depth to resist construction loads as a non-composite member; (b) what is the minimum required top chord depth, in conjunction with the topping slab, for ultimate strength; (c) what effect does including the topping slab have on the required prestressed reinforcement area and prestress force; (d) what changes to the top chord's transverse and longitudinal reinforcement are required to ensure composite action?

Many areas of investigation are available to refine the design procedure's approach to ultimate strength design and potentially reduce some of its conservatism. Developing a more accurate method of predicting the shear force and the inflection point location in each chord, possibly as a function of the extent of cracking in the chords, is one area. Better estimates of these parameters may result in reduced chord moments, resulting in less top chord depth and longitudinal reinforcement. Another area for investigation that may result in a less conservative design is using truss models to design the ITO girder for ultimate strength. Since truss models do not rely on the assumption of an inflection point location, this approach also has the potential to yield a less conservative design.

There are also avenues to explore related to the ITO girder's service load behavior. One area is predicting the ITO girder's deflections. While the IT girder's deflections give a good indication of the ITO girder's deflections for this cross-section, with the opening sizes specified, a more accurate estimate is desirable. Another area to investigate is the effect of rounding or chamfering the openings' corners to reduce the cracking at service loads with a less abrupt cross-section change.

An area that needs investigation is the ITO girder's economics. An estimate of the costs and the benefits associated with providing the openings is needed to evaluate the feasibility of producing this structural member. The costs include the additional fabrication labor to bend the transverse reinforcement, fabricate the reinforcement cage, place the strands, and create the openings. Some of the openings' potential benefits, associated with reducing a building's floor-to-floor height, are the reduced cladding area, the reduced size of the foundation elements, the reduced size and operating cost of HVAC equipment, and the increased revenue possible from the additional stories that can be placed within the same height envelope.

There are also areas for investigation that could directly affect the fabrication costs noted above, which may improve the ITO girder's economic feasibility. One area is developing a more efficient system for creating the openings. Foam blocks used for the test specimens were effective, but difficult to remove, and not reusable. Another area for improvement is the placement of the transverse reinforcement. This research used closed-loop stirrups for the transverse reinforcement, which caused the fabricator to have to thread the prestressed reinforcement through the cage. This is in contrast to the typical approach for IT girders, where the strand is stretched in the empty casting bed, and the transverse reinforcement cage is lowered onto it. If a reinforcement scheme can be developed for the ITO girder that allowed this typical practice to occur, it would reduce the fabrication labor and the casting bed's cycle time.

REFERENCES

Abdalla, H. and Kennedy, J. B., "Design of Prestressed Concrete Beams with Openings," Journal of Structural Engineering, Vol. 121, No. 5, May 1995a, pp. 890-898.

Abdalla, H. and Kennedy, J. B., "Design Against Cracking at Openings in Prestressed Concrete Beams," PCI Journal, Vol. 40, No. 6, Nov-Dec 1995b, pp. 60-75.

ACI Committee 318, "Building Code Requirements for Structural Concrete (ACI 318-99) and Commentary (ACI 318R-99)," American Concrete Institute, Farmington Hills, MI, 1999.

ASCE-ACI Committee 445 on Shear and Torsion, "Recent Approaches to Shear Design of Structural Concrete," Manual of Concrete Practice, 1999, pp. 445R1-445R-43.

Barney, G. B., Corley, W. G., Hanson, J. M, and Parmelee, R. A., "Behavior and Design of Prestressed Concrete Beams with Large Web Openings," PCI Journal, Vol. 22, No. 6, November-December 1977, pp. 32-61.

Canadian Precast/Prestressed Concrete Institute, "CPCI Metric Design Manual, Third Edition," Canadian Precast/Prestressed Concrete Institute, Ottawa, Ontario, Canada.

Colaco, Joseph P., "A Stub-Girder System for High-Rise Buildings," AISC National Engineering Conference, May 1972.

Collins, M. P. and Mitchell, D., "Prestressed Concrete Structures," Response Publications, Toronto and Montreal, 1997.

Cook, W. D. and Mitchell, D., "Studies of Disturbed Regions near Discontinuities in Reinforced Concrete Members," ACI Structural Journal, Vol. 85, No. 2, 1988, pp. .

International Code Council, Inc., "International Building Code/2000," International Code Council, Inc., Falls Church, VA, 2000.

Kennedy, J. B. and Abdalla, H., "Static Response of Prestressed Girders with Openings," Journal of Structural Engineering, Vol. 118, No. ST2, Feb 1992, pp. 488-504.

Mander, J. B., Priestley, M. J. N., and Park, R., "Theoretical Stress-Strain Model for Confined Concrete," Journal of Structural Engineering, Vol. 114, No. 8, Aug 1988, pp. 1804-1826.

Mansur, M. A., Lee, Y. F., Tan, K. H., and Lee, S. L., "Tests on RC Continuous Beams with Openings," Journal of Structural Engineering, Vol. 117, No. 6, 1991a, pp. 1593-1606.

Mansur, M. A., Huang, L. M., Tan, K. H., and Lee, S. L., “Deflections of Reinforced Concrete Beams with Web Openings,” ACI Structural Journal, Vol. 89, No. 4, July-Aug 1992, pp. 381-389.

Mansur, M. A., Tan, K. H., and Lee, S. L., “Design Method for Reinforced Concrete Beams with Large Openings,” ACI Journal, Vol. 82, No. 4, July-Aug 1985, pp. 517-524.

Mansur, M. A., Tan, K. H., Lee, Y. F., and Lee, S. L., “Piecewise Linear Behavior of RC Beams with Openings,” Journal of Structural Engineering, Vol. 117, No. 6, 1991b, pp. 1607-1621.

Pensiero, J., “An Introduction to Truss Models and Their Application in the Design of Precast and Prestressed Concrete Connections,” M.Sc. Thesis, Civil Engineering Department, Lehigh University, 1989.

Pessiki, S., Prior, R., Sause, R. and Slaughter, S., “Review of Existing Precast Concrete Gravity Load Floor Framing Systems,” PCI Journal, Vol. 40, No. 2, March-April 1995a, pp. 52-68.

Pessiki, S., Prior, R., Sause, R., Slaughter, S., van Zyverden, W., “Assessment of Existing Precast Concrete Gravity Load Floor Framing Systems,” PCI Journal, Vol. 40, No. 2, March-April 1995b, pp. 70-83.

Pessiki, S., van Zyverden, W., Sause, R., Slaughter, S., “Proposed Concepts for Floor Framing Systems for Precast/Prestressed Concrete Office Buildings,” PCI Journal, Vol. 42, No. 5, September-October 1997, pp. 66-76.

Precast/Prestressed Concrete Institute, “PCI Design Handbook: Precast and Prestressed Concrete, Fifth Edition,” Precast/Prestressed Concrete Institute, Chicago, IL, 1999.

Ragan, H. S. and Warwaruk, J., “Tee Members with Large Web Openings,” PCI Journal, Vol. 12, No. 4, August 1967, pp. 52-65.

Rogowsky, D. M. and MacGregor, J. G., “Design of Reinforced Concrete Deep Beams,” Concrete International: Design & Construction, Vol. 8, No. 8, 1986, pp. 49-58.

Savage, J. M., Tadros, M. R., Arumugasaamy, P., and Fischer, L. G., “Behavior and Design of Double Tees with Web Openings,” PCI Journal, Vol. 4, No. 1, January-February 1996, pp. 46-62.

Schlaich, J., Shafer, K, and Jennewein, M., “Toward a Consistent Design of Structural Concrete,” PCI Journal, Vol. 32, No. 3, 1987, pp. 74-150.

Slaughter, S., Sause, R. and Pessiki, S., “Development of a Framework for Structural Floor Framing Systems to Accommodate Nonstructural Requirements,” Journal of Architectural Engineering, Vol. 3, No. 3, September 1997, pp. 109-117.

Tan, K. H., Mansur, M. A., and Huang, L. M., “Reinforced Concrete T-beams with Large Web Openings in Positive and Negative Moment Regions,” ACI Structural Journal, Vol. 93, No. 3, May-June 1996, pp. 277-289.

Tan, K. H. and Mansur, M. A., “Design Procedure for Reinforced Concrete Beams with Large Web Openings,” ACI Structural Journal, Vol. 93, No. 4, July-Aug 1996, pp. 404-411.

Thompson, J. M. and Pessiki, S. P., “Experimental Investigation of Precast, Prestressed Concrete Inverted Tee Girders with Multiple Web Openings for Service Systems,” ATLSS Report No. 01-12, Center for Advanced Technology for Large Structural Systems, Lehigh University, Bethlehem, PA July 2001.

Vecchio, F. J. and Collins, M. P., “The Modified Compression-Field Theory for Reinforced Concrete Elements Subjected to Shear,” Journal of the American Concrete Institute, Vol. 83, No. 2, March-April 1986, pp. 219-231.